A Modelling Study of Air Pollution in Urban Areas

by

Tara AbuBakir Ali Rasoul

A thesis submitted to the University of Birmingham for the degree of
DOCTOR OF PHILOSOPHY

School of Geography, Earth and Environmental Sciences
College of Life and Environmental Sciences
University of Birmingham

August 2019

UNIVERSITY OF BIRMINGHAM

University of Birmingham Research Archive

e-theses repository

Abstract

Anthropogenic NO_x emissions from traffic have the potential to change atmospheric chemical composition, and lead to the production of pollutants that can have an adverse impact on human health and the environment. In this study, the formation and loss of nitryl chloride, nitrogen dioxide and secondary inorganic (nitrate) aerosol are explored using a zero dimensional (0-D) box model based on the near-explicit Master Chemical Mechanism (MCM).

$ClNO_2$ production, photolysis, chlorine atom sources, and chlorine chemical reactions are incorporated into a box model. The performance of the model was evaluated against measurements. The model was able to reproduce the $ClNO_2$ diurnal profile close to the observations. The evaluated model was then used to explore the effect of the projected increase in mean summer temperature of the UK by 2050 on the formation and impacts of $ClNO_2$ chemistry.

The box model was used to explore six NO_x emissions scenarios to investigate the effect of temporal NO_x emission distribution (changing emissions with time) from vehicles on a number of tropospheric chemical species. The change in NO_2 mixing ratios from different emission scenarios were used to estimate the number of deaths, due to exposure to NO_2. The scenarios in which NO_2 concentrations were very different to the base case were used in a case study to examine the best way of reducing NO_2 concentrations.

Finally, the box model was used to predict the formation of nitrate aerosol from N_2O_5 heterogeneous reactions. The effects of temporal NO_x emissions and $ClNO_2$ chemistry on the concentration of nitrate aerosol were also investigated.

The results obtained from this study showed the capability of the 0-D box model in predicting gas phase chemical compounds and aspects of particulate matter from heterogeneous reactions, and in simulating NO_x emission scenarios and their impacts on air quality.

This thesis is dedicated to the memory of

my father and my grandmother

Acknowledgments

Contents

List of Figures

List of Tables

Chapter 1 Introduction

This chapter presents an overview of atmospheric composition in general with a focus on the chemistry of the troposphere / boundary layer in urban areas, and highlights some of the main pollutant formation mechanisms in polluted environments. A focus upon the chemistry of a newly identified pollutant sources, $ClNO_2$, and pollutants such as NO_2, and nitrate aerosol provides the context for subsequent chapters of the thesis.

1.1 Atmospheric composition

The Earth's atmosphere is a thin, gaseous film surrounding our planet which consists mainly of nitrogen (78%) and oxygen (21%), the remaining 1% is comprised of argon, carbon dioxide with tiny amounts of other gases (trace gases) such as methane, non-methane hydrocarbons, ozone, nitrogen oxide species, and carbon monoxide. The atmosphere also contains water vapour and solid and liquid aerosol particles that scatter and absorb solar radiation.

The bulk composition of dry air (nitrogen, oxygen and a small amount of trace gases) is well mixed and relatively constant to an altitude of about 80 kilometres, they are called permanent gases (Table 1.1), whereas a small fraction made up from the trace gases (<0.04%) are variable (Table 1.2) and yet have significant impacts on atmospheric chemistry (Lutgens et al., 2010). Water vapour in the atmosphere is also variable according to temperature and altitude. The concentration of trace gases can be changed via natural and anthropogenic activities (Meszaros, 1993).

Table 1. 1 Permanent gases of the atmosphere dry air (Aguado and Burt, 2010)

Atmospheric constituent	% by volume
Nitrogen (N_2)	78.08
Oxygen (O_2)	20.95
Argon (Ar)	0.93
Neon (Ne)	0.002
Helium (He)	0.0005
Xenon (Xe)	0.00009
Hydrogen (H_2)	0.00005

Table 1. 2 Variable gases and their typical abundance in the atmosphere (Aguado and Burt, 2010)

Atmospheric constituent	% by volume
Water Vapour (H_2O)	0.25
Carbon Dioxide (CO_2)	0.036
Ozone (O_3)	0.01

The atmosphere is divided into four vertical layers based on the variation of temperature with altitude, which are the troposphere, stratosphere, mesosphere and thermosphere (Figure 1.1). Each of these layers differs in temperature, composition, stability and rate of vertical mixing (Peixoto and Oort 1992; Brasseur et al., 1999).
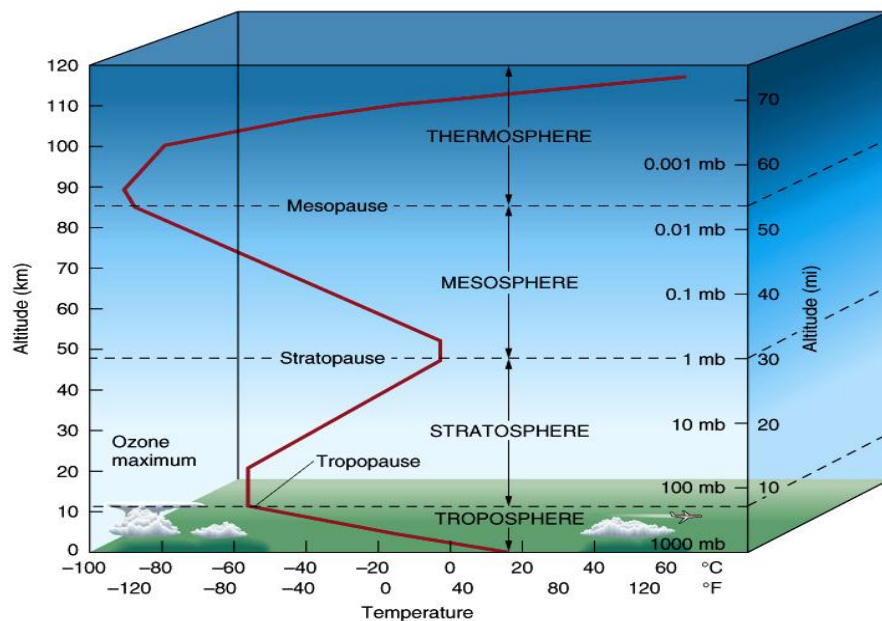
Figure 1. 1 The atmospheric layers based on temperature variation (Aguado and Burt, 2010)

The Troposphere

The lowest layer of the atmosphere contains about 90% of the atmospheric mass. The altitude of the tropopause varies according to latitude and season (Arya, 1999). Therefore, in the polar region, the troposphere can reach up to 8 or 9 km, whereas over the equator, where the air is warm, it can reach up to 16 km (Barry and Chorley, 2010). In addition, the troposphere is deeper in summer than in winter (Aguado and Burt, 2010).

The temperature in the troposphere decreases with increasing altitude at an average rate of ~6.5 °C km^{-1}, called the environmental lapse rate. Unsaturated air cools at a constant rate of 1°C per 100 meters. The rate of changing temperature of unsaturated air parcel with height is known as dry adiabatic rate.

The temperatures can also increase with increasing altitude in a situation called 'inversion' indicates the stability of the atmosphere. Temperature inversion mostly occurs on clear nights, as the air above the ground cools at a faster rate than the surrounding, and when ascending to a higher altitude the temperature of the air parcel become colder and denser than the surrounding air and tend to descend to its original position. Therefore, the air above the ground becomes colder than the air aloft.

Unlike other layers of the atmosphere, the troposphere is unstable with respect to vertical mixing. It is the region where almost all weather phenomena occur. The troposphere is relatively wet, containing about 0.1-4% of water vapour depending on temperature and altitude (Liang, 2013). It also contains many trace gases that are produced from natural and anthropogenic sources, such as methane (CH_4), carbon dioxide (CO_2), nitrous oxide (N_2O), carbon monoxide (CO), ammonia (NH_3), hydrogen sulphide (H_2S), sulphur dioxide (SO_2) and ozone (O_3). The troposphere is comprised of two regions, which are the Boundary Layer (BL) and the Free Troposphere (FT).

Boundary Layer (BL): The boundary layer is the lowest part of the atmosphere, where people breathe. It extends from the surface to a height varying from a few tens meters to 1-2 km depending on the place and time (Holloway and Wayne, 2010). The greater intensity of surface heating leads to a thicker boundary layer during the daytime, and thinner boundary layer at night, and during cold seasons (Haby, 2011). Over the ocean, the Marine Boundary Layer (MBL) is thinner than over continental areas (Planetary Boundary Layer) because the MBL is more stable due to less surface heating than over the land. The variation in thickness of the BL is mainly due to wind speed and temperature; high wind speeds lead to more convection mixing and cause the PBL to expand (Haby, 2011). During the daytime, on a sunny day, the ground is heated due to absorption of solar radiation, which in turn leads to warming via conduction of heat into the thin layer of air just above the earth's surface. The warmed air expands and becomes less dense, thus buoyantly rises upward as a thermal. The raised thermal air replaces the cooler, more dense air aloft, hence vertical exchange occurs that enhances mixing in this layer called convection (Aguado and Burt, 2010). The top of the convection layer is often capped by an inversion layer, in which temperature increases with altitude. Although some mixing might occur between the inversion and mixed layer, pollutants are typically trapped below or within the inversion. Therefore, the concentration of pollutants increase when the inversion is closer to the ground (Jacobson, 2012).

At night, the surface layer cools and temperature inversions develop; hence, most of the turbulent mixing reduces within BL. Therefore, the nocturnal boundary layer becomes more stable; however, the rest of mixed layer forms a residual layer.

1.2 Chemical composition of troposphere

1.2.1 Nitrogen – containing compounds: Nitrogen Oxides (NO$_x$)

Nitrogen (N$_2$) is the most abundant gas in the earth's atmosphere, which is inert throughout the lower atmosphere; however, ammonia (NH$_3$) and nitrogen species that contain oxygen (except nitrous oxide (N$_2$O) which is virtually inert in the troposphere) are reactive and significant in atmospheric oxidation process (Hewitt and Jackson, 2009). Amongst these species are nitric oxide (NO), nitrogen dioxide (NO$_2$), nitric acid (HNO$_3$), the nitrate radical (NO$_3$), dinitrogen pentoxide (N$_2$O$_5$), and nitryl chloride (ClNO$_2$).

One of the most important groups in atmospheric chemistry is the nitrogen oxides (NO$_x$), which refers to the sum of NO and NO$_2$. The majority of NO$_x$ (nearly 90%) emitted from either natural or anthropogenic sources into the atmosphere is thought to be in the form of NO, however, this depends on the emission / combustion process in question (Finlayson-Pitts and Pitts Jr, 1999). Nevertheless, natural sources contribute a small fraction compared to the total emitted from anthropogenic sources (Seinfeld and Pandis, 1997). Natural sources include lightning and emissions from soil and plants, while fossil fuel combustion at high temperature is the predominant anthropogenic source of NO (the Zeldovitch mechanism). Chemical reactions and deposition are the major sink for NO removal from the atmosphere, Table 1.3 (Jacobson, 2012).

$$O + N_2 \rightarrow NO + N \qquad\qquad R1.1$$

$$N + O_2 \rightarrow NO + O \qquad\qquad R1.2$$
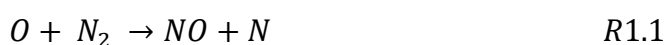
Table 1. 3 Source and sinks of nitrogen oxides [adapted from Jacobson, 2012; Seinfeld and Pandis, 1998].

sources	sinks
Fossil fuel combustion	Deposition
Soil released (natural and anthropogenic)	Chemical reactions
Biomass burning	
Lightning	
Photolysis and chemical reactions	

Reactions of nitrogen oxide lead to the production of secondary pollutants such as nitrogen dioxide (NO_2) and ozone (O_3) that have large impacts on air quality, and thus on human health and the environment.

NO_2 is a predominantly secondary pollutant that is produced via chemical reaction in the atmosphere, mainly from the oxidation of NO by O_3, and is removed by photolysis, chemical reaction or deposition (Jacobson 2012).

At wavelengths shorter than 420 nanometres (nm), NO_2 is photolysed to reform NO and a ground-state oxygen atom, $O(^3P)$. The latter combines with oxygen molecules forming O_3. O_3 further reacts with NO resulting in the conversion of O_3 back to O_2 and NO_2, thus NO, NO_2, and O_3 reach a photochemical steady state condition (PSS) in which no net O_3 production occurs (Seinfeld and Pandis, 1998). The ratio of NO to NO_2 can be derived from the reactions R1.3-R1.5, the so called Leighton ratio depends on the rate coefficient of reaction R1.5, photolysis frequency of NO_2 ($j(NO_2)$), and concentration of O_3 (Monks et al., 2015).

$$NO_2 + hv \, (< 420 \; nm) \rightarrow NO + O(^3P) \qquad\qquad R1.3$$

$$O(^3P) + O_2 + M \; \rightarrow O_3 + M \qquad\qquad R1.4$$

$$NO + O_3 \; \rightarrow NO_2 + O_2 \qquad\qquad R1.5$$
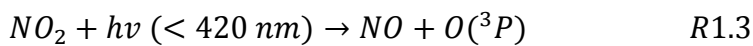
The above reactions recycle NO_x and O_3, and are significant in controlling O_3 concentration in the troposphere, however, if extra species such as carbon monoxide (CO), methane (CH_4), or non-methane hydrocarbons (NMHC) are present, then net O_3 production may occur. This arises as VOCs react with the hydroxyl radical (OH) which leads to the formation of peroxy radicals, which in turn convert NO to NO_2, leading to the net formation of tropospheric ozone (Figure 1.2).

$$O_3 + hv \rightarrow O(^1D) + O_2$$
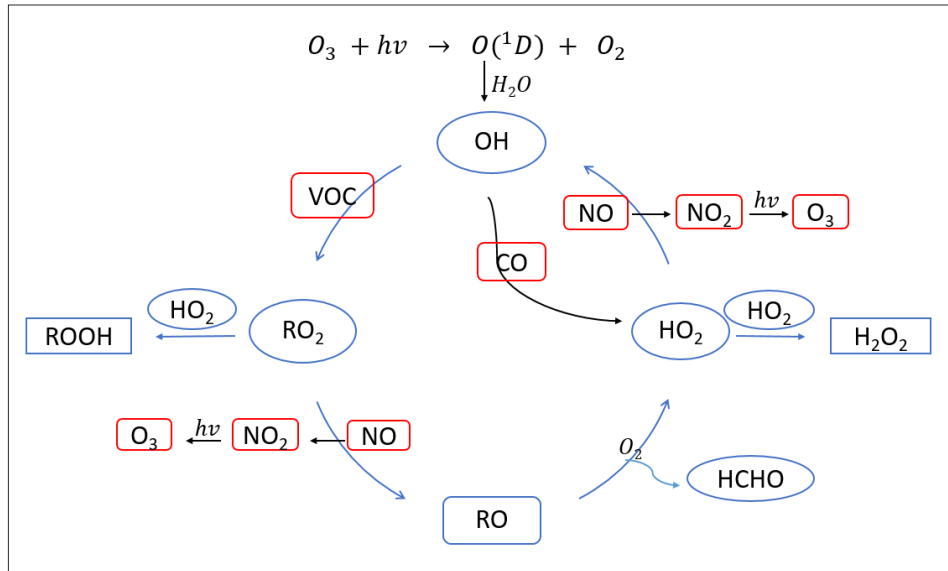
Figure 1. 2 Typical tropospheric chemistry; initiated by oxidations of VOC by OH leading to pollutant formation. Adapted from Bloss (2009).

1.2.2 Volatile organic compounds (VOCs)

VOCs are organic trace gases that have low boiling points and high vapour pressure, which usually evaporate from substances containing them (Jacobson, 2012). Most VOCs are emitted into the atmosphere from both natural and anthropogenic sources (Seinfeld and Pandis, 1997). Natural sources include vegetation and wetlands, whereas anthropogenic sources include transportation, petroleum refineries, and use of fossil fuels in general (Seinfeld and Pandis, 1997). In forested and heavily vegetated regions such as in the southeastern United States, VOCs emissions, mainly isoprene and terpenes, are a large local source of recurring high-ozone episodes (Brasseur et al., 1999, Winer et al., 1992). Alternatively, in urban and highly industrialized areas, many VOCs emitted from

anthropogenic sources, are the main contributors to photochemical ozone production (Mohamed et al., 2002).

Hydrocarbons / VOCs that are released into the atmosphere from vegetation sources are called biogenic hydrocarbons or biogenic volatile organic compounds (BVOCs), and VOC emitted from anthropogenic sources called AVOCs, hydrocarbons excluding methane may be termed non-methane hydrocarbons (NMHCs) or non-methane volatile organic compounds (NMVOCs).

1.2.3 Ozone

Ozone (O_3) is a secondary reactive oxidant gas that is chemically formed (in the troposphere) from reactions involving NO_x and VOC in the presence of sunlight (Figure 1.2), and removed from the atmosphere via photolysis, chemical reactions and deposition to the surface. O_3 is a greenhouse gas contributing to global warming, and a pollutant that can adversely affect human health, vegetation, and ecosystems. Anthropogenic emissions (mainly from traffic) of NO_x, CO, and VOCs is a main source of O_3 downwind of urban areas (Sillman, 2003). The lifetime of O_3 can be as little as 1-2 days if removed by dry deposition in the boundary layer, however, the average lifetime of O_3 in the troposphere has been estimated to be 22 days, making it a hemispheric pollutant (Fowler et al., 2008).

Controlling O_3 in the air is challenging, due to a non-linear relationship between the abundance of NO_x and VOCs and the rate of formation of ozone $P(O_3)$. When the NO_x concentration is low, the rate of O_3 production increases with increasing NO_x concentrations. However, the rate of O_3 production then changes to a situation where it decreases with increasing NO_x concentration in high NO_x environments. Therefore, in polluted urban areas (high NO_x), as air masses undergo transport from the (primarily anthropogenic) emission sources, O_3 formation moves from high NO_x (VOC limited), to low NO_x (VOC saturated) environment, where O_3 can build up and can persist in the air for several days or weeks, thus can be transported for long distances (Monks, 2005). The relationship between NO_x, VOC and $P(O_3)$ can be illustrated by isopleth plots as shown in figure 1.3.
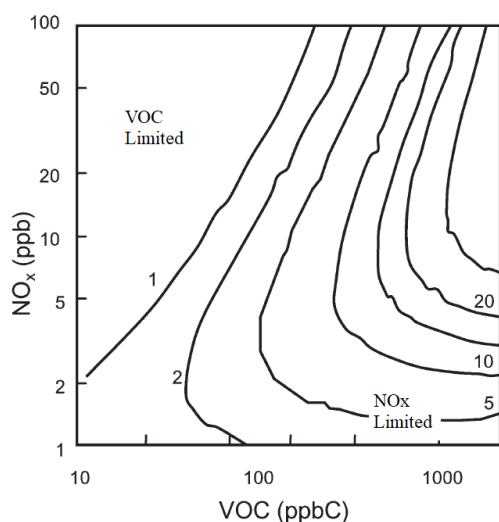
Figure 1. 3 Isopleth plots showing O_3 production rate (ppb h^{-1}) as a function of NO$_x$ (ppb) and VOC (ppbC) for mean summer daytime urban condition and clear sky [adapted from (Sillman, 1999)]

1.2.4 Aerosols

The term aerosol refers to gas, liquid or solid particles suspended in a gaseous medium. Aerosol particles or particulate matter (PM) refers to a mixture of solid and liquid particles suspended in the air that may either be emitted directly, known as primary aerosol (such as mineral dust from dry surfaces or soot from coal and biomass burning) or formed by gas-to-particle conversion process in the atmosphere (via nucleation, condensation and heterogeneous and multiphase chemical reactions) called secondary aerosol (e.g. sulphate from sulphur dioxide, SO_2) (Seinfeld and Pandis, 1997). Sources of aerosol include a variety of natural (e.g. wildfires, sea spray emissions, volcanic emissions, mineral dust from arid regions) and anthropogenic sources (e.g. fossil fuel combustion) (Hewitt and Jackson, 2009).

Aerosols have an adverse impact on human health and visibility degradation (Jacbson, 2012). Furthermore, aerosol particles can act as cloud condensation nuclei resulting in the formation of cloud or fog droplets, which can directly scatter solar radiation (Brasseur et al., 1999)

The oceans are the main source of sea salt aerosol particles in the atmosphere in term of mass concentrations, produced as a result of the bubble-bursting process (Manders et al.,

9

2010). The peak annual average concentrations of sea salt, up to 13 $\mu g\ m^{-3}$ have been found at the northern and southern coasts of Ireland and the UK, however, at a distance of 200-300 km from coastal areas, sea salt concentrations were found to be in a range of 2 - 5 $\mu g\ m^{-3}$ (Figure 1.4) (Manders et al., 2010). Sea salt has an important role in atmospheric chemistry. For instance, the uptake of dinitrogen pentoxide (N_2O_5) upon sea salt aerosol or any aerosol containing Cl^- leads to the production of nitryl chloride ($ClNO_2$) in the troposphere which has an adverse impact on the air quality. $ClNO_2$ acts as a reservoir for highly reactive chlorine atoms (Cl) and NO_2, both of which contribute to photochemical ozone production.
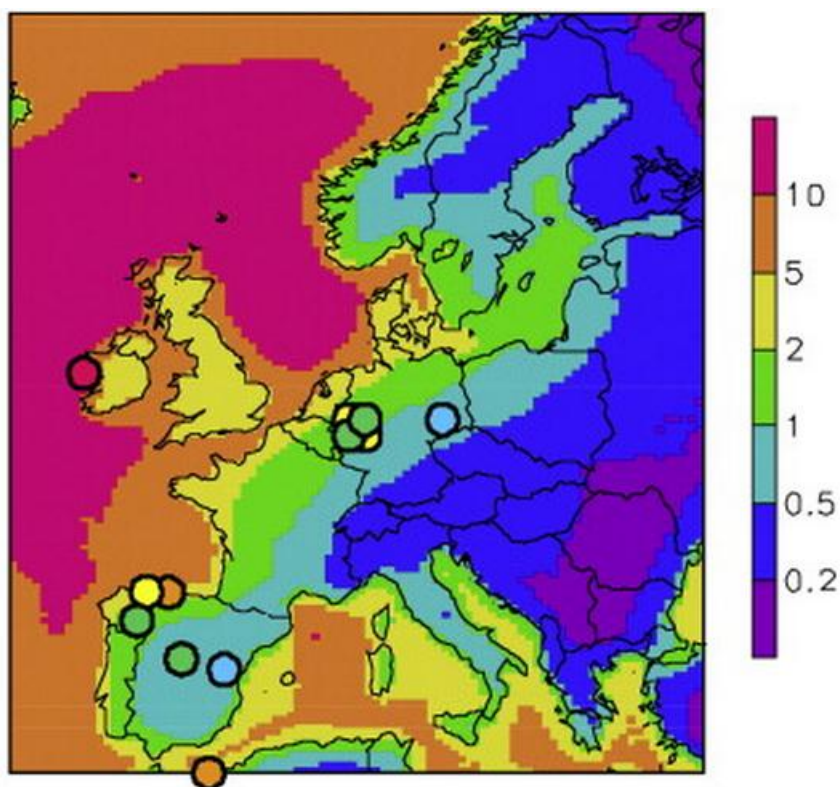
Figure 1. 4 The estimated annual average sea salt concentration ($\mu g\ m^{-3}$) across Europe for 2005. Filled circles indicate the concentration of sea salt (Manders et al., 2010)

The oxidation of biogenic and anthropogenic VOCs in the atmosphere followed by gas to particle conversion processes or the heterogeneous reactions of carbonyl result in the formation of Secondary Organic Aerosol (SOA), which accounts for a large fraction of

tropospheric aerosol (Kroll and Seinfeld, 2008). The oxidation processes of evaporated primary organic aerosols into the atmosphere may also lead to SOA formation (Xing et al., 2019). Low volatile compounds such as Aromatics (main components of vehicle emissions) and monoterpenes (biogenic emissions) are the most identified SOA precursors in urban and regional atmosphere (Kroll and Seinfeld, 2008, Vutukuru et al., 2006).

1.3 Chemistry of the troposphere

Emitted gases (trace gases) from both natural and anthropogenic sources may undergo a complex series of chemical and physical processes that eventually lead to their conversion into products that can be removed from the atmosphere via precipitation (rain and snow), or can be directly deposited onto the surface (Monks, 2005, Riedel and Lassey, 2008).

The OH radical acts as "detergent" as described by the Nobel Prize winner Paul Crutzen in cleansing the atmosphere from pollutants, for example non-methane hydrocarbons, as OH is highly reactive and can oxidize most of the atmospheric trace gases. Other radicals such as NO_3, and O_3 are less reactive than OH, but can also oxidize certain trace gases in the atmosphere into compounds that can be removed by precipitation and deposition as mentioned before (Riedel and Lassey 2008).

The atmospheric concentrations of oxidants such as OH and NO_3 are quite low, and as they are highly reactive molecules (particularly OH with concentrations typically of the order of 2×10^6 molecules cm^{-3}) with unpaired electrons in their outer orbitals which make them highly reactive with other chemical species (Riedel and Lassey, 2008; Monks, 2005). During the day NO_3 quickly photolysis to form NO or NO_2 (R1.32a and R1.32b). The concentration of NO_3 depends on NO_2 levels; high levels of NO at the surface results in the reduction of NO_3 concentrations due to NO reaction with NO_3, and at night NO_3 reaction with NO_2 to form N_2O_5 is the main removal pathway of NO_3 (Bannan et al., 2015).

The OH radicals can react with most VOCs (Monks, 2005), typically during day time when OH concentration is high and remove them from the atmosphere. The mechanism of OH reaction with saturated VOC (alkanes) proceeds via H-atom abstraction from C-H bond (less likely to O-H bond) (R1.6), while, with unsaturated compounds (C=C, aromatic

bond) such as alkenes and alkynes, the initiation reaction typically proceeds via H- atom addition to the carbon bond (R1.8). Under atmospheric conditions the products of OH reactions with VOC are quickly reacting with O_2 to form organic peroxy radicals (Brasseur et al., 1999).

$$OH + CH_3CH_3 \rightarrow CH_3CH_2 + H_2O \qquad\qquad R1.6$$

$$CH_3CH_2 + O_2 + M \rightarrow CH_3CH_2O_2 + M \qquad\qquad R1.7$$

$$OH + CH_2 = CH_2 + M \rightarrow HOCH_2 - CH_2 + M \qquad\qquad R1.8$$

$$HOCH_2 - CH_2 + O_2 + M \rightarrow HOCH_2 - CH_2O_2 + M \qquad\qquad R1.9$$
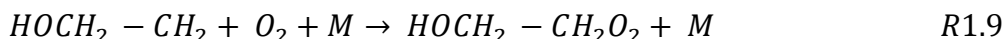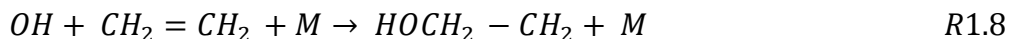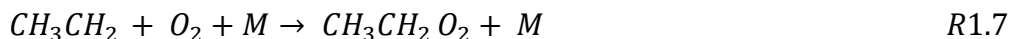
The oxidation of VOCs can also occur via their reactions with O_3, which are particularly important at night when OH reduced to their lowest levels. O_3 reactions with alkene result in the formation of a carbonyl species and Criegee biradical. The latter may decompose or stabilized by collisions (Brasseur et al., 1999):

$$O_3 + CH_2 = CH_2 \rightarrow CH_2O + (CH_2OO)^* \qquad\qquad R1.10$$

$$CH_2OO^* \rightarrow CO + H_2O \qquad\qquad R1.11a$$

$$\rightarrow CO_2 + H_2 \qquad\qquad R1.11b$$

$$\rightarrow 2H + CO_2 \qquad\qquad R1.11c$$

$$+ M \rightarrow CH_2OO + M \qquad\qquad R1.11d$$

Where the (*) denotes the excited biradical.

NO_3 radical is another important oxidant at night that oxidise VOCs mainly via addition of NO_3 to the double bonds (R1.12), and also via abstraction hydrogen atoms particularly from relatively weak $C - H$ bonds, such as in aldehydes (R1.13).

$$CH_2 = CH_2 + NO_3 + M + O_2 \rightarrow CH_2(ONO_2)CH_2O_2 + M \qquad\qquad R1.12$$

$$CH_3CHO + NO_3 + O_2 \rightarrow CH_3C(O)O_2 + HNO_3 \qquad\qquad R1.13$$
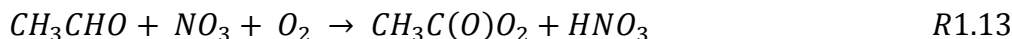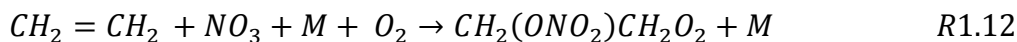
Chlorine atoms are highly reactive toward VOCs, with rate constants of factors of 10 to 200 larger than that for OH reactions with VOC (Riedel et al., 2014). The mechanism of Cl reactions with alkane proceeds via H- atom abstraction forming hydrochloric acid, HCl (R1.14), while with alkenes (e.g. ethene) the reactions proceed via Cl addition to the

double bonds forming chloro-carbonyl compounds (R1.15) (Atkinson and Aschmann, 1985, Wang and Finlayson Pitts, 2001):

$$Cl + RH + O_2 \rightarrow RO_2 + HCl \hspace{4cm} R1.14$$

$$Cl + CH_2 = CH_2 \rightarrow CH_2CH_2Cl \hspace{4cm} R1.15$$

1.3.1 Day-time chemistry

The OH radical in the free troposphere is primarily produced during daytime, from photolysis of O_3 in the presence of water vapour (H_2O) by ultraviolet light of wavelength < 310 nanometres (nm) (Monks, 2005):

$$O_3 + hv < 310nm \rightarrow O(^1D) + O_2 \hspace{3cm} R1.16$$
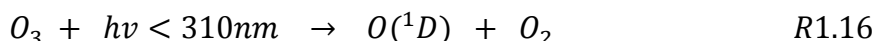
O_3 photolysis is the dominant source for the formation of electronically excited oxygen atoms $O(^1D)$ in the troposphere. The $O(^1D)$ can react with H_2O to form OH, or can react with other molecules, mainly O_2 or nitrogen (N_2), forming a ground state oxygen atom, $O(^3P)$, but with a smaller rate constant compared with interaction between $O(^1D)$ with H_2O. $O(^3P)$ further reacts with molecular oxygen producing tropospheric O_3:

$$O(^1D) + H_2O \rightarrow + 2OH \hspace{3cm} R1.17$$

$$O(^1D) + O_2 \rightarrow + O(^3P) + O_2 \hspace{3cm} R1.18$$

$$O(^1D) + N_2 \rightarrow + O(^3P) + N_2 \hspace{3cm} R1.19$$

$$O(^3P) + O_2 + M \rightarrow O_3 + M \hspace{3cm} R1.4$$
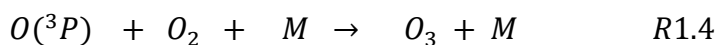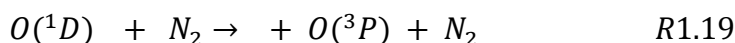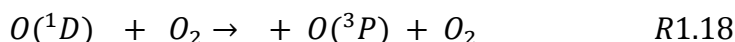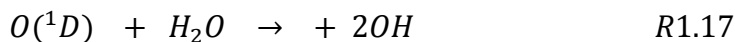
The OH production from O_3 photolysis is influenced by many factors such as humidity, pressure, temperature, and intensity of solar radiation. For example, OH concentrations are highest in tropical regions where humidity is high and solar zenith angle is small (Lelieveld et al., 2004). The fraction of $O(^1D)$ that generates OH is small, with most quenched to $O(^3P)$ via collisions with air molecules (O_2 and N_2) (R18 and R19) (Monks, 2005; Brasseur, 1999).

There are additional sources for OH formation which include the photolysis of nitrous acid (HONO), hydrogen peroxide (H_2O_2) and formaldehyde (HCHO), and the reaction of $O(^1D)$ with CH_4 (considered to be a small source) (Hewitt and Jackson, 2009; Brasseur, 1999).

The OH radical is ubiquitous throughout the troposphere due to the presence of O_3 and H_2O (Hewitt and Jackson, 2009). Furthermore, OH is highly reactive toward trace gases in the atmosphere so it has a very short lifetime of around a second (Monks 2005). Even though the OH concentrations are correspondingly highly variable, it has been accurately measured, typically in the range (1-5) x 10^6 molecules cm^3 in the boundary layer (Bloss et al., 2005c).

The OH radical reacts with many trace species in the troposphere to initiate a chain of reactions that recycle OH, forming peroxy and organic peroxy radicals (HO_2 and RO_2 respectively) and leading to the subsequent production of ozone. OH affects the lifetime of these species in the atmosphere (Solomon et al., 2007). The reaction of OH with either CO or CH_4 is the predominant chemistry in remote tropospheric environments (Monks, 2005):

$$OH \ + \ CO \ \rightarrow \ H \ + \ CO_2 \qquad\qquad R1.20$$

$$H \ + \ O_2 + \ M \ \rightarrow \ HO_2 \ + \ M \qquad\qquad R1.21$$

$$OH \ + \ CH_4 \ \rightarrow \ CH_3 \ + \ H_2O \qquad\qquad R1.22$$

$$CH_3 \ + \ O_2 + \ M \ \rightarrow \ CH_3O_2 \ + \ M \qquad\qquad R1.23$$
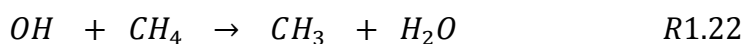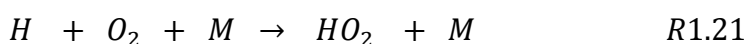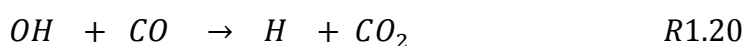
HO_2 has a short lifetime of about a minute in clean environments (less in a polluted area) might react with O_3 causing more O_3 loss or with another HO_2 forming hydrogen peroxide (H_2O_2). Alternatively, in polluted environments, HO_2 will predominantly react with NO to recycle OH and ultimately produce O_3 (Monks, 2005):

$$HO_2 \ + \ O_3 \ \rightarrow \ OH \ + \ 2O_2 \qquad\qquad R1.24$$

$$OH \ + \ O_3 \ \rightarrow \ HO_2 \ + \ O_2 \qquad\qquad R1.25 \qquad\qquad \text{Clean environment}$$

$$HO_2 + HO_2 + M \ \rightarrow \ H_2O_2 \ + \ O_2 \qquad\qquad R1.26$$

$$HO_2 + NO \ \rightarrow \ NO_2 \ + \ OH \qquad\qquad R1.27 \qquad\qquad \text{Polluted environment}$$

$$NO_2 + hv \ \rightarrow \ NO \ + \ O(^3P) \qquad\qquad R1.3$$
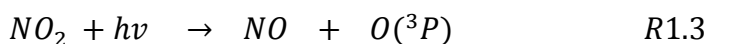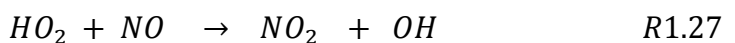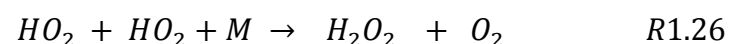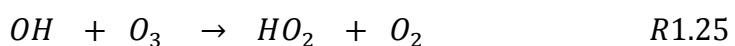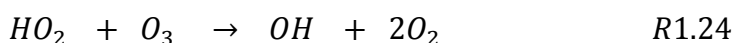
The organic peroxy radical (RO_2) such as methyl peroxy radicals (CH_3O_2) that are produced from the oxidation of CH_4 can be another sink for HO_2:

$$CH_3O_2 \; + \; HO_2 \quad \rightarrow \quad CH_3OOH \; + \; O_2 \qquad R1.28$$
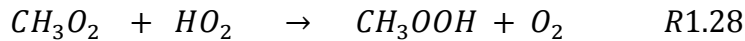
Conversely, in polluted environments, RO_2 mainly reacts with NO to form NO_2 (R1.21) which in turn rapidly undergoes photolysis at $\lambda \leq 420$ nm to yield a ground state oxygen atom $O(^3P)$ (R1.3). The latter further reacts with O_2 to form O_3 (R1.4). Thus, NO_x acts as a catalyst in O_3 production (Tang et al. 1998).

$$CH_3O_2 \; + \; NO \quad \rightarrow \quad NO_2 \; + \; CH_3O \qquad R1.29$$
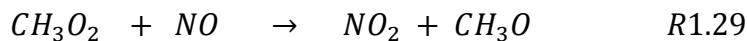
In urban areas where NO emissions are typically high (mainly from motor vehicles), NO reacts rapidly with O_3 to form NO_2 (R1.30). This reaction leads to O_3 reduction in urban areas. The photolytic lifetime of NO_2 is of the order of 100 seconds (Geyer, 2000).

$$NO \; + \; O_3 \; \rightarrow \; NO_2 \; + \; O_2 \qquad R1.30$$
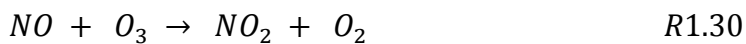
The three reactions (R1.3, R1.4, and R1.30) establish a null – cycle or a photochemical steady state (as described previously), which is the dominant chemistry in urban environments, that takes a few minutes or less to establish under typical mid-latitude boundary layer (Bloss, 2009).

In polluted, high NO_x conditions, the VOC oxidation and a photochemical steady state (PSS) cycles can be terminated when NO_2 reacts with OH yielding nitric acid (HNO_3), which is stable and can be efficiently removed from the atmosphere via dry or wet deposition.

From the above, it is clear that it is the combination of ozone and sunlight, leading to the formation of the hydroxyl radical, which oxidizes hydrocarbons and drives the daytime atmospheric chemistry. This oxidation results in conversion of NO to NO_2, forming O_3. At night there is no sunlight, hence the concentration of the OH radical falls. Instead, another chemistry mechanism dominates as explained in the following section.

1.3.2 Night-time chemistry

In 1979, the nitrate radical (NO_3) was first detected in a polluted region of the Los Angeles basin (Winer et al. 1980) and in a non-urban area, the Colorado Mountains (Noxon et al. 1980). Nonetheless, only in the last decade has the importance of this species and other nocturnal radicals such as dinitrogen pentoxide (N_2O_5) been fully recognized in terms of the effect of nocturnal chemistry on the next day's photochemistry and the role of heterogeneous reactions that occur during night-time (Brown and Stutz, 2012).

The nocturnal radicals, in particular NO_3 and N_2O_5 are important species in nighttime chemistry. The NO_3 radical is a reactive oxidizing agent in the troposphere (Wayne et al., 1991), as it has ability to react with a variety of unsaturated hydrocarbons and OVOCs, and hence affect their budgets in the atmosphere (Brown and Stutz, 2012). Moreover, nighttime chemistry has a noticeable impact on the formation of active radicals such as OH, HO_2 and RO_2 and on the budget of NO_x in the atmosphere (Brown and Stutz, 2012; Bloss, 2009). The reaction of NO_3 with isoprene and monoterpenes leads to the formation of secondary organic aerosols (SOA).

The reaction of NO_3 with VOCs, especially biogenic compounds such as isoprene, and monoterpenes, leads to the formation of SOA (Hoyle et al., 2011) via the addition of NO_3 to a double ($C = C$) bond forming RO_2 which this may further react with HO_2, NO_3, and RO_2, or isomerise to form SOA (Spittler et al., 2006, Kroll et al., 2006). Moreover, NO_3 can also react with aldehydes, and aerosol particles, in particular with soot, dust, and dry sodium salts, (Brown and Stutz 2012, Wayne 1991, Stutz et al. 2009).

More importantly, oxidation of VOCs by NO_3 leads to the formation of RO_2 at night (Platt et al. 1990). The RO_2 radicals can further undergo reactions with NO_3, NO, O_3 and other radicals forming many peroxides (Atkinson and Arey 2003). Finally, nighttime chemistry can also increase the production of ground level ozone during the following day (Osthoff et al., 2008).

Atmospheric chemistry during the daytime triggers the nighttime chemistry. Therefore, in a polluted, high NO_x region, most of the NO that is emitted mainly from traffic reacts rapidly with ozone to form NO_2 (R1.22) (in only a few minutes) (Wayne et al., 1991). With sunset, as photolysis slows, the NO_2 reaction with O_3 to form NO_3 becomes more efficient:

$$NO_2 \; + \; O_3 \quad \rightarrow \quad NO_3 + O_2 \qquad R1.31$$

This reaction (R1.31) is more significant when a high quantity of O_3 is present in the atmosphere (Mozurkewich and Calvert 1988). The time constant of this reaction is of the order of 15 hours at an ozone concentration of 30 ppbv and at 17 ℃ (290K) (Hewitt and Jackson 2009; Monks 2005). The rate of the reaction is strongly temperature dependent in which at 25 ℃ (298K), k = 3.2 x 10^{-17} cm^3 molecule^{-1} s^{-1}, however it slows down substantially at lower temperatures. For instance, at 0 ℃ (273K), k = 1.5 x 10^{-17} cm^3 molecule^{-1} s^{-1} (Sander et al. 2011; Brown and Stutz 2012), and the rate of NO_3 production is accordingly reduced.

Daytime concentrations of the NO_3 radical are low as it is efficiently photolysed by visible light (λ< 700 nm) to reproduce NO or NO_2 (Wayne et al., 1991, Brown and Stutz, 2012):

$$NO_3 \; + \; hv \; (< 700 \; nm) \; \rightarrow \; NO \; + \; O_2 \qquad R1.32a$$

$$+ \; hv \; (< 580 nm) \; \rightarrow \; NO_2 \; + \; O(^3P) \qquad R1.32b$$
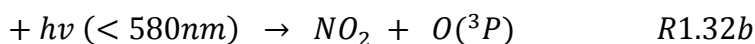
The photolysis frequency j(NO_3) for R1.32a ranges from 0.016-0.02 s^{-1} and j(NO_3) for R1.32b is 0.156- 0.19 s^{-1} (Johnston et al. 1996; Orlando et al. 1993). The lifetime of NO_3 is therefore extremely short, about 5 s in a clear sky and sunny day (Monks 2005).

Another fate of NO_3 is its reaction with NO which is significant near NO sources such as in urban areas where vehicle exhaust emissions are present in large quantities, and also near power plants (Brown and Stutz, 2012, Bloss, 2009):

$$NO_3 + NO \quad \rightarrow \quad 2NO_2 \qquad\qquad R1.33$$

According to Wayne (1991), the concentration of NO_3 depends heavily on temperature and the concentration of O_3, so NO_3 might exist in higher quantities when the concentration of O_3 is high which is typical during photochemical pollution episodes.

During the night-time, NO_3 radicals accumulate to levels that may range from a few ppt in a remote environment to several hundred ppt in polluted regions (Finlayson-Pitts et al. 1999) and reach an equilibrium with N_2O_5:

$$NO_2 \; + \; NO_3 \; + \; M \; \leftrightarrow \; N_2O_5 \; + \; M \qquad R1.34$$
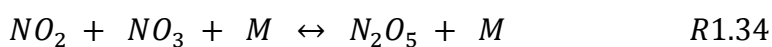
The formation of the NO_3 radical at night is always followed by the formation of dinitrogen pentoxide (N_2O_5). The latter is not stable; it decomposes efficiently back to NO_2

and NO_3 (Wayne et al., 1991; Brown and Stutz, 2012), with a lifetime with respect to thermal decomposition at 25 ºC (298 K) of about one minute (Bloss, 2009).

Formation of N_2O_5 at night has an important role in atmospheric chemistry as it influences the presence of NO_x and hence O_3 in the atmosphere for the subsequent day.

Formation of N_2O_5 represents an important sink for NO_x in the atmosphere, especially when it reacts with water forming HNO_3, which is stable and can be removed from the atmosphere by dry or wet deposition (Mozurkewich and Calvert 1988), or through the uptake of N_2O_5 on chloride containing aerosols forming nitrate chloride ($ClNO_2$) (Brown and Stutz 2012).

The hydrolysis of N_2O_5 on wet surfaces and other surface of atmospheric aerosol particles yielding two nitric acid molecules (HNO_3) also contribute to atmospheric acidification (Holloway and Wayne 2010):

$$N_2O_5 + H_2O_{(aerosol)} \rightarrow 2HNO_3 \qquad\qquad R1.35$$
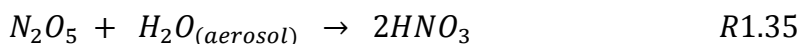
This heterogeneous reaction plays an important role in tropospheric chemistry as it efficiently removes NO_2 from the atmosphere; hence, less O_3 is produced on subsequent days (Stockwell et al. 2012). Over the last three decades, the significance of this reaction has been thoroughly studied. This thesis focuses on another important tropospheric night-time heterogeneous reaction of N_2O_5, and which leads to O_3 production, instead of depletion.

1.3.3 The uptake of N_2O_5 upon aerosol particles containing chloride

The heterogeneous reaction of N_2O_5 with aerosol particles can have a significant impact on air quality as this reaction leads to the formation of $ClNO_2$ and particulate nitrate in the atmosphere.
Laboratory studies by Tolbert et al. (1988) first reported that N_2O_5 reacts readily with HCl on ice surfaces, forming nitryl chloride at low temperature.

In a polluted environment a considerable amount of HCl can be released as a result of coal burning, which reacts with N_2O_5 to form $ClNO_2$ (Raff et al. 2009).

$$N_2O_5 + HCl_{(g\ or\ aq)} \rightarrow ClNO_{2(g)} + HNO_{3\ (g\ or\ aq)} \qquad R1.36$$

18
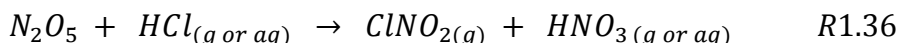
More importantly, N_2O_5 can heterogeneously react with sodium chloride (NaCl) or any chloride (Cl) containing particles to form $ClNO_2$, which may have a significant impact on air quality (Sodeau et al. 2000).

$$N_2O_5 + NaCl_{(aq)} \rightarrow ClNO_{2(g)} + NaNO_{3\,(aq)} \qquad R1.37$$
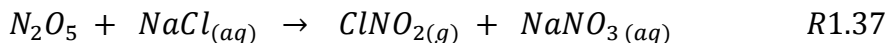
Osthoff et al. (2008), argued about the potential impact of $ClNO_2$ chemistry in the troposphere on air quality in regional and global scale.

Furthermore, significant nitrate particulate can be produced from the N_2O_5 heterogeneous reaction (for aerosol particle containing more nitrate particulate than chloride) in a rate comparable to that formed from the reaction of OH with NO_2 during the day (Geyer et al., 2001). The particulate nitrate (PNO_3^-) is a secondary inorganic aerosol, forms a significant fraction in both $PM_{2.5}$ and $PM_{(2.5-10)}$ which have been associated with an increase in mortality, visibility reduction , and climate change (Pope et al., 2009, Pan et al., 2016, Myhre et al, 2006).

1.3.4 Nitryl Chloride ($ClNO_2$)

In the troposphere, $ClNO_2$ can be formed and efficiently photodissociate at sunrise to yield NO_2 and a highly reactive Cl atom, but unlike stratosphere, here the produced Cl initiates the oxidation of VOCs and can enhance the formation of tropospheric O_3 (Mielke et al. 2011, Osthof et al. 2006). Furthermore, $ClNO_2$ acts as a reservoir for NO_x as it produces NO_2, which in turn undergoes photolysis during daytime to form more O_3 (Osthoff et al. 2008). This means that levels of NO_x increase (Brown et al. 2004).

The Cl atom released from $ClNO_2$ photolysis initiates VOCs oxidation to form RO_2. In polluted areas, RO_2 dominantly reacts with NO to form NO_2 and hence O_3 is produced as explained by the following general reactions:

$$ClNO_2 + h\nu < 839nm \rightarrow Cl + NO_2 \qquad R1.38 \text{ [(Atkinson et al., 2006a)]}$$

$$Cl + VOC \rightarrow RO_2 \qquad R1.39$$

$$RO_2 + NO \rightarrow NO_2 \qquad R1.40$$
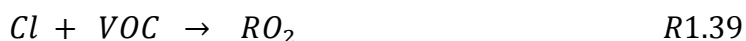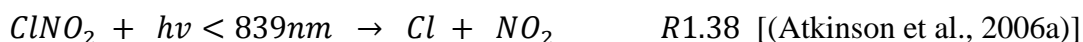
Through numerical modelling, it has been indicated that the Cl produced from $ClNO_2$ is sufficient to affect regional photochemistry (Osthoff et al. 2006). Moreover, $ClNO_2$ can recycle NO_x that would otherwise be removed from the gas phase.

While laboratory and chamber studies, such as the experiments by Finlayson-Pitts et al. (1989), Behnke et al., (1997), and Karlsson and Ljungstorm (1998) have detected $ClNO_2$ formation from reaction of N_2O_5 with NaCl or with HCl, no direct field measurements of $ClNO_2$ were made until 2006. Osthoff et al. (2008) reported the first direct measurement of this compound ($ClNO_2$) by using a chemical ionization mass spectrometer (CIMS) using iodide as a reagent ion at levels which exceeded all previous estimates (more than 1ppbv) in ambient air near Houston region, Texas (Figure 1.5). The authors provided evidence that the main source of $ClNO_2$ is the night-time reaction of N_2O_5 with chloride containing aerosol.
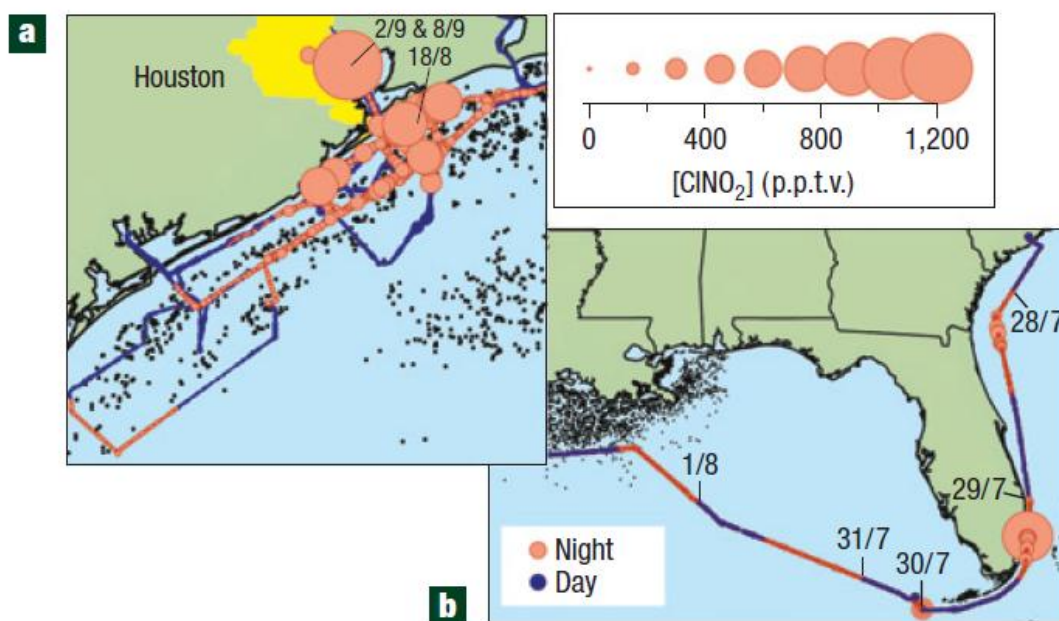
Figure 1. 5 Maps of study area showing measured $ClNO_2$. a) Houston, Texas has shown in yellow colour, and b) showing ship track along the United States southeast coastline. Red and blue circles indicate night and day time respectively, and the black dots indicate oil and natural gas platforms (Osthoff et al., 2008).

In February 2009, Thornton et al. (2010) carried out another study not in a marine but rather in a mid-continental urban environment near Boulder, Colorado in the middle of North America, a location 1400 km from the nearest coastline. The observed $ClNO_2$

mixing ratio consistently ranged from 100 - 450 pptv, corresponding to a third to a half value of that observed in polluted coastal areas of Texas (Thornton et al. 2010).

Similarly, in another mid-continental environment, Mielke et al. (2011) measured $ClNO_2$ via chemical ionization mass spectrometry (CIMS) in Calgary, Canada (a distance of 800 km from the open ocean) and confirmed the findings of Osthoff et al. (2008), showing that $ClNO_2$ can be generated via the reaction between N_2O_5 with chloride containing aerosol particles (R1.41). The maximum nocturnal mixing ratios of $ClNO_2$ reached 80-250 pptv.

$$N_2O_5 + Cl_{(aerosol)} \rightarrow ClNO_2 + PNO_3^- \qquad\qquad R1.41$$
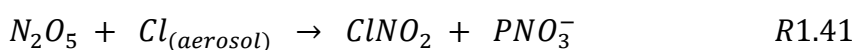
More observations and modelling studies have been conducted. Young et al. (2012) performed vertical measurements of $ClNO_2$ in Los Angeles and highlighted the even distribution of $ClNO_2$ in the lower layer with the ground surface considered as an important source. Kim et al. (2014) measured $ClNO_2$ at the ocean surface and emphasised the role of N_2O_5 uptake on aerosol particles in sustaining the high mixing ratio of $ClNO_2$ in the marine atmosphere.

Most early observations were undertaken in the USA and Canada, however, Phillips et al. (2012) reported the first study over continental Europe, specifically in Germany in a semi-rural area which is about 400 km from the nearest coastal region. The measured $ClNO_2$ in this study was also large, up to 800 pptv, which was observed over the majority of nights for one month (from 15th August – 16th September). The source of the $ClNO_2$ precursors was mainly sea salt and anthropogenic NO_x emissions.

In the UK, $ClNO_2$ was measured for the first time in an urban background area in North Kensington, London during the summer 2012 ClearfLo campaign, with a maximum mixing ratio of 724 ppt recorded (Bannan et al., 2015). In addition, Sommariva, et al., (2018) measured $ClNO_2$ in 2014-2016 at three different locations in the UK (Leicester, Penlee Point, and Weybourne) and in different seasons, and recorded maximum concentrations in winter, and they found sea salt to be the main source of chloride ions for locations 200 km away from the coast. In another study, Bannan et al. (2017) reported a $ClNO_2$ maxima of 65 ppt in spring 2013 in remote locations at the Weybourne Atmospheric Observatory on North Norfolk Coast, nearly 150 m from the shore in the UK, and Priestley et al. (2018) recorded 506 ppt in November 2014 in central Manchester.

$ClNO_2$ has become a subject of interest, thus, more measurement studies have been conducted in the last few years, mainly in the US, Canada, China, and Hong Kong such as

Riedel et al., (2012); Brown et al., (2013); Kercher et al., (2009); Mielke et al. (2013); Mielke et al. (2015); Wagner et al. (2013); Osthoff et al., (2018); Tham et al., (2014); Tham et al (2016); Wang et al., (2017); Liu et al., (2018); Zhou et al., (2018); Breton et al., (2018); Wang et al., (2016).

In a modelling study, Sarwar et al. (2014), found a substantial abundance of $ClNO_2$ (up to1ppb) from the heterogeneous chemistry of N_2O_5 on aerosol particles in many areas of the Northern Hemisphere, in particular over Western Europe and China. In this study, the Community Multiscale Air Quality model (CMAQ) was used, primarily to assess the impact of $ClNO_2$ formation on air quality. Two different air quality simulations were conducted for a period of two months in summer and two months in winter. The reaction of N_2O_5 uptake on aerosol particles and 25 gas phase reactions of chlorine with organic and inorganic species were incorporated into the model. A first simulation was performed in which the reaction of N_2O_5 on aerosol particles to produce HNO_3 only, while in a second simulation, the heterogeneous formation of $ClNO_2$ was also allowed to occur.

The results showed high production of $ClNO_2$ in the second simulation, especially during the winter as shown in Figure 1.6. In addition, the result illustrated the effect of $ClNO_2$ production on air quality through total nitrate reduction, enhancement of O_3 formation and increase in OH production, which enhances atmospheric oxidation capability and the formation of secondary pollutants.
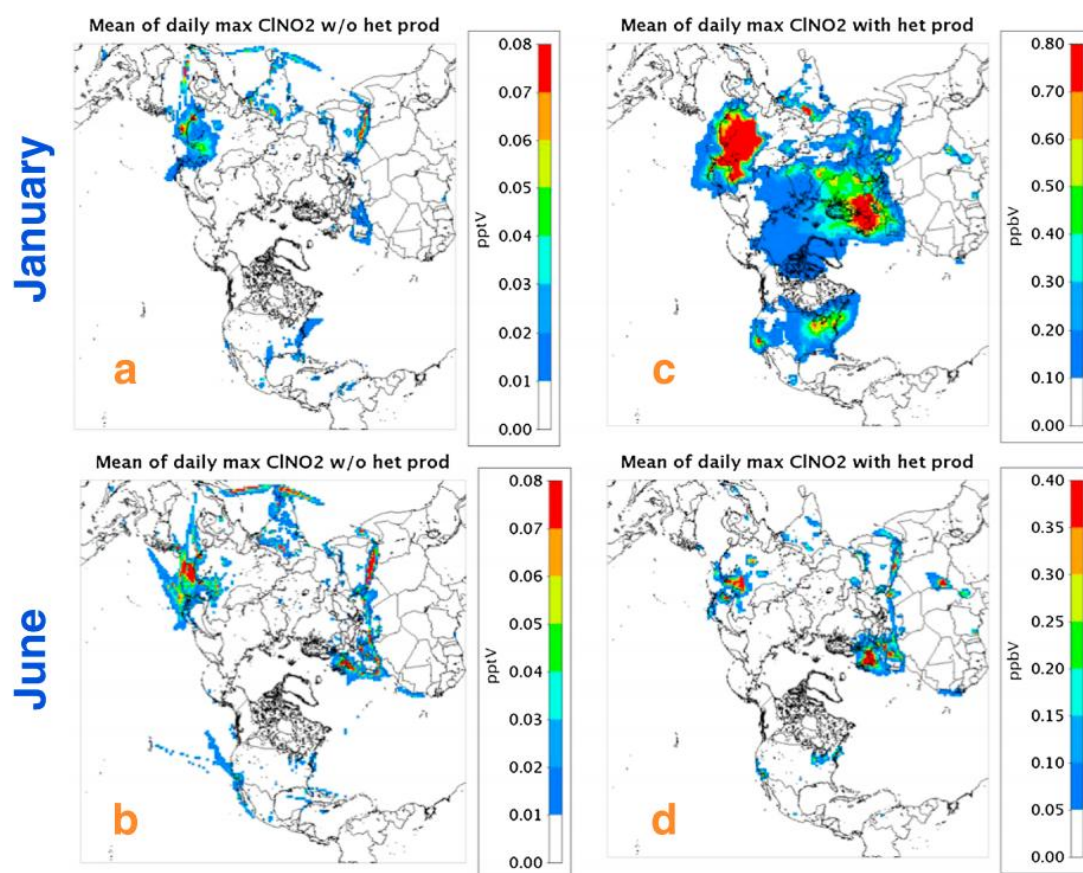
Figure 1. 6 Mean of ClNO$_2$ production (pptv) for (a) January and (b) June when the model run without (left) including the heterogeneous ClNO$_2$ production, and with (right) including the heterogeneous ClNO$_2$ production (ppbv) in (c) January and (d) June Sarwar et al. (2014).

A number of modelling studies on ClNO$_2$ formation and its impacts on air quality have been undertaken recently, such as Simon et al., (2009); Simon et al., (2010); Sarwar et al., (2012); Riedel et al., (2013); Xue et al., (2015); LI et al., (2016); Zhang et al., (2017); Liu et al., (2018); Li et al., (2018); and Yun et al., (2018).

All these studies showed that ClNO$_2$ in the boundary layer is primarily produced from uptake of N$_2$O$_5$ on aerosol containing chloride, whose source may be marine (sea salt) or anthropogenic; also, they illustrated many factors that might affect ClNO$_2$ production and its precursors such as:

- Water and chloride content within the particles (Behnke et al 1997; Sarwar et al. 2014),

- Environment and availability of nitrogen oxide (NO$_x$) (Thornton 2010)

- Temperature and season: Low temperatures of winter shift the $N_2O_5 - NO_3$ equilibrium to N_2O_5 and longer nights allow more N_2O_5 to accumulate, hence more $ClNO_2$ production is predicted (Sarwar et al. 2014).

1.3.5 Impact of ClNO$_2$ chemistry on photochemical ozone formation

As mentioned in the previous section, $ClNO_2$ influences the next day's photochemistry and enhances O_3 formation through its photodissociation to chlorine atoms and NO_2. The chlorine atoms are highly reactive with VOCs, with a rate coefficient (for some VOCs) nearly 200 times faster than that of OH (Breton et al., 2018). Moreover, as Cl peaks in the morning when OH concentrations are low, Cl atoms may be the dominant radicals in oxidizing VOCs at this time of day. The results of a modelling study by Bannan et al., (2015) emphasized the role of Cl atoms in oxidizing VOCs, particularly alkanes, alkenes, and alkynes in central London and confirmed the importance of considering Cl chemistry in determining VOC oxidation process.

The reaction of Cl with VOC can proceed via H atom abstraction by Cl or Cl addition to the double and triple carbon bonds or to the aromatic ring (Xue et al., 2015)

The general mechanism of reactions of Cl with VOC leading to the formation of alkyl and hence alkylperoxy radicals (via H atom abstraction) is given by Finlayson-Pitts (2003) (R1.42-R1.46):

$$Cl \ + \ R_1 CH \, R_2 \ \rightarrow \ HCl \ + \ R_1 \, C(H) \, R_2 \qquad\qquad R1.42$$

$$R_1 \, C(H) \, R_2 \ + \ O_2 \ \rightarrow \ R_1 \, C(H)(OO)R_2 \qquad\qquad R1.45$$
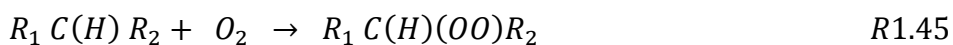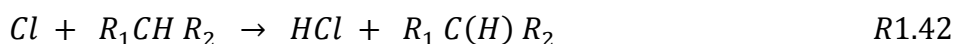
The radicals oxidize NO to NO_2. The latter undergoes photolysis to generate O_3:

$$R_1 \, C(H)(OO)R_2 \ + \ NO \ \rightarrow \ R_1 \, C(H)(O) \, R_2 + NO_2 \qquad\qquad R1.46$$
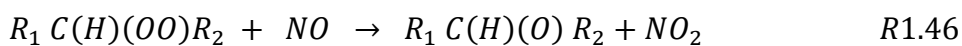
Where, R1 and R2 represent suitable alkyl groups

$$NO_2 + hv \ \rightarrow NO + O(^3P) \qquad\qquad R1.4$$

$$O(^3P) + O_2 + M \ \rightarrow O_3 + M \qquad\qquad R1.5$$

Riedel et al. (2014) showed that $ClNO_2$ has a significant influence on ozone, nitrogen oxide and other oxidants. For instance, including $ClNO_2$ in the Master Chemical

Mechanism (MCM) increased the production rate of RO_2 and hydrogen oxide radicals (HO_x = OH + HO_2) radicals in the morning by 2.2 times more than when the model excluded $ClNO_2$, thus more ozone was produced by ~200%. Zhang et al. (2017) simulated O_3 increases (up to 3.2%) from oxidation of VOC by Cl from $ClNO_2$ in China, using the WRF-Chem model. In a polluted environment in China, a 13% increase in O_3 specifically from $ClNO_2$ chemistry was observed in a box modelling study (Tham et al., 2016). In addition, Wang et al., (2016) in a box model study (MCM) observed 11-41% of O_3 increase from $ClNO_2$ in Hong Kong. In another MCM study, Xue et al., 2015 observed enhancements of O_3, RO_2, HO_2, and OH by 6.8, 120, 52.7, and 34.9% respectively due to $ClNO_2$ chemistry.

The impacts of $ClNO_2$ on O_3 vary according to the concentrations of $ClNO_2$. For instance, Osthoff et al. (2008) observed greatest photochemical ozone production from $ClNO_2$ chemistry near coastal urban areas (Houston) where VOCs exists at high concentration along with NO_x, sea salt and aerosol sources. Regarding the seasons, Sarwar et al. (2014) observed greater enhancement of O_3 by $ClNO_2$ chemistry in winter than in summer in the Northern Hemisphere, due to higher N_2O_5 abundance and thus $ClNO_2$ in winter than in summer.

1.4 Air pollution in urban areas

Air pollution on a local, regional, or global scale results from direct emissions of pollutants from natural and anthropogenic sources (industrial, road transport, and residential and commercial) into the atmosphere. Pollutants that are not emitted, such as O_3 are formed from chemical reactions involving primary emitted pollutants. Upon emission, the pollutants subject to dispersion, transport, chemical reactions, and removal from the atmosphere. All these processes affect the concentrations of pollutants as shown in Figure1.7. Some pollutants such as NO_2 and PM can be found in high concentrations at roadside locations in urban areas, and due to their direct effects on public health, legislation to limit their abundance have been established. In Europe, the Air Quality Directive and 4th Daughter Directive set limit values for PM_{10}, $PM_{2.5}$, NO_2, and O_3 that should not be exceeded as shown in Table 1.4.
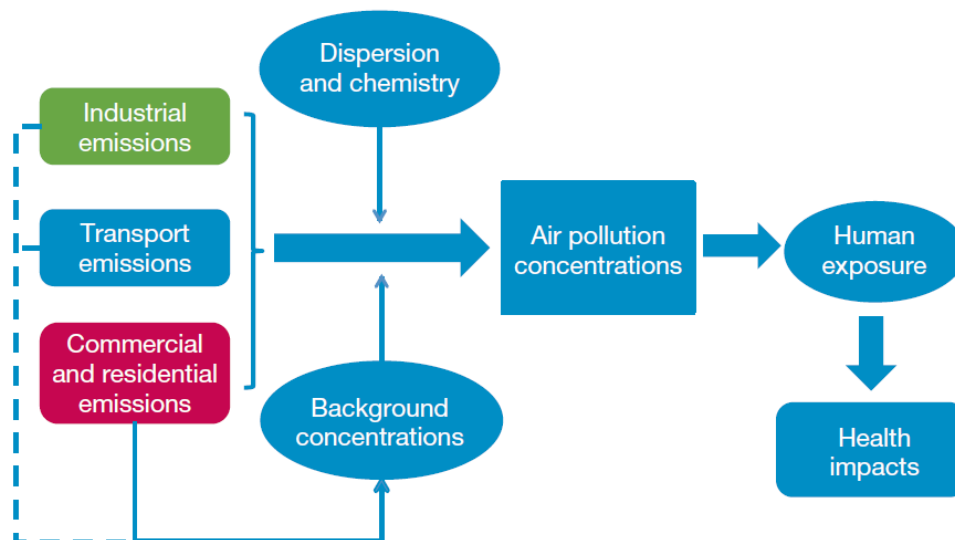
Figure 1. 7 Components of air pollution: sources, concentrations, and health impacts (Hitchcock et al., 2014).

Table 1. 4 Pollutant limit value as set by the EU Air Quality Directive. Adapted from European Commission (2008)

Pollutant	EU limit ($\mu g\ m^{-3}$)	Number of permitted exceedances each year
PM_{10}	40 (Annual mean)	n/a
	50 (24-hour mean)	35
$PM_{2.5}$	25 (Annual mean)	n/a
NO_2	40 (Annual mean)	n/a
	200 (Hourly mean)	18
O_3	120 (Daily 8-hour mean)	25 days (averaged over 3 years)

According to the Committee on the Medical Effects of Air Pollutants (COMEAP), for every $10\mu g\ m^{-3}$ increase in NO_2 concentrations, the rate of mortality increases by 2.5% (Defra, 2015; Hitchcock and Carslaw, 2016) The combined effects of NO_2 and PM on mortality has been estimated to result in 44,750 deaths annually (Hitchcock et al., 2014). In the UK transport is considered to be a major source of air pollution in urban areas, and

despite EU limit legislation, NO$_2$ concentrations in urban areas remain elevated (Hitchcock et al., 2014).

1.5 Modelling atmospheric chemistry

Atmospheric chemistry is the science that deals with the chemistry and meteorology factors that affect the composition of the atmosphere. Chemistry deals with the change in the concentrations of the atmospheric species, whereas, the dynamic process involves the transport and deposition of these species. Three approaches are available to study atmospheric chemistry, which are laboratory investigations, field measurements and numerical modelling. Laboratory studies explore and quantify kinetic and mechanistic parameters, while measurement data determine the actual composition of the atmosphere. Numerical modelling simulates atmospheric composition mathematically, from the emissions, chemical reactions, transport and removal processes of species, which can be used to predict their concentrations in any environment / point in time. There are zero, two, three-dimensional models according to spatial approach:

Zero- dimensional box models are the simplest kind of atmospheric model that consist of a single box of well mixed - air, and describe a detailed mechanism of the chemistry of the species in the atmosphere, but contains only a few meteorological parameters such as temperature, relative humidity, and atmospheric pressure. They do not consider dynamical processes, including transportation, dilution, and deposition. Therefore, this kind of model may not be ideal for predicting the long lived species that are highly affected by transport processes, instead other (two, three dimensional) models would be ideal.

1.5.1 The Master Chemical Mechanism

The Master Chemical Mechanism (MCM) describes detailed gas- phase chemical oxidation processes of methane and 142 primary emitted non-methane anthropogenic and biogenic VOCs in the troposphere including isoprene and monoterpenes ($\alpha - $ pinene, β-pinene, limonene). The MCM has been developed and updated by Jenkin et al., 1997; Jenkin et al., 2003; Saunders et al., 2003; Bloss et al., 2005; (Jenkin et al., 2012, Jenkin et

al., 2015a). The 142 VOCs were selected based on the speciation determined by the UK National Atmospheric Emissions Inventory (NAEI) (http://naei.beis.gov.uk/). The MCM performance has been evaluated using large, high quality dataset obtained from a set of outdoor smog-chamber experiments in the European Photoreactor (EUPHORE) (Bloss et al., 2005a), and data obtained from indoor chamber studies (Hynes et al., 2005), and from ambient field measurements.

The current version of the MCM (3.3.1) consists of 6700 chemical species and 17000 reactions, which is available free online at (http://mcm.leeds.ac.uk/MCM/help.htt). The kinetic data for the elementary chemical reactions of the VOC oxidation, such as rate coefficient, absorption cross sections, quantum yields, and photolysis rate that is utilised by the MCM were taken from published laboratory and experimental data, mostly from the International Union of Pure and Applied Chemistry (IUPAC) kinetics database (http://iupac.pole-ether.fr/) and Chemical Kinetics and Photochemical Data for Use in Atmospheric Studies (NASA) (Sander et al., 2015). However, kinetic data of a large number of unstudied chemical reactions have been estimated on the basis of analogy to the studied reactions of a smaller subset of similar chemical species, and by using structure-reactivity correlations (structure activity relationships – SARs) (Saunders et al., 2003, Bloss et al., 2005b, Pinho et al., 2006).

1.6 Research motivations and thesis outline

Many researchers have highlighted the impacts of $ClNO_2$ on air quality in coastal and marine environments worldwide (US, Europe, Asia). The literature also shows that $ClNO_2$ concentrations are higher in winter/spring than other seasons due to the reduction in N_2O_5 thermal decomposition at low temperatures. However, only a few measurement studies (Bannan et al., 2015; Bannan et al., 2018; Sommariva et al., 2018) have been carried out to detect and quantify $ClNO_2$ in the UK.

In addition, although the MCM explicitly describes the oxidation process of VOCs with OH, NO_3, and O_3 radicals, Cl radical reactions with inorganic and organic species have not been included except for alkane oxidation. Therefore, many researchers have developed chlorine chemical mechanisms to examine the influence of chlorine radicals, especially those released from $ClNO_2$, on O_3 increases in the atmosphere such as Tanaka et al. (2003); Sarwar et al. (2012); Riedel et al. (2014) and by Xue et al. (2015). These authors

also incorporated $ClNO_2$ formation (from the N_2O_5 heterogeneous reactions with aerosol particles) and loss chemistry into an MCM box model framework and aim to quantify the concentrations of $ClNO_2$ in a studied area. However, these studies did not explicitly investigate the effect of temperature on the formation of $ClNO_2$ concentration and hence its impact on air quality, nevertheless, this is significant influence, which needs to be explored, in particular with a potential future increase in global temperature.

In this thesis, an updated zero-dimensional box model based on the Master Chemical Mechanism (MCM) is applied to investigate the effect of temperature on the formation of $ClNO_2$ and its impacts on air quality in an urban area in the UK; mainly to predict the potential changes in $ClNO_2$ chemistry under future temperature increases due to climate change. In addition, the model is used to investigate the impact of emissions from traffic on air quality (focused on NO_2), and to assess the particulate nitrate formation from N_2O_5 heterogeneous reactions.

The principal stages and results of this work are described in this thesis as follows:

Chapter 2 introduces modelling approaches for the simulation of atmospheric chemistry, and the development and validation of a detailed mechanism for $ClNO_2$ production and impacts, based upon the MCM.

Chapter 3 describes the detailed heterogeneous chemistry of N_2O_5 reactions with aerosol particles and introduces a parameterisation for this.

Chapter 4 explores the impact of temperature on $ClNO_2$ formation and chemistry in current and future climates.

Chapter 5 investigates the effect of changing temporal NO_x emission distribution from traffic on air quality, focussing on NO_2. Accordingly, to assess the change in NO_2 concentration due to emission variations on the increase/decrease of mortality.

Chapter 6 investigates nitrate aerosol formation from N_2O_5 heterogeneous reaction first, and then assess the effects of changing temporal NO_x emission distribution and $ClNO_2$ chemistry on the concentration of nitrate aerosol.

Chapter 7 summarises the finding of this study, and the implications and the potential future works are discussed.

Chapter 2 Development of a numerical model mechanism for ClNO$_2$ formation

This chapter provides a general brief background on the atmospheric modelling technique by including different kinds of models, and describing different kinds of mechanisms. The main part of this chapter describes the modification and extension of the near explicit Master Chemical Mechanism to include sources of chlorine atoms (from photolysis of ClNO$_2$, Cl$_2$, HOCl, and ClONO$_2$) alongside incorporating inorganic and organic chlorine mechanism into a zero-dimensional box model.

The mechanism of ClNO$_2$ formation is not included, but described in Chapter 3.

2.1 Modelling tropospheric chemistry

Atmospheric modelling is used to describe the chemistry of the troposphere numerically, and to predict the concentration of pollutants in ambient air in past, present and future. Air pollution modelling can be used to identify the causes of air pollution in terms of emission sources and meteorological processes (Daly and Zannetti, 2007). Models are useful for policy makers aiming to reduce emissions, as the model can predict the consequences of changing emissions on the concentrations of pollutants (Derwent et al., 2010). In addition, modelling is not expensive compared to field measurements, and it can be used to predict pollutants in the future.

The results from atmospheric simulations must be evaluated for performance before applying a model to any study, which can be achieved by testing the results against ambient measurements or laboratory data.

There are several types of atmospheric model, categorised according to their domain size (the area that is simulated) which are microscale, mesoscale, regional, continental, and global model; and according to dimensionality (number of grid boxes), which are zero, one, two, and three-dimensional models as briefly explained below. The complexity of atmospheric models increases with dimensionality.

From complexity to simple (Figure 2.1):
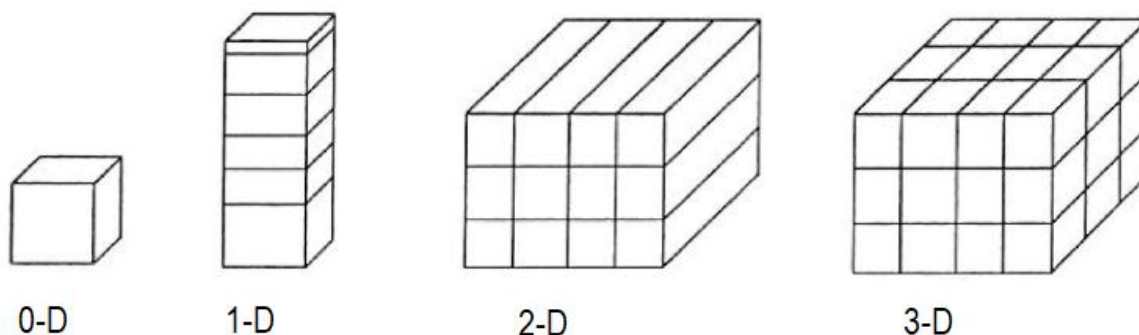
Figure 2. 1 Classifications of atmospheric model according to their dimensionality. Adapted from Seinfeld and Pandis (2012).

- **Three-dimensional (3-D) model**:

Considered as the most complex of the models, in which the concentrations of chemical species in 3-D models are simulated in three dimensions, i.e. vertically, horizontally, and attitudinally, and change with time. 3-D models are suitable for simulating atmospheric chemistry on a continental global scale.

- **Two-dimensional (2-D) model:** The chemical species in 2-D models are simulated in two dimensions, i.e. vertically and horizontally, and change with time. The model is suitable for simulating the global atmospheric chemistry, assuming that the concentrations of a chemical species are functions of latitude and altitude but do not depend on longitude (Seinfeld and Pandis, 1998).

- **One-dimensional (1-D) model:** Simulate chemical species in one dimension, i.e. vertically and change with time, but the concentrations do not vary horizontally (i.e. the concentrations are functions of height and time only).

- **Zero-dimensional (0-D) model: The 0-D model** is the simplest type of numerical models, which can be applied on a local or regional scale. This model normally consists of one box, by considering the modelled region as a single box.

There are two types of models that can predict changes in the chemical composition of an air parcel, which are Eulerian and Lagrangian models.

Eulerian models, also called grid cells, as the space domain (region) are divided into small boxes. In Eulerian models, the concentrations of chemical species are simulated in a fixed coordinate system, and there is transport (advection) of chemical species into or out of the box and also vertical mixing (the exchange of the air in the box with the air above the box). Example of Eulerian models is CALGRID, ARIA Regional model, and the Danish Eulerian Hemispheric Model (DEHM).

Lagrangian models, the box moves with the wind, allowing the exchange of air between the box and its surroundings. Examples of Lagrangian models are MOZART, STOCHEM, NAME, and Photochemical Trajectory Model.

Eulerian (0-D) box models, are the simplest models, in which the atmospheric domain is considered as a single box. The air in the box is assumed to be well mixed and the pollutant concentrations are homogeneous throughout the box, and vary with time only. Meaning that the pollutant emissions are evenly mixed with surrounding air (Collett and Oduyemi, 1997). The change in concentration of a chemical species with time ($\frac{dc}{dt}$) in the box is determined by:

- Emissions (Q): emissions of a chemical species per unit time (molecules s^{-1})

- Removal process (S): rate of deposition (molecules s^{-1})

- Transport (advection): transport of chemical species into and out of the box

- Chemistry: production rate of chemical species (molec cm^{-3} s^{-1})

- Ventilation: vertical exchange of air in the box with the air above the box (u)

- Background concentration (c_B)

A mass balance for the concentration of the chemical species (c), in the box of volume ($H\ dc\ dy$) is determined by the following equation (Seinfeld and Pandis, 1997):

Rate of change in concentration ($\frac{d(c\ dc\ dy\ h)}{dt}$) = emissions ($Q$) + production rate in the box volume ($R\ dc\ dy\ h$) − removal rate (S) + background concentrations and exchange

velocity due to advection as a function of mixing high and width of the box ($u\ h\ dy\ (c_B - c)$), mathematically expressed by:

$$\frac{d(c\ dc\ dy\ h)}{dt} = Q + R\ dx\ dy\ h - S + u\ h\ dy\ (c_B - c) \qquad\qquad Eq2.1$$

The removal rate due to deposition (S) can be presented by using the dry deposition velocity (vd) and the concentration (c) of the species:

$$S = v_d\ c \qquad\qquad Eq\ 2.2$$

Equation (Eq 2.1) can be simplified by dividing by $dc\ dy$:

$$\frac{dc}{dt} = \frac{Q}{h} + R - \frac{v_d}{h}\ c + \frac{u}{dx}\ (c_B - c) \qquad\qquad Eq2.3$$

If a vertical exchange of air is considered, the average speed of ventilation ($\acute{\omega}$) would be added to equation Eq 2.3:

$$\frac{dc}{dt} = \frac{Q}{h} + R - \frac{v_d}{h}\ c + \frac{u}{dx}\ (c_B - c) + \frac{\acute{\omega}}{h}\ (c_B - c) \qquad\qquad Eq\ 2.4$$

The ratio between the length of the box and advection can be used to determine the resident time (τ_r) of air over the area of the box (Eq 2.5):

$$\tau_r = \frac{dx}{u} \qquad\qquad Eq\ 2.5$$

2.2 Atmospheric chemical mechanism

Atmospheric chemistry is a branch of science involving elucidation of reactions of hundreds of chemical species under the influence of various physical and meteorological factors.

Gas phase chemical mechanism that describes degradation processes of emitted VOCs into the atmosphere and the consequent O_3 formation is an important component of atmospheric chemistry models.

Till now, many chemical mechanisms have been identified that mathematically describe the gas phase chemical processes of the primary emitted species from natural and anthropogenic sources. These chemical mechanisms consist of many different chemical

33

species, their chemical and photolysis reactions, together with rate constants, branching ratios and photochemical data derived from laboratory, simulation chamber and field measurements (Stockwell et al., 2012).

Most atmospheric chemical mechanisms explicitly describe the chemical reactions of inorganic species (NO, NO_2, O_3, OH, HO_2, and sulphur dioxide (SO_2)), which typically consist of around 45 reactions for about 20 species (Stockwell et al., 2012).

A comprehensive and explicit description of chemical reactions of all hydrocarbons emitted into the atmosphere in the atmosphere is yet to be developed as there would be millions of reactions, even of the known species (there will be many unknowns too) which is beyond the existing skills of scientists and computing infrastructure, especially for 3-D models (Stockwell et al., 2011). Therefore, these multi-step organic chemical reactions of a vast number of organic species are organised and simplified in a manageable and accurate form (Gery et al, 1989). Many mechanisms (near-explicit, surrogate, and aggregate) have been developed to describe the chemical processes of oxidation of VOCs that result in the formation of secondary pollutants like O_3. The differences between these mechanisms are in the organic representations, but they use similar or common kinetics data. Some types of chemical mechanisms are briefly described below:

- **The Carbon Bond Mechanism (CBM) Gery et al. (1988)**: Organic compounds are grouped based on the type of carbon bond: single, double, and carbonyl bonds. For example, PAR represents carbon single bond (alkane), OLE represents the double bond (alkene), and CAR represents the carbonyl group. This approach was initially considered as a success in predicting O_3 formation, as this mechanism can be easily implemented in air quality models, but now considered as "inappropriate" due to its grouping technique and simplicity in which few surrogate categories are used to represent each group consisting of many different types of chemical species (Gery et al., 1989).
- **The Regional Atmospheric Chemistry Mechanism (RACM)** (Stockwell et al., 1990, 1997): In this mechanism, the organic compounds of the same reactivity are lumped together to describe atmospheric chemical processes at the regional scale.
- **The Statewide Air Pollution Research Center** (SAPRC) (Carter, 1990): A detailed gas phase mechanism mainly designed for highly polluted urban

34

atmospheres. The latest version of this mechanism includes 119 species and 339 chemical reactions (Carter, 2010).

In surrogate mechanisms, the chemistry of a few selected hydrocarbons is explicitly described to represent the chemical processes of all organic species. The Empirical Kinetics Modelling Approach (EKMA), developed by Dimitrriades and Dodge, 1983), is an example of surrogate mechanisms. In the EKMA, the chemistry of less reactive alkane (butane) and more reactive alkene (propene) represent the chemistry of all organic species in the atmosphere.

There are some large chemical mechanisms which describe in detail chemistry of organic compounds in the atmosphere that are considered to be important, other reactions are assumed to have minor contributions and therefore have been neglected (Aumont et al., 2005). These mechanisms include NCAR (National Center for Atmospheric Research) Master Mechanism which comprise of 5000 oxidative reactions for 20 VOCs (Madronich and Calvert, 1990, Aumont et al., 2000), the SAPRC-99 (Statewide Air Pollution Research Center mechanisms that present the oxidation process of 400 primary emitted VOC (Carter, 2000), the Generator for Explicit Chemistry and Kinetics of Organics in the Atmosphere comprised of 350,000 species and 2 million chemical reactions (GECKO-A) (Aumont et al., 2005), and MCM (Master Chemical Mechanism) which includes more than 17,000 chemical reactions to describe the oxidation of 142 VOCs (Jenkin et al., 2015b).

The Master Chemical Mechanism (MCM) (Jenkin et al., 1997, 2003; Saunders et al., 2003): The MCM describes the detailed gas phase chemical degradation processes of a large number of primary emitted natural and anthropogenic VOC in the troposphere and the production of ozone and other secondary pollutants. The MCM has been evaluated against datasets obtained from chamber experiments and ambient field measurements, and the evaluations have shown that the MCM can reproduce the measured data well (Hynes et al., 2005, Stockwell et al., 2011).

The MCM has been continually updated to include more VOCs oxidation processes as summarised in Table 2.2.

The MCM has been simplified (so called near-explicit) to better understand complex interactions between the chemical species, and to reduce the computational cost of running it in a numerical atmospheric model, by implementing some strategies, such as limiting low probability reaction routes, simplifying the degradation process of less important

(minor) reaction products and parameterizing RO_2 self-reactions (Saunders et al., 2003). The near explicit MCM is however primarily implemented within 0-D box models that include simple dynamical processes, and cannot be used in complex model such as 3-D dynamical models. Therefore, a simplified mechanism such as the Common Representative Intermediates (CRI) mechanism (Jenkin et al., 2008) was developed as a subset of the MCM to present the degradation mechanism of the VOC and O_3 production.

Table 2. 1 A selection of chemical mechanisms

Mechanism	Type of development	Reactions	species	Referenes
Master Chemical Mechanism (MCM)	Near-explicit	17000	6700	Jenkin et al., 1997a
Common Representatives Intermediates (CRI)	Species lumped technique	570	250	Jenkin et al., 2008
Carbon Bond Mechanism (CBM)	Species lumped technique	82	33	Gery et al., 1988
Regional Atmospheric Chemistry Mechanism (RACM)	Species lumped technique	237	77	Stockwell et al., 1990
Statewide Air Pollution Research Center (SAPRC)	Chamber optimised	339	119	Carter, 1990
Empirical Kinetics Modelling Approach (EKMA)	species surrogated technique			Dimitriades and Ddge

Table 2. 2 Versions of the MCM

Mechanism	Reactions	species	VOC	Update
MCM v1	7000	2500	120	one biogenic species (isoprene)
MCM v2	10500	3500	123	Two biogenic species (isoprene, α-pinene)
MCM v3	12700	4400	125	Two biogenic species (isoprene, α and β-pinene)
MCM v3.1	13500	5600	135	Aromatic species
MCM v3.2	17000	6000	135	Biogenic species (β-caryophyllene)
MCM 3.3.1	17176	6700	142 and CH4	Isoprene chemistry updated to include 1926 reactions of 602 closed shell and free radical species

2.2.1 Mechanism reduction strategies

To amplify the size of a near explicit mechanism such as the MCM that can be used in complex atmospheric models like 3-D models, many techniques have been developed, mainly through (i) reduction of chemical species and reactions, (ii) or reduction via grouping of emissions in which the chemistry of one VOC is used to represent chemistry of a number of VOCs (Watson et al., 2008), and (iii) reduction via the use of surrogate species. The reduction of chemical species and reactions exclude redundant chemical species and reactions by using sensitivity tests (Heard et al., 1998). The redundant species can be identified through the investigation of the Jacobian system of which the effect of the change in the concentration of species on the rates of the reaction (with this species as a reactant) is identified. The redundant reactions can be identified through investigation of local rate sensitivities (Turanyi et al., 1989) to measure the effect of a perturbation in a rate parameter on the rate of production of important species (Whitehouse, et al., 2004).

Mechanism reduction can also be achieved through the identification of species that reacts very fast, which are assumed to be in equilibrium with slower species, where their rate of production and loss are nearly same. This method allows grouping species and reactions together, thus reducing the number of differential equations (Heard et al., 1998).

Furthermore, grouping of species with similar carbon bonds, reactivity, or molecular structure, whilst maintaining the explicit description of inorganic chemistry is another technique of mechanism reduction. Grouping of species may also be achieved via identification of surrogates in which a selected VOC is used to represent a number of VOC that have similar chemical reactivity and properties (Jacobson, 2005).

In Emissions lumping technique, selected anthropogenic VOCs are redistributed into suitable surrogate species with similar chemical properties of the redistributed VOCs within a number of VOC groups. This enables the redistributed VOCs to preserve the potential of O_3 formation by using the Photochemical Ozone Creation Potential (POCP) index as a standard (Watson et al., 2008). This method was used in the Common Representative Intermediates mechanism version 2 (CRI v2) to produce three reduced mechanisms (CRI v2-R1, CRI v2-R2, and CRI v2-R3). Further reduction in the number of representative VOCs in each VOC group was carried out by (Watson et al., 2008) that yielded two more mechanisms (CRI v2-R4 and CRI v2-R5). The CRI v2-R5 is the most

simplified mechanism that contains 19 NMVOCs to represent all anthropogenic species and is applied as a reference mechanism for global chemistry-transport models (Watson et al., 2008).

The Common Representative Intermediates mechanism (CRI) is a simplified mechanism that is developed as a subset of the MCM describing the O_3 formation from the degradation process of methane and 115 anthropogenic VOCs and biogenic VOCs including isoprene and monoterpenes (α- and β- pinene) (Jenkin et al., 2008). This reduction method was developed based on the number of NO to NO_2 conversions that occur during the VOC oxidation by OH and consequent intermediate oxidised products and radicals formation that result in O_3 formation. The amount of O_3 production is equivalent to the number of C-H and C-C bonds in the parent molecules. For example, methane reaction with OH radical leads to the formation of CO_2, four NO to NO_2 conversions occur, corresponding to the overall quantity of O_3 formation (4 molecules) and the number of reactive bonds. Based on this a single intermediate species can be used as a common representative for a group of intermediates and can be grouped together (Jenkin et al., 2008).

2.2.2 Protocol of the MCM

In the MCM, the degradation process of VOCs starts with oxidation of the primary emitted VOC by OH, NO_3, O_3, and Cl (with alkanes only), and by photolysis of the photoliable organic compounds forming intermediate products including RO and RO_2 radicals and Criegee intermediates, or the direct formation of oxygenated products (initiation reactions). These chemical reactions lead to the formation of several oxygenated products including carbonyls, hydroperoxides, peroxy acids, carboxylic acids, alkyl nitrate, PAN, and CO (Saunders et al., 2003).

The degradation process continues until CO_2, organic compounds, or radicals are produced, for which the subsequent chemistry is already represented in the MCM (Saunders et al., 2003). The description of the mechanism is illustrated in Figure 2.2.

Chemical kinetic data and the chemistry of the VOCs presented in the MCM are derived from the published laboratory and theoretical data, mainly from IUPAC Subcommittee on

Gas Kinetic Data Evaluation (Atkinson et al., 2001) and by the NASA/JPL Panel for Data Evaluation (DeMore et al., 1997, Sander et al., 2009). However, for the oxidation mechanisms of those compounds for which experimental kinetic data are unavailable, the rate constants can be predicted by applying structure-reactivity correlations (SARs), or by analogy with the studied reactions of a similar chemical species (Kwok and Atkinson, 1995).

In this study the near explicit MCM version 3.3.1 is extended to include some chemical process that needs it to fulfil the objectives of the study (section 2.4).
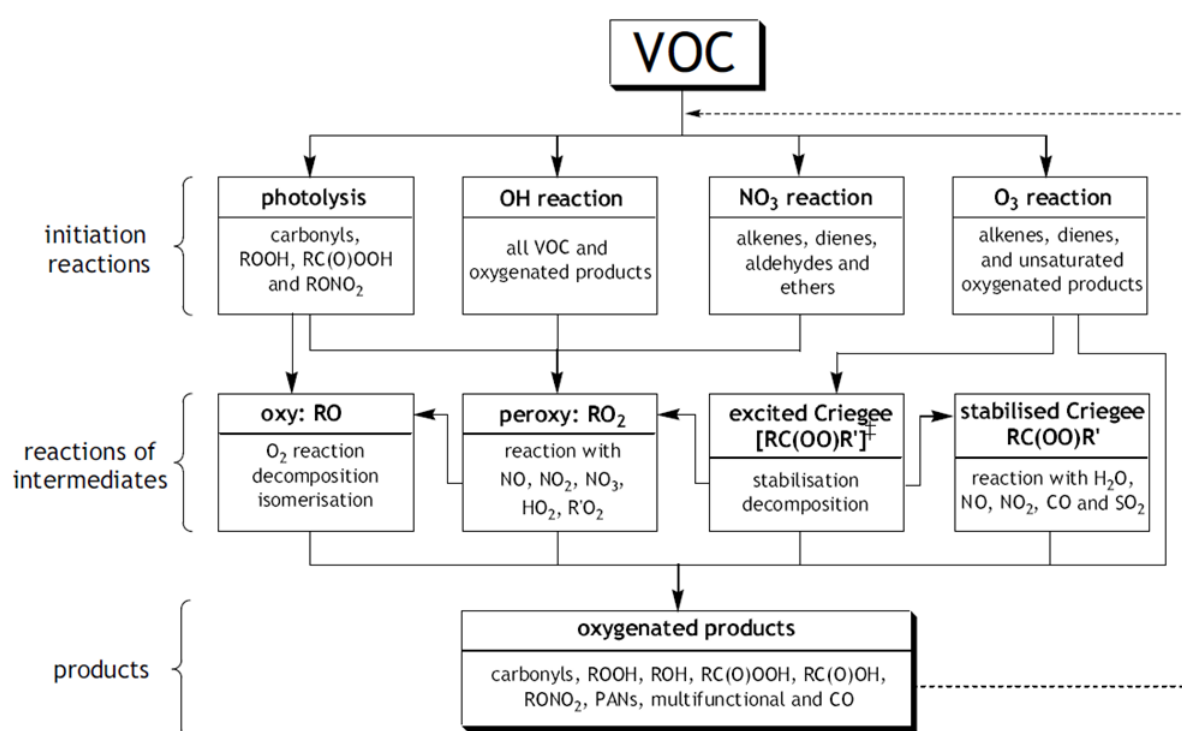
Figure 2.2 Flowchart describing the initiation, intermediate reactions, and product classes within the MCM protocol (Saunders et al., 2003)

2.3 Modelling approach

In this study, a 0-D box model was used to assess the $ClNO_2$ formation and its impact on air quality in an urban area in the UK (Chapter 4). The near explicit MCM is selected for this study as it describes the degradation of the individual VOCs in detail and it can be run within a 0-D box model. The same mechanism is updated to investigate the effect of diurnal emission distribution from traffic on the concentrations of NO_2 and a number of chemical species (Chapter 5), and to simulate nitrate aerosol formation in a rural and an urban area (Chapter 6).

2.3.1 Box model configuration

The air in the 0-D box model is assumed to be well mixed. Transport in and out of the box, dilution, ventilation, advection and background mixing is not included in the model. The chemical processes within the box model are the dominant processes for the chemical production and loss of species.

The main part of the box model is the chemical mechanism, which is a set of reactions describing the production and loss of chemical species in the troposphere. The chemical mechanism in the box model presented as a set of ordinary differential equations that determine the production and loss of each chemical species in the model. The concentration of a chemical species in chemical model can be determined by using differential equations, which calculate the rate of change in concentration of a species ($\frac{d[c_i]}{dt}$) as a function of the sum of all reactions that produce (P_i) and remove (L_i) a species (c_i):

$$\frac{d[c_i]}{dt} = P_i - L_i \quad i = 1,2,3, \dots \dots, N \qquad\qquad Eq\ 2.6$$

The concentration of a species c_i is calculated at time $t = t_n$, then at each time step: $t_{n+1} = t_n + \Delta t$ $\qquad\qquad Eq\ 2.7$

The production and loss terms are defined by the rate constant and the concentrations of the reactants:

$$P_i = \frac{d[c_i]}{dt} = k\,[C_i] \hspace{5cm} Eq\ 2.8$$

$$L_i = -\frac{d[c_i]}{dt} = -k\,[C_i] \hspace{5cm} Eq\ 2.9$$

In a chemical model there is one differential equation for each species (i), and N is the number of the species in the model. The rate constant may vary by several orders of magnitude as a function of time, which may result in lengthy processes in terms of computational times, and therefore stiffness may occur in chemical kinetic system.

To solve stiff differential equations numerically, software such as FACSIMILE can be used to calculate the concentration of a specious based on the concentration of the species from previous time step.

Applications of Facsimile include the chemical processes of OH and HO_2 in urban atmosphere, NO_x formation, and O_3 formation and destruction on a regional scale (Curtis and Sweetenham, 1987).

2.3.1.1 Photolysis reactions

In the MCM, the photolysis rates as a function of solar zenith angle (SZA) have been calculated for many compounds (inorganic, carbonyls, organic peroxides, and organic nitrates) using two stream (upward and downward photon flux) isotropic (transmitting light in all directions) scattering model that performed for clear sky conditions and at an altitude of 0.5 km (Saunders et al., 2003, Grenfell et al., 1999). In the MCM, the variation in photolysis rate coefficients j as a function of SZA has been described by the following format:

$$j_{s^{-1}} = l(cosSZA)^m \exp(-n.secSZA) \hspace{4cm} Eq2.10$$

Where, l, m, n are constant unique to each photolysis reaction (Jenkin et al., 1997, Wolfe et al., 2016). These parameters assigned for each reaction where absorption cross section and quantum yield were available. The latitude, longitude, and date were defined in order to calculate SZA as a function of solar declination.

Latitude and longitude of Leicester city, UK were defined in the box model and the date of the model simulation was set for August 1st, which started at 12:00 midnight (UTC). The physical parameters and chemical conditions that applied to the box model have been listed for each study.

For those species that photolysis rates are not included in the MCM, a scaling factor was used as explained in the following section (2.4.1).

2.4 MCM extension for modelling $ClNO_2$ chemistry

Despite detailed oxidation processes of 142 VOCs by OH, NO_3, and O_3 in the MCM (ve 3.3.1), there is a gap in the VOC oxidation processes initiated by Cl (except for alkanes). The sources of Cl are also not presented in the MCM. Herein, we extended the MCM scheme to include kinetics and reactions for Cl formation, and chemical reactions of Cl with inorganic and organic compounds.

2.4.1 Cl sources in the troposphere

A number of Cl potential sources in the troposphere have been recognised including OH reaction with hydrochloric acid (HCl), and photolysis of $ClNO_2$, chlorine (Cl_2), chlorine nitrate ($ClONO_2$), and hypochlorous acid (HOCl) (Riedel et al., 2014). Most of these sources are emitted from anthropogenic sources (Tanaka et al., 2003).

Maximum Cl produced from HCl reaction with OH occurs around midday when maximum OH produced from $O(^1D)$ reaction with H_2O (Riedel et al., 2014). Cl production from the photolysis of Cl_2 is important when direct emissions of Cl_2 are existing. The photolysis of $ClNO_2$ has been recognised as a dominant source of Cl in both continental and marine areas (Riedel et al., 2014).

The photolysis rates of these Cl sources are not included in the MCM, however, a number of researchers have calculated the photolysis rates of $ClNO_2$, Cl_2, HOCl, and $ClONO_2$ by using the Tropospheric Ultraviolet and Visible (TUV) Radiation Model (Madronich and

Flocke, 1999) (available at http://cprm.acd.ucar.edu/Models/TUV) and directly incorporated into the box model. While some studies used a scaling factor to calculate the photolysis frequencies of $ClNO_2$ ($jClNO_2$) in which the $j(ClNO_2)$ that calculated via the TUV model (Eq 2.11) was scaled to the photolysis rate of another species.

$$j = \int_{\lambda 1}^{\lambda 2} \sigma(\lambda)\,\theta(\lambda)\,l(\lambda)\,d\lambda \qquad\qquad Eq\ 2.11$$

Where, j (s^{-1}) is the rate of photolysis defined over all wavelength, λ (nm) and calculated for several different SZA, σ (cm^2 $molecule^{-1}$) is the absorption cross-section, θ is the quantum yield (molecules $photone^{-1}$), and l (photons cm^{-2} nm^{-1} s^{-1}) is the actinic flux (the intensity of solar flux). The data for the absorption cross section and quantum yield are available within the IUPAC database (Atkinson et al., 2006a). Table 2.4 shows sources of data for l and σ that used to calculate the photolysis rates of $ClNO_2$, Cl_2, $ClONO_2$, and HOCl in the model.

Table 2. 3 Methods applied in modelling studies to calculate photolysis rates of Cl sources. The actinic flux for most of the studies in the table were determined through using the TUV model (Eq 2.11). Bannan et al., (2015) measured the actinic flux by Metcon spectral radiometer.

Studies	Species	Approach
Tanaka et al. (2003)	$ClNO_2$, Cl_2, $ClONO_2$ and HOCl	J calculated via Eq 2.11, then scaled to jNO_2
Sarwar et al. (2012)	$ClNO_2$, Cl_2, and HOCl	J calculated via Eq 2.11, then scaled to jNO_2
Riedel et al. (2014)	$ClNO_2$ Cl_2, $ClONO_2$ and HOCl	Measured JNO_2 divided by 30 J calculated via Eq 2.11
Wang et al. (2016)	$ClNO_2$	scaled to measured jNO_2
Mielke et al. (2015)	$ClNO_2$	J calculated via Eq 2.11
Bannan et al. (2015)	$ClNO_2$, $ClONO_2$ and HOCl	J calculated via Eq 2.11, then scaled to jNO_2
Simon et al. (2009)	$ClNO_2$	J calculated via Eq 2.11, then scaled to jHCHO [$jClNO_2 = 10.05 \times jHCHO$]
Xue et al. (2015)	$ClNO_2$, Cl_2, $ClONO_2$ and HOCl	J calculated via Eq 2.11, then scaled to jNO_2

As shown in Table 2.3, most of previous studies scaled j(ClNO$_2$) (calculated from Eq 2.11) to measured or modelled j(NO$_2$), however, Simon et al. (2009), found that j(ClNO$_2$) better matched the photolysis rate of formaldehyde (j(HCHO)) in terms of the molecule's absorption cross section. In addition, both Riedel et al. (2014) and Simon et al. (2009) used a constant value (30 and 10.05) as a scaling factor to scale j(ClNO$_2$) to j(NO$_2$) and j(HCHO), respectively. Meaning that the constant values do not vary across all SZA, which may affect the accuracy of the diurnal variation in j(ClNO$_2$).

In this study the Cl sources that incorporated into the box model are photolysis reactions of ClNO$_2$, Cl$_2$, HOCl, ClONO$_2$, and OH reactions with HCl (R2.1-R2.5 and R2.14), as they are the most recognized Cl sources in the troposphere (Riedel et al., 2014, Xue et al., 2015).

$$ClNO_2 \quad + \quad hv \quad \rightarrow \quad Cl \quad + \quad NO_2 \qquad\qquad R2.1$$

$$HOCl \quad + \quad hv \quad \rightarrow \quad Cl \quad + \quad OH \qquad\qquad R2.2$$

$$Cl_2 \quad + \quad hv \quad \rightarrow \quad 2Cl \qquad\qquad R2.3$$

$$ClONO_2 \quad + \quad hv \quad \rightarrow \quad Cl \quad + \quad NO_3 \qquad\qquad R2.4$$

$$ClONO_2 \quad + \quad hv \quad \rightarrow \quad ClO \quad + \quad NO_2 \qquad\qquad R2.5$$
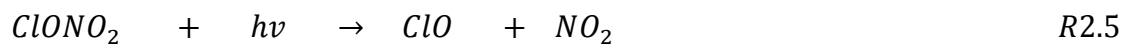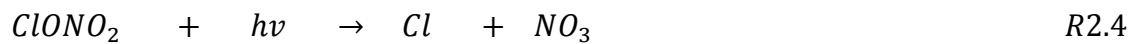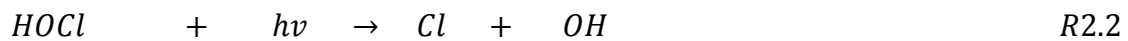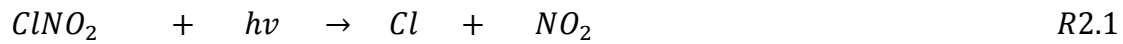
Here, the photolysis rate of ClNO$_2$ (j(ClNO$_2$)) is initially calculated by summing up the product of the actinic flux (I), the absorption cross section (σ), and the quantum yield (ϕ) for each wavelength (λ) at solar zenith angles (SZA) of 0, 10, 20, 30, 40, 50, 60, 70, and 86° via using equation Eq 2.11 (Table 2.5).

Table 2. 4 The sources of I and σ that used for the calculation of j(ClNO$_2$), j(Cl$_2$), j(CloNO$_2$), and j(HOCl)

Species	Species	References
ClNO$_2$	Φ σ	(Nelson and Johnston, 1981) (Ganske et al., 1992)
Cl$_2$	Φ σ	(Maric et al., 1993)
ClONO$_2$	Φ σ	(Goldfarb et al., 1997) (Burkholder et al., 1994)
HOCl	Φ σ	(Molina et al., 1980) (Barnes et al., 1998)

The actinic flux is determined via the (TUV) calculator (Madronich and Flocke, 1999) for several solar zenith angles (as mentioned above) under a standard condition of 300 Dobson units for ozone column, surface albedo of 0.1 and zero altitude with clear sky condition. The values of σ and ø for ClNO$_2$ are derived from Atkinson et al. (2006a).

The j(NO$_2$) and j(HCHO) are calculated from the TUV for those SZA mentioned above to identify the photolysis frequency that has the relatively similar wavelength spectrum to ClNO$_2$ across the different solar zenith angles. The calculated j(ClNO$_2$) j(NO$_2$), and j(HCHO) were normalised to their maximum value (at SZA=0) and compared with each other (Figure 2.3). The result shows that HCHO has a similar photolysis frequency variation with solar zenith angles (SZA) as ClNO$_2$, whereas NO$_2$ was different across most SZAs. Furthermore, the Action Spectra (absorption cross section * quantum yield) against wavelength is plotted for ClNO$_2$, NO$_2$, and two channels of HCHO photolysis reactions (R2.6a and b) demonstrate ClNO$_2$ and HCHO (particularly R2.6b) are well matched for Action Spectra across all wavelengths (Figure 2.4). The data for absorption cross section and quantum yield were derived from Sander (2011).

$$HCHO \ + \ hv \ \rightarrow \ H \ + \ HCO \qquad\qquad R2.6a$$

$$\rightarrow \ H_2 \ + \ CO \qquad\qquad R2.6b$$
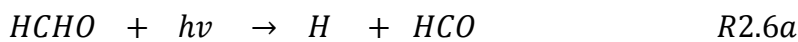
Therefore, j(ClNO$_2$) is scaled to j(HCHO) ((j(ClNO$_2$)/j(HCHO)). Then this ratio is used to define the scaling factor across several zenith angles. The scaling factor (Y) was determined from the j(ClNO$_2$)/j(HCHO) variability with SZA as shown in Figure 2.5, and incorporated into the model as Eq 2.12 to determine j(ClNO$_2$). Figure 2.6 demonstrates the modelled j(ClNO$_2$) for the 6 days of the model run period.

$$j(ClNO_2) = Y \times j(HCHO) \qquad Eq\ 2.12.$$
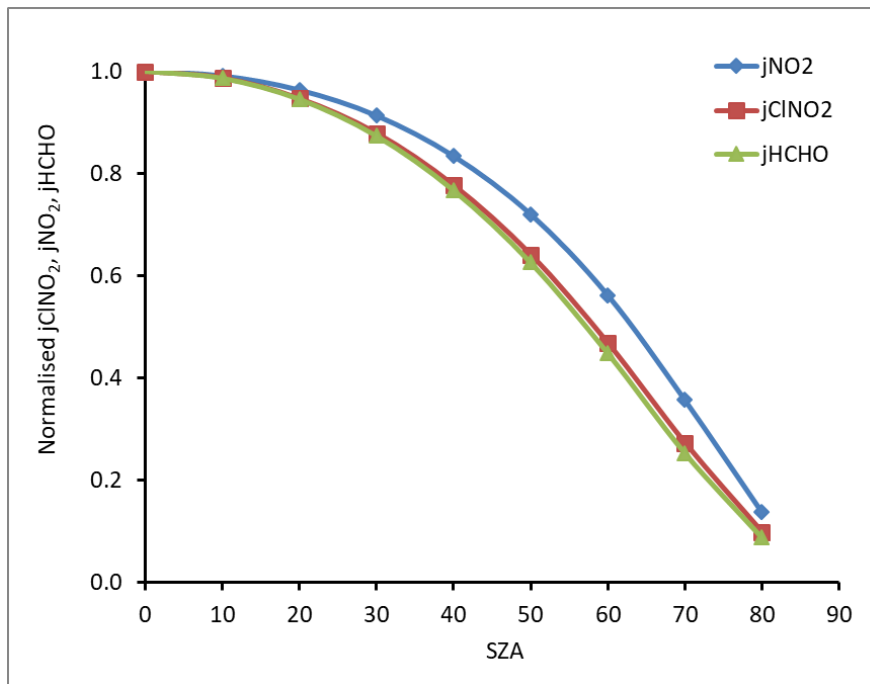
Figure 2. 3 Photolysis rates of ClNO$_2$ (red line), NO$_2$ (blue line) and HCHO (green line) as a function of SZA. The photolysis rates have been normalised to their maximum value at SZA=0.
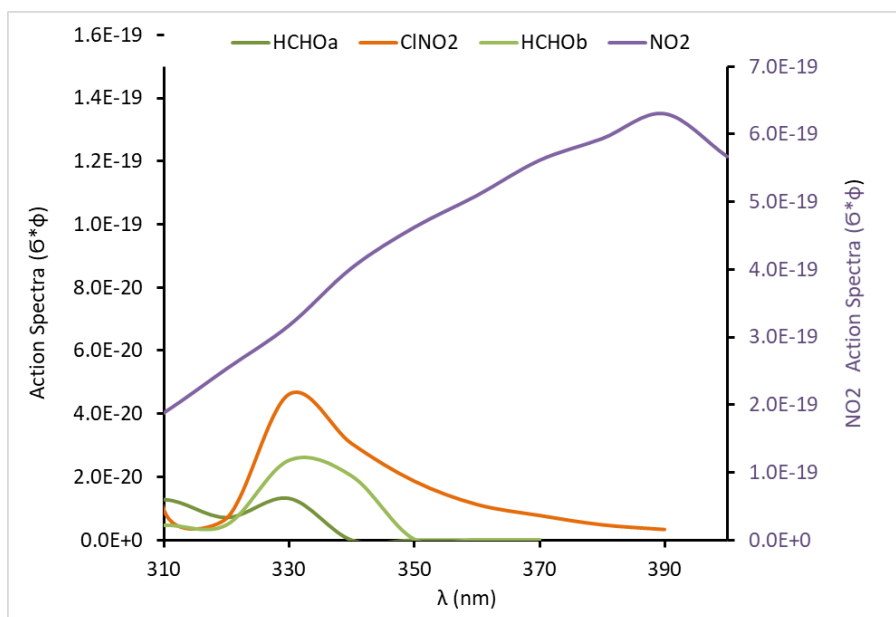
Figure 2. 4 Illustrates the Action Spectra ($\sigma * \phi$) via wavelength (λ for NO_2 photolysis (Right), and $ClNO_2$, HCHO (both channels) photolysis (Left).

$$y = 4.21216E\text{-}06x^3 - 1.33605E\text{-}04x^2 + 2.55911E\text{-}03x + 1.23423E\text{+}01$$
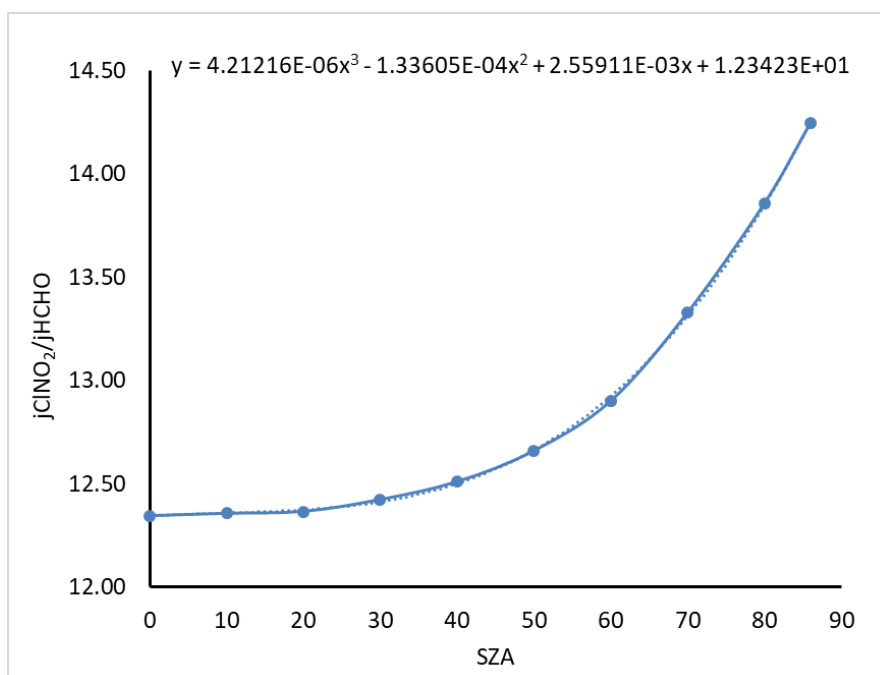
Figure 2. 5 Determination of the scaling factor (Y) factor from the ratio of $j(ClNO_2)$ to $j(HCHO)$ as a function of SZA.
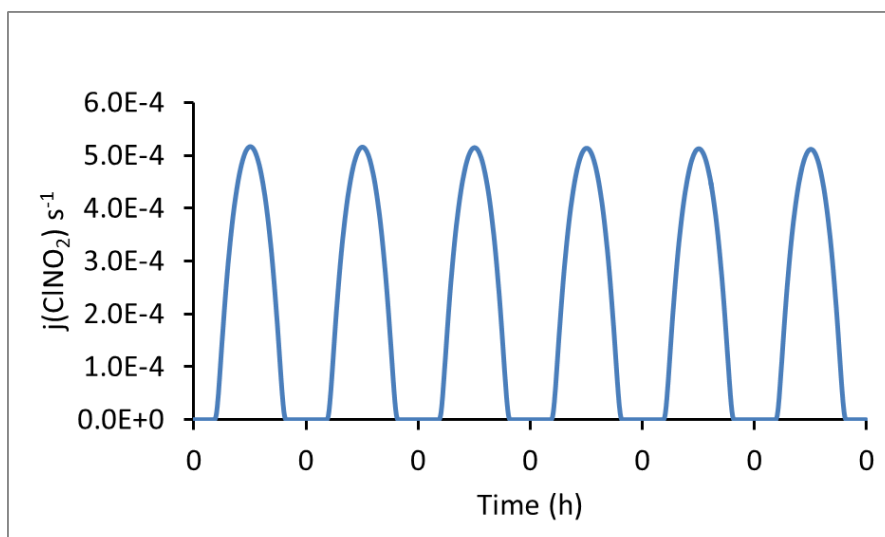
Figure 2. 6 Modelled j(ClNO$_2$) for 6 days of the model run, calculated for clear sky, under slandered atmospheric condition of 300 Dobson units for ozone column, surface albedo of 0.1 and zero altitude

This method of determining j(ClNO$_2$) is more accurate than methods used in previous studies (Riedel et al. 2014; Simon et al. 2009) as the scaling factor is not constant but varies throughout the day, which decreases errors that may possess in scaling j(ClNO$_2$) to j(HCHO). The difference between the scaling factor calculated for this study and that used by Simon et al., (2009) is shown in Figure 2.7, in which the difference between the two factors considerably increases from SZA 70 to reach more than 4 factors at SZA 86°.

$$y = 4.21216E\text{-}06x^3 - 1.33605E\text{-}04x^2 + 2.55911E\text{-}03x + 1.23423E\text{+}01$$
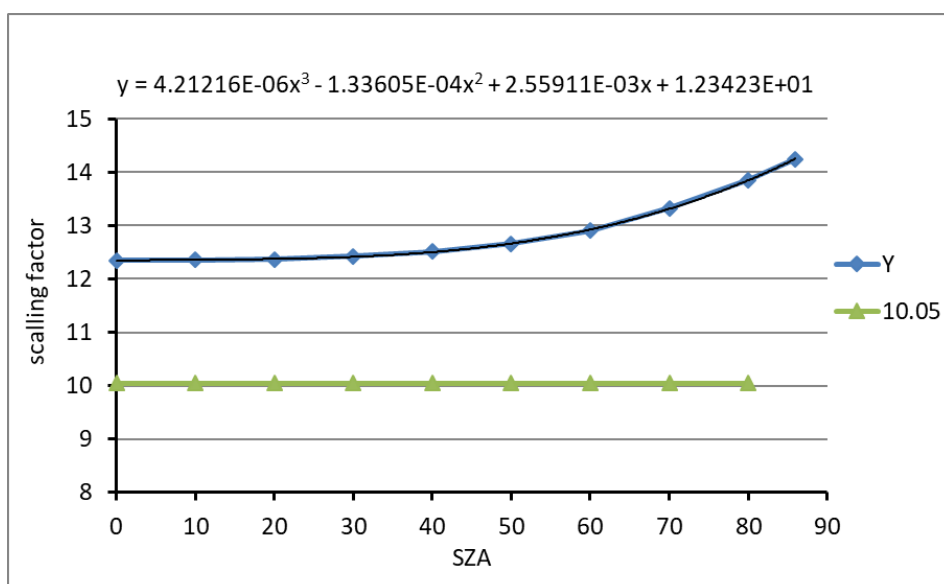
Figure 2. 7 Comparison between the scaling factors (Y) calculated in this study and the factor (10.05) that used by Simon et al. (2009). The blue line represents Y and the green line represents 10.05.

48

Table 2. 5 Photolysis rates from TUV model calculated at 12:00 UTC on August, 1st, 2014 for Latitude (52o.62 N), and Longitude (-1o.12 W), 0.1 albedo, ozone column of 300 Dobson units, and zero altitude

SZA	jHCHO [TUV]	jNO$_2$ [TUV]	$jClNO_2 = \int_{\lambda1}^{\lambda2} I(\lambda)\sigma(\lambda)\emptyset(\lambda)d\lambda$
0	5.01E-05	9.78E-03	6.19E-04
10	4.95E-05	9.69E-03	6.11E-04
20	4.74E-05	9.42E-03	5.86E-04
30	4.38E-05	8.93E-03	5.44E-04
40	3.85E-05	8.16E-03	4.81E-04
50	3.14E-05	7.04E-03	3.97E-04
60	2.25E-05	5.50E-03	2.90E-04
70	1.27E-05	3.49E-03	1.69E-04
80	4.40E-06	1.35E-03	6.09E-05
86	1.43E-06	4.52E-04	2.03E-05

The photolysis rates of chlorine (j(Cl$_2$)), chlorine nitrate (j(ClONO$_2$)), and hypochlorous acid (j(HOCl)) are calculated in the same way as for j(ClNO$_2$). Their photolysis rates are initially calculated by Eq 11, and then scaled to the photolysis rate of NO$_2$, rather than j(HCHO) because they have nearly similar absorption spectrum as a function of wavelength across different SZA as NO$_2$ (Tanaka et al. (2003). The ratio, j(X)/j(NO$_2$), was plotted for different SZA, and from the polynomial equation as shown in Figure 2.8, the scaling factor (Y) used to determine the photolysis rate, as listed in Table 2.6.

The approach of using a scaling factor to estimate the photolysis rates is quite reasonable because this scaling method simplifies the execution and reduces the number of mathematical calculations within the model (Tanaka et al. 2003; Simon et al. 2009).
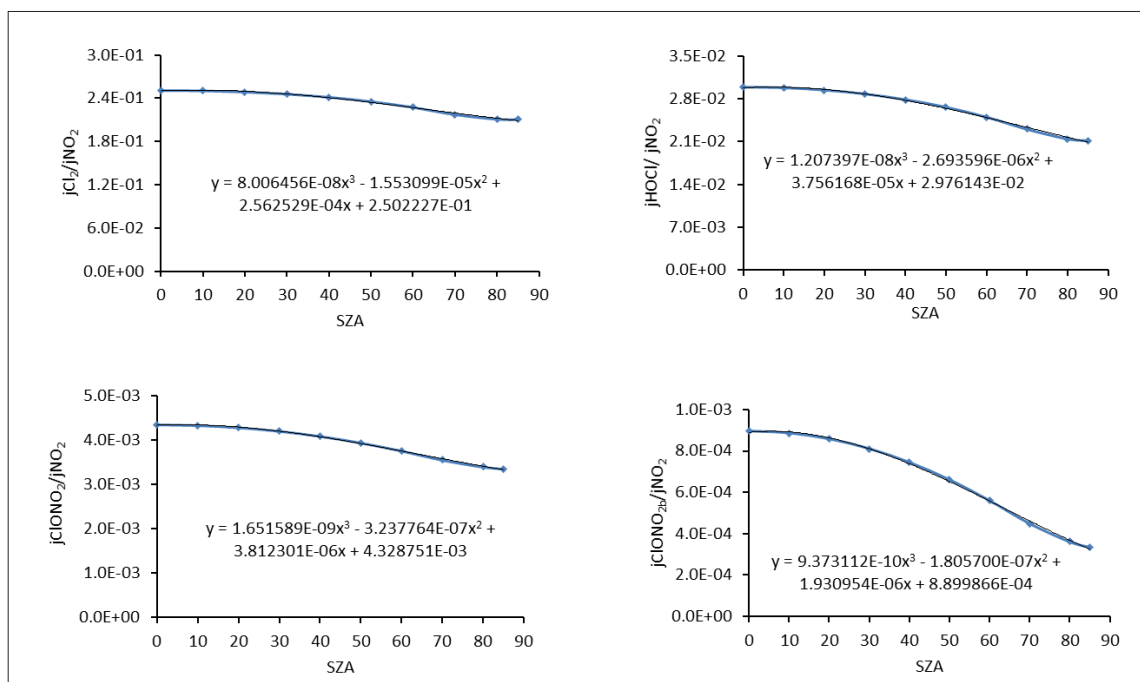
Figure 2. 8 Illustrates calculation of the photolysis rates of $ClONO_2$, Cl_2, and HOCl as a function of SZA

Table 2. 6 Photolysis reactions presented in the model

Reaction No.	Photochemical reactions	Photolysis rate (j)	Sources
1	$ClNO_2 + hv = Cl + NO_2$	$Y_1 \ x \ jHCHO$	This study
2	$Cl_2 + hv = 2Cl$	$Y_2 \ x \ jNO_2$	This study
3	$HOCl + hv = OH + Cl$	$Y_3 \ x \ jNO_2$	This study
4	$ClONO_2 + hv = NO_3 + Cl$	$Y_4 \ x \ jNO_2$	This study
5	$ClONO_{2b} + hv = NO_2 + ClO$	$Y_5 \ x \ jNO_2$	This study

2.4.2 Cl reaction with inorganic compounds

Many researchers have previously developed chlorine mechanisms (Cl reactions with inorganic and organic compounds) which are not presented in the MCM, mainly to assess chlorine formation or to quantify the effect of chlorine on O_3 formations or loss (Tanaka

et al., 2003, Sarwar et al., 2012, Riedel et al., 2014, Faxon et al., 2015, Bannan et al., 2015, Xue et al., 2015, Zhang et al., 2017).

In this study, 15 inorganic Cl reactions (R2.7- R2.21) are incorporated into the model. These reactions are selected based on those previous studies that mentioned above as they thought that these selected reactions might be important in the troposphere. The Cl reaction with O_3 (R2.7) is believed to be the major source of monochloride (ClO) formation in the troposphere, which might be a dominant reaction specifically in the afternoon when the concentrations of the VOC are normally in lower levels (Riedel et al., 2014, Wofsy and McElroy, 1974). In polluted urban areas, the ClO will predominantly react with NO to from NO_2 and recycle Cl into the system (R2.16) (Badia et al., 2017, Wofsy and McElroy, 1974, Saiz-Lopez and von Glasow, 2012).

ClO_x (Cl + ClO) reactions with HO_x (OH + HO_2) (R2.8, 2.9, 2.17, 2.18, 2.19) can modify HO_2/OH ratio and the HO_x balance may be shifted to OH, in which Cl atoms are not recycled with the oxidation cycle (Faxon et al., 2015, Saiz-Lopez and von Glasow, 2012).

$ClONO_2$ formation (R2.20) has been included in the previous modelling studies (and this study) because it was predicted that 23-33% of Cl reaction with O_3 forming ClO (R2.7) in the troposphere can lead to $ClONO_2$ formation (Riedel et al., 2014). Furthermore $ClONO_2$ decomposition reaction is also included in the model, as excluding this reaction in the model simulation led to an overprediction of Cl concentrations. Moreover, Tanaka et al. (2003) found that the omission of $ClONO_2$ formation and loss in their box model simulation study led to an overprediction of O_3 productivity.

The rate constants for the 15 inorganic reactions are mostly derived from Sander et al. (2009) and Atkinson et al. (2006b).

$$Cl \quad + \quad O_3 \qquad \rightarrow \quad ClO \quad + \quad O_2 \qquad\qquad R2.7$$

$$Cl \quad + \quad HO_2 \qquad \rightarrow \quad HCl \quad + \quad O_2 \qquad\qquad R2.8$$

$$Cl \quad + \quad HO_2 \qquad \rightarrow \quad ClO \quad + \quad OH \qquad\qquad R2.9$$

$$Cl \quad + \quad H_2O_2 \qquad \rightarrow \quad HCl \quad + \quad HO_2 \qquad\qquad R2.10$$

$$Cl \quad + \quad NO_3 \qquad \rightarrow \quad NO_2 \quad + \quad ClO \qquad\qquad R2.11$$

$$Cl + ClONO_2 \rightarrow Cl_2 + NO_3 \qquad R2.12$$

$$OH + HOCl \rightarrow ClO + H_2O \qquad R2.13$$

$$OH + Cl_2 \rightarrow HOCl + Cl \qquad R2.14$$

$$OH + HCl \rightarrow Cl + H_2O \qquad R2.15$$

$$ClO + NO \rightarrow Cl + NO_2 \qquad R2.16$$

$$ClO + HO_2 \rightarrow HOCl + O_2 \qquad R2.17$$

$$ClO + OH \rightarrow Cl + HO_2 \qquad R2.18$$

$$ClO + OH \rightarrow HCl + O_2 \qquad R2.19$$

$$ClO + NO_2 + M \rightarrow ClONO_2 + M \qquad R2.20$$

$$ClONO_2 + M \rightleftarrows ClO + NO_2 + M \qquad R2.21$$
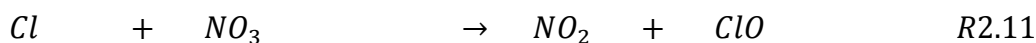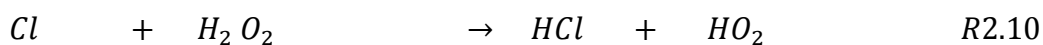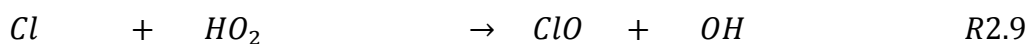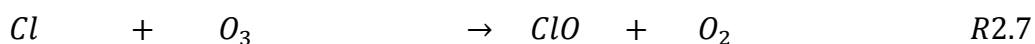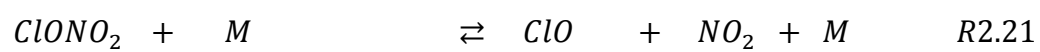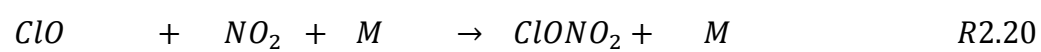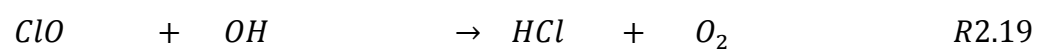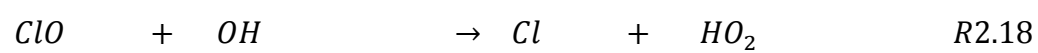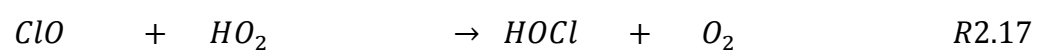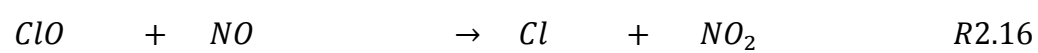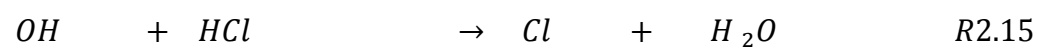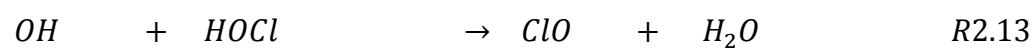
Table 2. 7 List of Cl reactions with inorganic compounds with their reaction rate coefficients that presented in the box model.

No.	Chemical reactions	Rate coefficient	Sources
1	$Cl + HO_2 = HCl + O_2$	3.50D-11	IUPAC
2	$Cl + HO_2 = ClO + OH$	7.5D-11*EXP(-620/TEMP)	IUPAC
3	$Cl + H_2O_2 = HCl + HO_2$	1.1D-11*EXP(-980/TEMP)	IUPAC
4	$C + NO_3 = NO_2 + ClO$	2.40D-11	IUPAC
5	$Cl + O_3 = ClO + O_2$	2.8D-11*EXP(-250/TEMP)	IUPAC
6	$Cl + ClONO_2 = Cl_2 + NO_3$	6.2D-12*EXP(145/TEMP)	IUPAC
7	$ClO + HO_2 = HOCl + O_2$	2.2D-12*EXP(340/TEMP)	IUPAC
8	$ClO + NO = Cl + NO_2$	6.2D-12*EXP(295/TEMP)	IUPAC
9	$ClO + NO_2 + M = ClONO_2 + M$	$k_{(ClO+NO_2)}$determined from: $$k_0 = 1.60x\,10^{-31}\left(\frac{T}{300}\right)^{-3.4}[N_2]$$ $$k_\infty = 1.5\ x\ 10^{-11}$$ $$F = 0.5$$	(Tanaka et al., 2003)
10	$OH + ClO = HO_2 + Cl$	1.80D-11	NASA
11	$OH + ClO = HCl + O_2$	1.20D-12	IUPAIC
12	$OH + Cl_2 = HOCl + Cl$	3.6D-12*EXP(-1200/TEMP)	IUPAC
13	$HCl + OH = Cl + H_2O$	1.7D-12*EXP(-230/TEMP)	IUPAC
14	$OH + HOCl = ClO + H_2O$	5.00D-13	IUPAC
15	$ClONO_2 + M = ClO + NO_2 + M$	k_{ClONO_2} determined from: $$k_{eq}x\ k_{(ClO+NO_2)}$$ $$k_{eq} = 5.20x10^{25}\exp\left(-\frac{12000}{T}\right)\left(\frac{T}{300}\right)^{3.4}$$	(Tanaka et al., 2003)

2.4.3 VOC inclusion into the box model

The tropospheric organic chemistry is complex, as thousands of chemical species are emitted from both natural and anthropogenic sources into the atmosphere (Fuentes et al. (2000); Simon et al. (2010); Stockwell et al. (2011). To simplify the model simulation a limited number of the VOCs should be included into the model.

The selection of the VOCs is usually carried out based on the individual VOC contribution to O_3 formation in the atmosphere. The concentrations and chemical reactivity of each VOC, typically with OH are the main factors that determine the role of the VOC in O_3

formation, because, OH is a dominant radical in removing VOCs in the atmosphere and subsequent formation of peroxy radicals, thus O_3 formation. Total OH reactivity, denoted as k'_{OH} can be defined as the sum of the product of the rate coefficient of OH reaction with VOC and the concentration of each VOC:

$$k'_{OH} = \sum k_{(OH+VOC)_1}[VOC_1] + k_{(OH+VOC)_2}[VOC_2] + \cdots \qquad Eq\ 2.13$$

$$k'_{Cl} = \sum k_{(Cl+VOC)_1}[VOC_1] + k_{(Cl+VOC)_2}[VOC_2] + \cdots \qquad Eq\ 2.14$$

In this study we aimed to include those VOCs that are highly reactive toward the Cl atoms. Therefore, based on the proposed Cl reactions with VOCs in previous studies (Riedel et al., 2014; Sarwar et al., 2012), 15 VOCs are selected to initially calculate their reactivities with OH via equation Eq 2.13 (Figure 2.9A), then their reactivities toward Cl atoms were calculated via equation Eq 2.14 (Figure 2.9B). The concentrations of the VOCs were derived from the average measured concentrations (in August 2003) during the TORCH campaign (Tropospheric Organic Chemistry experiment) carried out in a rural area in Essex, UK (Lee et al. 2006).

The results show that acetaldehyde is the most reactive species toward OH (31%), while, methanol was the most reactive species with Cl (37%).

The relatively less reactive VOCs toward Cl (VOCs reactivity $< 2\ s^{-1}$) are not included in the model, which are: 1-butene, trans-2-butene, cis-2-butene, 1,3-butadiene, and butanal. The remaining 10 VOCs (methanol, ethanol, formaldehyde, acetaldehyde, isoprene, toluene, m-xylene, ethene, propene, and acetylene), which account for ~97% of the total Cl reactivity from all 15 species are incorporated into the model, with their subset mechanisms extracted from the MCM3.3.1. The reason for not including the all 15 VOC into the model is to reduce model complexity, hence, the model running duration time would not be highly affected by inclusion of the Cl mechanism.

In order to obtain an accurate representation of the VOC, the concentration of each VOC was multiplied by a factor to maintain the total OH reactivity of $3.396\ s^{-1}$ as calculated for 65 measured VOC during the TORCH campaign (Lee et al., 2006). The increase of VOC concentrations, and thus, OH reactivity would minimise the errors that may arise from not including the all 65 VOCs in the model. Table 2.8 summarizes the initial VOC

concentrations (after multiplying by a factor) that included in the model, which were kept constant throughout the simulations.

A)

B)
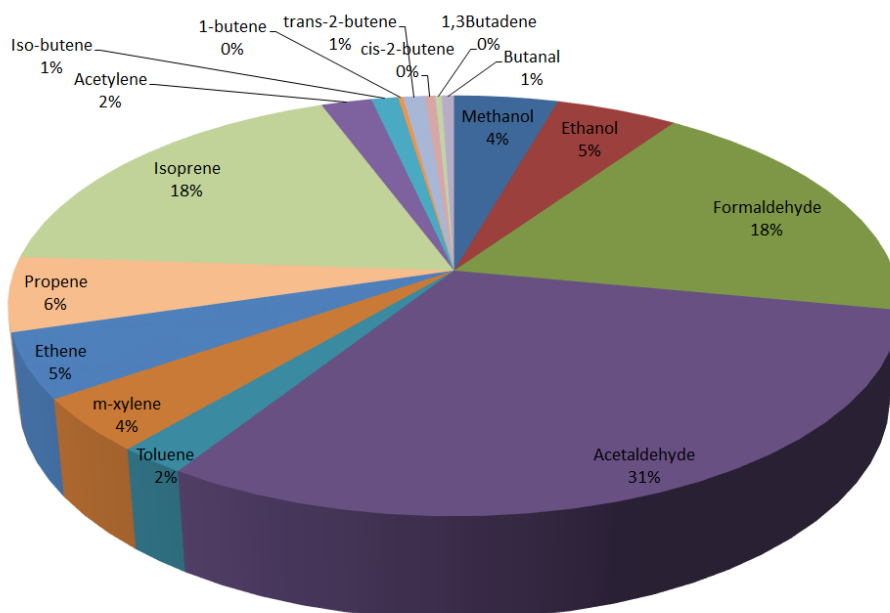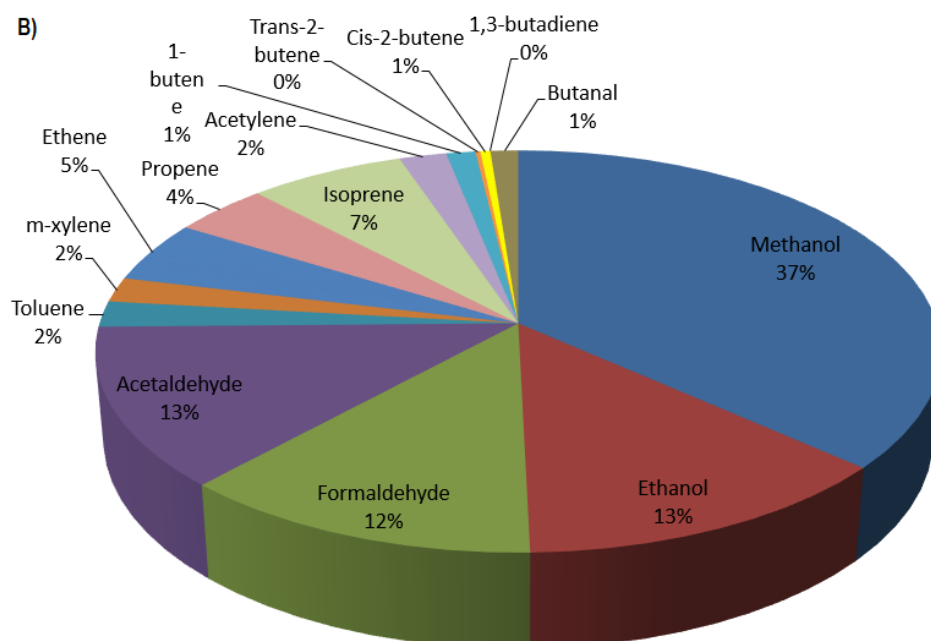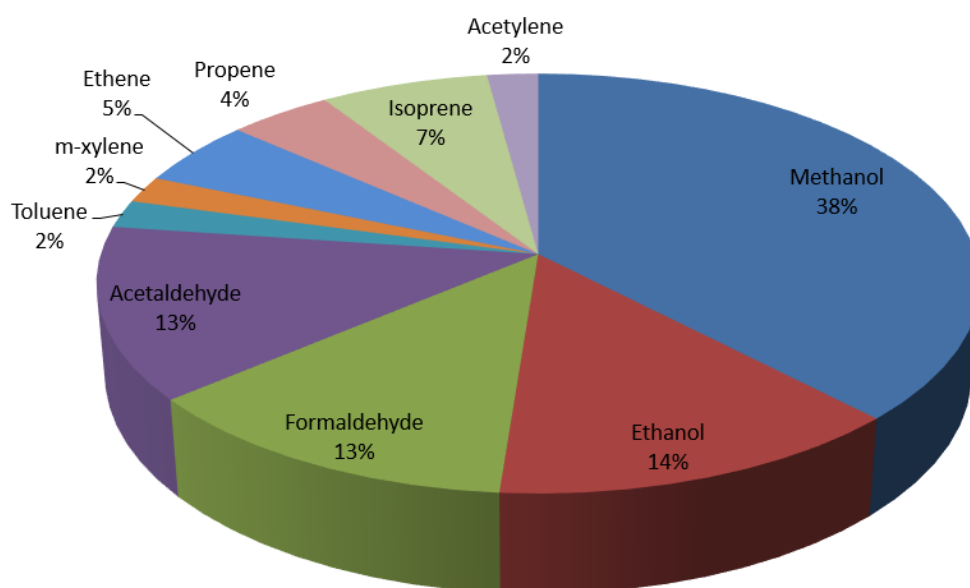
Figure 2. 9 Pie chart showing A) OH reactivity with 15 VOCs, B) Cl reactivity with 15 VOCs, and C) Cl reactivity with 10 VOC, after excluding the less reactive species, which are incorporated into the model with their concentrations set to their measured VOC (after application of a scaling factor) during TORCH campaign.

Table 2. 8 Mixing ratio of measured VOCs from TORCH campaign, and modified VOCs (after application of a scaling factor factor) used in the model simulations. The initial measured VOC multiplied by a factor of 1.8 to obtain total OH reactivity close to the measured (TORCH) reactivity

	The TORH measurements	Modified ([initial VOC] * 1.8)
VOCs	**Mixing ratio (pptv)**	**Mixing ratio (pptv)**
Methanol	3785	6813
Ethanol	1214	2185
Formaldehyde	1610	2898
Acetaldehyde	1528	2750
Isoprene	134	241
Toluene	281	506
M-xylene	135	243
Ethene	469	844
Propene	148	266
Acetylene	395	711

2.4.4 Cl reactions with organic compounds

Several studies have revealed that VOC (especially alkane) oxidation by Cl are at least 2 orders of magnitude faster than their oxidation by OH (Chang et al., 2002; Riedel et al., 2014; Tanaka et al., 2003). The atmospheric lifetime of some alkanes with the presence of 1.4×10^5 atoms- cm^{-3} of Cl would be 14 hours, while, with OH of $\sim 10^6$ molecules cm^{-3} the lifetime would be more than 10 days (Suh and Zhang, 2000).

Including a comprehensive Cl chemistry with organic compounds within the MCM box model is therefore necessary to avoid the underestimation of any potential impact of Cl on air quality. Chlorine reactions with only alkanes are presented in the current near explicit mechanism, MCM ve3.3.1.

The general approach based on previous studies for Cl reactions with organic compounds is that Cl reacts with organic compounds via H-atom abstraction from the O-H and H-C bonds (R2.22) or by Cl addition to the $C = C$ double and triple $C \equiv C$ bonds, or Cl

addition to the aromatic ring. The Cl reactions with organic compounds mostly produce RO_2 and HO_2, which then converts NO to NO_2, thus form O_3.

$$Cl + RH \rightarrow HCl + R \qquad\qquad R2.22$$

Cl-VOC reactivity differs from that of OH-VOC, as the rate constant of Cl-VOC being at least 2 orders of magnitude larger than that of OH-VOC especially for alkanes which are less reactive toward OH (Young et al., 2014). Moreover, H abstraction by Cl mechanism may be differ from the H abstraction by OH, such as in alcohols in which H abstraction by Cl mostly occurs from C-H bonds and not O-H bond (R2.25) (Grosjean, 1997), whereas, the H abstraction by OH may involve either C-H (R2.23) or O-H bonds (R2.24) (Seinfeld, 1989):

$$RCH_2OH + OH \rightarrow H_2O + RCHOH \qquad R2.23$$

$$RCH_2OH + OH \rightarrow H_2O + RCH_2O \qquad R2.24$$

$$RCH_2OH + Cl \rightarrow HCl + RCHOH \qquad R2.25$$
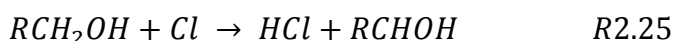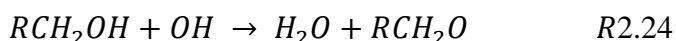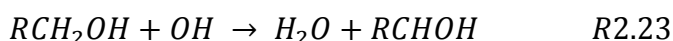
Most of the products of the Cl-VOC reactions that proceed by hydrogen abstraction exist in the MCM, so their chemistry is already presented. In such cases, the Cl atoms are recycled back into the system, mainly via HCl reaction with OH. However, the products of those reactions that are proceeded by Cl addition to the carbon bond are mostly new and their chemistry needs to be defined via assigning an analogy species that form from the same VOC reaction with OH, to avoid permanent loss of Cl.

Below is explained the Cl chemical reactions with the 10 parent VOCs (and the fate of the new products) that are incorporated in the MCM-based box model

2.4.4.1 Cl reactions with alcohols [methanol (CH_3OH) and ethanol (C_2H_5OH)]

Alcohol reaction with Cl is assumed to occur by hydrogen (H) atom abstraction (Xue et al., 2015) from the H-C bond, similarly as OH reaction with the alcohol (Grosjean, 1997) to form HCl and either a RO_2 or an HO_2 together with a carbonyl species (Xue et al., 2015).

Products of Cl reaction with methanol are proposed to be HCl, HO_2 and HCHO (Ohta et al., 1982), while $HOCH_2CH_2O_2$ and HCl is produced from the Cl reaction with ethanol.

These products are available in the MCM in which $HOCH_2CH_2O_2$ reacts with NO forming NO_2. Rate constants are derived from the IUPAC database (Atkinson et al., 2006b):

$$Cl \ + \ CH_3OH \quad \rightarrow \quad HO_2 \qquad + \quad HCHO \quad + \quad HCl \qquad \text{R2.26}$$

$$Cl \ + \ C_2H_5OH \quad \rightarrow \quad CH_3CHO \quad + \quad HO_2 \quad + \quad HCl \qquad \text{R2.27}$$

$$Cl \ + \ C_2H_5OH \quad \rightarrow \quad HOCH_2CH_2O_2 \ + \ HCl \qquad\qquad \text{R2.28}$$
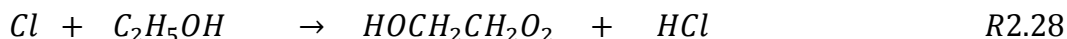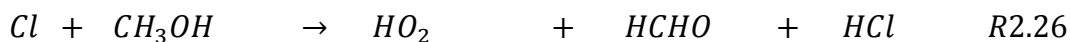
2.4.4.2 Cl reactions with aldehyde [formaldehyde (HCHO) and acetaldehyde (CH$_3$CHO)]

Cl reaction with HCHO and CH$_3$CHO proceeds via H abstraction by Cl as proposed by previous studies, forming products, already presented in the MCM which are HCl and HO$_2$ from HCHO, and CH$_3$CO$_3$ and HCOCH$_2$O$_2$ from CH$_3$CHO reactions (Grosjean, 1997, Atkinson et al., 2006b). In the MCM, CH$_3$CO$_3$ react with HO$_2$ and NO to form NO$_2$. Rate constants were taken from Atkinson et al. (2006b):

$$Cl \ + \ HCHO \qquad \rightarrow \quad HO_2 \qquad\quad + \quad CO \qquad\quad + \quad HCl \qquad \text{R2.29}$$

$$Cl \ + \ CH_3CHO \quad \rightarrow \quad CH_3CO_3 \quad + \quad HCl \qquad\qquad\qquad \text{R2.30}$$

$$Cl \ + \ CH_3CHO \quad \rightarrow \quad HCOCH_2O_2 \quad + \quad HCl \qquad\qquad \text{R2.31}$$
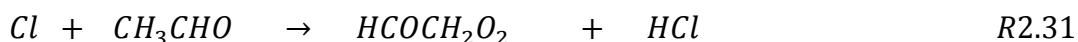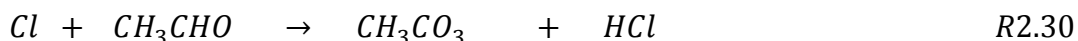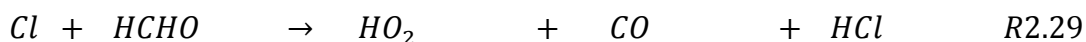
2.4.4.3 Cl reactions with dialkenes [isoprene (C$_5$H$_8$)]: $CH_2 = C(CH_3)CH = CH_2$

Isoprene reaction with Cl is believed to have a potential to play an important role in O$_3$ formation (Suh and Zhang, 2000). The mechanism of this reaction and the products is not clear and considered as complex (Xue et al., 2015). Fan and Zhang, (2004) proposed that the reaction proceeds mostly by Cl addition forming Cl–isoprene adduct radicals (ISOCl). The latter react with OH to form chloroalkenyl peroxy radicals (ISOClO$_2$) under atmospheric condition (Fan and Zhang, 2004). In the presence of NO, ISOClO$_2$ reacts with NO forming chloroalkenyl alkoxy radicals (ISClO) and NO$_2$. Xue et al., (2015) used a simple mechanism based on the Carbon Bond Mechanism (CBM) (Gery et al., 1989) to represent the Cl-isoprene reaction, and they proposed that ISOClO further degraded to form ISOClCHO, but no further reaction of ISOClCHO was presented. The proposed Cl-

isoprene reaction products (ISOClO$_2$ and ISOClO, and ISOClCHO) were therefore not present in the MCM.

Here, we modified ISOClO to ISOPAO as the latter is a product of OH reaction with isoprene, which is already present in the MCM. By this, a potential underestimation of Cl affects O$_3$ formation can be avoided as in the MCM, ISOPAO undergoes a rapid isomerisation reaction to form HMACR, HCHO, and HO$_2$ via a series reactions involving a peroxy radical C524O$_2$ formation (Jenkin et al., 2015b). C524O$_2$ also reacts with NO forming NO$_2$. The rate constant for Cl reaction with isoprene (R2.32) used here was suggested by Tanaka et al., (2003). They proposed that the rate of Cl reaction with isoprene is 4.5 times higher than that of OH ($k_{Cl+C5H8} = 4.75 \, x \, (k_{OH+C5H8)}$).

$$Cl \quad + \quad C_5H_8 \quad \rightarrow \quad ISOClO_2 \qquad\qquad R2.32$$

$$ISOClO_2 \quad + \quad NO \quad \rightarrow \quad ISOPAO \quad + \quad NO_2 \qquad R2.33$$

2.4.4.4 Cl reactions with aromatics [toluene (C$_7$H$_8$) and m-xylene (C$_8$H$_{10}$)]

The reactions of Cl atoms with aromatics via addition of Cl to the aromatic ring is very slow, thus, the reactions assumed to proceed via H abstraction from non-ring alkyl substitutes, to form HCl and RO$_2$ (Xue et al., 2015). Therefore, Cl reactions with toluene and m-xylene were suggested to proceed via hydrogen abstraction from the methyl group. The experimental rate constant data determined by Shi and Bernhard (1997) is used for both toluene and m-xylene.

$$Cl \quad + \quad C_7H_8 \quad \rightarrow \quad C_6H_5CH_2O_2 \quad + \quad HCl \qquad R2.34$$

$$Cl \quad + \quad C_8H_{10} \quad \rightarrow \quad C_8H_{10}O_2 \quad + \quad HCl \qquad R2.35$$
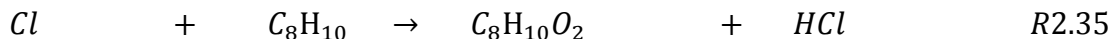
2.4.4.5 Cl reactions with ethene (C$_2$H$_4$) and propene (C$_3$H$_6$)

Cl reactions with alkenes proceed mainly by the addition of Cl to the carbon double bond forming chlorinated compounds such as formyl chloride and chloroacetone, which can serve as a long lived (> 1 month) reservoirs for Cl (Baker et al., 2016). The product of Cl-ethene reaction is present in the MCM. The rate constant of ethene-Cl is derived from Riedel et al., (2014).

$$Cl \quad + \quad C_2H_4 \quad \rightarrow \quad CH_2ClCH_2O_2 \qquad R2.36$$
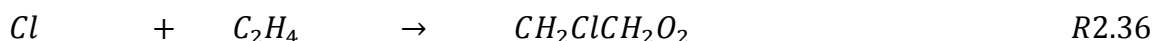
The atmospheric lifetime of propene in the presence of Cl with concentrations of $\sim 1 \times 10^5$ atoms cm^{-3} is suggested to be 11 hours, while in the presence of OH, the lifetime will be as long as 107 hours (Ezell et al., 2002). The reaction of Cl with propene is rather complex (Xue et al., 2015). Atkinson et al. (2006b) proposed C_3H_6Cl formation from Cl reaction with propene without providing further degradation of the product, which may cause a permanent loss of Cl. However, Riedel et al., (2014) presented the Cl- propene reaction scheme, which they suggested that the reaction proceed via abstraction of hydrogen (10%) (R2.37) and by addition of Cl in to the double bond (90%) (R2.39 and R2.41).

The H atom abstraction will result in the formation of HCl and a new peroxy radical ($CH_2C_2H_3O_2$) (R2.37) which is not available in the MCM. The new radical was proposed to react with NO forming 2-Propenal (ACR) (R2.38) and its chemistry is present in the MCM. The rate constant of this reaction was taken from Riedel et al., (2014).

Depending on the Cl selectivity of attack, Riedel et al., (2014) suggested that 50% of Cl addition to propene will lead to the formation of $CH_2ClCHOOCH_3$ (R2.39), which in turn reacts with NO to form $CH_2ClCOCH_3$ (R2.40). The chemistry of the latter is present in the MCM. The rate constant of this reaction was taken from Riedel et al., (2014).

Whereas, 40% of Cl reactions with Propene proposed to form $CH_3CHClCH_2OO$ (R2.41). The degradation mechanism of this product is given by Riedel et al. (2014). Some of the suggested products of these reactions (R2.41-R2.57) have been investigated in polar regions (Riedel et al., 2014, Keil and Shepson, 2006).

Cl- propene reaction via hydrogen abstraction (10%):

$$Cl \quad + \quad C_3H_6 \quad \rightarrow \quad CH_2C_2H_3O_2 \quad + \quad HCl \qquad R2.37$$

$$CH_2C_2H_3O_2 \quad + \quad NO \quad \rightarrow \quad ACR \quad + \quad HCl \qquad R2.38$$

Cl- propene reaction via Cl addition to the carbon double bond:

A) $(CH_2 = CH - CH_3)$ (50%)

Cl $+$ C_3H_6 $\rightarrow$ $CH_2ClCHOOCH_3$ $\qquad$ R2.39

$CH_2ClCHOOCH_3$ $+$ NO $\rightarrow$ $H_2ClCOCH_3$ $\qquad$ R2.40

B. $(CH_3 = CH - CH_2)$ (40%)

New products, which are not available in the MCM, are bolded

Cl $+$ C_3H_6 $\rightarrow$ $\mathbf{CH_3CHClCH_2OO}$ $\qquad$ R2.41

$\mathbf{CH_3CHClCH_2OO}$ $+$ NO $\rightarrow$ $\mathbf{CHOCHClCH_3}$ $\qquad$ R2.42

$\mathbf{CHOCHClCH_3}$ $+$ OH $\rightarrow$ $\mathbf{C_2H_5OClCO_3}$ $\qquad$ R2.43

$\mathbf{C_2H_5OClCO_3}$ $+$ HO_2 $\rightarrow$ CH_3CHClO_2 $\qquad$ R2.44

$\mathbf{C_2H_5OClCO_3}$ $+$ HO_2 $\rightarrow$ $\mathbf{CH_3CHClCO_3H}$ $\qquad$ R2.45

$\mathbf{CH_3CHClCO_3H}$ $+$ OH $\rightarrow$ $\mathbf{C_2H_5ClCO_3}$ $\qquad$ R2.46

$\mathbf{CH_3CHClCO_3H}$ $\rightarrow$ CH_3CHClO_2 $+$ OH $\qquad$ R2.47

$\mathbf{C_2H_5ClCO_3}$ $+$ HO_2 $\rightarrow$ $\mathbf{CH_3CHClCOOH} + O_3$ $\qquad$ R2.48

$\mathbf{CH_3CHClCOOH}$ $+$ OH $\rightarrow$ CH_3CHClO_2 $\qquad$ R2.49

$\mathbf{C_2H_5OClCO_3}$ $+$ NO $\rightarrow$ CH_3CHClO_2 $+ NO_2$ $\qquad$ R2.50

$\mathbf{C_2H_5OClCO_3}$ $+$ NO_2 $\rightarrow$ $\mathbf{2\ ClPPN}$ $\qquad$ R2.51

$\mathbf{2\ ClPPN}$ $+$ OH $\rightarrow$ $ClETAl$ $+$ CO $+ NO_2$ $\qquad$ R2.52

$\mathbf{2\ ClPPN}$ $\rightarrow$ $\mathbf{C_2H_5ClO_3}$ $+$ NO_2 $\qquad$ R2.53

$\mathbf{C_2H_5ClO_3}$ $+$ NO_2 $\rightarrow$ CH_3CHClO_2 $\qquad$ R2.54

$\mathbf{C_2H_5ClO_3}$ $\rightarrow$ CH_3CHClO_2 $\qquad$ R2.55

$\mathbf{C_2H_5ClO_3}$ $\rightarrow$ $\mathbf{CH_3CHClCOOH}$ $\qquad$ R2.56

$\mathbf{CHOCHClCH_3}$ $+$ hv $\rightarrow$ CH_3CHClO_2 $+ HO_2 + CO$ $\qquad$ R2.57

2.4.4.6 Cl reaction with Acetylene (C_2H_2)

Cl reaction with acetylene initiates with Cl addition to the triple bond. It was reported that Cl reaction with acetylene is temperature and pressure dependent (Wallington et al., 1990). The rate constant of this reaction was taken from Carter (2010).

$$Cl \quad + \quad C_2H_2 \quad + \quad M \quad \rightarrow \quad ClCHO \quad + \quad CO \quad + \quad HO_2 + M \quad R2.58$$
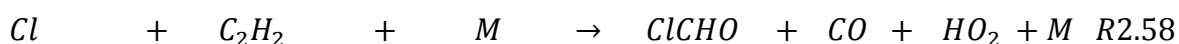
2.4.4.6 Cl reaction with organic acids and nitrates

Following Xue et al., (2015), Cl reactions with organic acids (including formic acid (HCOOH), acetic acid (CH_3CO_2H), propanoic acid (PROPACID)) and organic nitrates for five C1-C4 alkyl nitrates are added into the model.

Cl reacts with organic acids via H atom abstraction forming HCl and RO_2. The rate constant of Cl reactions with HCOOH and CH_3CO_2H is taken from the IUPAC database, but the rate constant for Cl reaction with PROPACID was estimated from:

$$\frac{k_{(cl+CH_3CO_2H)}}{k_{(OH+CH_3CO_2H)}} \; x \; k_{(OH+CH_3CO_2H)} \qquad Eq2.15$$

For organic nitrates, Cl reactions with alkyl nitrates are assumed to proceed via H atom abstraction forming HCl, NO_2 and carbonyl compounds with rate constants are taken from the IUPAC database.

Table 2. 9 Organic chlorine chemistry presented in the model

No.	Species	Chemical reactions	Rate coefficient	Sources
1	Alcohols	$Cl + CH_3OH = HO_2 + HCHO + HCl$ $Cl + C_2H_5OH = CH_3CHO + HO_2 + HCl$ $Cl + C_2H_5OH = HOCH_2CH_2O_2 + HCl$	$7.1x10^{-11}\exp(-\dfrac{75}{T})$ $6.0x10^{-11}\exp\left(\dfrac{155}{T}\right)x0.92$ $6.0x10^{-11}\exp\left(\dfrac{155}{T}\right)x0.08$	IUPAC
2	Alkenes	$Cl + C_2H_4 = CH_2ClCH_2O_2$ $Cl + C_3H_6 = CH_2C_2H_3O_2 + HCl$ $Cl + C_3H_6 = CH_2ClCHOOCH_3$ $Cl + C_3H_6 = CH_3CHClCH_2OO$ $CH_3CHClCH_2OO + NO = CHOCHClCH_3$ $CHOCHClCH_3 + NO_3 = C_2H_5ClCO_3$ $CHOCHClCH_3 + OH = C_2H_5ClCO_3$ $C_2H_5ClCO_3 + HO_2 = CH_3CHClO_2$ $C_2H_5ClCO_3 + HO_2 = CH_3CHClCO_3H$ $CH_3CHClCO_3H + OH = C_2H_5ClCO_3$ $CH_3CHClCO_3H + hv = CH_3CHClO_2 + OH$ $C_2H_5ClCO_3 + HO_2 = CH_3CHClCOOH + O_3$ $CH_3CHClCOOH + OH = CH_3CHClO_2$ $C_2H_5ClCO_3 + NO = CH_3CHClO_2 + NO_2$ $C_2H_5ClCO_3 + NO_2 = 2ClPPN$ $2ClPPN + OH = ClETAl + CO + NO_2$ $2ClPPN = C_2H_5ClO_3 + NO_2$ $C_2H_5ClCO_3 + NO_3 = CH_3CHClO_2$ $C_2H_5ClCO_3 = CH_3CHClO_2$ $C_2H_5ClCO_3 = CH_3CHClCOOH$ $CHOCHCLCH_3 + hv = CH_3CHCLO_2 + HO_2 + CO$	$1x10^{-10}$ $0.1x2.7x10^{-10}$ $0.40x2.7x10^{-10}$ $0.50x2.7x10^{-10}$ $2.9x10^{-12}\exp(\dfrac{350}{T})$ [1] $3.24x10^{-12}\exp\left(-\dfrac{1860}{T}\right)$ [2] $4.9x10^{-12}\exp(\dfrac{405}{T})$ [3] $KAPHO_2 x0.44$ [4] $KAPHO_2 x0.41$ [5] $4.42x10^{-12}$ [6] $jPERPROACID$ [7] $KAPHO_2 x0.15$ [8] $1.2x10^{-12}$ [9] $6.7x10^{-12}\exp(\dfrac{340}{T})$ [10] $KFPAN$ [11] $1.27x10^{-12}$ [12] $1.7x10^{-3}\exp(-\dfrac{1280}{T})$ [13] $KRO_2NO_3 x1.74$ [14] $1.0x10^{-11}x0.7$ [15] $1.0x10^{-11}x\,0.3$ [16] $jpropanal$ [17]	IUPAC IUPAC IUPAC IUPAC MCM MCM MCM MCM MCM MCM MCM MCM MCM MCM MCM MCM MCM MCM MCM MCM MCM
3	Alcohols	$Cl + CH_3OH = HO_2 + HCHO + HCl$ $Cl + C_2H_5OH = CH_3CHO + HO_2 + HCl$ $Cl + C_2H_5OH = HOCH_2CH_2O_2 + HCl$	$7.1x10^{-11}\exp(-75/T)$ $6.0*10^{-11}\exp(155/T)*0.92$ $6.0*10^{-11}\exp(155/T)*0.08$	IUPAC IUPAC IUPAC

4	Aldehyde	$HCHO + Cl = HCl + HO_2 + CO$	$8.1 \times 10^{-11} \exp(-34/T)$	IUPAC
		$Cl + CH_3CHO = CH_3CO_3 + HCl$	$8.0 \times 10^{-11} * 0.99$	IUPAC
		$Cl + CH_3CHO = HCOCH_2O_2 + HCl$	$8.0 \times 10^{-11} * 0.01$	IUPAC
5	Aromatic	$Cl + C_7H_8 = C_6H_5CH_2O_2 + HCl$	5.9×10^{-11}	Shi& Bernhard (1997)
		$Cl + mxyl = mxylO_2 + HCl$	1.4×10^{-10}	
6	Dialkene	$Cl + C_5H_8 = ISOClO_2$	$4.75 * 2.7 \times 10^{-11} \exp(390/T)$	Xue et al., (2015)
7	Alkayne	$C_2H_2 + Cl = ClCHO + CO + HO_2$	4.97×10^{-11}	Carter (2010)
8	Organic acids and nitrates	$Cl + CH_3OOH = CH_3O_2 + HCl$	$5.9 \times 10^{-11} * 0.6$	IUPAC
		$Cl + CH_3OOH = HCHO + OH + HCl$	$5.9 \times 10^{-11} * 0.4$	IUPAC
		$Cl + HCOOH = HO_2 + HCl$	1.9×10^{-13}	IUPAC
		$Cl + CH_3CO_2H = CH_3O_2 + HCl$	2.65×10^{-14}	IUPAC
		$Cl + PROPACID = C_2H_5O_2 + HCl$	$1.2 \times 10^{-12} * 0.033$	Xue et al., (2015)
		$Cl + CH_3NO_3 = HCHO + NO_2 + HCl$	2.4×10^{-13}	IUPAC
		$Cl + C_2H_5NO_3 = CH_3CHO + NO_2 + HCl$	4.7×10^{-12}	IUPAC
		$Cl + NC_3H_7NO_3 = C_2H_5CHO + NO_2 + HCl$	2.2×10^{-11}	IUPAC
		$Cl + IC_3H_7NO_3 = CH_3COCH_3 + NO_2 + HCl$	3.8×10^{-12}	IUPAC
		$Cl + NC_4H_9NO_3 = C_3H_7CHO + NO_2 + HCl$	8.5×10^{-11}	IUPAC

Notes: Most of chlorine chemistry (chemical reactions between Cl and VOC with the rate constant) used in this study was derived from the MCM, Sander et al. (2009), Atkinson et al. (2006b), Riedel et al., 2014, and Xue et al., (2015).

(1) k from MCM for $NC_3H_7O_2 + NO$
(2) k from MCM for $propanal + NO_3$
(3) k from MCM for $propanal + OH$
(4) k from MCM for $C_2H_5CO_3 + HO_2$
(5) k from MCM for $C_2H_5CO_3 + HO_2$
(6) k from MCM for $PERPROACID + OH$
(7) j from MCM for $PERPROACID$
(8) k from MCM for $C_2H_5CO_3 + HO_2$
(9) k from MCM for $PROPACID + OH$

(10) k from MCM for $C_2H_5CO_3 + NO$
(11) k from MCM for $C_2H_5CO_3 + NO_2$
(12) k from MCM for $PPN + OH$
(13) k from MCM for PPN decomposition
(14) k from MCM for $C_2H_5CO_3 + NO_3$
(15) k from MCM for $C_2H_5CO_3 + RO_2 = C_2H_5O_2$
(16) k from MCM for $C_2H_5CO_3 + RO_2 = PROPACID$
(17) j from MCM for $propanal$

2.5 Chapter summary

Reactions of chlorine atoms with organic and inorganic compounds are important due to its potential to affect air quality. The main updates to the mechanisms that previously developed for Cl chemistry in the troposphere are the photolysis calculations performed in this study for $ClNO_2$, $HOCl$, CL_2, and $ClONO_2$. The photolysis rates of these compounds are calculated more accurately than other studies performed before, as the scaling factors used for the calculation of the photolysis rate coefficient are not constant, but vary with the SZA, which provided an accurate photolysis diurnal profile.

In this study we modified and extended the Cl atoms reactions with isoprene to more explicitly present the degradation of the first product ($ISOClO_2$) of the reaction, which have not been presented in previous studies. This allows us to decrease the underestimation of Cl impacts on air quality in general and O_3 in particular as the reaction of Cl with isoprene plays an important role in the formation of O_3 in the troposphere as proposed by previous literature.

It is important to mention that the number of the VOCs and their chemistry that included in the model are selected carefully, based on literatures and their reactivity toward OH and Cl, so as to capture the effect of Cl on the radicals (OH, HO_2, RO_2), thus O_3 formations precisely. However, there are still some uncertainties, which need to be investigated. For example, it is unknown whether the products that form from the Cl reactions with VOCs may react with Cl, and at what rates. This can affect the Cl budget in the atmosphere and the subsequent RO_2 or HO_2 formations.

Chapter 3 Model development and evaluation

In this chapter an overview of $ClNO_2$ formation process from N_2O_5 heterogeneous reaction is recapped from Chapter 1 (Introduction). The process of the model development for use with the Master Chemical Mechanism (MCM) is comprehensively presented in terms of parameters, chemical reactions, and mathematical equations that have been integrated into the model framework. Finally, model evaluation is presented.

3.1 Heterogeneous N_2O_5 reaction with aerosol particle

From figure 3.1, at night with the reduction of photolysis in the evening, the NO_2 accumulates and reacts with O_3 to form NO_3 radicals (R1.3 and R1.31) which can oxidize VOCs at night when other radicals, such as OH, are limited.

$$NO_2 + hv \ (< 420 \ nm) \rightarrow NO + O(^3P) \hspace{2cm} R1.3$$

$$NO_2 \ + \ O_3 \ \ \rightarrow \ \ NO_3 \ + \ O_2 \hspace{2cm} R1.31$$
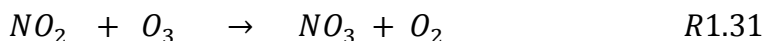
During the night, the NO_3 radical accumulates to levels that may range from a few ppt in a remote environment to several hundred ppt in polluted regions (Finlayson-Pitts et al. 1999) and can react with NO_2 to form N_2O_5. The latter is thermally unstable and may decompose back to NO_3 and NO_2 and set up an equilibrium with NO_3 (R1.34). N_2O_5 can react homogeneously with water vapour $(H_2O_{(g)})$ to form HNO_3 with the rate constants of around $2.5x10^{-22}$ cm^3 molecule^{-1} s^{-1} and $1.8x10^{-39}$ cm^6 molecule^{-2} s^{-1} for the second and third order reactions (R3.1 and 3.2 respectively) (Wahner et al. 1998), or it can react heterogeneously with particles to form HNO_3 or $ClNO_{2,}$ with a relatively much faster rate coefficient than the homogeneous reactions.

$$NO_2 \ + \ NO_3 \ + \ M \ \leftrightarrow \ N_2O_5 \ + \ M \hspace{2cm} R1.34$$
$$N_2O_{5(g)} \ + \ H_2O_{(g)} \ \rightarrow \ 2HNO_{3(g)} \hspace{2cm} R3.1$$
$$N_2O_{5(g)} \ + \ 2H_2O_{(g)} \ \rightarrow \ 2HNO_{3(g)} \ + \ H_2O_{(g)} \hspace{2cm} R3.2$$
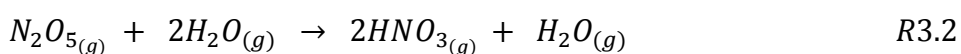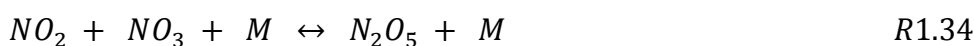
N_2O_5 can rapidly react with aerosol containing H_2O (hydrolysis) to produce HNO_3 which, during the night, is a primary mechanism for removing NO_x in the atmosphere, as NO_3 and N_2O_5 are rapidly photolysis during day time, thus N_2O_5 can only build up at night. Thereby, N_2O_5 hydrolysis leads to a reduction in NO_x levels in the atmosphere for the following day (Li et al. 2016). If there is Cl^- present in the aerosol however, the product of the reaction of N_2O_5 and aerosol will be $ClNO_2$ that can then photolyse and release NO_2, hence extends the lifetime of NO_x in the atmosphere.

3.2 $ClNO_2$ formation mechanism
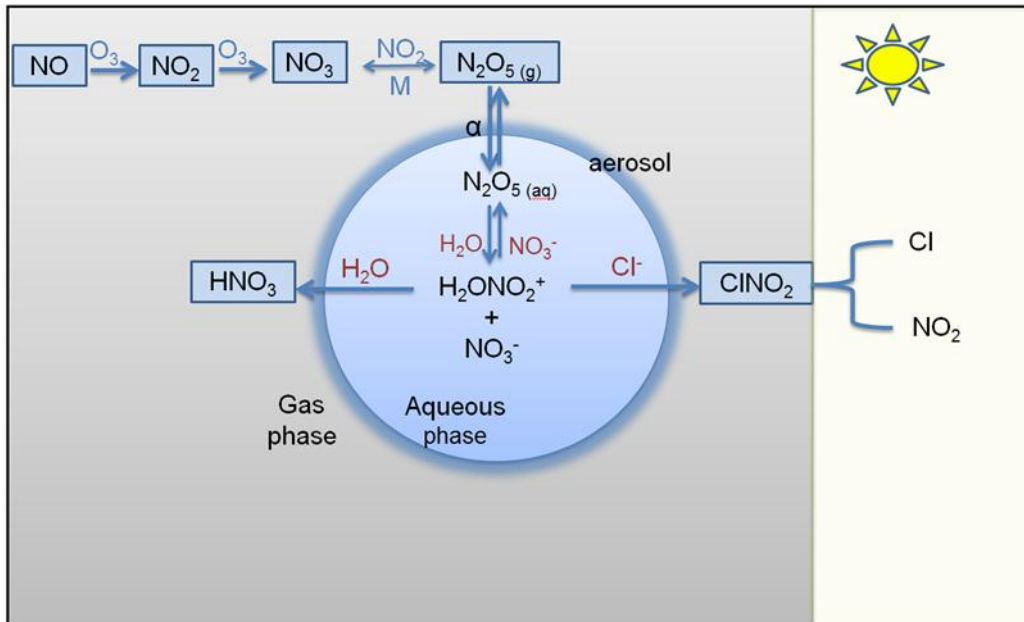
Figure 3. 1 The process of the heterogeneous reaction of N_2O_5 with aerosol particle and the formation of either $ClNO_2$ or HNO_3 (updated from Bertram and Thornton, 2009)

$ClNO_2$ formation is thought to proceed through the following reactions (R3.3-R3.7), as proposed by Bertram and Thornton (2009); Herrmann et al. (2015):

$$N_2O_{5(gas)} \quad \rightarrow \quad N_2O_{5(aq)} \qquad\qquad R3.3$$

$$N_2O_{5(aq)} + H_2O_{(l)} \quad \rightarrow \quad H_2ONO^+_{2(aq)} + NO^-_{3(aq)} \qquad R3.4$$

$$H_2ONO^+_{2(aq)} + NO^-_{3(aq)} \quad \rightarrow \quad N_2O_{5(aq)} + H_2O_{(l)} \qquad R3.5$$

$$H_2ONO_{2(aq)}^+ + H_2O_{(l)} \quad \rightarrow \quad H_3O_{(aq)}^+ + HNO_{3(aq)} \qquad\qquad R3.6$$

$$H_2ONO_{2(aq)}^+ + Cl_{(aerosol)}^- \quad \rightarrow \quad ClNO_2 + H_2O_{(l)} \qquad\qquad R3.7$$
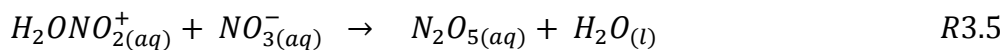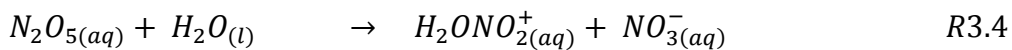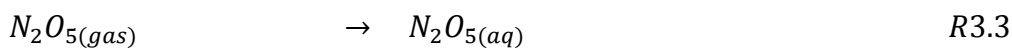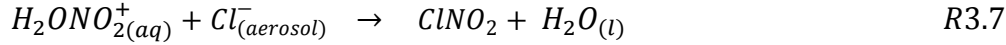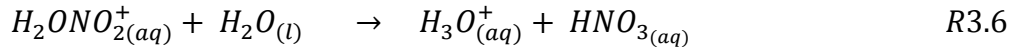
From Figure 3.1, The heterogeneous reaction of N_2O_5 with aerosol begins when the gas phase N_2O_5 diffuses into the surface of aerosol and accommodates onto the aerosol surface which hydrates and converts to the aqueous phase N_2O_5 (N_2O_{5aq}) (R3.3). The latter reacts with water, $H_2O_{(l)}$ (hydrolysis) to form the hydrated intermediate ($H_2ONO_2^+{}_{(aq)}$) (R3.4), however, if the aerosol contains more particulate nitrate (NO_3^-) than $H_2O_{(l)}$, the $H_2ONO_2^+$ will predominantly convert back to $N_2O_{5(aq)}$ (R3.5). Otherwise, the $H_2ONO_2^+$ will continue to either react with $H_2O_{(l)}$ to form nitric acid (HNO_3) (R3.6) or with a halide (for example chloride) to form nitryl chloride ($ClNO_2$) (R3.7) (Figure 3.1). Therefore the product of the heterogeneous reaction is thought to depend on the concentration of $H_2O_{(l)}$ and chloride within the aerosol particle (Bertram and Thornton 2009). The products HNO_3 or $ClNO_2$ (when chloride presents in the aerosol) can either remain in the liquid droplet, undergo more chemical reactions or diffuse out into the gas phase (Ravishankara, 1997).

The probability of N_2O_5 gas phase reaction with aerosol particle that result in the N_2O_5 removal from the gas phase is expressed as the uptake coefficient ($\gamma_{N_2O_5}$). Based on laboratory experiments, Bertram and Thornton (2009) parameterized the uptake coefficient of N_2O_5 on aerosol particles ($\gamma_{N_2O_5}$) as a function of the ratio between $H_2O_{(l)}$ and NO_3^- and Cl^- to NO_3^- since they suggested that these three components in aerosol are controlling $\gamma(N_2O_5)$:

$$\gamma_{N_2O_5} = A.k_{3.4}' \left(1 - \frac{1}{\frac{k_{3.6}[H_2O_l]}{k_{3.5}[NO_3^-]} + 1 + \frac{k_{3.7}[Cl^-]}{k_{3.4}[NO_3^-]}} \right) \qquad\qquad Eq3.1$$

The derivation of this reaction is given below (Eq 3.2 – Eq 3.12):

The change in the rate of the concentration N_2O_5 ($\frac{dN_2O_5}{dt}$) is determined from reactions R3.4 and R3.5

$$\frac{d[N_2O_5]}{dt} = k_{3.5}[H_2ONO_2][NO_3^-] - k_{3.4}[N_2O_5][H_2O] \qquad\qquad Eq\ 3.2$$

$$\frac{d[H_2ONO_2]}{dt} = k_{3.4} [N_2O_5] [H_2O] - k_{3.5} [H_2ONO_2][NO_3^-] - k_{3.6} [H_2ONO_2][H_2O]$$

$$- k_{3.7}[H_2ONO_2][Cl^-] = 0 \qquad Eq\ 3.3$$

$$[H_2ONO_2] = \frac{k_{3.4} [N_2O_5] [H_2O]}{k_{3.6} [H_2O] + k_{3.5} [NO_3^-] + k_{3.7}[Cl^-]} \qquad Eq\ 3.4$$

Substitute Eq 3.4 into Eq 3.2:

$$\frac{d[H_2ONO_2]}{dt} = k_{3.5} [NO_3^-] \left[\frac{k_{3.4} [N_2O_5] [H_2O]}{k_{3.6} [H_2O] + k_{3.5} [NO_3^-] + k_{3.7}[Cl^-]} \right]$$

$$- k_{3.4}[N_2O_5][H_2O] \qquad Eq3.5$$

The pseudo first-order heterogeneous rate constant of the irreversible N_2O_5 loss ($k_{N_2O_5}$) from gas phase to aerosol as derived from the kinetic theory of gases or free-molecule regime can be determined using the following equation: (Wagner et al., 2013).

$$k_{N_2O_5} = \frac{\gamma_{N_2O_5}\,\omega\,S_A}{4} \qquad Eq3.6,$$

The mean molecular speed of N_2O_5 (ω) is determined by:

$$\omega_{N_2O_5} = \sqrt{\frac{8RT}{\pi\,(M_{w_{N_2O_5}})}} \qquad Eq3.7,$$

where, R is the ideal gas constant (8.31451 JK^{-1} mol^{-1}), T is temperature, and M_W is the molecular weight of N_2O_5 (Mielke et al., 2013).

The $k_{N_2O_5}$ is in a linear relationship with the N_2O_5 uptake coefficient ($\gamma_{N_2O_5}$), aerosol surface area density, S_A (cm^{2}m^{-3} of air), and mean molecular speed of $\omega_{N_2O_5}$ (ms^{-1}).

Assuming that the N_2O_5 reaction occurs throughout the entire particle volume (V), the value of $\gamma_{N_2O_5}$ can be expressed as equation Eq 3.8:

$$\gamma_{N_2O_5} = \frac{4\,x\,\left(-\frac{d[N_2O_{5(aq)}]}{dt}\right)\,x\,V}{\omega\,S_A\,[N_2O_{5\,(g)}]} \qquad Eq3.8$$

$\gamma_{N_2O_5}$

$$= \frac{4 \, x - \left(\left[\frac{k_{3.5} \, [NO_3^-] \; x \; k_{3.4} \, [N_2O_5] \, [H_2O]}{k_{3.6} \, [H_2O] \; + \; k_{3.5} \, [NO_3^-] \; + \; k_{3.7}[Cl^-]} \right] - k_{3.2f} \, [N_2O_5] \, [H_2O] \right)}{\omega \, S_A \, [N_2O_{5\,(g)}]} \qquad Eq3.9$$

$\gamma_{N_2O_5}$

$$= \frac{4 \, x \, k_{3.2f} \, [N_2O_5] \, [H_2O] \left(- \frac{k_{3.5} \, [NO_3^-]}{k_{3.6} \, [H_2O] \; + \; k_{3.5} \, [NO_3^-] \; + \; k_{3.7}[Cl^-]} + 1 \right) x \, V}{\omega \, S_A \, [N_2O_{5\,(g)}]} \qquad Eq3.10$$

$$= \frac{4}{\omega} \, x \, \frac{V}{S_A} \, x \, \frac{[N_2O_{5(aq)}]}{[N_2O_{5\,(g)}]} \, x \, k'_{3.4} \, x \left[1 - \frac{[H_2O] \; x \; k_{3.5} \, [NO_3^-]}{k_{3.6} \, [H_2O] \; + \; k_{3.5} \, [NO_3^-] \; + \; k_{3.7}[Cl^-]} \right] \qquad Eq3.11$$

The Henry's law coefficient (K_H) is defined as the ratio of the partial pressure of a chemical compound in the air to concentrations of that compound in liquid at constant temperature. Thus $\frac{[N_2O_{5aq}]}{[N_2O_{5g}]} = K_H$

The N_2O_5 reaction with particle containing water (R3.4) can be proceed in the presence of water in the particle, otherwise R3.4 will be suppressed by containing nitrate ions. Therefore, the rate constant ($k_{3.4}$) of the reaction R3.4 is determined as a function of H_2O_l to trace the H_2O_l limitation that was observed in the nitrate particles (NO_3^-), and defined as defined as $k'_{3.4}$.

The mean measured value in the experiment by Thornton, for $K_{H_{N_2O_5}}$ and $\frac{V}{S_A}$ were 51 and 3.75×10^{-8} m respectively.

The rate constant of R3.4 reaction ($k_{3.4}$), $k_{3.6}/k_{3.5}$, and $k_{3.7}/k_{3.5}$ were estimated quantitatively. The value of $k_{3.4}$ was calculated as a function of H_2O_l effect, using an uncertainty- weighted least square fit: $k'_{3.4} = \beta - \beta. \exp^{(-\delta \, [H_2O_l]}$ Eq3.12

where, β represents the slope between $k_{3.4}$ and H_2O_l, which is calculated to be $1.15 \times 10^6 \pm 3 \times 10^5 \, s^{-1}$, and δ is the uncertainty, determined to be $1.3 \times 10^{-1} \pm 5 \times 10^{-2} \, M^{-1}$.

For solid particles, the value of $k'_{3.4}$ was assumed to be zero.

$\frac{4}{\omega} * \frac{V}{SA} * K_H$ was calculated by Bertram and Thornton (2009) to be 3.2×10^{-8} s and designated by *A* (an empirical pre-factor). To recall that ω is the mean speed of the

molecule N_2O_5 (ms^{-1}), v is total particle volume concentration (m^3 m^{-3}), S_a is the total particle surface area concentration (m^2 m^{-3}), and K_H is Henry's law coefficient ($K_H =$ [N_2O_{5aq}] / [N_2O_{5g}])

The final equation will be:

$$\gamma_{N_2O_5} = A \cdot k'_{3.4} \left(1 - \frac{1}{\frac{k3.6[H2O(l)]}{k3.5[NO3^-]} + 1 + \frac{k3.7[Cl^-]}{k3.4[NO3^-]}} \right)$$ Eq 3.1

The ratios of $k_{3.6}$ to $k_{3.5}$ and $k_{3.7}$ to $k_{3.5}$ have been estimated to be 0.06 ± 0.01 and 29 ± 6 respectively.

The $\gamma_{N_2O_5}$ is determined as a function of the ratio between $H_2O_{(l)}$ and NO_3^- and Cl$^-$ to NO_3^- ·Bertram and Thornton (2009) suggest that these three components in aerosol are controlling $\gamma_{N_2O_5}$. For example, the presence of chloride in aerosol enhances the N_2O_5 uptake and results in the formation of $ClNO_2$ which alternatively, may be suppressed by the increase of NO_3 content in the aerosol (Morgan et al. 2012). In general the value of uptake coefficients (γ) varies greatly according to the particle chemical composition, relative humidity (RH), aerosol water content, and temperature (Chang et al., 2011; Wagner et al., 2013).

For instance, $\gamma_{N_2O_5}$ is observed to be reduced at:

-   Lower relative humidity (Thornton et al., 2003) and lower water content in aerosol because the molecules of N_2O_5 can not dissociate to NO_2^+ and NO_3^- if there is not enough water content in the particle (Mentel et al., 1999).
-   High concentration of nitrate ions (NO_3^-) within the aerosol (Mentel et al., 1999).
-   High temperature associated with more evaporation, thus less liquid results in a lower N_2O_5 uptake coefficient.

The N_2O_5 uptake coefficient ($\gamma_{N_2O_5}$) has been measured in the laboratory on aerosol surfaces, water droplets, and ice surfaces. The value of $\gamma_{N_2O_5}$ on sea salt particles range between 0.006 to 0.04 at RH of 30% and 77% respectively. The value of $\gamma_{N_2O_5}$ calculated by the model in this study is 0.035, which is close to the upper limit of the range (0.04). The concentration of water, nitrate and chloride used in this study is explained in the following sections:

3.2.1 Chloride ion concentration in aerosol

Chloride ions (Cl$^-$) are produced mechanically mainly in coastal areas from the evaporation of sea spray as a result of evaporation or wind induced wave breaking. In urban areas chloride forms mainly from a road deicing salt during the winter months (Harrison and Yin, 2004; Thornton et al., 2010). Chloride particulate may be also produced from gaseous hydrochloric acid (HCl) emissions, mainly from combustion sources, particularly from the coal power stations and incinerators (Harrison et al.,1999).

Moreover, chloride can form as a secondary product in the form of ammonium chloride in fine mode from the reaction of ammonia with HCl, however, ammonium chloride (NH_4Cl) is highly volatile, thus exists in tiny amounts in aerosol (Harrison and Yin, 2004).

The abundance of Cl from NaCl is very likely to exist in urban areas as it is influenced by transport of NaCl from coastal areas, also from the road spray of NaCl during the winter and due to less direct HCl emissions as mentioned in the previous paragraph, this study will consider NaCl as a main source of Cl. According to The Airborne Particles Expert Group, APEG (1999), chloride (in the coarse mode) of marine origin accounts for nearly 75% of total UK chloride, particularly from the sea salt. Non-marine chloride arises anthropogenically from road spray of NaCl (in coarse mode) during the cold and dry weather in winter. Typical concentration of chloride in aerosol is estimated at 1 - 3 μgm^{-3} (Harrison and Jones, 1995).

 In Birmingham the mean concentration of chloride ions in PM_{10} measured over six months in four seasons of 1995-1996 was 1.9 $\mu g\ m^{-3}$ with a minimum and maximum concentration of 0.7 $\mu g\ m^{-3}$ and 3.6 $\mu g\ m^{-3}$ respectively (Turnbull and Harrison, 2000). Furthermore, in a study conducted by Laongsri (2012), in Birmingham, chloride ions in coarse ($PM_{2.5-10}$) and fine ($PM_{2.5}$) particle mode were about 0.83 ± 0.03 $\mu g\ m^{-3}$ and 0.73 ± 0.02 $\mu g\ m^{-3}$ respectively mainly attributed to the influence of anthropogenic sources such as re-suspension of sea salt on the road. Recently, Sommariva, et al., (2018) measured 1.49 $\mu g\ m^{-3}$ of mean daily concentration of chloride ions in PM_{10} in Leicester over August in 2014. This value (1.49 $\mu g\ m^{-3}$) has been used in this study for the calculation of N_2O_5 uptake coefficient, to estimate $ClNO_2$ yield.

3.2.2 Aerosol water content estimation using a single hygroscopicity parameter kappa

Atmospheric particles absorb or lose water as the ambient relative humidity changes to retain in thermodynamic equilibrium with the ambient environment (Walker et al., 2011). The ability of atmospheric aerosol particles to uptake water and form a liquid droplet or activate to a cloud condensation nucleus (CCN) as a function of chemical composition of particles and relative humidity is called aerosol hygroscopicity.

Atmospheric aerosol particles may show a hysteresis behaviour in the process of absorbing water (Sjogren et al., 2007) (Figure 3.2). Upon hydration, a solid (soluble) particle absorbs water and dissolves to make a saturated aqueous droplet at a certain relative humidity called the deliquescence relative humidity (DRH). Whereas, during dehydration (decreasing relative humidity) the water evaporates and the solute crystallizes at a lower relative humidity (the Efflorescence Relative Humidity, ERH) than the DRH (Mikhailov et al., 2009). Figure 3.2 illustrates the hysteresis behaviour of NaCl.

Atmospheric soluble solid substances have a DRH of higher than 50% (Mikhailov et al., 2009). If the relative humidity further increases, additional water condenses onto the salt solution to maintain a thermodynamic equilibrium. Sea salt mainly composed of sodium chloride (NaCl), exists as dry particles at low RH (Randles et al, 2004), and with increasing RH the particle grows in size.
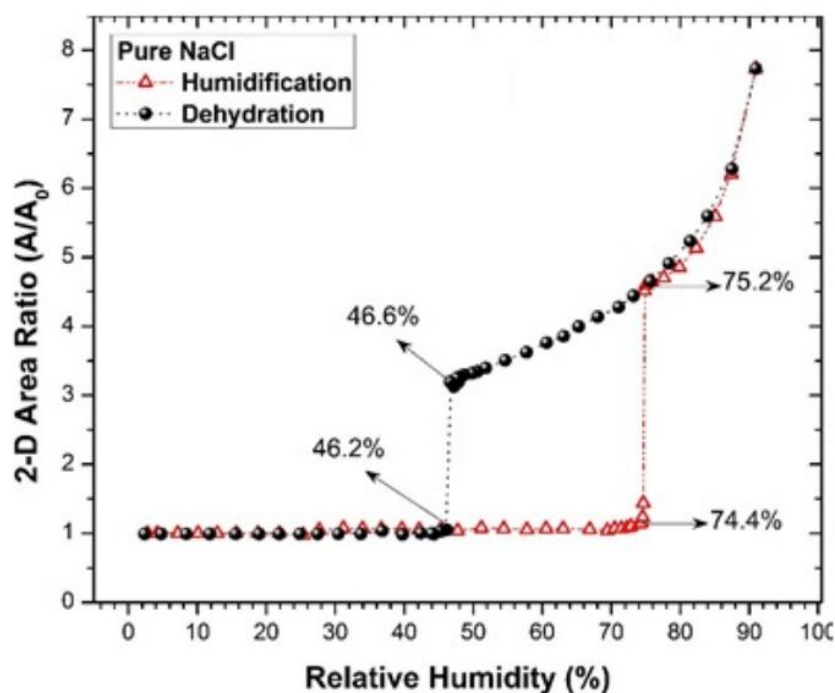
Figure 3. 2 Hysteresis behaviour in terms of deliquescence and crystallization as a function of relative humidity illustrated for a pure NaCl particle. The particle size on the Y-axis was determined via measuring the two-dimensional (2-D) surface area (the ratio between the areas of the particle at a given RH to the area of the particle before starting the hydration process (Gupta et al., 2015). Humidification, ---△--- (increasing RH from ~ 3% to ~ 95%), and ---●--- dehydration (decreasing RH from ~95% to ~3%).

A single parameter (called kappa (k)) represents the Kohler theory describes the hygroscopicity behaviour of atmospheric aerosol particles; k represents a quantitative measure of the ability of aerosol particle to absorb water (Friedman et al, 2013, Petters and Kreidenweis, 2007). Values of kappa vary according to the chemical composition of the aerosol particles. Atmospheric particles, depending on their chemical composition can uptake water at relative humidity < 100% (Stock et al., 2011). For highly soluble (hygroscopic) substances such as NaCl, the typical value of kappa can reach as high as 1.4, however, for less hygroscopic substance, kappa can range 0.01 to 0.05, or even zero for a non-soluble (non hygroscopic) compounds (Petters and Kreidenweis, 2007).

Inorganic salts, mainly ammonium sulphate and sodium chloride in aerosols are highly hygroscopic and can activate into a cloud condensation nuclei, CCN (aerosol particles serve as the nuclei of the atmospheric cloud droplet) at the diameter around 100 nm in supersaturation conditions (RH > 100%) (Sullivan et al. 2009).

The hygroscopic properties of aerosol particles can be modelled by k-Köhler theory which presents the equilibrium relationship between water vapour saturation ratio (ambient relative humidity) and the size of aerosol particle (Topping and McFiggans, 2012).

The Köhler equation proposed by Petters and Kreidenweis (2007) combines water activity and relative humidity via equation Eq3.13:

$$RH = \alpha w \exp\left(\frac{4\sigma_{s/a M_w}}{RT\rho_w D}\right) \qquad\qquad Eq3.13$$

The activity of water (αw) is the ratio of the water vapor pressure (p_w) above the particle to saturation vapor pressure ($p\circ_w$). If the particle is at equilibrium with its ambient environment, the water activity of the solution would be equal to the relative humidity divided by 100 (RH/100) in scale 0.0 to 1.0, which simplifies the equilibrium calculations for atmospheric aerosol, as the water activity for all liquid aerosol solution would be fixed for each RH (Seinfeld and Pandis, 1998; Kreidenweis et al., 2008),

$$\alpha w = \frac{P_w}{P_w^\circ} = \frac{RH}{100} \qquad\qquad Eq3.14$$

Petters and Kreidenweis (2007) parameterized water activity as a function of the hygroscopicity parameter (kappa, k) and the volume of the dry particle (solute, V_s) and the wet particle (V_w):

$$\frac{1}{\alpha w} = 1 + k\,\frac{V_s}{V_{w\,(RH)}} \qquad\qquad Eq3.15$$

The volumes can be presented by their volume equivalent diameters; the volume of dry particle and water can be determined by $Vs = \frac{4}{3}\pi.\,r_s^3$ and by $Vw = \frac{4}{3}\pi.\,r_w^3$ respectively. The Köhler equation can be expressed by combining equations Eq 3.13 and Eq 3.15 as expressed below:

$$S_D = \alpha w = \frac{RH}{100} = \frac{D^3 - D_d^3}{D^3 - D_d^3\,(1 - kappa)}\;exp\left(\frac{\frac{4\sigma_s}{a M_w}}{RT\rho_w D}\right) \qquad\qquad Eq3.16$$

where, $S_{(D)}$ is the water vapor saturation ratio (RH/100), $\sigma s/a$ is the surface tension of the solution droplet per air interface = 0.072 J/m^2 , Mw is the molecular weight of water, R is the universal gas constant= 8.314 J/ K. mol, T is temperature = 298.15 K, ρw is the density of water=1000kg m^{-3}, and D_d and D represent the diameter of the particle in dry condition (RH=0) and wet diameter in a humidified environment respectively.

The density and hygroscopicity parameter (kappa, k) derived from Petters and Kreidenweis (2007) of some dry particles have been summarized in the table 3.1.

Table 3. 1 Physical properties of some dry inorganic components [Adapted from Kreidenweis et al., 2008]. The compounds presented in the table are: sodium chloride (NaCl), ammonium sulphate ($(NH_4)_2SO_4$), ammonium nitrate (NH_4NO_3), sodium sulphate (Na_2SO_4), black carbon (BC)

Compound	Density (g/cm^3)	Kappa	DRH% (298.15K)
NaCl	2.17	1.28	75.3
$(NH_4)_2SO_4$	1.70	0.61	80.2
NH_4NO_3	1.72	0.67	62.1
Na_2SO_4	2.66	0.80	84.2
BC	2.0	0	
Dust	2.65	0	

The aerosol water content for different kappa values was calculated as shown in Table 3.2. It can be seen that the aerosol water content value depends on RH and kappa value. For example, maximum aerosol water content (50.84 M) is recorded when RH is 90% and kappa is 1.2. However minimum water content (21.72) is recorded when RH is 65% and kappa is 0.36.

Table 3. 2 Summarise estimated water content in aerosol using different values of kappa and relative humidity

RH%	Kappa	[H$_2$O] M	Particle
90	1.2	50.84	PM10
90	0.36	42.22	PM10
90	0.36+0.16	45.55	PM10
90	0.36- 0.16	35.65	PM10
65	0.36	21.72	PM10
75	1.28	44.07	PM10

In this study the aerosol water content calculations were incorporated into the model framework via using equation Eq3.16. The water content was calculated for PM_{10} particle, which assumed to be a sphere. In addition, a dry diameter of 200 nm has been selected to apply in the Kohler equation because within urban areas most particles, in terms of surface area which is an important factor for the heterogeneous reaction is found mostly within the accumulation mode (diameter: 100nm -1µm) (Vu et al., 2015, Jacob, 2000) especially within the range 100-500nm (Seinfeld and Pandis 1998) as shown in Figure 3.3 Finally, the relative humidity value used in the calculation is assumed to be 90%.
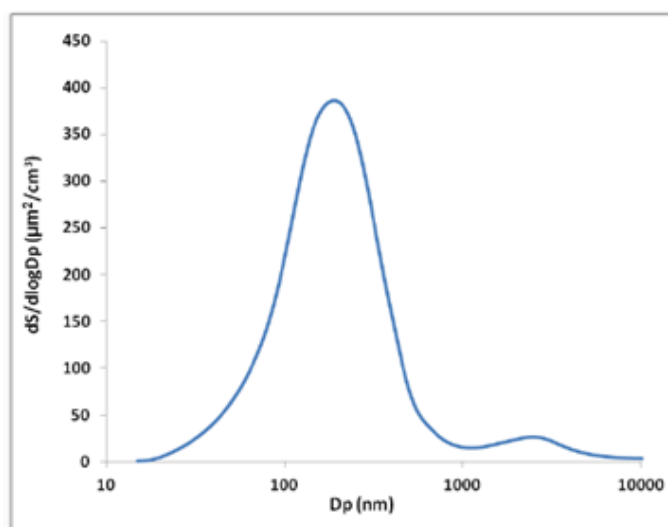
Figure 3. 3 Particle distribution in terms of surface in an urban background in North Kensington, London during 24th-29th July 2012 (Vu et al., 2015)

3.2.3 The heterogeneous reactions of N_2O_5 with aerosol

Previous studies considered the formation of HNO_3 as the only chemical path of the heterogeneous reaction between N_2O_5 with aerosol (Chang et al., 2011) until 2006 when the high quantity of $ClNO_2$ (about 1ppb) was observed in a field campaign in Houston (Osthoff et al., 2008).

As N_2O_5 chemistry has many paths, it is important to know which path is more likely to occur under different atmospheric conditions. The gas phase reaction of N_2O_5 with H_2O (both bi and termolecular components) is slow (R3.1 and R3.2), with rate constants of around 2.7×10^{-22} cm^3 molecule^{-1} s^{-1} and 1.8×10^{-39} cm^3 molecule^{-1} s^{-1} respectively (Wahner

et al., 1998, George et al., 1994). The hydrolysis of N_2O_5 in the aqueous phase (reaction of N_2O_5 on wet surfaces, meaning with water on the surface of aerosol, in aerosol containing water or in cloud droplet) occurs sufficiently fast (R1.35) (Wahner et al., 1998) which is considered as the main source of HNO_3 formation in the atmosphere at night because the gas phase reaction of OH with NO_2 is the main source of HNO_3 during the daytime.

$$N_2O_{5(g)} + H_2O_{(l)aerosol} \rightarrow 2HNO_{3(aq)} \qquad\qquad R1.35$$
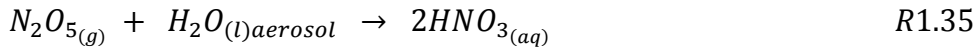
The pseudo first-order rate constant of N_2O_5 reaction with aerosol containing chloride is calculated in this study to be around 2×10^{-6} s^{-1} for ambient temperature of 287.5 K, aerosol surface area of 1×10^{-6} cm^2 cm^{-3}, and uptake coefficient of 0.034.

The uptake coefficient of N_2O_5 on aerosol is uncertain as it depends on many factors, including aerosol composition, relative humidity, and temperature (Brown et al., 2006, Chang et al., 2011, Bertram et al., 2009).

The atmospheric lifetime of N_2O_5, which is longer than that for NO_3 ranges between a few minutes in a humid environment to days in a dry environment (Brown and Stutz, 2012), depending mainly on:

(i) Relative humidity

In a humid environment (80% RH) and a temperature of 25℃ the lifetime of N_2O_5 may not exceed 20 minutes (Brown and Stutz, 2012) due to the homogeneous and heterogeneous exceed 20 minutes (Brown and Stutz, 2012) due to the homogeneous and heterogeneous hydrolysis of N_2O_5. As stated before, the heterogeneous hydrolysis of N_2O_5 on a surface of the particle is more rapid than the homogenous gas phase reaction of N_2O_5 with water vapour, which is the main loss of NO_3, and N_2O_5 in the atmosphere and the major source of HNO_3 in the atmosphere:

At low RH, below the deliquescent point (< ~75% RH), the surface of a solid particle surrounded by a thin halo of water as the water is only wetted the particle (Wise et al., 2008). Therefore, the uptake coefficient of N_2O_5 on a particle ($\gamma_{N_2O_5}$) before the deliquescent point is relatively small (Escorcia, 2010), hence, the lifetime of N_2O_5 would be rather long. For instance, the lifetime of N_2O_5 can be longer in a condition of

relative humidity less than 50%, mainly because a thin layer of water or liquid is available for N_2O_5 to react, hence the salt particles would be relatively dry (Atkinson et al., 1986).

(ii) Temperature

The atmospheric lifetime of N_2O_5 decreases with increasing temperature. For instance, at a temperature around 270K the N_2O_5 lifetime is ~700 s, which decrease to ~ 40 s at a higher temperature of around 290K due to thermal decomposition of N_2O_5 (Brown and Stutz, 2012) which mostly occur in the morning with the sunrise (Wood et al., 2005).

The low temperature of winter and high concentration of NO_x, in several areas of the Northern Hemisphere shifts the $N_2O_5 - NO_3$ equilibrium to N_2O_5 as observed by Sarwar et al., (2014) and because of the long night of winter, more N_2O_5 accumulates as at low temperatures the rate of thermal dissociation of N_2O_5 to NO_3 and NO_2 is reduced (Brown and Stutz, 2012), hence more $ClNO_2$ production is predicted (Sarwar et al., 2014). Therefore, the reaction of N_2O_5 with NaCl, thus, $ClNO_2$ production might be more significant in colder regions (Finlayson-Pitts et al. 1989).

Here, we have calculated the equilibrium rate constant (k_{eq}) of N_2O_5-NO_3 at different temperature ranging between 284 to 292 K (11 – 19 ℃), using the equation Eq 3.17 (Brown and Stutz, 2012). From Figure 3.4, it can be noticed that the maximum rate coefficient of the N_2O_5 formation is occurring at lower temperature (284 K), the rate is declining as the temperature increases to reach its minimum value around 290K.

$$keq = 5.50x10^{-27} \exp\left(\frac{10724}{T}\right) \qquad\qquad Eq3.17$$
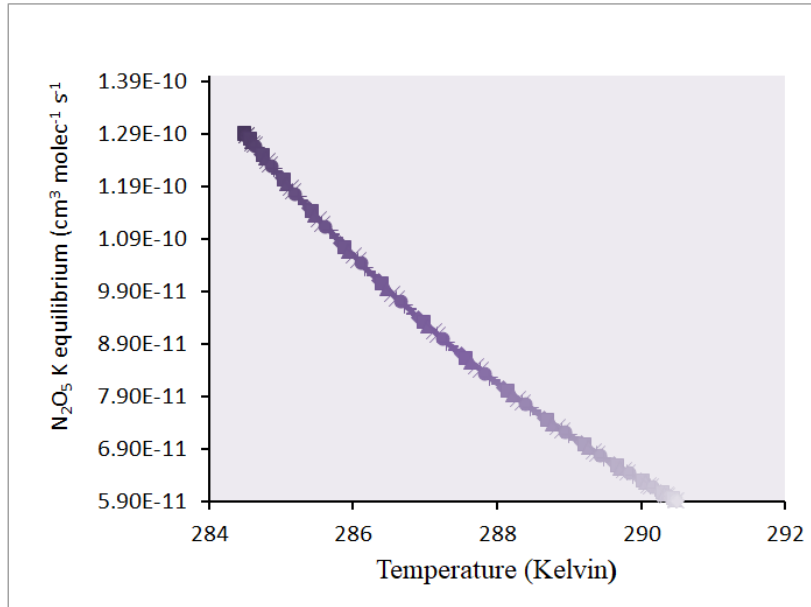
Figure 3. 4 Calculated the equilibrium rate constant of N_2O_5-NO_3 as a function of temperature
$[N_2O_5] = keq\ [NO_2][NO_3]$

(iii) Photolysis

The cold temperature in the stratosphere makes thermal decomposition of N_2O_5 insignificant; rather the photolysis of N_2O_5 in the daytime at wavelengths below 400 nm (R 3.8) becomes a significant process for removing N_2O_5 in the atmosphere and releasing NO_x (Brown and Stutz, 2012). In the stratosphere, the lifetime of N_2O_5 is in the range of months to years (Brown and Stutz, 2012).

$$N_2O_5 + hv\ (\lambda < 400\ nm)\ \rightarrow\ NO_3 + NO_2 \qquad\qquad R3.8$$
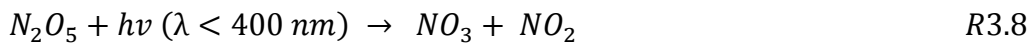
In the troposphere, the photolysis of N_2O_5 is too slow (Brasseur et al., 1999), however, at sunrise the mixing ratio of N_2O_5 rapidly decreases to nearly zero due to the rapid photolysis of NO_3 which is in thermal equilibrium with N_2O_5 (Kim et al., 2014).

(iv) Aerosol composition

The lifetime of N_2O_5 varies from a few minutes if the dominant aerosol composition is highly hygroscopic components such as inorganic salts (example: sea salt or sulphate) to days with a prevailing organic aerosol environment (Brown and Stutz, 2012).

(v) Aerosol surface area

Alongside with high relative humidity, sufficient aerosol surface area can limit the atmospheric lifetime of N_2O_5. A study carried out by Brown et al. (2009), indicated that the lifetime of N_2O_5 was relatively short in the environment with large aerosol surface area. The reason is that more surface area means more surfaces available for the reaction of N_2O_5 to take place, thus more loss of N_2O_5. Therefore, the loss of N_2O_5 is linearly proportional to the aerosol surface area.

3.2.4 Yield of $ClNO_2$

The yield of $ClNO_2$ ($\emptyset_{ClNO_2}$) from the reaction of N_2O_5 with aerosol has been measured in laboratory by passing a specific quantity of N_2O_5 over a wet NaCl bed in a tube containing N_2 or ambient air, the result was a 100% (1.0) yield of $ClNO_2$ which was calculated from the loss of N_2O_5 (Finlayson-Pitts et al., 1989, Behnke et al., 1997, Kercher et al., 2009).

The $\emptyset_{ClNO_2}$ can be determined by the efficiency of $ClNO_2$ formation from the N_2O_5 heterogeneous reaction with an aerosol particle (Riedel et al., 2014). Therefore, it is the competition of whether the intermediate H_2ONO_2 reacts with $H_2O_{(l)}$ forming HNO_3 (R3.5) or H_2ONO_2 reacts with Cl^- and producing $ClNO_2$ (R3.7). According to Behnke et al. (1997), Bertram and Thornton (2009), Roberts et al. (2009), and Sarwar et al. (2014), the yield of $ClNO_2$ from the uptake of N_2O_5 upon aerosol depends mainly on Cl^- abundance in the particle and the particle's liquid water content $[H_2O_{(l)}]$ which is expressed via the equation Eq 3.18,

$$\emptyset_{ClNO_2} \; or \; \gamma = \frac{k_{3.7}[H_2ONO_2^+][Cl^-]}{k_{3.7}[H_2ONO_2^+][Cl^-] + k_{3.6}[H_2ONO_2^+][H_2O]} \qquad Eq3.18$$

$$= \frac{[H_2ONO_2+](k_{3.7}[Cl^-])}{[H_2ONO_2+](k_{3.7}[Cl^-]) + k_{3.6}[H_2O]\}} = \frac{1}{1 + \frac{k_{3.6}[H_2O]}{k_{3.7}[Cl]}} \qquad Eq3.19$$

Where, the ratio between $k_{3.6}$ and $k_{3.7}$ determined by Bertram and Thornton (2009) to be 483 ± 175 while Roberts et al. (2009) estimated a constant of 485:

$$\emptyset_{ClNO_2} = \frac{1}{1+\frac{[H2O(l)]}{483[Cl^-]}}$$
$$Eq3.20$$

The above equation is based on the probability of whether N_2O_5 reacts with H_2O to form HNO_3 or reacts with Cl^- forming $ClNO_2$.

The reaction of N_2O_5 with aqueous particles containing Cl^- is rapid with $\gamma_{N_2O_5}$ about 0.03, and the yield of $ClNO_2$ approached 100% when Cl^- concentration is more than 4mole (Behnke et al., 1997, Thornton and Abbatt, 2005). Nevertheless, Bertram and Thornton (2009) observed the increasing of $\gamma_{N_2O_5}$ with increasing $[Cl^-]$ and the yield of $ClNO_2$ approaches 100% with $[Cl^-]$ as low as 1mole. As reported by (Brown and Stutz, 2012), the reaction of $NO_2^+_{(aq)} + Cl^-_{(aq)} = ClNO_{2(aq)}$, is nearly 450-480 times more rapid than

$NO_2^+_{(aq)} + H_2O_{(l)} = HNO_{3(aq)} + H^+_{(aq)}$, thus, existing a small amount of Cl^- in aerosol results in a large yield of $ClNO_2$.

3.2.5 The rate constant of ClNO$_2$ formation

The pseudo first-order heterogeneous rate constant (rate of N_2O_5 uptake coefficient) of the irreversible N_2O_5 loss from gas phase to aerosol due to the reaction on the surface of the aerosol or in the condensed phase is expressed by equation Eq 3.6 (Ravishankara, 1997):

$$k_{N_2O_5} = \frac{\gamma_{N_2O_5}\,\omega\,S_A}{4} \qquad Eq3.6$$

Where, (γ) is the uptake coefficient of N_2O_5, which is defined as a fraction of a gas molecule undergoing collision with particle surfaces leading to loss of N_2O_5 from the gas-phase (Chang et al. 2011), S_A is the aerosol surface area density (cm^2 m^{-3}), and ω is the mean speed of the molecule N_2O_5 (ms^{-1}).

Within the model, the pseudo first-order heterogeneous rate constant of $ClNO_2$ and HNO_3 formation is calculated using the equations:

$$\frac{dClNO_2}{dt} = \frac{\emptyset\gamma_{N_2O_5}\,\omega\,S_A}{4}$$
$$Eq3.21$$

$$\frac{dHNO_3}{dt} = \frac{(1-\emptyset)\gamma_{N_2O_5}\,\omega\,S_A}{4} \qquad\qquad Eq3.22$$

Φ represents the yield of ClNO$_2$ or HNO$_3$. The aerosol surface area value used in this study is 1×10^{-6} cm^2 cm^{-3} which is within the range of $1\times10^{-6} - 4\times10^{-6}$ cm^2 cm^{-3} that was measured in the UK as part of the RONOCO (ROle of Night-time chemistry in controlling the Oxidising Capacity of the atmOsphere) project from July 2010 to January 2011 (Morgan et al., 2015).

3.3 Model validation

In order to evaluate the performance of the model, the modelled ClNO$_2$ formation has been compared with ClNO$_2$ measured by Chemical Ionization Mass Spectrometry (CIMS) in Leicester on August 2014 during the fieldwork performed by the University of Leicester at the AURN monitoring station located in the University campus (Figure 3.9) (Sommariva et al., 2018).

The data measured in Leicester are used in this study to establish the initial experimental conditions of the box model. The mean temperature (287.5 K), mean mixing ratios of NO, NO$_2$, O$_3$ (5.95, 10.93, and 20.45 ppbv) as shown in Figure 3.5, and mean concentrations of chloride, and nitrate particulate aerosol (1.49 and 3.57 μgm^{-3}) recorded over August 2014 in Leicester were used. The ten primary VOCs were integrated into the model with their initial mixing ratios taken from measurements during the TORCH campaign carried out in a rural area in Essex, UK in 2003 (Lee et al.,2006) (explained in Chapter 2.4.3). Detail of the model input data is listed in Table 3.3.
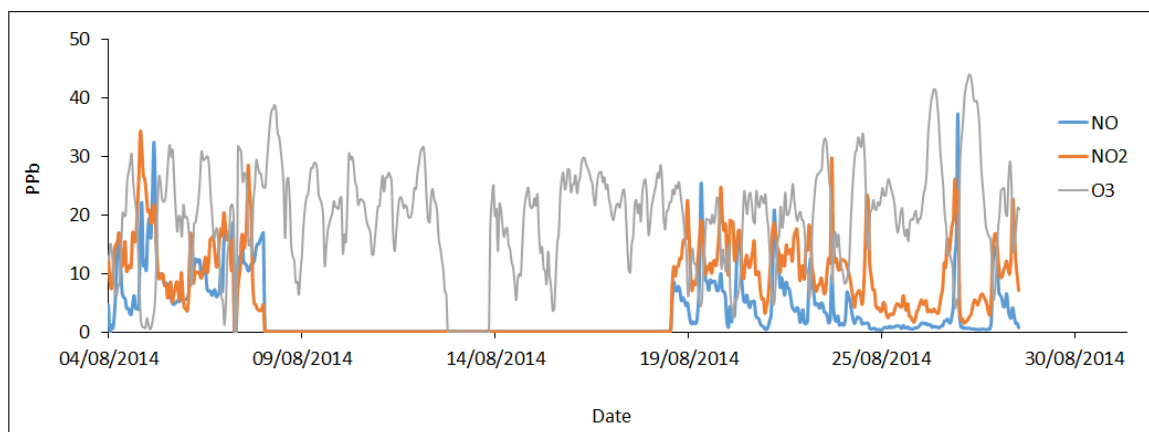
Figure 3. 5 Diurnal profile of NO, NO$_2$, and O$_3$ measured in Leicester during August 2014. Blue, orange, and the grey line represent NO, NO$_2$, and O$_3$ respectively. No data measured for NO and NO$_2$ during the period of 8th August at 7 am to 19th August at 11 am, and O$_3$ from 13th August at 7am to 14th August at 10 am.

Ambient ozone and nitrogen oxides (NO$_x$) emissions rate have been integrated into the model as this is important to sustain the key chemical species (OH, HO$_2$, NO, NO$_2$, O$_3$, and ClNO$_2$) in a steady state level. These species are assumed to be in a steady state level if the variations in their peak concentration remain < 5% for the whole model run period, which is 6 days in this study.

The amount of emissions (ENO$_x$) that has used in this study close to the emission rate (6.94x10^9 molec cm^{-3} s^{-1}) that was used by Bright et al. (2011) which was calculated for an urban major road (Bristol Road in Birmingham) by using the UK Road Vehicle Emission Factors, 2009. Vehicle emissions per kilometre driven were determined using vehicle speed emission factors, vehicle fleet composition data, and total activity. The number of vehicles per hour on the major road was rounded to the nearest 500 to become 1500 vehicles per hour, which represents moderate traffic flow for a 30 mile per hour speed limit (Figure 5.1).

Traffic is assumed to be the main source of NO$_x$ emissions in the model, and the primary emissions of NO and NO$_2$ were estimated to be 90% and 10% respectively, of the total NO$_x$ emissions. The 10% represents the lowest value of the estimated range (10-15%) of NO$_2$ primary emissions in London (Carslaw et al., 2011, Grice et al., 2009).

In urban areas, traffic volume often peaks during the weekday morning and evening due to the daily commute to and from work or school (Knibbs et al., 2011, Ragettli et al., 2013),

resulting in a greater emission of pollutants when compared to off-peak times or in rural areas (Hitchcock and Carslaw, 2016). Figure 3.6 shows typical average hourly distribution of traffic trips in the UK on weekdays and weekends during 1997-1999. During weekdays, driver's journeys peak in the morning and the afternoon, while travel during the weekend peak around middle of the day (Charlton and Baas, 2002).

Therefore, NO_x emissions peak for two hours during the morning and evening, i.e. during 'peak-rush hour' scenario is included in the model (Figure 3.7), that represents a typical emission condition in the UK urban areas during weekdays, i.e. when traffic activity is high.
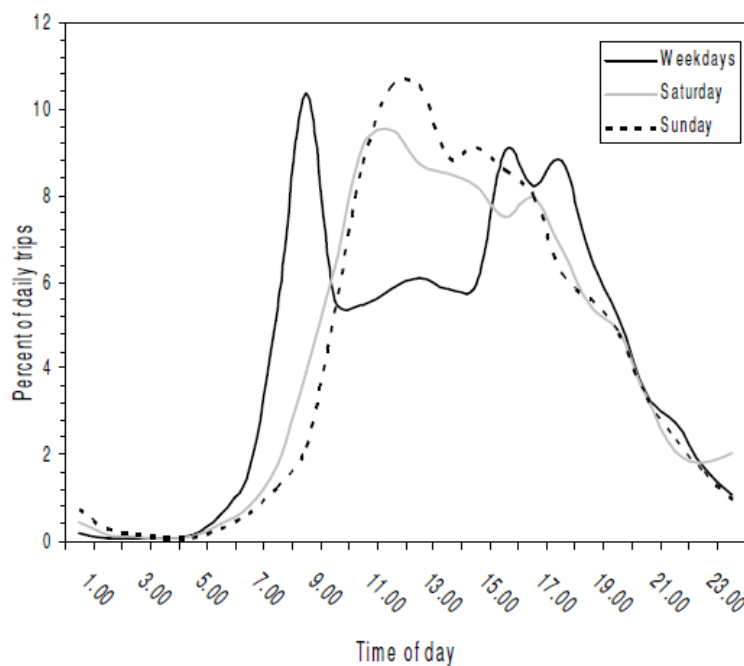
Figure 3. 6 Hourly distribution of traffic trips during weekdays, weekends in the UK (Charlton and Baas, 2002).
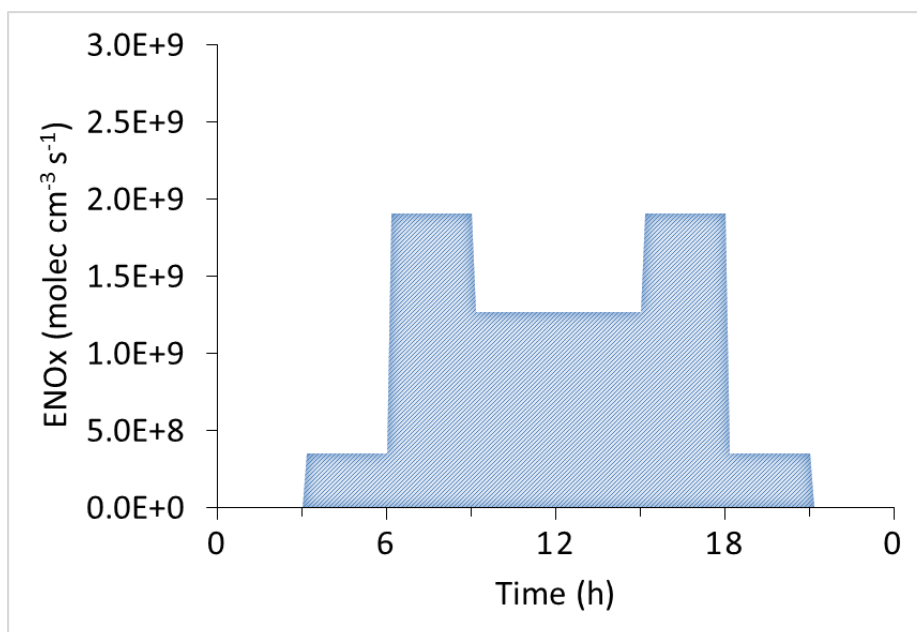
Figure 3. 7 Modelled NO$_x$ emissions scenario represents a typical emission condition in the UK urban areas during weekdays.

The model was simulated for a period of 6 days with a one-minute time step. The first 5 days used as a spin up period to minimize the effect of initial conditions on the concentrations of the output chemical species from the model simulation, as well as to allow the short/intermediate or long lived species like O$_3$ to reach a steady state level (Figure 3.8).
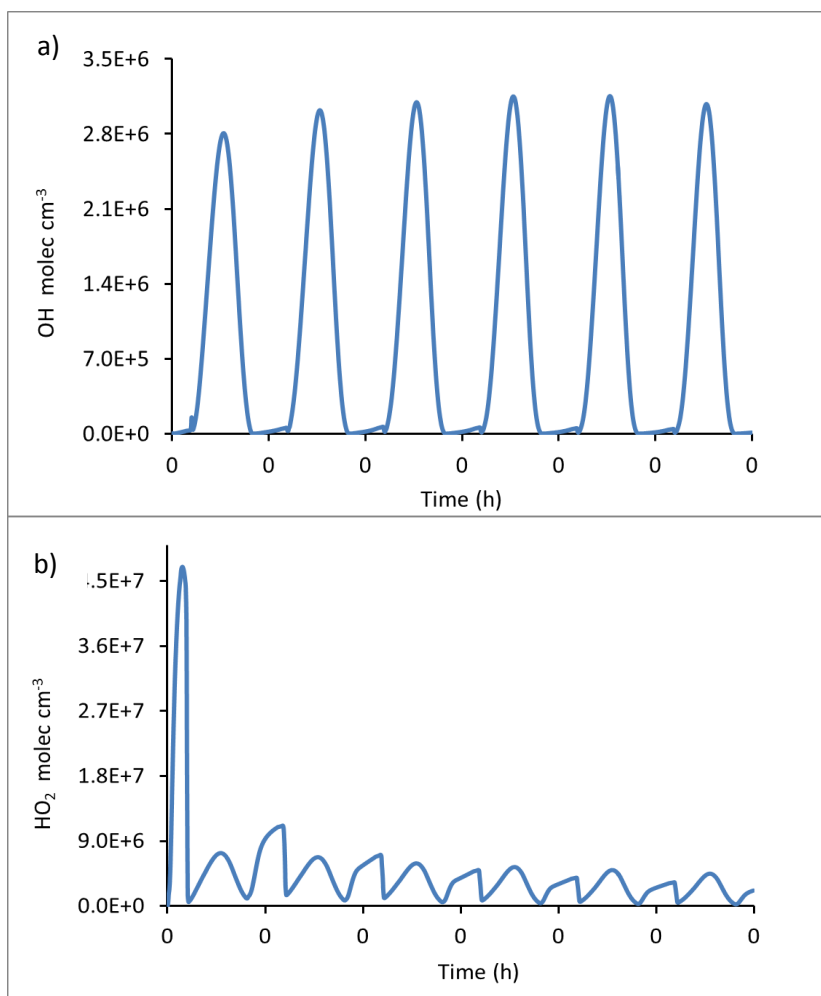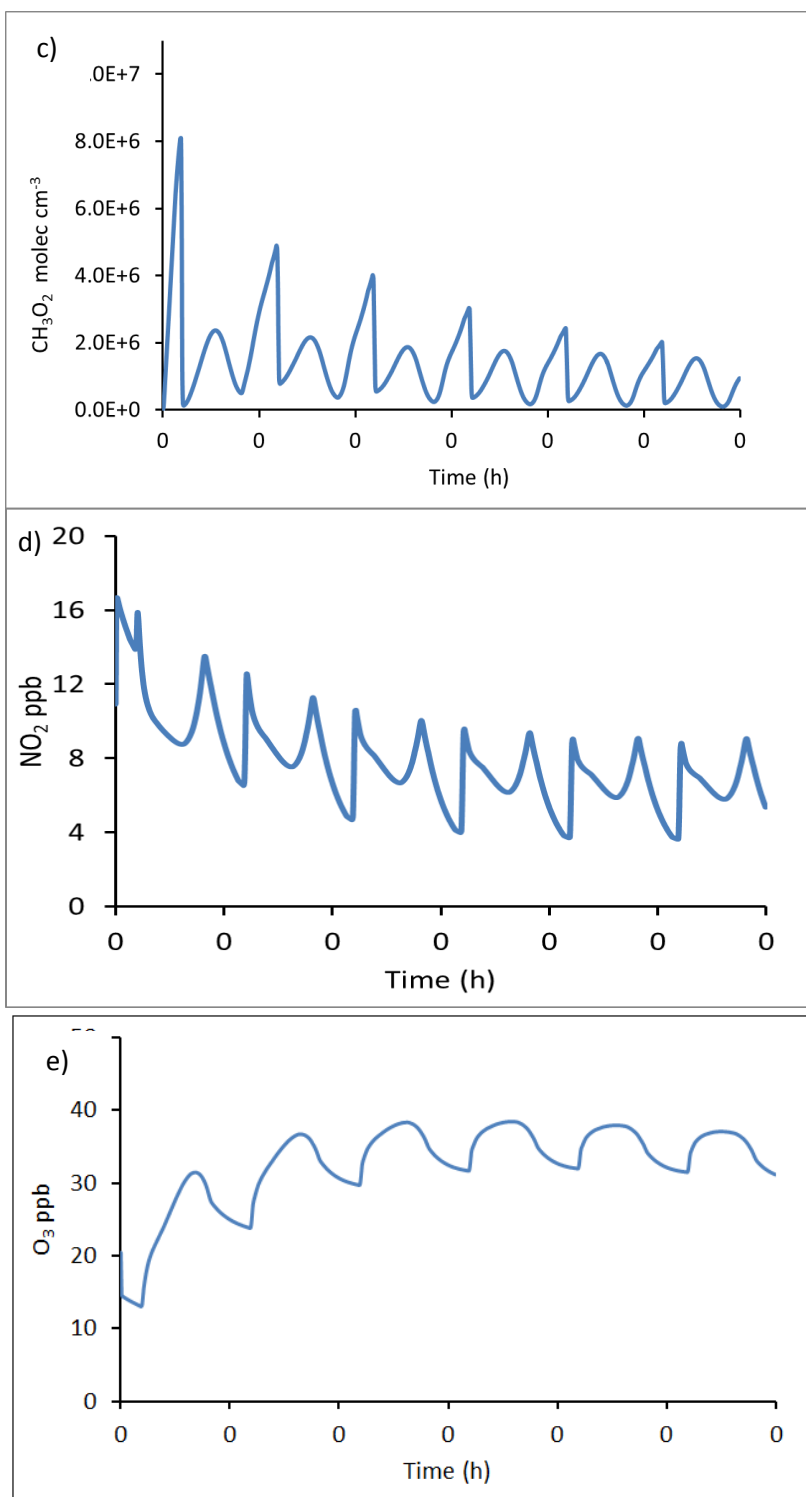
Figure 3. 8 Shows the concentrations of short lived species [a) OH, b) HO_2, c) CH_3O_2], intermediate and long lived species [d) NO_2, e) O_3] are in steady state level on the 6th day of the model simulation

Table 3. 3 Initial chemical and physical data applied to the box model

Chemical parameters	Chemical formula	Model input	Physical parameters	Model input
Nitric oxide	NO	5.95 ppb	Latitude	52° 62´ N
Nitrogen dioxide	NO_2	10.93 ppb	Longitude	-1°12 W
Ozone	O_3	20.45 ppb	Day	1
Methane	CH_4	1800 ppb	Month	8
Formaldehyde	HCHO	2898 ppt	Year	2014
Acetaldehyde	CH_3CHO	2750 ppt	Start time	12.0 Midnight (UTC)
Toluene	C_7H_8	506 ppt	Temperature	287.5 K
Mxylene	C_8H_{10}	243 ppt	Pressure	1013.25 hPa
Isoprene	C_5H_8	241 ppt	Ideal gas constant	$8.314\ J\,K^{-1}\,mol^{-1}$
Ethene	C_2H_4	844 ppt	Water vapour (H_2O)	2%
Propene	C_3H_6	266 ppt	Nitrogen (N_2)	78.09%
Methanol	CH_3OH	6813 ppt	Oxygen (O_2)	20.79%
Ethanol	C_2H_5OH	2185 ppt		
Acetylene	C_2H_2	711ppt		
Chloride aerosol	Cl	$1.49\ \mu g\ m^{-3}$		
Nitrate aerosol	NO_3	$3.57\ \mu g\ m^{-3}$		

The measured average $ClNO_2$ mixing ratio for the period from 20th to 28th August 2014 which peaked at ~60 ppt is compared with the modelled $ClNO_2$ (peaked at 112.86 pptv) (Figure 3.10A). Since data for NO, NO_2, and O_3 was not recorded before 20th August, thus the comparison is made for that period (20th to 28th August) only.

However, the modelled $ClNO_2$ mixing ratio which peaked at 112.86 pptv, is comparable with the measured $ClNO_2$ on the 10th August with the peak 114.97 pptv (Figure 3.10B).
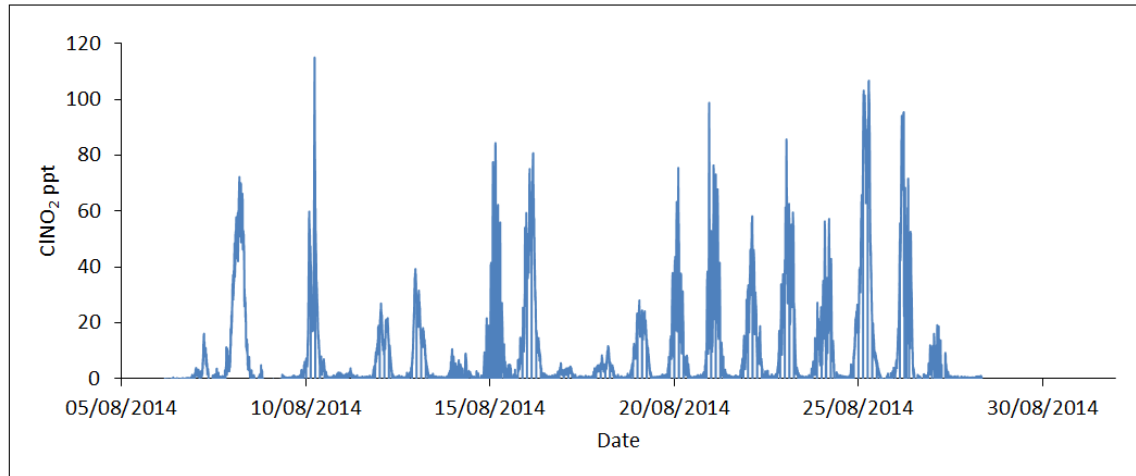
Figure 3. 9 Measured ClNO$_2$ mixing ratio in Leicester on the 10th August 2014 during fieldwork performed by the University of Leicester at the AURN monitoring station on the University campus (Sommariva et al., 2018).

As shown in Figure 3.10A and B, the modelled and measured ClNO$_2$ mixing ratios have relatively same pattern as both modelled and measured ClNO$_2$ peaked in the early morning, followed by almost complete depletion around 3pm as ClNO$_2$ is readily photolysis to release chlorine. The frequency distribution of the modelled and measured ClNO$_2$ was investigated and the result revealed that the modelled ClNO$_2$ has a same distribution (Right skewed) as the measured, with low ClNO$_2$ mixing ratio (< 10ppt) shows a high frequency in both cases (Figure 3.11).
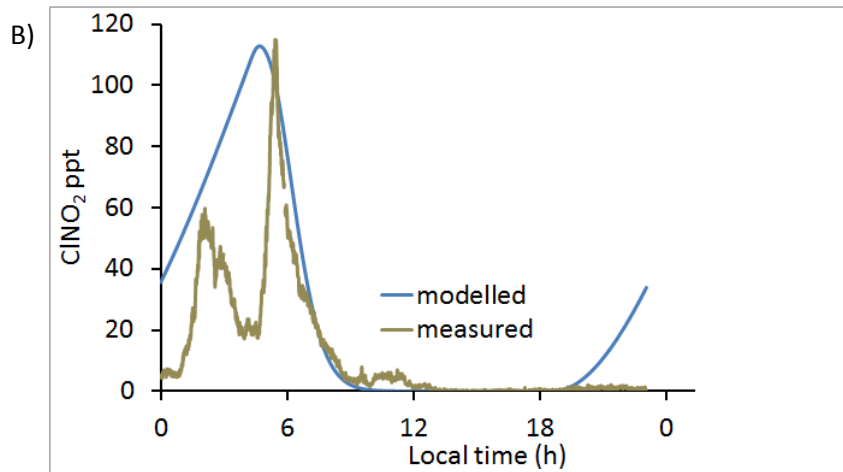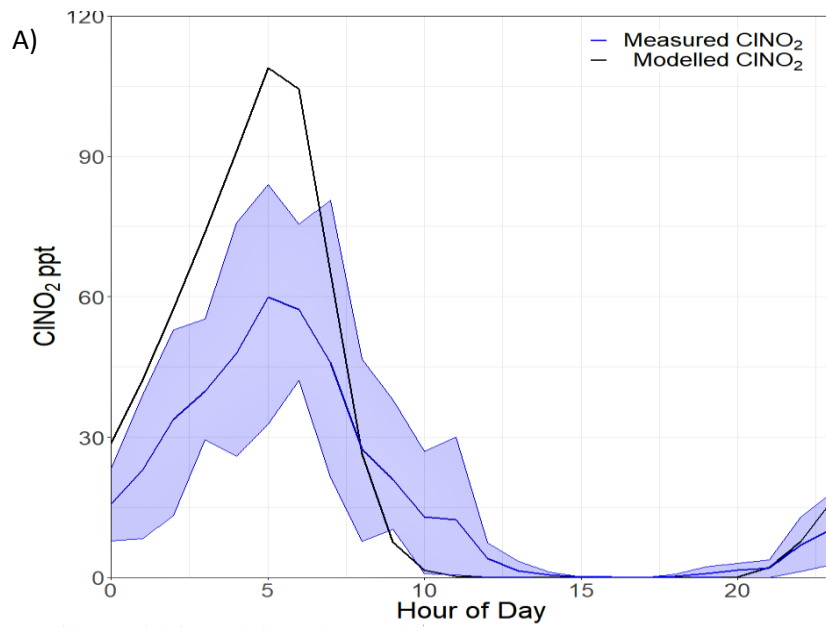
Figure 3. 10 A) Comparisons between modelled with mean measured ClNO$_2$ over 20-28th August 2014 in Leicester, and **B)** comparison between modelled and measured ClNO$_2$ on 10th August 2014 in Leicester
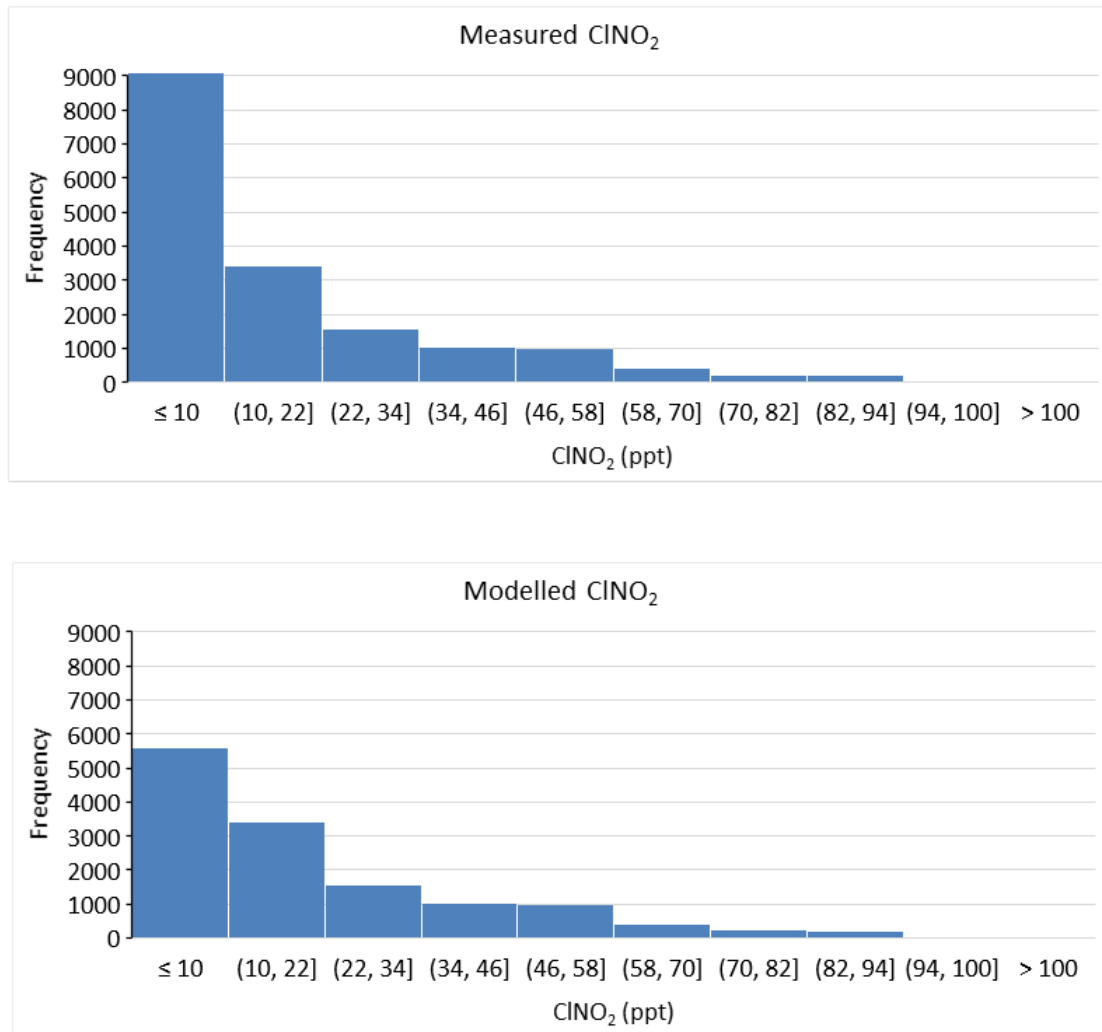
Figure 3. 11 Positive-Right-skewed distribution of modelled and measured (over the August 2014) $ClNO_2$.

The general discrepancies between modelled and measured $ClNO_2$ mixing ratios may be related to the variation in emissions or abundance of NO_x and VOC, which can affect NO_x, O_3, N_2O_5, and thus $ClNO_2$ concentrations. The differences could also be related to meteorological factors such as rainfall or wind speed, which can considerably affect the measurements (Oikonomakis et al., 2018). For example, there is a decrease in measured $ClNO_2$ from 4 to 5am of the local time and an increase in modelled $ClNO_2$ from 6pm which is not observed in the measurement (Figure 3.10B). According the weather station of Met Office (https://www.metoffice.gov.uk/climate/uk/summaries/2014/august), August 2014 was wet and the coolest August since 1992, with rainfall and showers almost every day.

Further to evaluate the model, the simulated and average measured NO, NO_2 and O_3 over August 2014 are compared (Figure 3.12). The model relatively well reproduced measured NO_2 and O_3, but not for NO as the modelled NO peaked at 3 ppb whereas the average measured NO peaked at ~13 ppb, which may be related to the difference in the amount of NO emissions between the model and measurement.
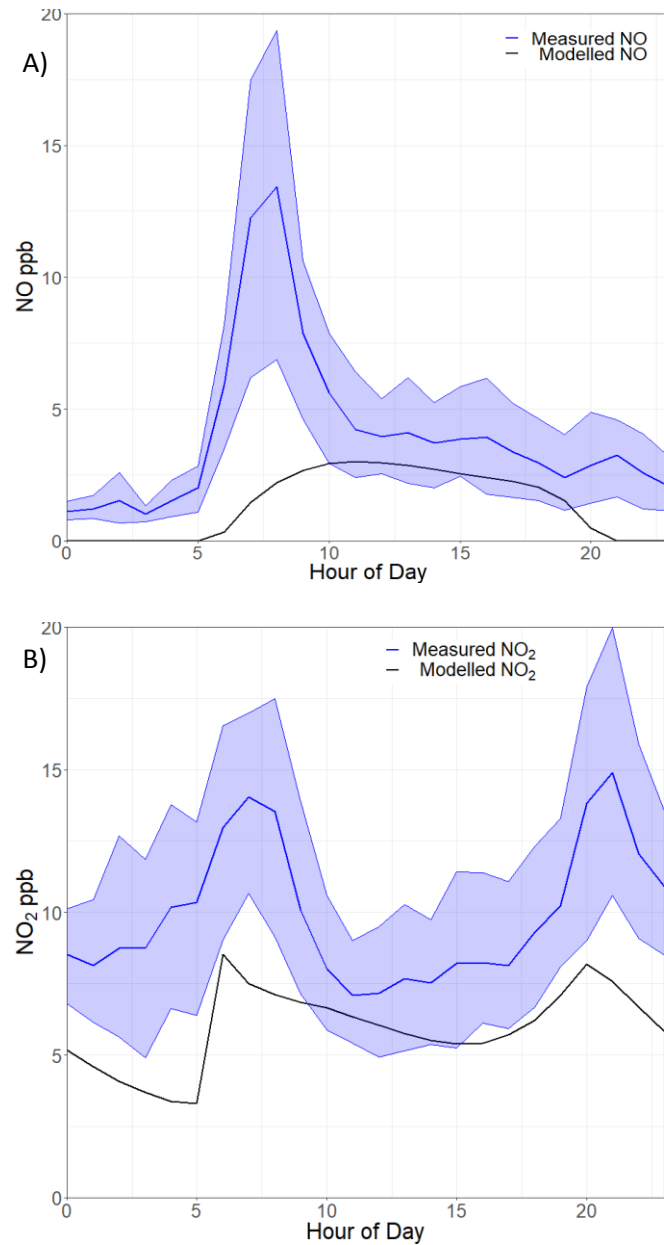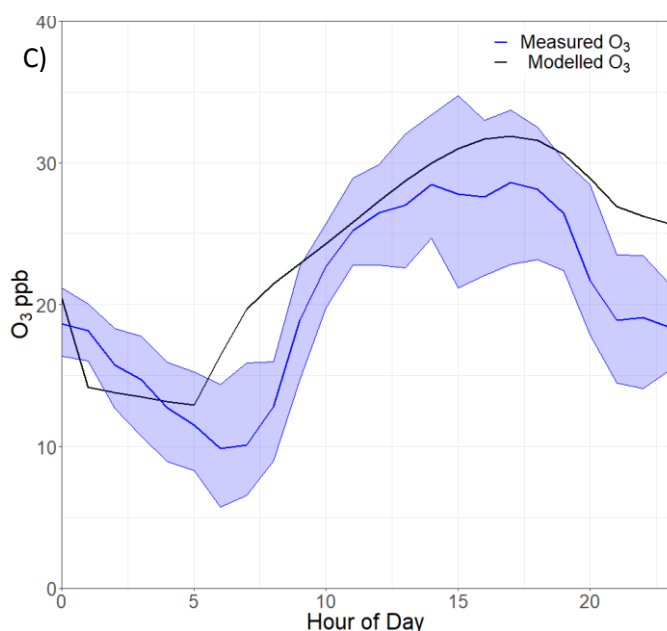
Figure 3. 12 Comparison between model diurnal with mean measured A) NO, B) NO$_2$. C) O$_3$ for the period $20 - 28^{th}$ August 2014 in Leicester

3.4 Chapter summary

The MCM box model has been developed to include parameters and reactions describe the N$_2$O$_5$ reaction with aerosol particles. Each single parameter that involved in the N$_2$O$_5$ heterogeneous reactions and ClNO$_2$ formation have been explained in detail, highlighting the main factors that can affect the atmospheric lifetime of N$_2$O$_5$.

The developed model (Chapter 2 and Chapter 3) has been evaluated against measurements to examine the accuracy of the model. The model and measurements are in good agreement for predicting ClNO$_2$ concentrations. Therefore, the model can be used to investigate N$_2$O$_5$ and ClNO$_2$ chemistry and to predict the concentrations of the chemical species in the atmosphere.

The following chapters of this thesis describe the use of the developed MCM box models for the investigation of effect of temperature on ClNO$_2$ formation and chemistry (Chapter 4), the effect of diurnal emission distribution from traffic on the concentrations of the atmospheric chemical species (Chapter 5), and finally to predict the nitrate aerosol formation from N$_2$O$_5$ heterogeneous reactions in the atmosphere.

Chapter 4 Impact of temperature on the formation of ClNO$_2$ in current and 2050s urban atmosphere

In this chapter, the influence of temperature upon the production and impact of ClNO$_2$ chemistry on air quality was examined, as this is of particular importance in future climate with potentially increasing global temperatures. The effect of ClNO$_2$ chemistry on the enhancement of atmospheric OH, HO$_2$, RO$_2$, NO$_2$ and O$_3$ concentrations was assessed at the baseline temperature and at a projected increase in temperature by 2.9^{o}C by the 2050s, and the results were compared.

4.1 Introduction

4.1.1 Projected ClNO$_2$ and Cl production level in 2050s

The UK Climate Projections 2009 (UKCP09) were developed to understand and prepare for climate changes of the UK under current and future projections of global greenhouse gas emissions. The UKCP09 provide projections on the climate change for the land and marine areas in the UK in a greater temporal and spatial detail than previous UK climate projections, with 25 km resolution. UKCP09 has ability to deal with the uncertainty that might be faced in the future (Murphy et al., 2009).

In order to determine the probability of climate change, the UKCP09 developed the CDF (the Cumulative Distribution Function) which shows a probability level of a certain climate change variable for a certain location and month of the year for three emissions scenarios (low, medium, and high CO$_2$ emissions) (Jenkins, 2009). The CDF presents the percentile of the probability level at which climate change is not likely to exceed a certain value.

According to UKCP09 (2010), the projected mean daily temperature in summer 2050 (the central year of the time period (2040 - 2059) for the West Midlands at the 10, 50 and 90% probability will be 1.2, 2.6, and 4.4 ℃ respectively under medium CO_2 emission scenarios and will be 1.4, 2.9, and 4.8 ℃ under a high emission scenario. The changes in temperature have been projected relative to a baseline period (1961-1990) with the central year 1975. The probability percentile indicates that it is very unlikely that the projected temperature change or warming to be less than 1.2 ℃; 50% means the "central estimate" which is a term given by UKCP09 for a median value that predicted to be 2.6 ℃, and the 90% indicate that it is very likely that the warming to be less than 4.4 ℃. These temperature projections are based on a large number of climate model simulations and observations.

4.2 Method

The model developed and evaluated in Chapter 2 and 3 was used in this study to examine the influence of temperature upon the production and impact of $ClNO_2$ chemistry as this is of particular importance in future climate with potentially increasing global temperatures. The model developments included selecting ten VOCs based on their reactivity toward Cl atoms, N_2O_5 uptake parameterization, chemistry of $ClNO_2$ formation and loss, and Cl atom reactions with inorganic and organic species. The same physical parameters and the initial conditions used for model evaluation (Chapter 3) are used for this study, except for temperatures that are set for the aim of this study. The model was simulated for a period of 6 days with a 10-minutes time step. The 6th day of the model run was used for the analysis.

4.3 Results and discussion

Having considered the temperature change in 2050, it is important to investigate the response of $ClNO_2$ formation and its impact on air quality at predicted future temperatures. To address this the model was run at two different temperatures:

- Average temperature over 30 years for the baseline period (1961-1990) which is 287.8K calculated for the Midlands from Met Office data:

- Change at 90% probability which represents an extreme case under high emission scenario equivalent to +4.8 °C for 2050 (292.6K).
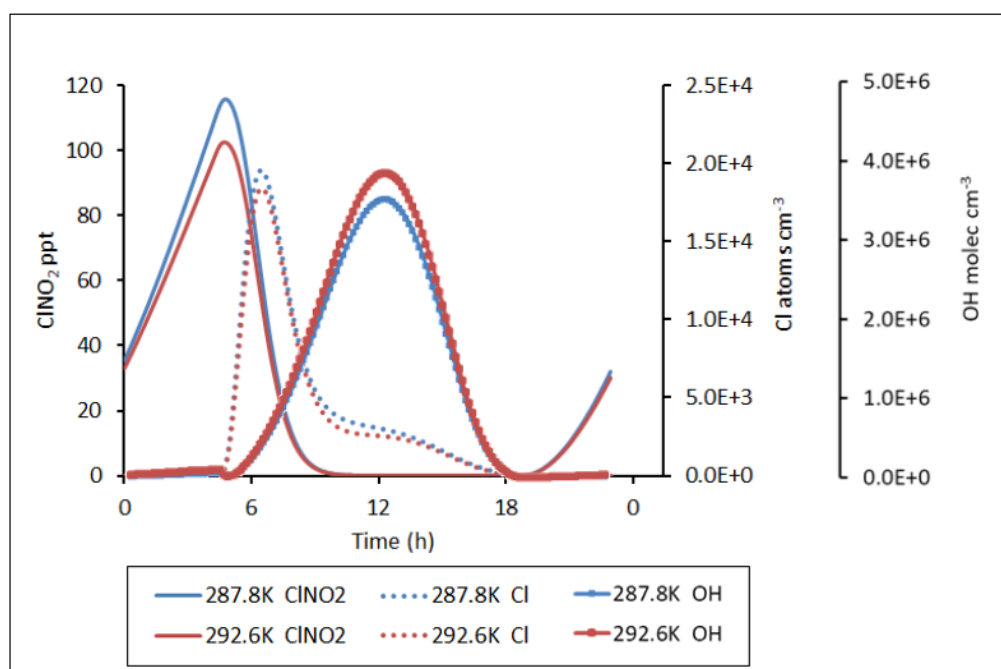
Figure 4. 1 The concentrations of $ClNO_2$, Cl, and OH as predicted by the model at a constant average temperature (287.8 K) of the baseline time period and the projected temperature (292.6K) in 2050

Figure 4.1 shows that an increase in temperature from 287.8 to 292.6 K has resulted in a decrease in the $ClNO_2$ mixing ratio by 6 ppt (10%) as an average from 12am to 10am and by 13 ppt for the peak in $ClNO_2$ at 5am. This decrease arises because greater N_2O_5 concentrations predicted at 287.8 K than at 292.3 K (Figure 4.2b) as at higher temperatures N_2O_5 thermally decomposes more rapidly to NO_2 and NO_3, and thus greater NO_3 concentrations have predicted at 292.6 than at 287.8 K (Figure 4.2c). Therefore, at lower temperatures more N_2O_5 builds up which can then react with aerosol to form $ClNO_2$. This result is in agreement with previous modelling studies (Finlayson-Pitts et al., 1989, Riedel et al., 2014, Sarwar et al., 2014).

It is to be noted that the model predicted greater N_2O_5 production rate at 292.3 K than at 287.8 K (Figure 4.2a), because the only source for N_2O_5 production in the model is NO_2

reaction with NO_3 (R1.34), but there are more than one N_2O_5 removal processes including thermal decomposition and its uptake on aerosol, which the latter is more efficient at lower temperature.

a)

b)
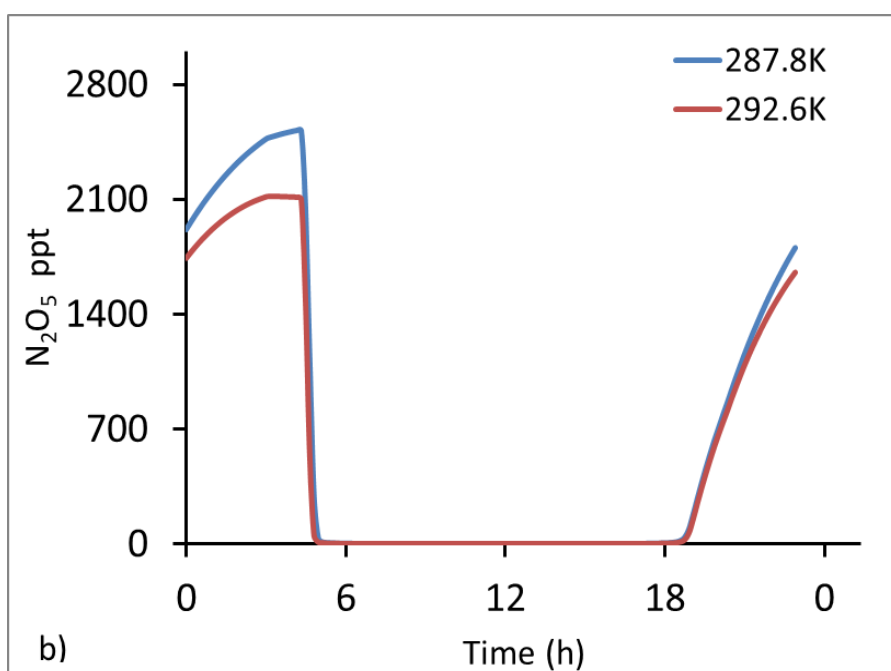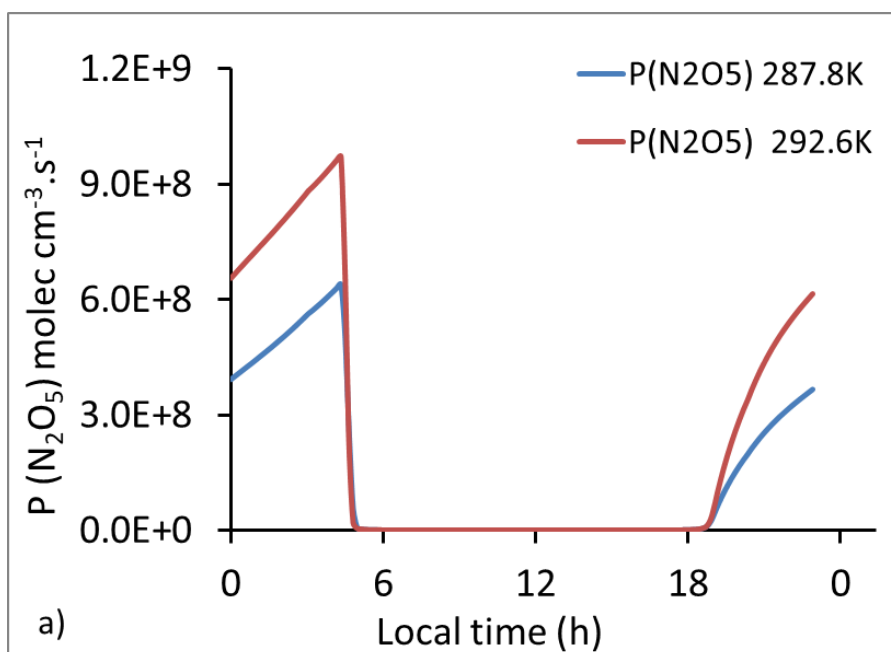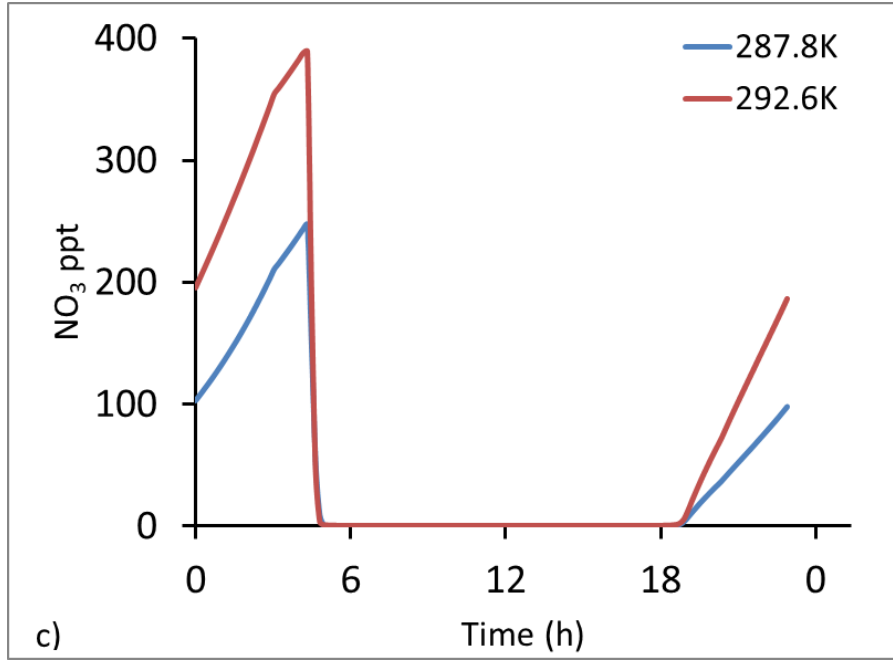
Figure 4. 2 The effect of temperature upon a) N_2O_5 production rate $P_{(N_2O_5)}$ calculated via $k_{(NO_2+NO_3)}[NO_2][NO_3]$, b) the mixing ratio of N_2O_5 and c) the mixing ratio of NO_3.

To investigate the sensitivity of $ClNO_2$ to temperature and NO_x in more detail the model was run 55 times, initialised with different temperatures (267-315 K) and NO_x mixing ratios (5 - 55 ppb) but holding the initial O_3 mixing ratio constant, at 20 ppbv. Each model run is for 6 days and the peak $ClNO_2$ level from the last day is plotted against the NO_x mixing ratio and temperature (Figure 4.3). The model results showed that $ClNO_2$ mixing ratios increase as NO_x mixing ratio increases from 10 to 35 ppb and temperature increases from 267K (6^oC) to 291K ($18\ ^oC$), and then $ClNO_2$ decreased as NO_x increases from 35 to 55ppb and temperature from 291 K to 315 K. A maximum $ClNO_2$ occurs at temperatures between 6 and 14 ^oC and NO_x mixing ratios between 25 and 35 ppb. The $ClNO_2$ was low when NO_x was either low (5- ~12 ppb) or very high (45 – 55 ppb) across all temperatures. This result shows that the temperature has a limited impact on $ClNO_2$ if NO_x is low or high, however, it does significantly affect $ClNO_2$ when NO_x is ranged between 15 - 45 ppb. Sommariva et al. (2018) found that the highest $ClNO_2$ concentration occurs between the O_3 limited regime and NO_2 limited regime. The results presented here further emphasize the role of temperature on $ClNO_2$, if the condition locates between the NO_x and O_3 limited regime.
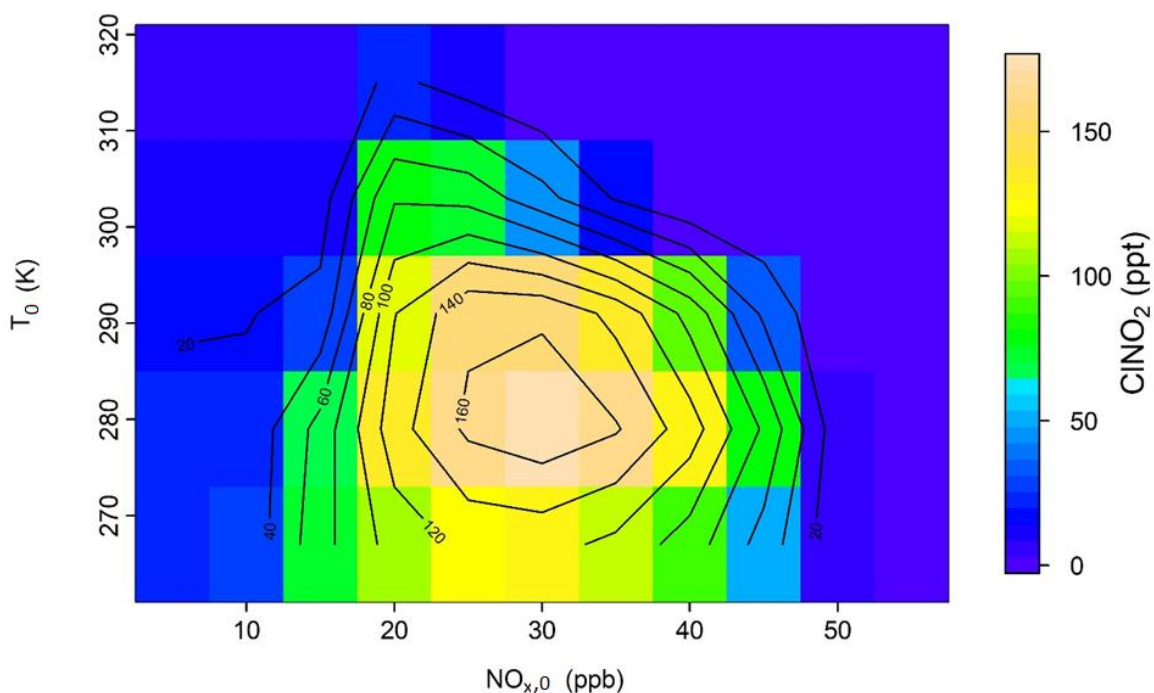
Figure 4. 3 Isopleths showing the sensitivity of $ClNO_2$ mixing ratio to temperature as a function of NO_x. T_0 and NO_{x0} represent the initial conditions of temperature and NO_x.

Recalling that $ClNO_2$ photolysis release chlorine atoms, the model predicted greater Cl concentrations at 287.8 than at 292.6 K by ~10 % as an average from 5 am to 7 pm with Cl maximum concentrations reaching 1.96×10^4 and 1.83×10^4 atoms cm^{-3} at 6:40 am for 287.8 and 292.6 K respectively (Figure 4.1).

A peak in Cl production in the morning arises from $ClNO_2$ photolysis. Then, the productions of Cl atoms are decreasing rapidly before noon as $ClNO_2$ is largely depleted by this time. However, Cl released from $ClNO_2$ is oxidised principally by HO_2 and O_3 to form ClO, which reacts with NO to form Cl which this caused Cl to remain slightly elevated from 10:00am to ~06:00 pm. In addition, the reaction of HCl with OH becomes an important source of Cl atoms (maximum ~ 3×10^4 molec $cm^{-3}s^{-1}$) in the afternoon (Figure 4.4). The photolysis of $ClONO_2$ is also a source of Cl (maximum production rate ~9.4×10^3 molec $cm^{-3}s^{-1}$), but Cl production from photolysis of Cl_2, and HOCl is negligible. It is worth noting that without $ClNO_2$ chemistry in the model, the other sources of Cl will not be produced and since $ClNO_2$ favoured to lower temperature, so at the higher temperature of 292.6 K Cl production rates are lower from all these sources. Reactions R4.1 - R4.6 summarise sources of Cl atoms incorporated into the model:

$$ClNO_2 \ + \ h\nu \ \rightarrow \ Cl \ + \ NO_2 \qquad\qquad R4.1$$

101

$$ClO + NO \rightarrow Cl + NO_2 \qquad R4.2$$

$$HCl + OH \rightarrow Cl + H_2O \qquad R4.3$$

$$ClONO_2 + hv \rightarrow Cl + NO_2 \qquad R4.4$$

$$Cl_2 + hv \rightarrow 2Cl \qquad R4.5$$

$$HOCl + hv \rightarrow Cl + OH \qquad R4.6$$
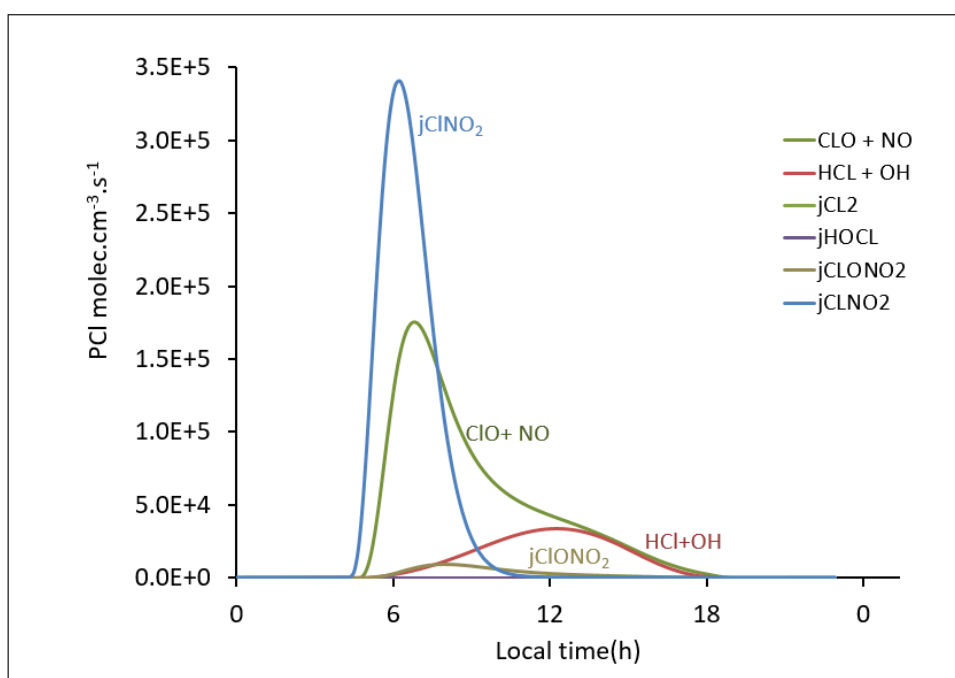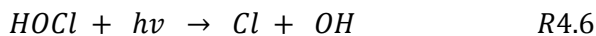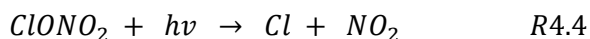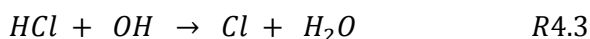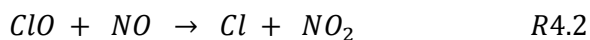
Figure 4. 4 Cl production rates (PCl) from different sources at 287.8K as calculated from the model. Maximum PCl from j(HOCl) and j(Cl$_2$) is very low, around 85 and 3.5 molec.cm^{-3}.s^{-1} respectively.

4.3.1 Impact of temperature upon the effect of ClNO$_2$ on RO$_2$ and HO$_x$

The chlorine atoms released from the photolysis of ClNO$_2$ initiate the oxidation of VOC to produce RO$_2$. To assess the influence of ClNO$_2$ on air quality, the model was run with and without ClNO$_2$ chemistry for both temperatures, 287.5K and 292.3K. In the model without ClNO$_2$ chemistry the heterogeneous reaction of N$_2$O$_5$ reacts with aerosol containing water and will only produce HNO$_3$. Therefore the differences between the two models is the

formation of Cl atoms and NO_2 from N_2O_5 reactions with aerosol containing chloide and producing $ClNO_2$ and HNO_3.

$ClNO_2$ has a distinctive effect on RO_2 in two ways. Cl (formed from $ClNO_2$) can either react with HO_2, which can then form OH, oxidising VOCs to form RO_2, or the Cl can directly oxidise VOCs to RO_2. In polluted environments RO_2 reacts primarily with NO to form either HO_2, alkyl nitrate or closed shell oxygenated VOCs (Riedel et al., 2014). In addition, HO_2 reacts with NO to form OH, and hence more RO_2 can form.

The model results show that after 5am when $ClNO_2$ starts to photolyse, the concentrations of OH, HO_2, and RO_2 rapidly increase (Figure 4.5), with the maximum increase occurred at 5:30-5:40 am for OH and HO_2, and at 6 am for RO_2 (Table 4.1).

OH and HO_2 are highly enhanced by $ClNO_2$ formation as shown in Table 4.1, which this enhancement are resulted in an increase in the concentration of HCHO by approximately 20% in the morning (Figure 4.6). Moreover, O_3 reaction with alkenes (C_2H_4, C_3H_6, and C_5H_8) especially during night time is another source of HCHO (R4.7- R4.9), however the model predicted tiny contribution to the HCHO formation from these sources. From Figure 4.7a , the main sources for HCHO formation in the model are OH reaction with CH_3OH (R4.10) followed by Cl reaction with CH_3OH (R4.11), and the main HCHO loss that predicted by the model are HCHO photolysis (R4.12 and R4.13), followed by HCHO reaction with OH (R4.14).

O_3 + C_2H_4 → $HCHO$ + CH_2OOA R4.7

O_3 + C_3H_6 → $HCHO$ + CH_3CHOOA R4.8

O_3 + C_5H_8 → $HCHO$ + $MVKOOA$ R4.9

CH_3OH + OH → HO_2 + $HCHO$ R4.10

CH_3OH + Cl → HO_2 + $HCHO$ + HCl R4.11

$HCHO$ + hv → HO_2 + $H2$ + CO R4.12

$HCHO$ + hv → → CO + $2HO_2$ R4.13

OH + $HCHO$ → HO_2 + CO R4.14
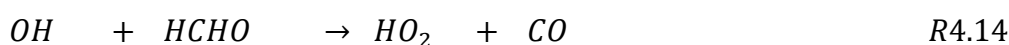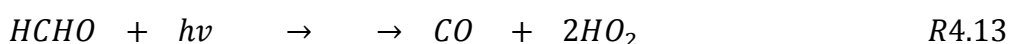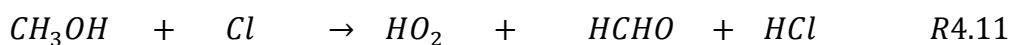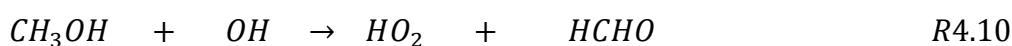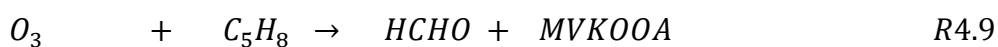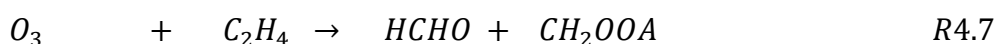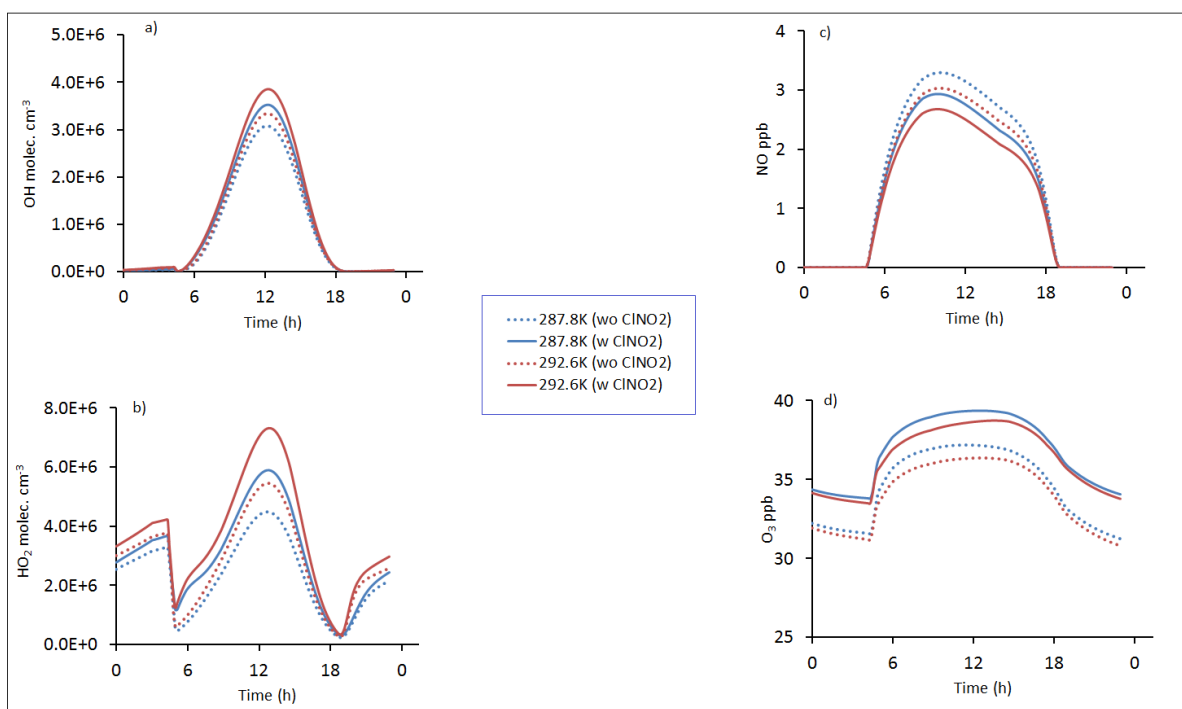
Figure 4. 5 Impact of ClNO$_2$ chemistry on a) OH, b) HO$_2$, c) NO, and d) O$_3$ concentrations at temperatures of 287.8 and 292.6 K.
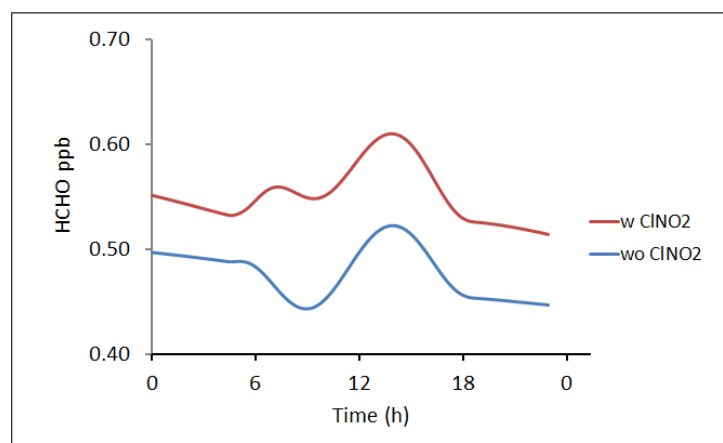
Figure 4. 6 Increase in HCHO mixing ratio when ClNO$_2$ chemistry is included into the model. The blue and red lines indicate the mixing ratio of HCHO before and after activating ClNO$_2$ chemistry in the model respectively.
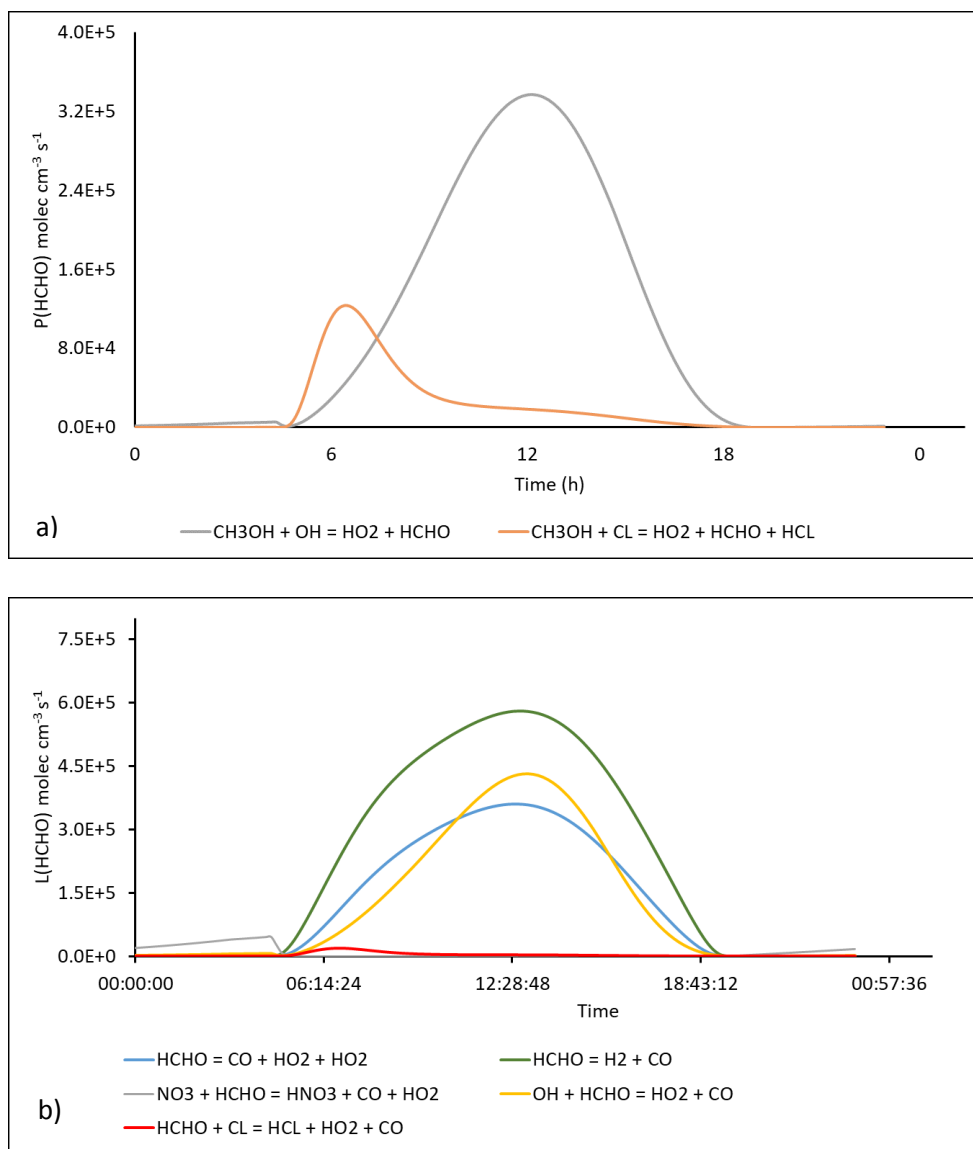
Figure 4. 7 The main sources for the (a) production and (b) Losses for HCHO in the model

During daytime, CH_3O_2 is the main RO_2 that predicted by the model, which its concentration is greater at 292.6 K than at 287.8K (Figure 4.8). Figure 4.9 shows that $CH_3O_2NO_2$ decomposition followed by OH reaction with CH_4 are the main sources for CH_3O_2 formation in the model.

The model has predicted more RO_2 in the evening for a short time (from 07:30 to 08:00pm) than during the day. Most of these elevated RO_2 comes from the products of toluene (mainly 2-Methylphenol or CRESOL) and to a lesser extend meta-xylene chemistry. Figure 4.10b shows the impact of 11 produced RO_2 from toluene chemistry only on the sum of RO_2 that are produced mainly by the OH oxidations during the day. As NO abundance become low (nearly zero) by 07:30pm, these RO_2 builds up until after

08:00pm. From then the concentrations of NO_3 will start to increase and become a dominant radical that react with RO_2, thus RO_2 concentrations start to decline. During the day greater RO_2 is produced when $ClNO_2$ chemistry is included in the model than without, however, at night the opposite effect occurs. The reason is because during the day Cl atoms released from $ClNO_2$ with extra formation of OH from $ClNO_2$ react with VOCs to form RO_2, thus RO_2 levels are elevated above those in the model without $ClNO_2$. Inclusion of $ClNO_2$ chemistry in the model is enhanced NO_3 abundance (figure 4.10c), which reacts with RO_2, however, NO_3 also react with some VOCs, such as C_2H_4, C_5H_8, and meta-xylene, but it mostly reacts with RO_2. Therefore, more NO_3 in model with $ClNO_2$, then more RO_2 will remove from the system, and thus the abundance of RO_2 will be less. Furthermore, more NO_3 are formed at 292.6 K than at 287.8K, so less RO_2 are lost at 292.6K at night. Further studies (measurements and modelling) are important to investigate the behaviour of VOCs particularly toluene at night.

Generally, the enhancement of OH, HO_2, and RO_2 by chlorine atoms is higher at 287.8K than at 292.6K as more $ClNO_2$, hence more Cl produced at 287.8K than at 292.6K (table 4.1):

Table 4. 1 Maximum peak enhancement of OH, HO_2, and RO_2 concentrations by $ClNO_2$ chemistry**.**

Chemical compounds	287.8 K	292.6 K	Peak time
OH	92%	78%	5:30-5:40 am
HO$_2$	166%	133%	5:40 am
RO$_2$	125%	93%	6:00 am
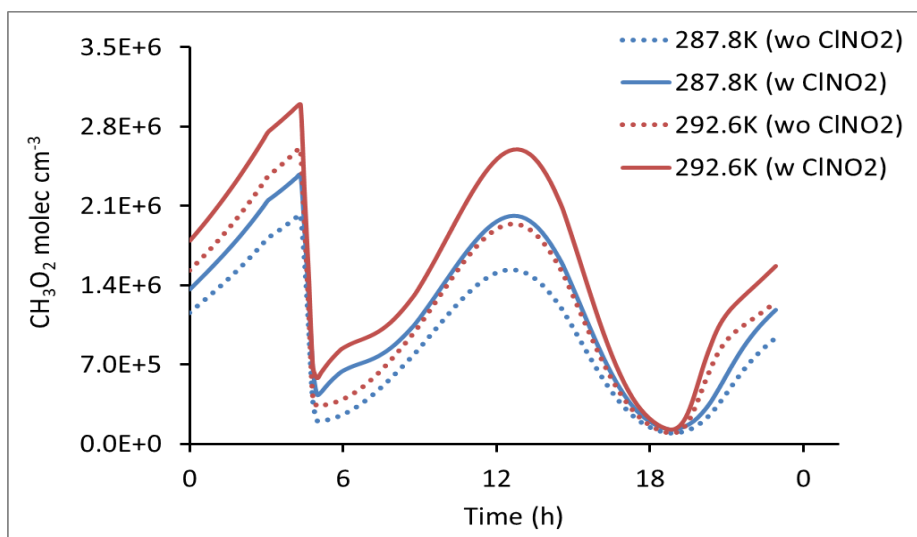
Figure 4. 8 Impact of ClNO$_2$ on the concentrations of CH$_3$O$_2$ in with and without ClNO$_2$ chemistry cases at temperatures of 287.8 and 292.6 K.
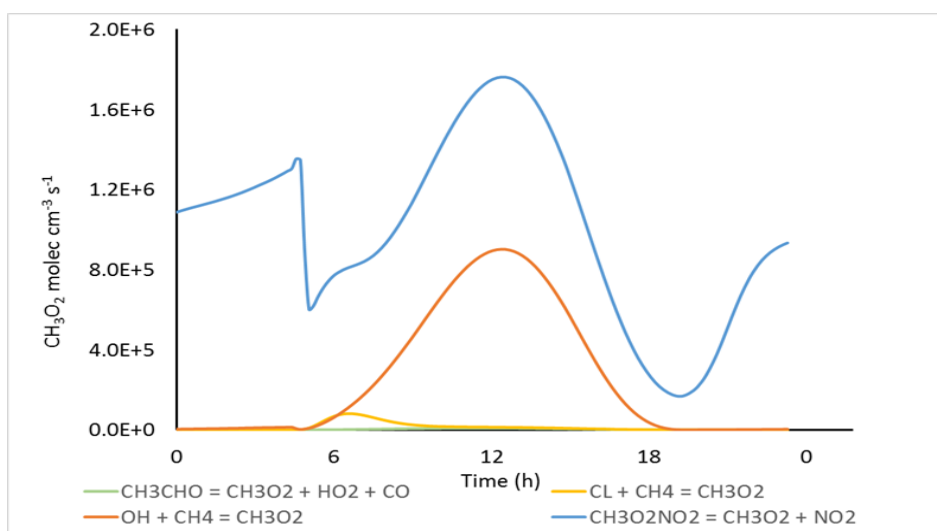
Figure 4. 9 Main sources of CH$_3$O$_2$ in the model
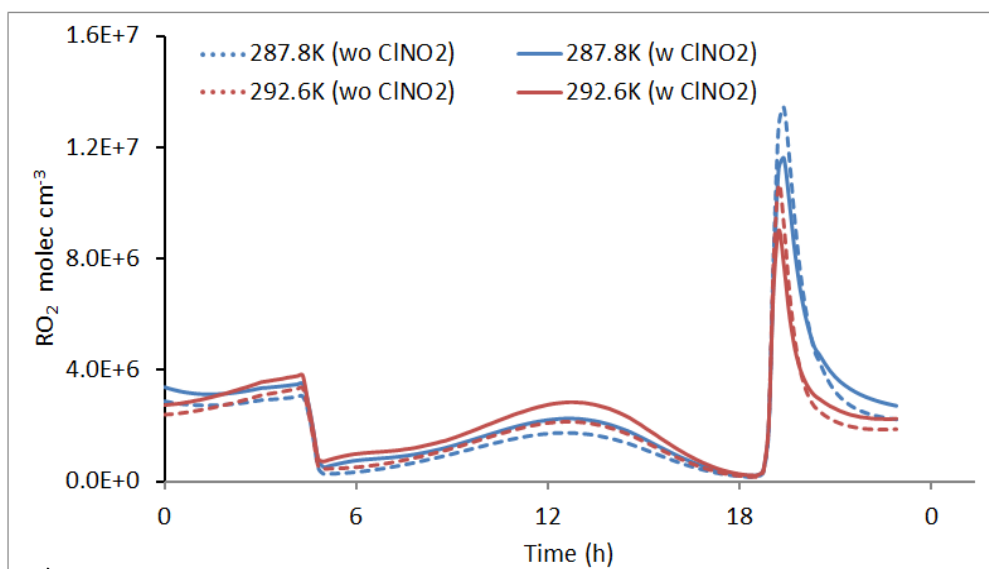
a)
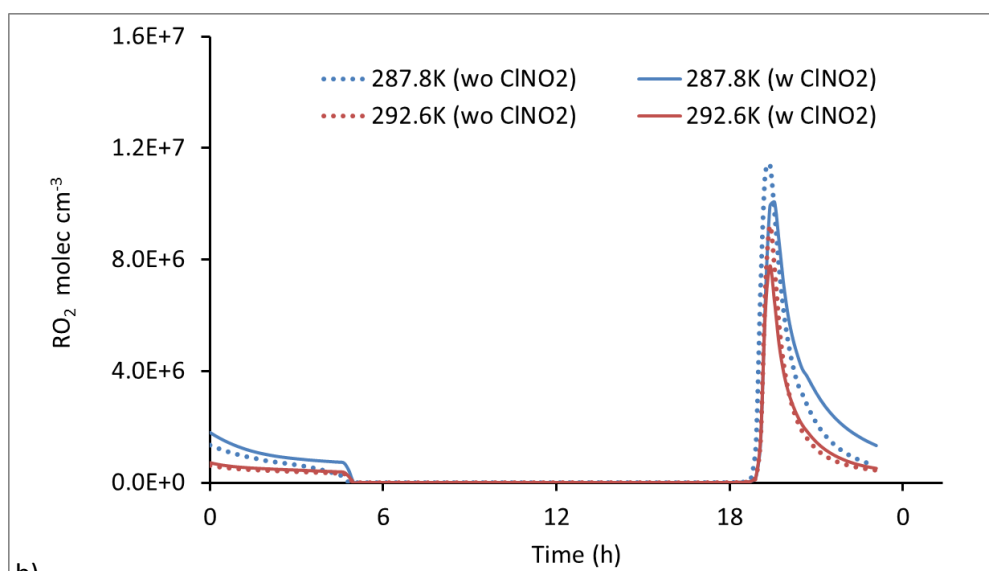
b)
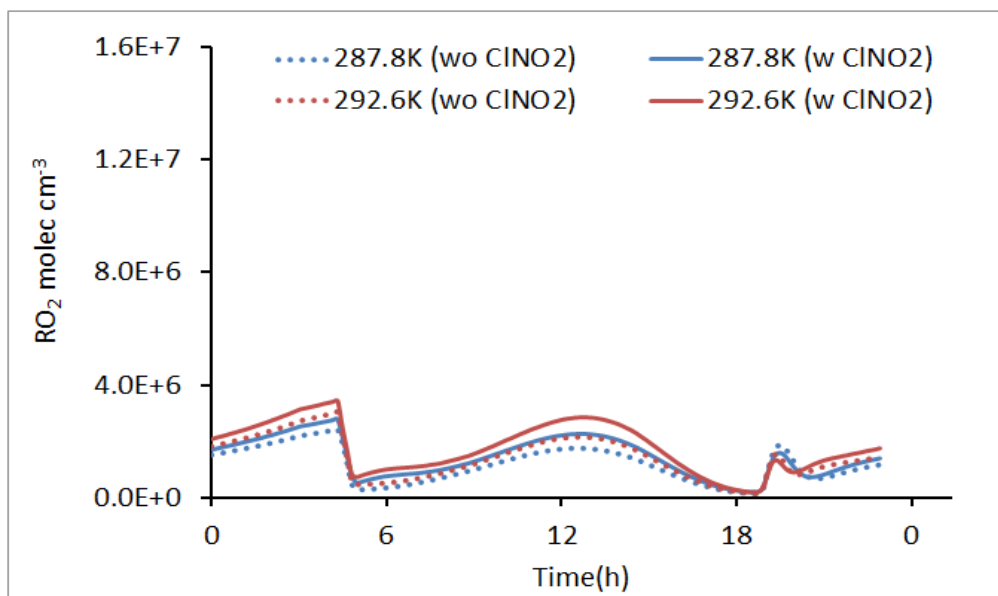
c)

Figure 4. 10 Impact of $ClNO_2$ on the concentrations of RO_2 **a)** the sum of 448 produced RO_2 species for runs with and without $ClNO_2$ chemistry, **b)** sum of 11 RO_2 produced from toluene chemistry, **c)** sum of RO_2 when the 11 RO_2 from toluene chemistry is excluded

a)

b)
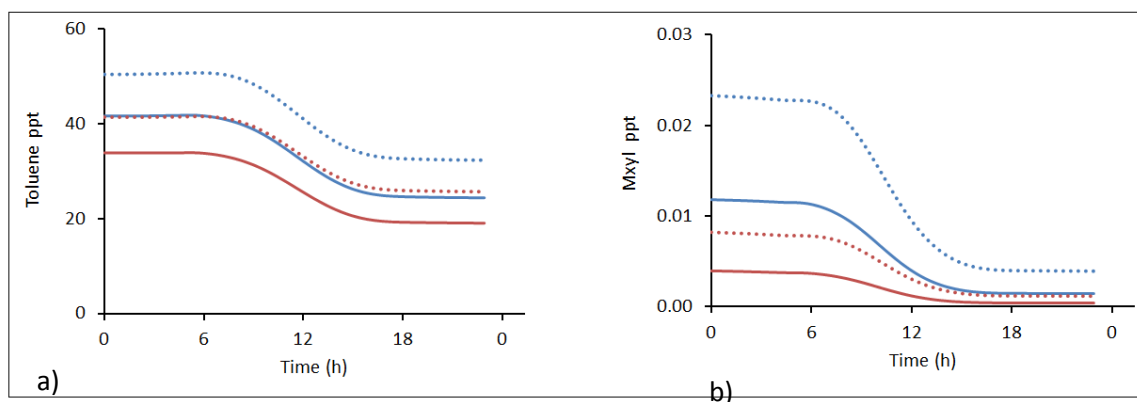
Figure 4. 11 Influence of $ClNO_2$ on **a)** toluene and **b)** m-xylene for model runs with and without $ClNO_2$ chemistry

4.3.2 Impact of temperature upon the effect of $ClNO_2$ on O_3 formation

The inclusion of $ClNO_2$ chemistry in the model has resulted in an increase in the mixing ratio of O_3 by 2.17ppb (6.7%) and 2.31ppb (7%) on average over 24 hours at 287.8 K and 292.6 K respectively. Releasing Cl atoms and NO_2 from the photolysis of $ClNO_2$ is thought to be the main cause of O_3 increase as the RO_2 formation from the VOC oxidation by Cl will result in the formation of NO_2, HO_2, and OH and thus increase O_3 concentrations (Liu et al., 2018, Riedel et al., 2014, Sarwar et al., 2014, Wang et al., 2016, Liu et al. 2018; Riedel et al. 2014; Sarwar et al. 2014; Wang et al. 2016) (R4.15-R4.19):

$$Cl \; + \; VOC \; \rightarrow \; RO2 \qquad\qquad R4.15$$

$$RO_2 \; + \; NO \; \rightarrow \; NO_2 \; + \; RO \qquad\qquad R4.16$$

$$RO \; + \; O_2 \; \rightarrow \; HO_2 \; + \; HCHO \qquad\qquad R4.17$$

$$HO_2 \; + \; NO \; \rightarrow \; NO_2 \; + \; OH \qquad\qquad R4.18$$

$$NO_2 \; + \; hv \; \rightarrow \; NO \; + \; O(^3P) \qquad\qquad R4.22$$

$$O(^3P) \; + \; O_2 \; + \; M \; \rightarrow \; O_3 \; + \; M \qquad\qquad R4.19$$
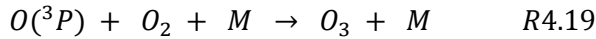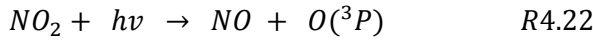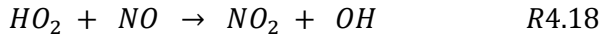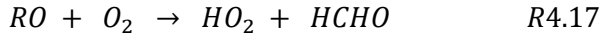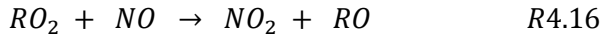
A greater O_3 mixing ratio is predicted at 287.8 than 292.6 K, and the model results show the O_3 production rate (P_{O3}) (calculated via equation Eq 4.1) is on average (from 5am to 7pm) 9% higher at 292.6 than 287.8 K(Figure 4.12).

It is important to mention that the initial model (before adding $ClNO_2$ chemistry) has predicted less O_3 mixing ratio at higher temperature (Figure 4.5d), but more P_{O3} (Figure 4.12) at higher temperature. The reason is that O_3 mixing ratio in the model is solely depends on NO_x and VOC concentrations, whereas, more other factors such as the RO_2 and HO_2 concentrations along with the rate coefficient of their reactions with NO will also affect P_{O3}. Since less NO and NO_2 are produced at higher temperature (292.6 K), so the abundance of O_3 was also less. Alternatively, there were more OH, HO_2, and RO_2 at higher temperatures; hence, the rate of O_3 production was greater at higher temperature.

$$P_{O3} = k_{HO2+NO} \, [HO_2][NO] + \Sigma \, k_{RO2+NO} \, [RO_2][NO] \qquad Eq \; 4.1$$

Where, k_{HO2+NO} is the rate coefficient for reaction HO_2 with NO, $\Sigma\ k_{RO2+NO}$ is the rate coefficient for the reaction of NO with the sum of 448 RO_2, $[HO_2]$, $[NO]$, and $[RO_2]$ is the concentrations of HO_2, NO, and RO_2.
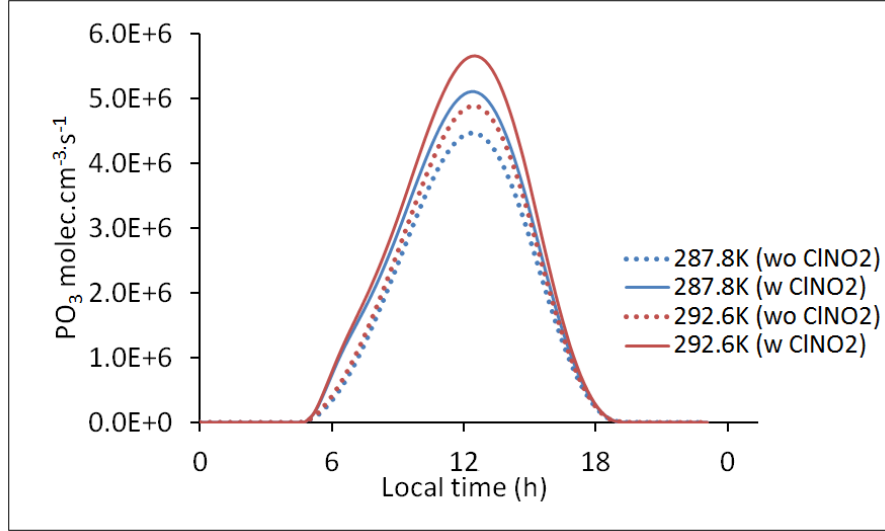
Figure 4. 12 Impact of $ClNO_2$ chemistry on the enhancement of O_3 production rate.

4.3.3 Impact of temperature upon the influence of $ClNO_2$ on NO_2

Including $ClNO_2$ chemistry in the model resulted in a decrease in the mean mixing ratio of NO_2 from sunrise to noon by 0.43 ppb (6%) at 287.5 K and 7% at 292.3 K (figure 4.13a). This result is similar to the modelling study by Riedel et al. (2014) and Liu et al. (2017) in which $ClNO_2$ resulted in the decrease of NO_2 from sunrise to noon by 6%. Higher production of OH and RO_x ($RO_2 + NO_2$) by $ClNO_2$ chemistry resulted in faster removal of NO_2 to form nitric acid (HNO_3), acyl peroxy nitrates (PAN), and alkyl nitrates ($RONO_2$) (Riedel et al., 2014) (R4.20-R4.23) as shown in figure 4.13. Also Li et al. (2016) ascribed the decrease in NO_2 by $ClNO_2$ to faster transforming of NO and NO_2 to form total nitrate.

$$OH\ +\ NO_2\ \rightarrow\ HNO_3 \qquad\qquad R4.20$$

$$RO_2\ +\ NO\ \rightarrow\ RONO_2 \qquad\qquad R4.21$$

$$RO_2\ +\ NO_2\ \rightarrow\ PAN \qquad\qquad R4.22$$

$$CH_3O_2\ +\ NO_2\ \leftrightarrow\ CH_3O_2NO_2 \qquad\qquad R4.23$$
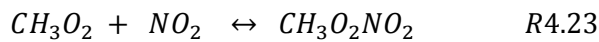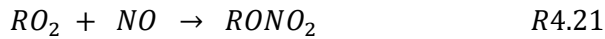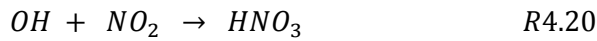
The main sink of NO_2 during the day is HNO_3 formation from the reaction of NO_2 with OH. The presence of $ClNO_2$ enhanced the formation of HNO_3 by 3% (for both 287.5 and 292.3 K) from 5 am to noon, relative to the model without $ClNO_2$ chemistry. The reaction of RO_2 with NO_2, which is considered as a termolecular reaction that involves a third body molecule (N_2 or O_2) depends on temperature and pressure. At low temperatures RO_2NO_2 have an atmospheric lifetime of days, which can build up in the upper troposphere (Calvert et al. 2015), however, at higher temperatures peroxy nitrate (RO_2NO_2) such as methoxy nitrate ($CH_3O_2NO_2$) is unstable and will decompose to reform RO_2 and NO_2 (R4.23). Therefore, more $CH_3O_2NO_2$ concentrations are occurred at 287.8 than at 292.6 K (Figure 4.13d). The decomposition rate of $CH_3O_2NO_2$ is calculated from the model simulation and was 16% higher at 292.6 than 287.6K (average during daytime). In addition, oxidation of non-methane volatile organic compounds (NMVOCs) results in the formation of PAN. The extra formation of NO_2 from $ClNO_2$ chemistry resulted in a mean increase of PAN over 24 hours by 12% and 8% for temperatures 287.8 and 292.6 K respectively (Figure 4.13b). At lower temperatures, PAN acts as a reservoir for NO_x allowing long distance transport. With an increase in temperature, PAN decomposes to release NO_x into the atmosphere and can result in an increase in O_3 and OH (Fischer et al. 2014). Therefore, liberating NO_2 from $ClNO_2$ photolysis is counterbalanced by the formation of O_3, HNO_3, $CH_3O_2NO_2$, and PAN (Li et al., 2016; Liu et al., 2017; Riedel et al., 2014).
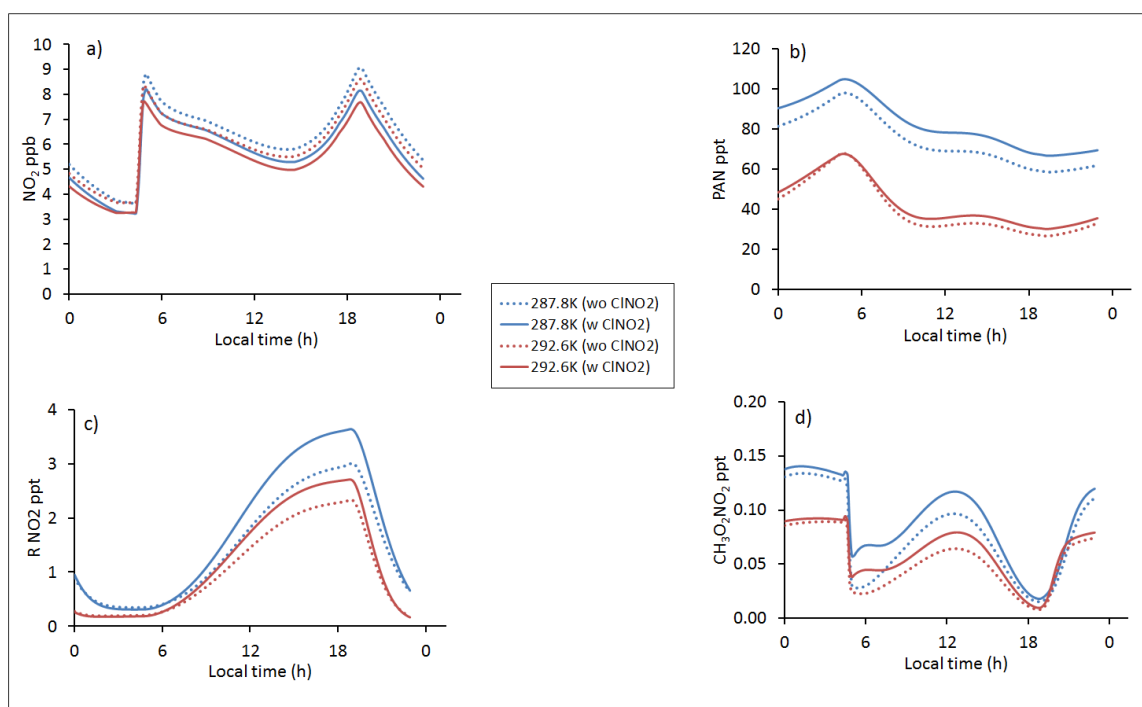
Figure 4. 13 Mixing ratio of: **a)** NO$_2$, **b)** PAN, **c)** RNO$_2$, and d) CH3O$_2$NO$_2$ in both cases (with and without ClNO$_2$ chemistry at temperatures 287.8 and 292.6 K.

4.4 Conclusion

A box model study using the MCM was used to investigate the effect of temperature on the formation and chemistry of ClNO$_2$. The model is comprehensively updated to include the parameterization of N$_2$O$_5$ uptake on the aerosol and the subsequent ClNO$_2$ formation, alongside gas-phase chlorine chemistry. The updated model has been evaluated against ClNO$_2$ observations in an urban area, which show that the model was able to capture the production of ClNO$_2$.

This study aimed to investigate the impact of projected future mean temperature increase by 2.9 ^{o}C by 2050s on the formation and impact of ClNO$_2$ chemistry on a number of chemical species, which are important in urban air quality. The model predicted that with a projected increase in temperature by 2.9^{o}C the average concentration of ClNO$_2$ and thus Cl atoms would decrease by 10%. Therefore, the effect of ClNO$_2$ on the enhancement of OH, HO$_2$, RO$_2$, and HNO$_3$ was greater at lower temperatures, but the effect is not significant (1% in average across the day) at higher temperature for O$_3$. Moreover, the inclusion of

113

$ClNO_2$ in the model has decreased NO_2 levels, but the decrease is less at 287.8 than at 292.6K; meaning higher NO_2 levels at 287.8 K. Recycling NO_2 from $ClNO_2$ is counterbalanced by more O_3, HNO_3, $CH_3O_2NO_2$, and PAN formation, in agreement with previous studies.

The sensitivity of $ClNO_2$ to temperature as a function of NO_x was investigated and indicated that the maximum $ClNO_2$ occurred at temperatures ranging from 279 to 291K when NO_x is between 25 and 35 ppb. A minimum $ClNO_2$ was predicted when NO_x is less than 15 ppb or more than 45ppb. In these two cases temperatures have limited effect on the $ClNO_2$ variations, however temperature does significantly affect $ClNO_2$ when NO_x is ranged between 15 and 45 ppb. Therefore, polluted urban environment (25-35ppb NO_x) coupled with cold to moderate temperature represent a typical condition for high $ClNO_2$ formation.

Figure 4.14 shows the summary of $ClNO_2$ impacts on air quality as a function of NO_x as expected by the model (from the sensitivity test). The figure shows that $ClNO_2$ chemistry has a small impacts in low (5-15 ppb) and high (45-55 ppb) NO_x mixing ratio, whereas, the impacts will be greatest when NO_x are in the range 25-35 ppb. Therefore, a more polluted air will be expected in areas with NO_x ranging 45-55 ppb and when temperature ranging from 279 to 291K as a more O_3 pollutant produced from $ClNO_2$ chemistry will release into the air.

Hence, it is important for the air quality regulator and policy maker to consider the results raised from this study while they set up regulations in controlling NO_x emissions. Many countries are set regulations to limit NO_x emissions in order to improve air quality in urban areas such as in US (Pusede et al., 2016).

This work is an extension of previous studies and further emphasize the important role of temperature on $ClNO_2$ formation, chemistry, and on its seasonal and geographical distribution which explained in terms of NO_2 and O_3 limited regimes by Somariva et al., (2018). The results raised from this work suggest the significance of more modelling and observation studies to probe $ClNO_2$ and its precursor gases relationship with temperature especially in polluted environments coupled with high temperature environment.

Finally, it is well known that the rise in global temperatures will result in increase in BVOCs emissions (Peñuelas and Staudt, 2010), therefore the production of a highly reactive species such as isoprene could increase as global temperature rise, which can

affect NO_x and O_3 budget in the atmosphere. In low NO_x environment, isoprene reacts directly with O_3, thus reduces O_3 levels in the atmosphere, but at high NO_x conditions isoprene oxidation by OH leads to NO_2 formations and hence increases O_3 levels (Pacifico et al., 2009). Modelling studies are therefore important to investigate temperature effects on BVOC emissions and the consequent effects on air quality.
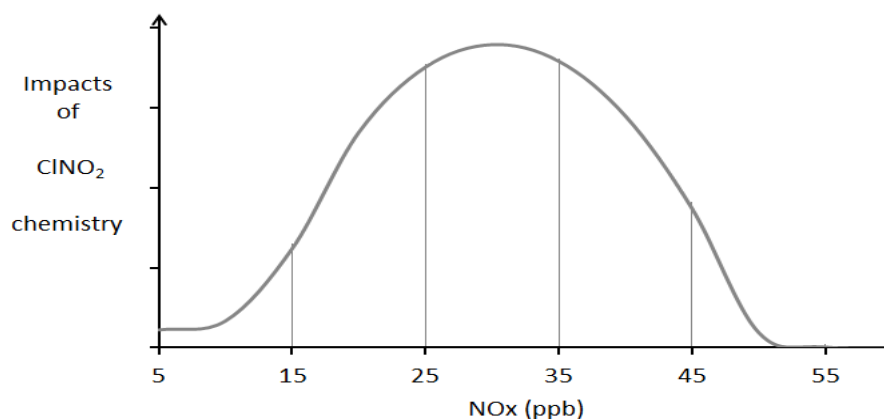
Figure 4. 14 Impacts of $ClNO_2$ chemistry on the Cl + VOC reactivity as a function of NOx

Chapter 5 Impacts of changing diurnal emission distribution from traffic on urban air quality (NO$_2$)

In this chapter, the model that has been further developed for simulating the ClNO$_2$ chemistry (Chapter 4) is used first to examine the impact of diurnal variations in traffic emissions on the concentrations of OH, HO$_2$, NO, NO$_2$, NO$_3$, N$_2$O$_5$, and ClNO$_2$ in an urban area in the UK. Then the effect of changing NO$_2$ concentrations (due to emission variation) on the number of deaths was examined. Accordingly, recommendations on controlling NO$_2$ are provided at the end of the chapter.

5.1 Introduction

Urban regions are characterised by high anthropogenic emissions (Wang et al., 2017), with the concentration of pollutants being considerably influenced by local sources, such as emissions from vehicles, industrial processes and product distribution, and residential activities (Salmond and McKendry, 2009). Currently, road transport forms the main source of emissions within urban areas in developed nations (Vardoulakis et al., 2003, Hitchcock et al., 2014), with the main air pollutants from vehicle exhausts being: Nitrogen Oxides (NO$_x$= NO+NO$_2$); particulate matter (PM); and Volatile Organic Compounds (VOCs). The direct emissions of NO$_2$ from vehicles are estimated to be around 15% of NO$_x$ emissions in inner London in 2014, with the percentage varying according to the type of vehicle and fuel (Carslaw et al., 2016, Malley et al., 2018). NO$_2$ is also formed in the atmosphere as the result of the reaction between NO and O$_3$, and is known as secondary NO$_2$.

It has been estimated that for every 10 μgm^{-3} increase in the annual concentration of NO$_2$ there is a corresponding 2.5% increase in the all-cause mortality rate (Defra, 2015; Hitchcock and Carslaw, 2016). Defra has estimated that 23,500 total annual deaths in the UK are due to exposure to NO$_2$, with an annual cost to the country of approximately £13.3 billion (Defra, 2016; Hitchcock and Carslaw, 2016). In a modelling study Mills et al.

(2016), found an increase in 10 μgm^{-3} of NO_2 in an hour would increase the risk of all-cause mortality in all age group by 0.22% (with a 95 percent confidence interval (Cl): − 0.15 to 0.60) and by 0.92% (95% Cl :0.58 to 1.72) in 24 hours.

Studies undertaken in a number of European cities (including London) have established a relationship between daily exposure to NO_2 and cardiovascular diseases and asthma (Zmirou et al., 1996, Poloniecki et al., 1997, Sunyer et al., 1997). Nhung et al. (2018) found a strong association in Hanoi, Vietnam between short-term (i.e. daily) exposure to NO_2 and hospital admissions for pneumonia, bronchitis, and asthma in children under eighteen. Also, excess mortality risks from cardiovascular diseases in Kermanshah, Iran were attributed to NO_2 (Khaniabadi et al., 2017).

Furthermore, NO_2 is a precursor for the formation of secondary pollutants such as O_3 (at ground level) and nitrate aerosol. NO_2 can be also converted into acids in the atmosphere via diverse chemical pathways in both gas and liquid phases causing acid rain, which can affect crop yields and species diversity (Singh and Agrawal, 2007).

Although there are over 700 Air Quality Management Areas (AQMAs) throughout the UK primarily set for exceedance of permitted levels of NO_2 (Defra, 2016), direct NO_2 emissions from diesel vehicles remain a major issue, due to the high proportion of light and heavy-duty vehicles powered by diesel. In 2017 diesel vehicles accounted for 50% of all car fleets in the UK compared with only 7.4% in 1994 (Holgate, 2017).

As mentioned in Chapter 3, in urban areas, traffic volume often peaks during the weekday morning and evening due to the daily commute to and from work or school (Knibbs et al., 2011, Ragettli et al., 2013), resulting in a greater emission of pollutants when compared to off-peak times or in rural areas (Hitchcock and Carslaw, 2016). During weekdays, driver's journeys peak in the morning and the afternoon, while travel during the weekend peak around middle of the day (Figure 3.6) (Charlton and Baas, 2002).

This different pattern of traffic distribution for urban roads in the UK may result in different concentrations of pollutants between weekdays and weekends. For example, the mean NO_2 concentration measured at the roadside in 2017 was noticeably lower (28.4 μg m^{-3}) during weekends in comparison to weekdays (35.9 μg m^{-3}). This difference was

attributed to the lower level of traffic during weekends (Defra, 2018). Pollutant concentrations also vary according to the road type.

Commuters (pedestrians) are more exposed to poor air quality at the roadside of major roads than on minor roads as a result of greater traffic density and higher emissions (Hitchcock and Carslaw, 2016; Rivas et al., 2017). Figure 5.1 illustrates the average hourly variations in vehicles on a major (Bristol Road) and urban minor road for Monday (as a typical week day) as calculated by Bright et al. (2011). From figure 5.1, at 9 am, more than 2000 vehicles were recorded on major road compared to only 185 vehicles on minor road.
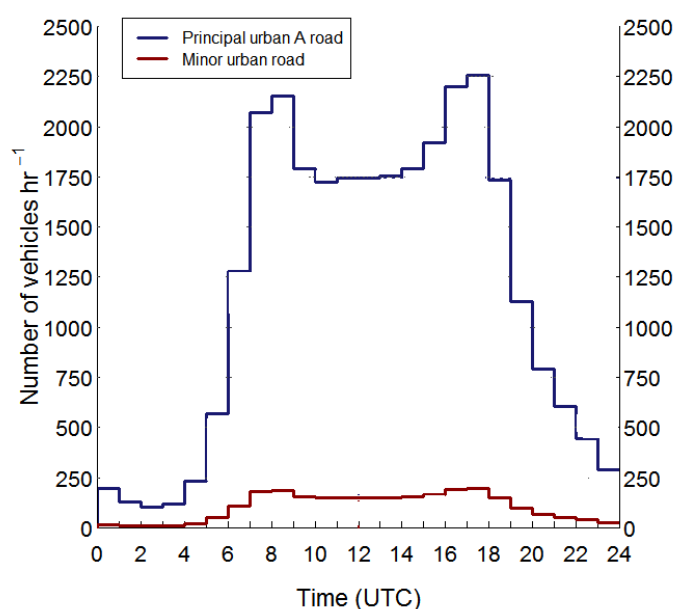
Figure 5. 1 Number of average vehicles per hour on a typical weekday for a) major road (four lane road) and b) urban minor road (two lane road) in 2008 (Bright et al., 2011).

The control of ambient NO_2 concentrations especially from the transportation sector remains a challenge in many European countries, due to ineffective reduction in NO_x emissions from diesel vehicles via emissions limits legislations/ the Euro standards which mismatch the real world vehicle driving performance (Carslaw et al., 2016).

The presence of NO_x and VOCs in the atmosphere in the presence of sunlight is the main source of ozone in the lower atmosphere, which is a greenhouse gas and a pollutant capable of adversely impacting human health and vegetation (Wang and Mauzerall, 2004).

It is therefore important to control NO_x and VOC emissions, in order to also control O_3 pollution (Gao, 2007).

Recalling that during daytime, the hydroxyl radical oxidizes VOCs in the presence of NO_x and sunlight, resulting in the formation of O_3 in the troposphere. During the night, OH^- radicals reach their minimum concentration, but O_3 and nitrate radicals (NO_3) become more predominant in oxidizing VOCs, particularly alkenes, cresols, and isoprene (McLaren et al., 2010). $ClNO_2$ can also be produced during the night which is not reactive, but can, at sunrise, readily undergo photolysis, thus releasing NO_2 and highly reactive chlorine atoms (Cl) capable of oxidizing VOCs and enhancing O_3 formation in the atmosphere (Riedel et al., 2014). Emissions, meteorology, and chemistry are all capable of altering the concentration of NO_2 (Malley et al., 2018), and subsequently the magnitude of its impacts on air quality.

In urban areas, particularly at roadside locations, the concentrations of NO_2 are significantly influenced by total road NO_x emissions and by the proportion of directly emitted NO_2 from vehicles (Grange et al., 2017). A number of studies have been undertaken to quantify the impacts of the temporal and spatial distributions of NO_x emissions on the annual concentration of NO_2. (Syafei and Zhang, 2015) examined the variation in peak concentration of NO and NO_2 in relation to the time of day, day of the week, and seasons throughout the year. They found that the time of peak concentration varies according to location and season, demonstrating that peak concentrations were closely associated with traffic congestion. In addition, Fujita (2013) has examined O_3 variation in relation to the day of the week. Cardelino (1998) studied the daily and the hourly variability of traffic emissions in weekends and weekdays for rural and urban principle and minor roads in and around the Atlanta Metropolitan Area. They analysed traffic counter data, and observed difference in emission distribution between weekdays (have two typical peaks), and weekend (one peak or steady). They also emphasized the importance of temporal emissions variability on O_3 concentrations; however, they did not investigate the impact of emission distributions on O_3 or any pollutant concentrations. Kassomenos et al. (2006) also used collected data from different roads in Athens, Greece to study the temporal and spatial distribution of emissions, but also they used emissions inventory model (COPERT) to determine the spatial and daily variation of emissions rate of pollutants (CO, NO_x, O_3, PM_{10}, and VOCs) according to the emissions distribution. They found high emission rates of NO_x and PM_{10} during the morning rush hour.

However, to our best of knowledge, no study has previously explored the impact of temporal emission variation of NO_x on air quality- i.e., how changing emission distribution with time could affect the concentrations of the atmospheric chemical species including pollutants like NO_2 and O_3.

The focus of this study is to examine the impact of changing the temporal distribution of NO_x emissions, based on traffic distribution patterns with time of the day, upon the concentrations of a number of chemical species with the main focus on NO_2, and consequently on the mortality rate in an urban area. The results of this work will be beneficial for the improvement of air quality management regulations to control air pollution related to emissions from traffic and implementation of abatement measures.

5.2 Methods

The developed model (Chapter 2 and Chapter 3) was used for this study with some updates, explained in the following section. The initial conditions for the simulations is same as for the $ClNO_2$ study (Chapter 4) which was constrained with the measured data in Leicester in August 2014 (Sommariva et al., 2018). The initial conditions comprised of mean NO, NO_2, and O_3 mixing ratios of 5.95, 10.93, and 20.45 ppbv respectively, and mean temperature of 14.5^oC over August 2014 (as for the model validation), (Sommariva et al., 2018). Initial mixing ratios of the 10 primary VOCs included in the model were taken from measurements during the TORCH campaign (the Tropospheric Organic CHemistry experiment) in Essex (Lee et al., 2006). The VOCs considered are ethene, formaldehyde, acetaldehyde, propene, methanol, ethanol, isoprene, m-xylene, toluene, and acetylene. The model was run for 1st August and simulated for six days with a ten minute time step. The first five days were used as a spin up period to reduce the effect of the initial conditions and allow the moderate/long-lived species like O_3 to react and reach a steady state level.

In order to examine how the varying distribution of traffic emissions can affect air quality, we have established six emission scenarios (Figure 5.2), each of which has a unique pattern of emission reflecting an idealised real condition on the road. A model run was conducted for each of these six scenarios. The differences between these scenarios take into account the variations in the distribution of NO_x emissions (ENO_x) over twenty-four hours, reflecting the distribution pattern of traffic on the road, whilst at the same time

maintaining a constant total emission over a twenty four hour period; i.e. the emission is varying with time of the day (increase and decrease) in each scenario, but the total emission summed over a 24 hour period remains the same for all the scenarios.

Traffic is assumed to be the main source of NO_x emissions in the model, and, the temporal (daily/hourly) variations in traffic flow greatly affect the emission profile.

The same amount of emissions (ENO_x) that was used to constrain the model in Chapter 3 (for model evaluation) and chapter 4 was used for this study. Flux out of the box via ventilation or advection is not considered, as the chemical processes are the main loss of pollutants within the box model.

The six NOx emissions scenarios included in the model are:

A. **Scenario A: Base case**: This emission scenario was used to constrain the model in Chaptr 3 (for model evaluation) and chapter 4, so it has represented as a baseline emissions scenario in which NO_x emissions peak for two hours during the morning and evening, i.e. during 'peak-rush hour. This represents a typical emission condition in the UK urban areas during weekdays, i.e. when traffic activity is high.

B. **Scenario B: Shortened peak-duration case**: Peak rush hours is reduced from two hours (base case: scenario A) to thirty minutes. This case can represent school start and end times (i.e. between 8:30-9:00 and 15:00-15:30) during school term. The dropping off of children has been associated with idling engines, resulting in increased air pollutant concentrations near schools (Ryan et al., 2013), particularly for those located close to busy roads and traffic junctions (Holgate, 2017).

C. **Scenario C: One peak lasting between 6am to 6pm**. In this case, the traffic flow is assumed to be smooth, with no peak rush hour or congestion issues. Road traffic congestion is a deviation from smooth driving flow.

D. **Scenario D: Three peaks during the daytime** (1) between 6:30 and 8am; (2) between 12:30 and 1:30pm; and (3) between 4:30 and 6pm. This case may occur in areas with ineffective route control and frequent congestion, potentially due to road work or an event taking place.

E. **Scenario E: Night peak case**: Emissions during the day are steady (i.e. the absence of any peak in emissions), but peak instead at night, i.e. between 9pm to 3am. This case can represent an area such as in Delhi, where a regulation has been put in place inhibiting heavy duty vehicles within city roads during daytime, i.e. they are

restricted to night time only in the city, in order to reduce air pollution during the day (Gulia et al., 2018).

F. **Scenario F: Steady case**: the presence of constant emissions during both the day and night. This case represents an area with a steady flow of traffic during twenty-four hour period.
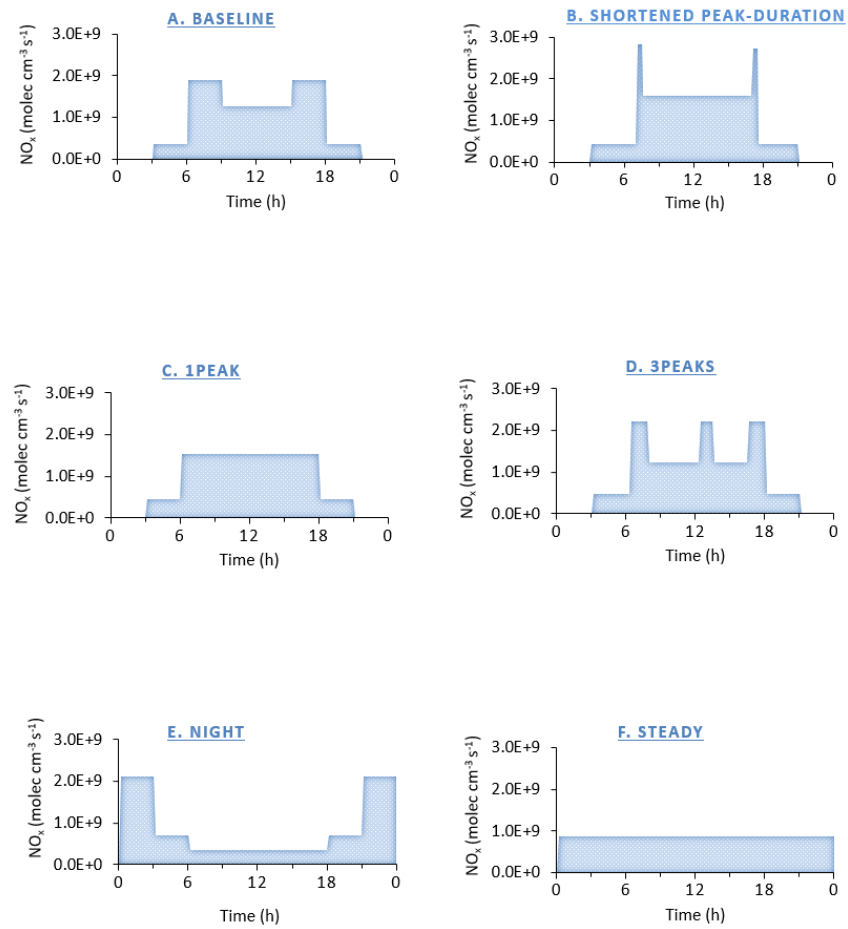
Figure 5. 2 Six modelled NO_x emissions scenarios, reflecting different distribution patterns of road traffic, whilst the total amount of NO_x emitted per day was held constant

5.3 Results and discussion

This study applied six contrasting emissions distribution scenarios, reflecting hypothetical differences in temporal traffic distribution, whilst at the same time maintaining the same total cumulative NO_x emission over a twenty-four hour period in each scenario.

Even though total ENO_x emissions would be same in all scenarios, ENO_x variations as a function of time are expected to change the pollutant levels in the atmosphere as temporal emission variation could perturb the chemical processes between atmospheric species, which are not linear. For example, the concentration of NO_2 is dominated by local NO_x road emissions (Hood et al., 2018). However, the effect of NO_x emissions on NO_2 background concentrations could be non-linear due to the rate of NO to NO_2 conversion processes which is slower near the road, i.e. close to NO sources due to low O_3 in urban areas (titration process), but it increases at downwind side, and this results in decreases in NO_x (but increase in NO_2) concentration with distance from the emission source (Hood et al., 2018).

5.3.1 Impact of temporal emission distribution pattern on atmospheric chemical species
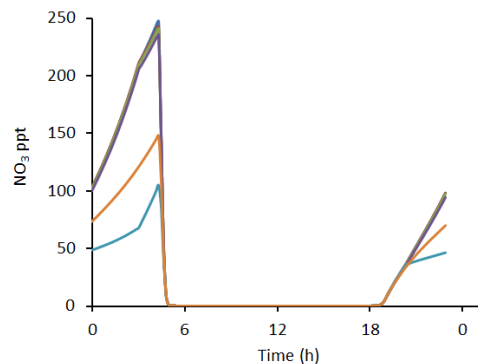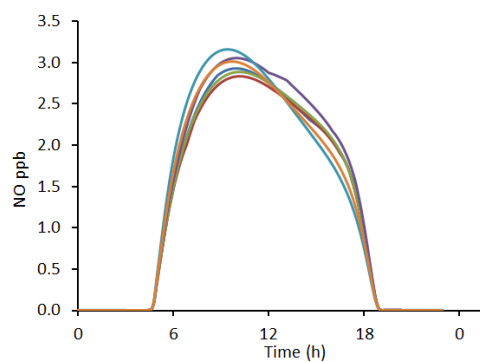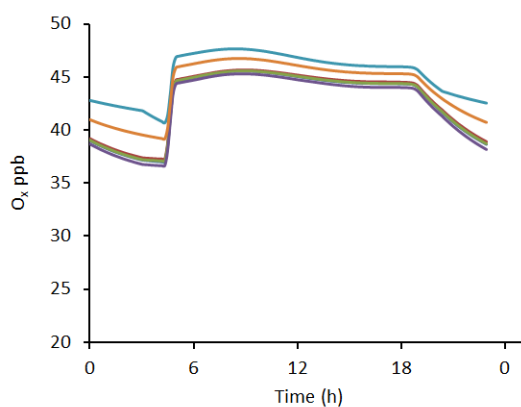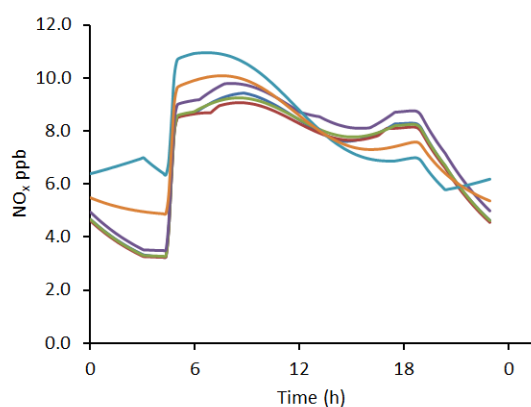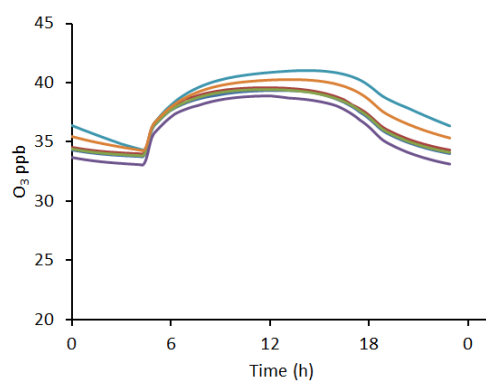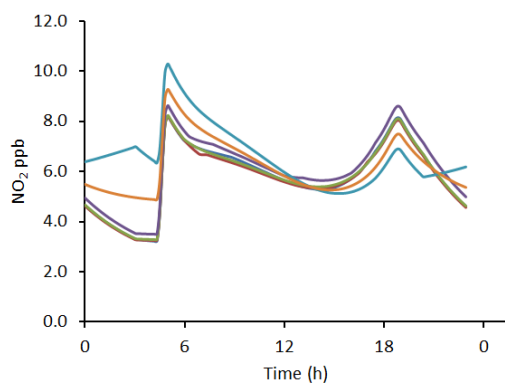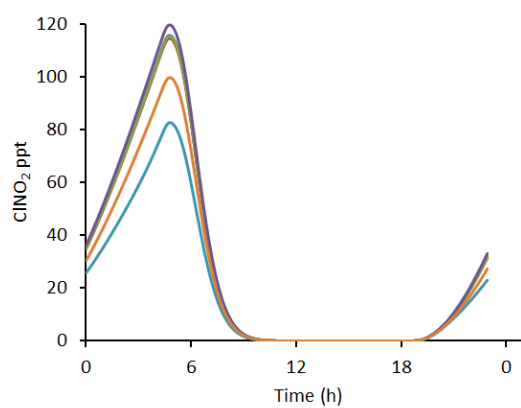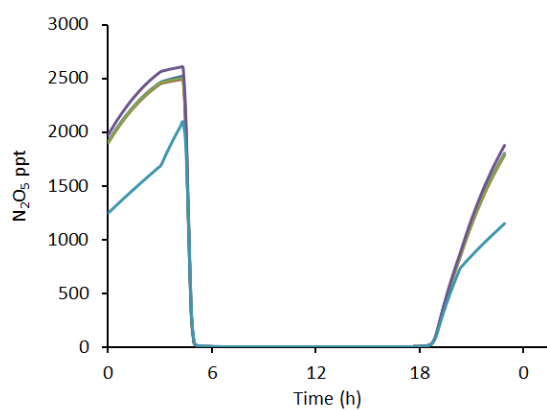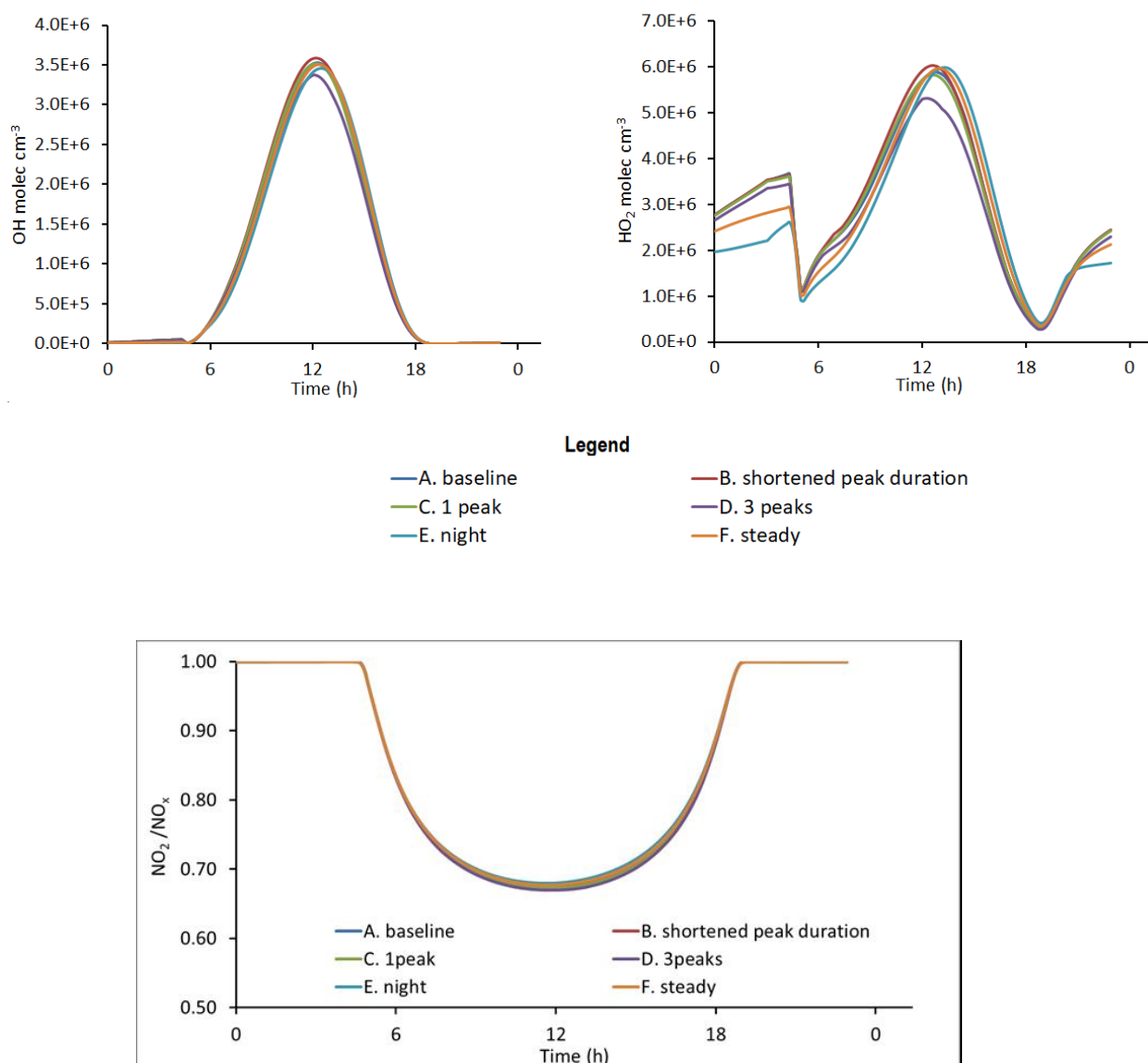
Figure 5. 3 The modelled results of the concentrations of eight atmospheric chemical species: OH and HO$_2$ (molec cm^{-3}); NO, NO$_2$, O$_3$, NO$_x$, O$_x$ (ppb); NO$_3$, N$_2$O$_5$, ClNO$_2$ (ppt), and for NO$_2$/NOx ratio for the six NO$_x$ emission scenarios. The blue line is baseline, red line is shortened peak duration, green line is 1 peak, purple line is 3 peaks, Aqua line is night, and orange line is steady case.

Day-time chemistry

As shown in Figure 5.3, during the morning (i.e. from 5am to approximately noon), the greatest NO, NO$_2$, NO$_x$, and O$_x$ mixing ratios occurred in scenario E followed by scenario F. In the afternoon, and until around 9 pm, NO, NO$_2$, NO$_x$, and O$_x$ (NO$_2$+O$_3$) reached

minimum levels in scenario E but, by contrast, the highest levels in the scenario 'D'. This pattern occurred as a result of emissions being at their lowest during the day in scenario E, but at their highest in scenario D. High levels of NO emissions during the day in scenario D led to faster titration of O_3, resulting in the concentration of the latter decreasing in scenario D case. The low emissions of NO during the day allowed O_3 to build up and increase its concentration in the scenario E, due to a slow NO_x titration process (Jin et al., 2008). The low concentration of O_3 caused OH and HO_2 to also fall to a low level in the scenario D compared to the other five scenarios. However, their concentrations were nearly similar in the other scenarios.

The model predicted extremely low concentrations of NO_3, N_2O_5, and $ClNO_2$ during the day, in all scenarios, because of photolysis of NO_3.

Night-time chemistry

From figure 5.3, during the night, NO primarily reacts with O_3 and the NO_3 radical to form NO_2. Thus, the NO concentration decreases to zero at night in all cases. Figure 5.3 demonstrates that the NO_2 mixing ratio decreases during the night (i.e. between 7:40pm to 4:20am) in all scenarios by more than > 5 ppb (3 ppb in scenario F), apart from scenario E. In E scenario NO_2 decrease by ~1ppb from 7:40 -9:10 pm, but from 9:10 pm to 3am, NO_2 increases again by ~1 ppb (i.e. when NO_x emissions are highest between 9 pm – 3 am), but, then decreases between 3am and 5am by ~0.6 ppb as NO_x emissions decreases from 3am. Similarly, maximum concentrations of NO_x and O_x are occurred in scenario E (Table 5.2). This shows the linear relationship between NO_2 concentration and NO_x emissions at night.

Generally, in all cases NO_2 concentrations reach a minimum value at 4:20 am as most of NO_2 is removed to produce NO_3 radicals, which peak at this time.

The lowest peak of NO_3 mixing ratio (105 ppt) was found to occur in scenario E, whereas, the greatest NO_3 (~247 ppb) was found in scenario A. The high NO_x emissions at night increased NO_3 consumption through its reaction with NO and VOCs (Stutz et al., 2004). Consequently, minimum NO_3, N_2O_5, and $ClNO_2$ occurred in scenario E; with a difference in mixing ratio to scenario D of 156%, 49%, and 48% respectively. Herein, the non-linear relationship between high NO_x emissions (and thus NO_2) and NO_3 and so N_2O_5 and $ClNO_2$ is apparent, as high emissions at night has resulted in more NO_3 removal.

In addition, from midnight to 3am, the minimum HO_2 (2.08×10^6 molec.cm^{-3}) occurred in scenario E compared to scenario D (3×10^6 molec.cm^{-3}), as most HO_2 reacts with NO_3 during the night to form NO_2. Moreover, the excess of NO_2 resulted in a greater formation of PAN, HO_2NO_2, and RNO_2 than NO_2 reaction with O_3 to form NO_3. Therefore, scenario E included maximum HO_2NO_2, RNO_2, and peroxyacetyl nitrate (PAN) concentrations (13%, 6%, and 3%) respectively compared to scenario B, in which minimum concentrations of HO_2NO_2, RNO_2, and PAN occurred (Figure 5.4).

$$HO_2 + NO_3 \; \rightarrow \; OH + NO_2 \hspace{4cm} R5.1$$

$$HO_2 + NO_2 \; \rightarrow \; HO_2NO_2 \hspace{4cm} R5.2$$
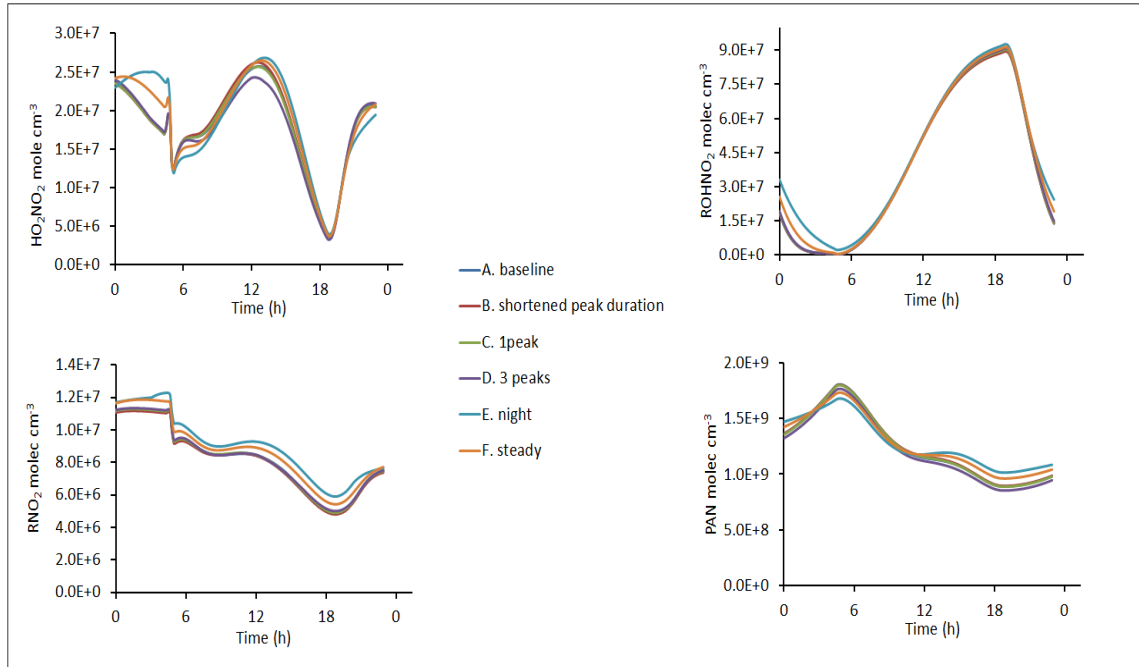
Figure 5. 4 Shows greatest concentrations (molec cm^{-3}) of HO_2NO_2, RNO_2, $ROHNO_2$, and PAN levels in 'night' case compared to other scenarios. : The blue line is baseline, red line is shortened peak duration, green line is 1 peak, purple line is 3 peaks, Aqua line is night, and orange line is steady case.

Table 5. 1 Demonstrates the a) maximum, b) average (over 24 hours) concentrations of a number of chemical species in each scenario over the final 24 hours of the model run period. The (bold, underline) and (bold, italic, underline) values indicate the highest (peak) and lowest values respectively. The unit for OH, HO_2, and Cl is molec.cm^{-3}; for NO, NO_2, and O_3 is ppb; and for NO_3 and N_2O_5 is ppt.

a)

Scenarios	OH	HO_2	NO	NO_2	NO_3	N_2O_5	O_3	$ClNO_2$	Cl
Baseline	3.53E+06	5.89E+06	2.94	8.20	**_246.94_**	2518.02	39.36	115.71	1.96E+04
Shortened peak duration	**3.59E+06**	**6.04E+06**	**_2.84_**	**_8.18_**	242.08	2490.45	39.62	114.74	1.94E+04
1 Peak	3.52E+06	5.84E+06	2.89	8.23	240.87	2503.10	39.40	115.20	1.95E+04
3 Peaks	**_3.38E+06_**	**_5.32E+06_**	3.05	8.63	235.72	**2605.26**	**_38.92_**	**119.53**	**2.02E+04**
Night	3.46E+06	6.01E+06	**3.16**	**10.29**	**_105.01_**	**_2093.49_**	**41.00**	**_82.64_**	**_1.36E+04_**
Steady	3.51E+06	5.98E+06	3.02	9.26	148.16	2266.87	40.30	99.70	1.66E+04

	OH	HO₂	NO	NO₂	NO₃	N₂O₅	O₃	ClNO₂	Cl

b)

Scenarios	OH	HO$_2$	NO	NO$_2$	NO$_3$	N$_2$O$_5$	O$_3$	ClNO$_2$	Cl
Baseline	1.03E+06	2.97E+06	1.304	5.81	**<u>44.66</u>**	664.91	36.91	27.27	3.10E+03
Shortened peak duration	**<u>1.05E+06</u>**	**<u>3.03E+06</u>**	***<u>1.27</u>***	***<u>5.74</u>***	44.55	658.91	37.17	27.03	3.10E+03
1 Peak	1.03E+06	2.96E+06	1.302	5.81	44.28	661.89	***<u>36.28</u>***	**<u>28.13</u>**	3.09E+03
3 Peaks	***<u>9.77E+05</u>***	2.73E+06	**<u>1.38</u>**	6.11	43.33	**<u>688.61</u>**	37.90	23.39	**<u>3.14E+03</u>**
Night	1.00E+06	***<u>2.68E+06</u>***	1.33	**<u>6.62</u>**	***<u>20.07</u>***	611.451	**<u>38.57</u>**	***<u>19.36</u>***	***<u>2.17E+03</u>***
Steady	1.02E+06	2.83E+06	1.31	6.19	29.53	***<u>571.61</u>***	37.91	23.40	2.65E+03

Table 5. 2 Mixing ratios of NOx (NO + NO$_2$) and Ox (NO$_2$ + O$_3$) in each scenario, averaged over the final 24 hours of the model run period. The (bold, underline) and (bold, italic, underline) values indicate the highest (peak) and lowest values respectively. The units are ppb.

Scenarios	NO$_x$	O$_x$
Baseline	7.11	42.72
Shortened peak duration	***<u>7.01</u>***	42.91
1 Peak	7.11	42.76
3 Peaks	7.94	***<u>42.40</u>***
Night	**<u>7.95</u>**	**<u>45.20</u>**
Steady	7.50	44.09

5.3.2 Impact of temporal emission distribution pattern on ClNO$_2$ chemistry

The influence of changing emission distribution from traffic on ClNO$_2$ chemistry, in terms of its impact on the concentrations of OH, O$_3$, and NO$_2$ is examined through running the model without the inclusion of ClNO$_2$ chemistry and compared with outputs of models where ClNO$_2$ included. For this section three emissions scenarios are selected including Scenario B. shortened peak duration, Scenario D. 3 peaks, and Scenario E. night and compared with the Scenario A. baseline. The results show little differences in the enhancement of OH and O$_3$, and the reduction of NO$_2$ by ClNO$_2$ chemistry between each scenario (Figure 5.5).
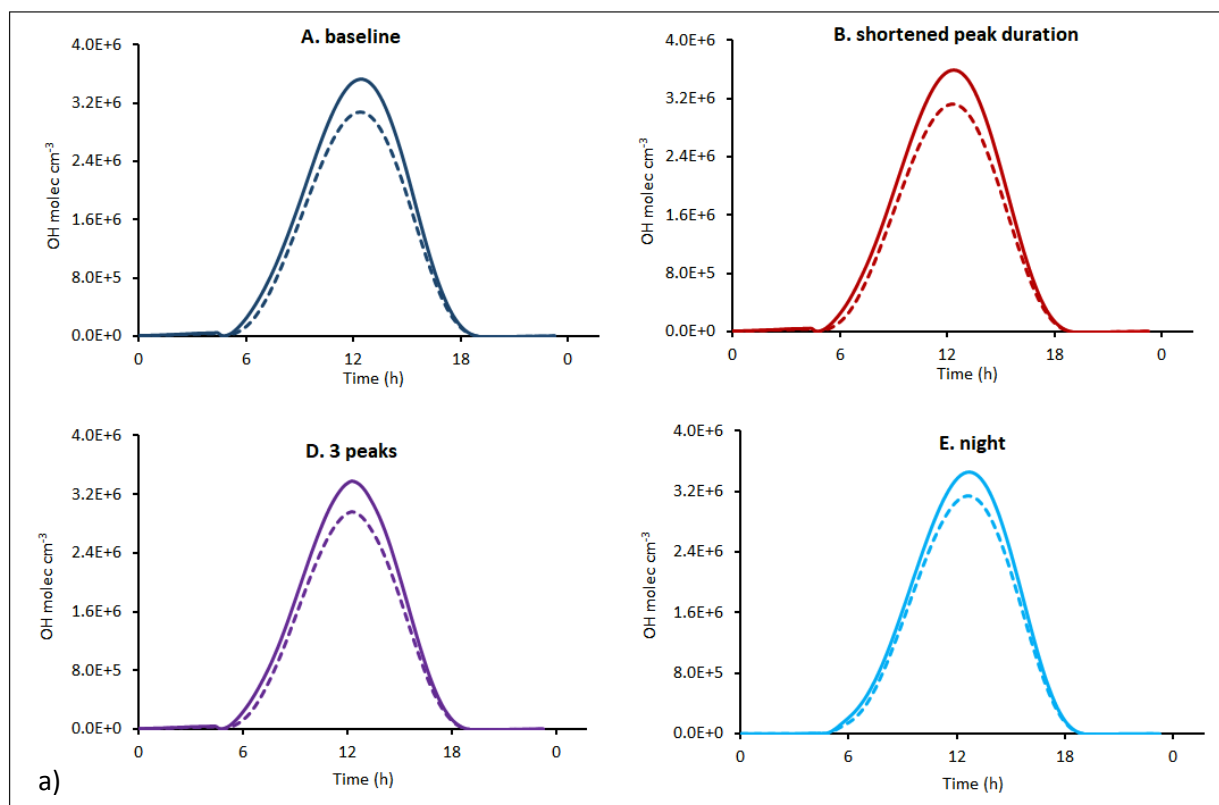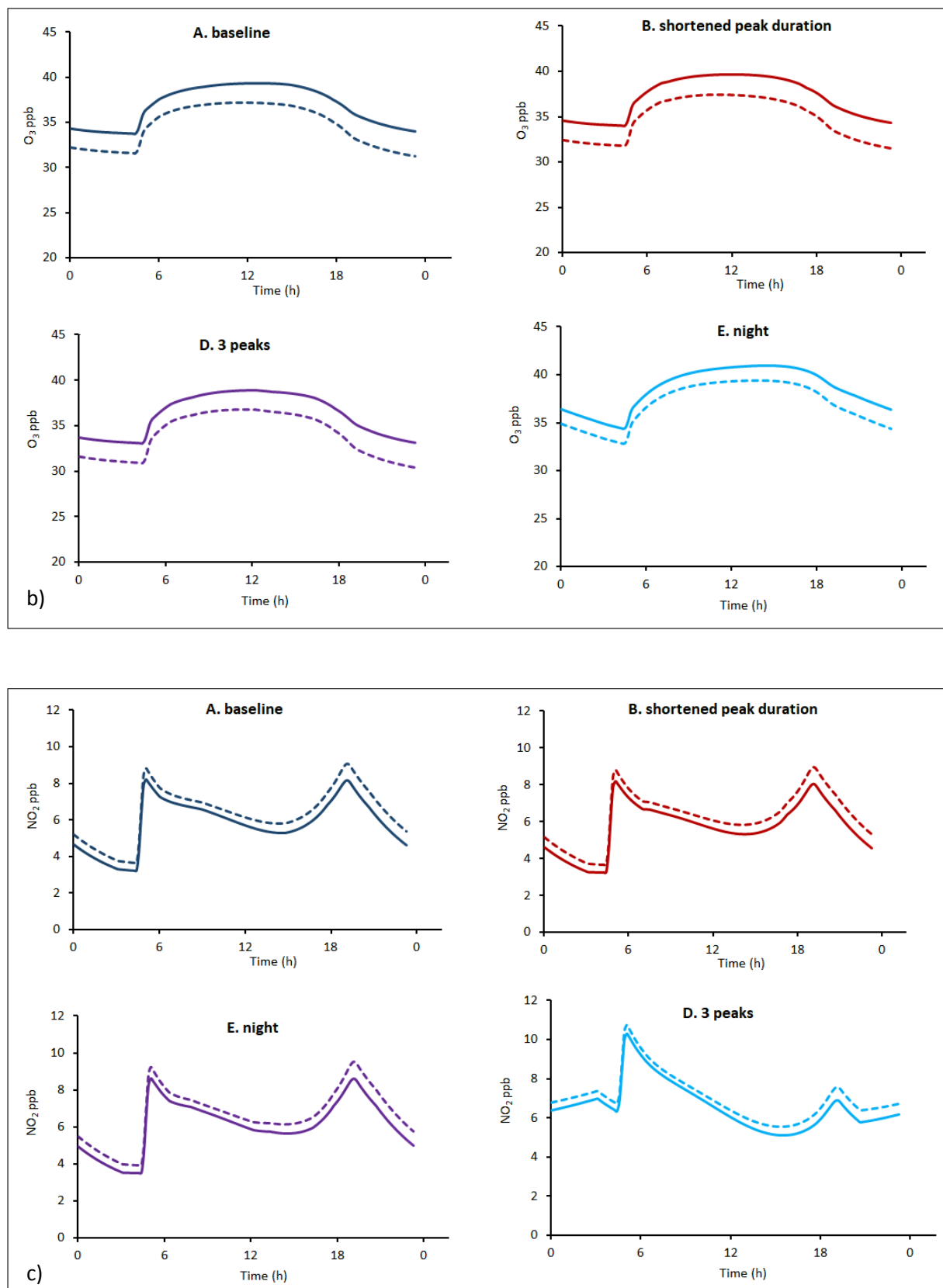
Figure 5. 5 Comparisons between emissions scenarios for the impacts of $ClNO_2$ chemistry on the enhancement of a) OH, b) O_3, c) NO_2

5.4 Air pollution control in urban areas

It has been well known that the fraction of NO_x emitted as NO_2 mainly from diesel vehicles has increased in the past decade in urban areas, specifically from 1995 to 2010 in most of the European countries, with substantially higher concentrations at busy roadsides. (Grange et al., 2017, Carslaw et al., 2016).

It is important to note that both short (hour) and long-term (annual) exposure to NO_2 has been linked to adverse effects on human health (Malley et al., 2018).

The results from the model simulations demonstrate that a variation in NO_x emissions on the road with time can affect air quality, even if total emitted NO_x is constant. The concentration of the pollutant differs between the morning, evening, and night, reflecting the complexity of atmospheric chemistry, and hence the difficulty in developing strategies to reduce air pollutants.

To examine how temporal variations in emission distributions can affect the NO_2 abundance in the urban atmosphere, the average mixing ratio of NO_2 during the day (7am-7pm), in the morning only (6-10am), and in the evening only (4-8pm) were calculated for each scenario and compared as shown in figure 5.6.

Multiple emission peaks during the day such as in scenarios D, B, and A have resulted in a high NO_2 mixing ratio on average from 7am-7pm, with the highest NO_x appearing in the scenario D. Alternatively, if emissions are higher during the night and lower during the day (E), the NO_2 mixing ratio reaches its maximum level in the morning (i.e. 6-10am) and its lowest levels in the evening (i.e. 4-8pm). Furthermore, if emissions are assumed to be constant over twenty-four hours, the NO_2 mixing ratio is highest in the morning (i.e. slightly lower than the E case).

The overall results show that the mean NO_2 concentration was significantly changed when the traffic distribution changed from A to E and F cases. Whereas, NO_2 levels do not change significantly between A, B, C, and D cases.

The percentage difference in NO_2 levels for each scenario was determined with respect to scenario A as this scenario is representative of typical current emission patterns during weekdays in the UK (Table 5.3). The changes in NO_2 were calculated by taking the

average in the morning and evening for each scenario and the percentage differences related to scenario A were then derived.

Table 5. 3 Summary of the change in average NO_2 mixing ratios in each scenario as related to the base case A. For the morning (7 to 10am), evening (4 to 8pm), and over 24 hours.

	NO_2 (ppb)		
Scenarios	Morning	Evening	24 hours
B. Shortened peak duration	-2.50%	-0.97%	-0.73%
C. 1 Peak	-0.81%	-0.18%	0.15%
D. 3 Peaks	3.99%	4.89%	5.25%
E. Night	18.64%	-13.4%	14.05%
F. Steady	9.46%	-7.71%	6.67%

Table 5.3 and figure 5.6 clarify that,1 peak emissions (scenario C) have a relatively small effect on NO_2 mixing ratio, but frequent peaks in emissions (scenario D) have resulted in ~4-5% increase in NO_2 at all times. Night and steady scenarios (E and F) have resulted in NO_2 increases by more than 18% and 9% respectively in the morning and by more than 14% and 6% average over 24 hours. In contrast, in the evening NO_2 in scenarios E and F has decreased by more than 13% and 7% respectively.

The shortened peak duration (scenario B) resulted in NO_2 decreases during the morning and evening, and over 24 hours. This scenario can be therefore considered as the most effective approach in reducing NO_2.
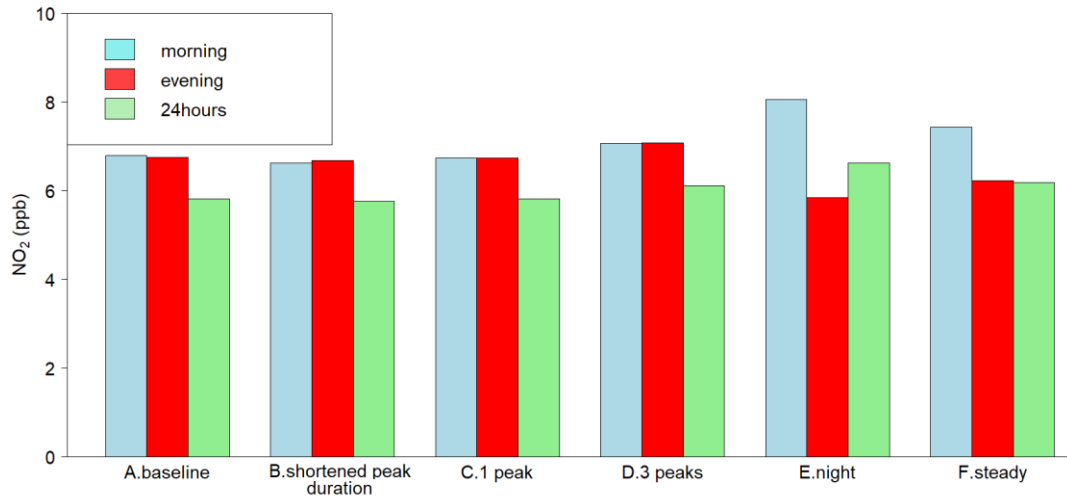
Figure 5. 6 Comparison between cases according to the time of day for NO_2 mixing ratio [The Y axis represents the mean values of NO_2 mixing ratio over 6 to 10am (morning), 4 to 8pm (evening), and 7am to 7pm (average over a day)]

5.4.1 Health implications

To protect human health, the European Union (EU) has established objectives and limit values for pollutants. In the UK, hourly (short term) and annually (long term) average limit value for NO_2 concentrations have been set to 200 and 40 μgm^{-3} respectively, and to not be exceeded more than 18 times per a year for the former (Defra, 2004). The objectives for short and long-term limit values aim to offer protection from exposure to a high concentration of NO_2 over a short and long period. Therefore, in the UK those areas with high concentrations of NO_2 (i.e. higher than the limit value set for NO_2 by the European Union) would be identified by a local authority as areas in need of air quality management, with measures being set to reduce the concentrations in these areas (Defra, 2004).

The rate of all-cause mortality increases by 2.5% for every 10 μgm^{-3} increase in the annual mean concentration of NO_2 (Defra, 2015:3; Hitchcock and Carslaw, 2016).

According to the Office for National Statistics, there were 525,048 deaths registered in England and Wales in 2016 (Defra, 2016). Amongst these around 23,500 (~ 4.5%) deaths per year were related to exposure to NO_2 (Defra, 2016). In order to assess the effect of changing NO_x emission distribution on the mortality, assumptions and simple calculations

were used as described below. Scenarios B and E were selected for the calculation as they represent the best and worst scenarios respectively related to the decrease and increase in NO_2 concentrations.

First, we assume that, this value (23,500) is the number of deaths for scenario A over one year related to the scenario without NO_2 concentrations (i.e. 501,548 deaths per year).

Second, a 10 μgm^{-3} increase of NO_2, the number of deaths increases by 2.5%, to be 587.5.

- For B. shortened peak duration: Over 24 hours, NO_2 in the base case is 5.81 ppb (11.10 μgm^{-3}), and in scenario B is 5.76 ppb (10.97 μgm^{-3}) with the difference 0.13 μgm^{-3}.

  The decrease in the number of deaths in Scenario B $= \frac{0.13 \; x \; 587.5}{10} = $ ~8 people/year (1.2%).

  $23500 - 8 = 23492$ the number of deaths per year if emission distribution changed from scenario A to scenario B.

For morning (6-10am): the number of deaths decreases by 2.5%, equivalent to ~ 19 people/year.

- For E. night: Over 24 hours, NO_2 in base case is 5.81 ppb (11.10 μgm^{-3}), and in scenario E is 6.62 ppb (12.66 μgm^{-3}) with the difference 1.56 μgm^{-3}.

  The increases in the number of deaths in Scenario E $= \frac{1.56 \; x \; 587.5}{10} = $ ~92 people/year (14%).

For morning (6-10am): the number of deaths increases by 18.6% related to the base case, equivalent to 142 deaths per year.

To sum up, the change in diurnal emission distribution from scenario A to scenario B resulted in a decrease in the number of deaths/ year due to NO_2 by 8 (1.2%) for the case if NO_2 mixing ratio averaged over 24 hours. However, the number of deaths is more decreased by 19 (2.5%), when it was calculated for morning case (NO_2 averaged over the morning, from 6-10am).

In contrast, the number of deaths is increased by 92 (14%), when the diurnal emission distribution changed from scenario A to scenario E for 24 hours case. For the morning case (6-10am) the number of deaths is further increased by 142 (18.6%).

It is important to bear in mind that the above rough calculation does not take into account many factors that can affect pollutant concentration in the air including chemistry, road and engine conditions, meteorological factors, and season.

Further modelling studies capable of identifying the effects of the diurnal variation of emission distribution on mortality would be important to trace road traffic distribution/driving effects on human health/mortality, i.e. geographical methods (Elliot and Cuzick, 1992) or high resolution dispersion modelling study (Colvile et al., 2001). Furthermore, there is a need for long term observation of emissions on road, i.e. to identify the annual rate of mortality for days/roads with no congestions or peaks and when there is a peak rush hour or a traffic jam.

Table 5. 4 Summary of the change in average NO_2 mixing ratios (Δ) in each scenario as related to the base case (A) and the effect of the changes on the number of deaths. The concentration of NO_2 averaged over the morning (7 to 10am), evening (4 to 8pm), and over 24 hours.

Scenarios	Morning		Evening		Averaged over 24 hours	
	ΔNO_2	Δ people/yr	ΔNO_2	Δ people/yr	ΔNO_2	Δ people/yr
B. shortened peak duration	- 2.5%	- 19	- 1.0%	- 8	- 1.2%	- 8
C. 1 peak	- 0.8%	- 6	- 0.2%	- 1	0.0%	0
D. 3 peaks	+ 3.9%	+ 30	+ 4.9%	+ 37	+ 5.2%	+ 34
E. night	+ 8.6%	+ 142	- 13.4%	- 102	+ 14.1%	+ 92
F. steady	+ 9.4%	+ 71	- 7.8%	- 59	+ 6.6%	+ 43

5.4.2 Measures to reduce NO_2

The increase in NO_2/NO_x ratio has a significant impact on the concentration of NO_2, as has been observed at a number of sites in London (Carslaw, 2005). The results from this modelling study suggest that emissions of NO_x that are low during the day but high at night (scenario E) result in an increase in NO_2 concentrations during the morning (7-10 am) by ~19%, but a decrease in the evening (4-8 pm) by ~13% (Table 5.3) compared to scenario A (base case).

In Delhi for example, the majority of heavy goods vehicles (HGVs) are based on diesel (Guttikunda and Goel, 2013), which is the main source of primary NO_2 emissions. Therefore, restrictions are applied on HGVs on city roads during the day to reduce the daytime exposure rate, however, the low boundary layer at night will decrease the dispersion of emissions (Guttikunda and Goel, 2013, Kumar et al., 2015).

5.5 Diurnal traffic emissions distribution effects on NO_2 levels in the city of Delhi, India: a case study

According to Guttikunda and Goel (2013), the transport sector is a major contributor of NO_x emissions in Delhi, India, and emissions from this sector comprises of more than 50% of the total NO_x emissions from all sources. In Delhi, the majority of NO_x emissions are attributed to diesel vehicles (Guttikunda and Goel, 2013). Thus, policies were implemented in Delhi to restrict the movement of heavy commercial duty trucks into the city to night-time only (9 pm- 6am) to reduce NO_x emissions and re-suspension of dust (Guttikunda and Goel, 2013). However, it has been shown that this policy measure negatively affected Delhi air quality, due to meteorological factors, especially the low boundary layer at night, when the cold wind passing through the city at night (Kumar et al., 2015). Low mixing layer results in reduced dispersion and thus pollutants build up in the ambient air (Guttikunda and Goel, 2013).

In section 5.4, we found the maximum NO_2 mixing ratio in the morning and over 24 hours when NO_x emissions are low during the day, but high at night (scenario E) compared to NO_2 in other scenarios as predicted by the model (Figure 5.3). This emission pattern (scenario E) is well suited to represent the Delhi case. A steady scenario (F) on the other hand could also represent traffic operation in Delhi if emissions at night are nearly same as in daytime. Here, it is important to understand the effect in the change of the amount of NO_x emissions on NO_2 mixing ratio in these two emissions scenarios (E and F). For this purpose, sensitivity tests are conducted to assess the response of NO_2 levels upon increase or decrease of NO_x emissions in scenarios E and F.

Herein, five simulations were performed with different total NO_x emissions (ENO_x), but the initial concentration of NO_2 kept constant in all simulations. Scenario E is the baseline

(ENO$_x$ = 1.48x10^6 molec cm^{-3} s^{-1}), and then these emissions were changed in each simulation: decreased to half of that amount (-50%); increased by half (50%) of ENO$_x$; doubled (200%); tripled (300%); and increased by five (500%) and ten times (1000%) of ENO$_x$.

The simulation results depicted in Table 5.5 show slight similarities in the percentage changes of NO$_2$ mixing ratio (averaged over 24 hours of the final day of the model run, averaged over the morning 6-10 am, and averaged over the evening 4-8 pm) between scenarios E and F that were produced from the six cases of varying total of NO$_x$ emissions.

In general, if total NO$_x$ emission rate can be reduced by half of that in the baseline, NO$_2$ mixing ratio will be decreased by 87% and 88% in night and steady cases (scenario E and F) respectively. Alternatively, NO$_2$ will approximately linearly increase if emissions increased by 50%, 200%, and 300% of the baseline, however, the NO$_2$ increase slows when emissions are increased by 500% and 1000% times as shown in Figure 5.7. The reason is because, NO$_2$ titration process increased approximately linearly when NO$_x$ emissions increased by 50%, 200%, and 300% of emissions in the baseline. However, with more increase in NO$_x$ emissions (by 500% and more), the titration process slows down, as most O$_3$ are removed via titration, and the system becomes saturated with NO$_x$. Thus, in high NO$_x$ condition, the addition of more emissions will have less impact on the NO$_2$ mixing ratio, and the relationship between NO$_2$ mixing ratio and emissions becomes less linear.

It is also important to notice that, in both scenarios (E and F), the response of change in NO$_2$ levels to emissions variations (increase or decrease) was greater in the morning than in the evening, and maximum NO$_2$ occurred in the morning than in the evening in these two scenarios (E and F) as shown in Figure 5.7. This means that the high emissions at night but low in the day (scenario E) or when emissions is identical in day and night (scenario F), will cause NO$_2$ to build up in the morning, due to lack of sunlight to remove NO$_2$ and high emissions at night will increase NO$_2$ budget in the morning. Therefore, the condition in the morning in the both scenarios (E and F) is saturated with NO$_x$; the NO titration process is slow (Hood et al.) due to lower O$_3$ concentrations near the source, and the response of NO$_2$ levels to changes in emissions (increase or decrease) will be less linear. Alternatively, in the evening, the condition can represent as a low NO$_x$, and thus the

increase or decrease in NO_x emissions will affect NO_2 mixing ratio due to faster NO titration process, due to high O_3 in the afternoon.
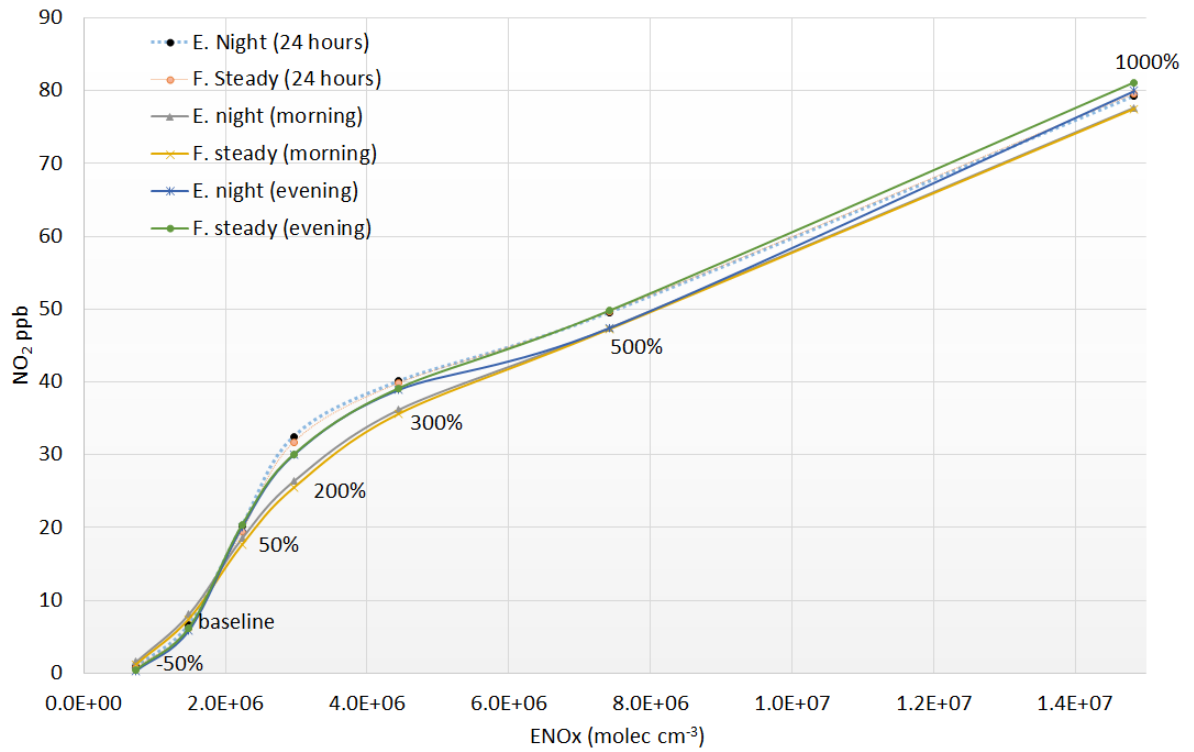
Figure 5. 7 Response of NO_2 to changing total NO_x emissions in E and F scenarios.

- - • - - NO_2 mixing ratio averaged over 24 hours for night (scenario E);

—•— NO_2 mixing ratio averaged over 24 hours for steady (scenario F);

—▲— NO_2 mixing ratio averaged over the morning (6-10 am) for night (scenario E);

—✕— NO_2 mixing ratio averaged over the morning (6-10 am) for steady (scenario F);

—✳— NO_2 mixing ratio averaged over the evening (4-8 pm) for night (scenario E);

—•— NO_2 mixing ratio averaged over the evening (4-8 pm) for steady (scenario F)

Table 5. 5 Percentage of NO$_2$ levels change in response to NOx emission variations, compared with NOx emissions in the base case.

Cases	E. night			F. steady		
	Averaged 24 hours	Morning	evening	Averaged 24 hours	Morning	evening
x 0.5	-87%	-81%	-94%	-88%	-84%	-92%
x 1.5	204%	129%	242%	216%	137%	228%
x 2.0	392%	227%	413%	416%	243%	385%
x 3.0	506%	349%	566%	548%	380%	531%
x 5.0	648%	488%	740%	707%	536%	703%
x 10.0	1097%	863%	1267%	1193%	944%	1209%

5.6 Conclusion

The results of this modelling study indicate that the diurnal distribution pattern of emissions influences the concentration of pollutants. Significant changes to NO$_2$ related to the baseline scenario A took place (from highest to lowest) in scenarios E. night, F. steady, and D. 3 peaks. The highest NO and NO$_2$ concentrations in the '3peaks' scenario made the OH reactions with NO$_2$ preferable over its reaction with VOC. Thus, removing OH and NO$_2$ from the system resulted in lower concentrations of O$_3$ and OH. The lowest concentrations of N$_2$O$_5$ and ClNO$_2$ occurred in the night (E) scenario, as high emissions resulted in an additional conversion of NO$_2$ to PAN, RNO$_2$, and HO$_2$NO$_2$. Maximum NO$_2$ occurred in night scenario 'E' in the morning (between 6 to 10am). This therefore creates greater exposure to high NO$_2$ during the morning. From a simple calculation, reducing the duration of peak rush hour from 2 hours to 30 minutes resulted in a decrease in NO$_2$ concentrations by 0.08 μgm^{-3}, and consequently the number of deaths decreased by 0.02% (equivalent to ~ 5 person). However, the night emission scenario (E) resulted in an increase in NO$_2$ concentrations by 1.55 μgm^{-3}, which increased the number of deaths by 0.6% (equivalent to > 91 persons). This calculation can also be applied to estimate the

impact of diurnal emission distributions on the economic cost of human health degradation due to increases/ decreases in urban NO_2 levels.

This study therefore recommends better traffic management by local authorities to reduce NO_2 concentrations, by reducing the duration of the time peak rush hour during weekdays and the school term. In a study conducted in July 2003 to measure airborne particulates in urban areas in Leeds, UK, Lingard et al. (2006) observed lower particle concentrations during off-peak hours (i.e., free-flow traffic conditions) than during peak hours. They observed that during off-peak hours, vehicles held at red lights for a much shorter time than during peak-hours, which this resulted in less road congestion and better driving performance, as during peak- hours, most drivers accelerate hard on the light change.

Although reducing peak rush hour to thirty minutes may be not realistic in real life, it is important to be considered in transport management. For example, improving traffic flows, as suggested by Hitchcock and Carslaw (2016). Reducing the volume of traffic can be achieved by many ways such as reducing cost of public transport, staggered working hours (staggered working shift) (Elston, 1979).

The results from the sensitivity tests conducted to examine the impact of increases/ decreases in total NO_x emissions on NO_2 levels for both night (E) and steady (F) scenarios (Delhi case) demonstrated that NO_2 decreases by ~88% (as average over 24 hours), and by more than 90% (in the evening) in both scenarios if total emissions reduces by a half,- 50%. This implies that the public will be exposed to less NO_2 in the air.

In contrast, NO_2 approximately linearly increases with increasing emissions by 50%, 200%, and 300% of the emissions in the baseline. This approximate linearity relationship will be reduced as emissions increase more by 500% and 1000% as the system will be more saturated with NO_x, and less O_3 will be available for titration process, that makes the effect of emissions on NO_2 less important. This indicates the importance in controlling NO_x emissions to not reach a saturated level as it is case in developing countries, where an increase / decrease of emissions will be less effective on NO_2 concentrations.

These results indicate that any change in traffic conditions (flow) must be coupled with tail-pipe emissions reduction measures (for example, improve NO_x reduction catalysts in diesel fuel vehicles), because changing traffic flow only does not reduce NO_2 abundance (averaged over 24 hours) in the air, it rather can increase NO_2 level as in scenario E. It is

also important to consider and differentiate the meteorological factors and atmospheric chemistry between day and night when planning traffic management. The differences in boundary layer high between day and night, temperature, relative humidity, and wind speed are important factors that affect pollutant dispersion. Furthermore, photochemical chemistry is the daytime chemistry driver, while, VOC oxidations by NO_3 and O_3 radicals is the main nighttime atmospheric process at night. For example, in the absence of sunlight at night, the main removal of NO_2 will be $ClNO_2$ or HNO_3 formation from heterogeneous reaction, which affect the following day NO_2 budget in the atmosphere.

Chapter 6 Modelling heterogeneous inorganic nitrate aerosol formation

In this chapter, the model developed in Chapters 2 and 3 is further extended to include nitrate aerosol particulate formation and loss reactions, to explore the use of the box model to predict nitrate aerosol formation from N_2O_5 hydrolysis. The model was evaluated with measurement data from AURN monitoring stations. In addition, the model was run applying two of the emissions scenarios that were developed in Chapter 5 to examine the effect of diurnal variation in emission distribution from traffic on nitrate formation in an urban area. Finally, the impact of $ClNO_2$ chemistry on nitrate aerosol concentrations is assessed.

6.1 Introduction

Atmospheric particulate matter (PM) is a pollutant that has been associated with increased mortality (Pope III et al., 2009, Kumar et al., 2006, American Lung Association, 2006), visibility reduction (Pan et al., 2016; Watson, 2002), and climate change (Myhre et al., 2013). Primary PM is emitted to the atmosphere from natural (such as sea spray, biomass burning and re-suspension of soil) and anthropogenic (power plant, road transport, biomass burning) sources, whereas secondary PM is formed from the oxidation of gas phase precursors (Harrison and Yin, 2004). The main components of PM in urban areas are thought to be organic compounds, sulphate, nitrate, ammonium, sea salt, trace metals, mineral compounds, and biological materials (Harrison and Yin, 2004, Jimenez et al., 2009). Reducing these components (from anthropogenic sources) is necessary in order to reduce PM concentrations in the atmosphere. Figure 6.1 illustrates the main chemical composition of PM_{10} and $PM_{2.5}$ in Birmingham city centre, UK. Moreover, Jimenez et al. (2009) measured the mass concentration and mass fractions of inorganic and organic constitutes in sub-micrometre aerosols (fine (100-1000 nm) and ultrafine (<100 nm)) by the Aerosol Mass spectrometer (AMS) in the Northern Hemisphere in winter and summer (Figure 6.2). More nitrate and sulphate concentrations present in aerosol in summer than in winter in UK urban area.

The main inorganic aerosol components are: sulphate (SO_4^{2-}), ammonium (NH_4^+), and nitrate aerosol (PNO_3^-) and considered as the main fraction of $PM_{2.5}$ (particles with aerodynamic diameter $\leq 2.5\mu m$). However, PNO_3^- which is a secondary inorganic aerosol, mainly forms from NO_x oxidation and can be found in both accumulation (100 nm < diameter <1 μm) and coarse (diameter > 1 μm) modes. PNO_3^- forms a significant fraction in both $PM_{2.5}$ as NH_4NO_3 from the reaction of NH_3 and HNO_3 (R6.2), and coarse aerosol mode ($2.5\mu m$-$10\mu m$) from HNO_3 chemistry (Seinfeld and Pandis, 2016, Petetin et al., 2016). According to Putaud et al. (2010), PNO_3^- contributes to an average of 6-16% and 6-20% of $PM_{2.5}$ and PM_{10} in Europe, respectively.
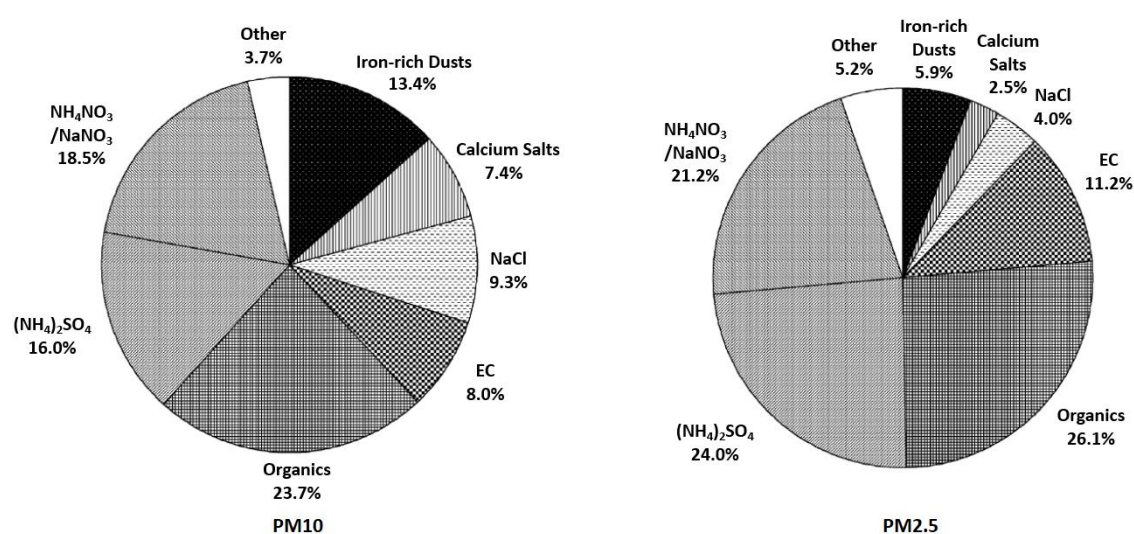
Figure 6. 1 Main chemical composition of PM_{10} (left), and $PM_{2.5}$ (right) measured in Birmingham city centre (Harrison and Yin, 2008).
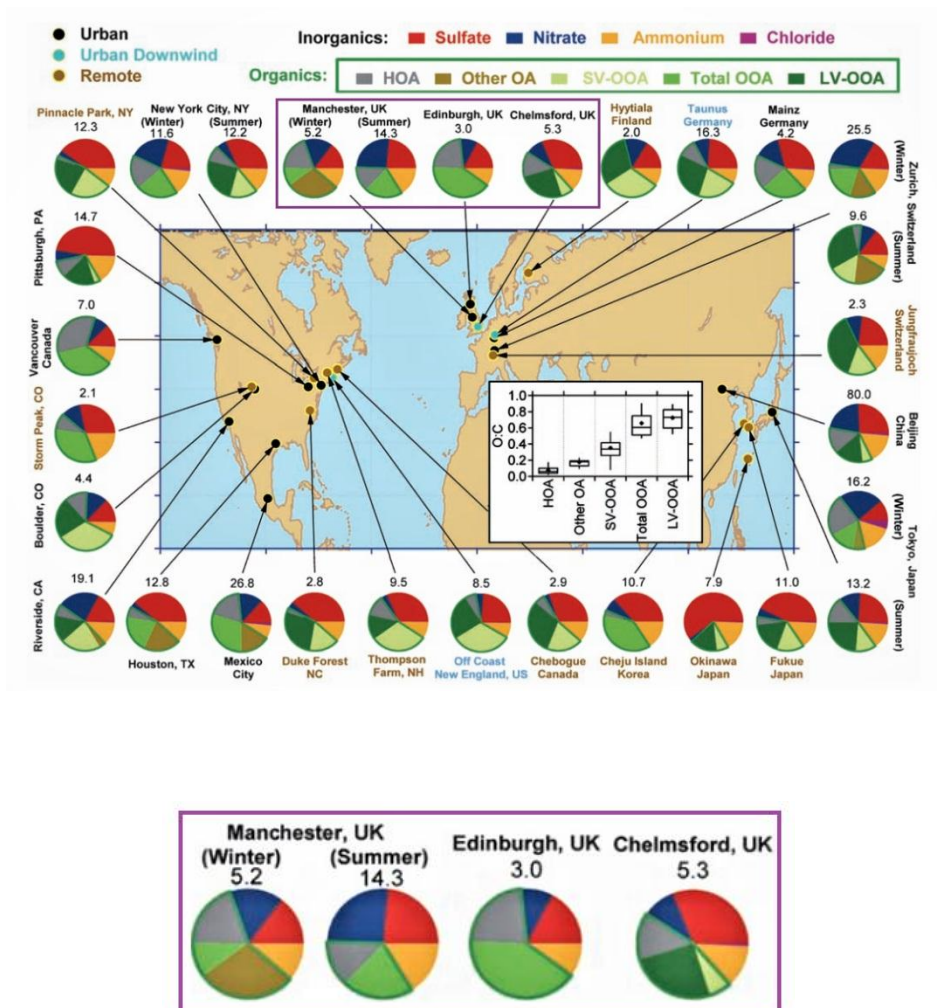
Figure 6. 2 Main chemical composition of submicron aerosol in the UK (Jimenez et al., 2009)

The main source of nitrate aerosol during the daytime is thought to be the chemical reaction between gas phase nitric acid (HNO_3) and ammonia (NH_3) and other alkaline compounds (Seinfeld and Pandis, 2016, Wen et al., 2018). Xue et al. (2014) showed that rapid production of nitrate was observed around noon in Hong Kong, which was consistent with elevated gas phase HNO_3 production from hydroxyl radical (OH) reaction with nitrogen dioxide (NO_2) (R6.1). The authors also observed that the reaction of gas phase N_2O_5 with aerosol (R6.4 and R6.5) was a dominant nitrate source in the afternoon due to elevated NO_2 concentrations and reduced nitrate (NO_3), and N_2O_5 photolysis loss (Xue et al., 2014).

The homogenous formation of nitrate (in the form of ammonium nitrate (NH_4NO_3)) is highly dependent on temperature and relative humidity. Low temperature and low relative humidity shift the equilibrium to an NH_4NO_3 aerosol (R6.3) (Bauer et al., 2007):

145

$$OH + NO_2 + M \quad\quad \rightarrow \quad HNO_{3(g)} + M \quad\quad\quad\quad R6.1$$

$$HNO_{3(g)} + NH_{3(g)} \quad\quad \leftrightarrow \quad NH_4NO_{3(s)} \quad\quad\quad\quad R6.2$$

$$HNO_{3(g)} + NH_{3(g)} \quad\quad \leftrightarrow \quad NH_{4(aq)}^+ \; + \; NO_{3\,(aq)}^- \quad\quad R6.3$$

$$NO_3 + h\nu \, (< 700 \; nm) \; \rightarrow \; NO + O_2 \quad\quad\quad\quad R1.32a$$

$$NO_3 + h\nu \, (< 580 \; nm) \; \rightarrow \; NO_2 + O(^3P) \quad\quad\quad R1.32b$$
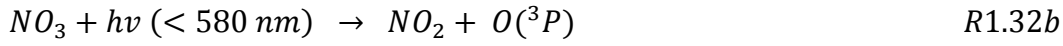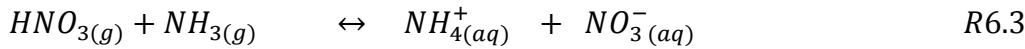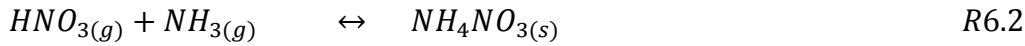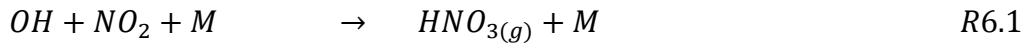
At night as photolysis ceases, PNO_3^- formation from the heterogeneous reaction of N_2O_5 with aerosol containing H_2O is thought to be efficient and comparable or even greater than PNO_3^- formation from the daytime reaction of HNO_3 and NH_3 (Pathak et al., 2009, Shon et al., 2013, Wang et al., 2017, Xie et al., 2009). The concentration of N_2O_5 is limited in the daytime due to rapid NO_3 photolysis (j(NO_3) ranges between 0.02 s^{-1} (R1.32a) and 0.156 s^{-1} (R1.32b) at noontime) (Brown and Stutz, 2012). However, in a polluted environment with high NO_x emissions and in cloudy conditions, the N_2O_5 reaction with aerosols can play an important role in the formation of PNO_3^- (Su et al., 2017).

The reaction of N_2O_5 with aerosols containing water produces either two PNO_3^- molecules (R6.4) or PNO_3^- and $ClNO_2$ (R6.5) if the aerosol contains chloride (Cl$^-$) (Pusede et al., 2016):

$$N_2O_{5(g)} + H_2O_{aerosol} \quad\quad \rightarrow \quad 2PNO_3^- \quad\quad\quad\quad R6.4$$

$$N_2O_{5(g)} + Cl_{aerosol} \quad\quad \rightarrow \quad ClNO_2 + PNO_3^- \quad\quad R6.5$$
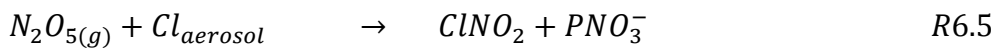
Abundance of the precursor gases (NO_x, and NH_3) and meteorological factors, such as temperature and humidity, play an important role in PNO_3^- formation (Xu and Penner, 2012, Xue et al., 2014). Low temperature limits N_2O_5 thermal decomposition resulting in more N_2O_5 accumulation, thus the heterogeneous reactions with aerosol will be more dominant than at high temperature (Griffiths et al., 2003). Therefore, PNO_3^- formation is suggested to be significant at cold temperatures and at night (Shon et al., 2013).

This study highlights the role of N_2O_5 heterogeneous reactions in the formation of nitrate particulate in rural and urban areas; taking into account the impact of NO_x emission distribution from traffic on particulate nitrate formation.

Many modelling studies have used a simple box model or the Community Multiscale Air Quality Modelling System (CMAQ) to evaluate nitrate aerosol formation from N_2O_5 heterogeneous reactions (Wang et al., 2018, Wagner et al., 2013, Yun et al., 2018, Xue et al., 2014, Deng et al., 2010, Wang et al., 2017, Li et al., 2016, Zheng et al., 2015).

However, to our knowledge, there are no studies, which have used a detailed chemical mechanism such as the MCM for modelling nitrate aerosol formation from N_2O_5 reactions with aerosol. Moreover, those modelling studies that have been used for simulating nitrate or $ClNO_2$ formation used a constant value for the N_2O_5 uptake on aerosol coefficient (γ), or this value was calculated from the measured NO_2, O_3 and nitrate radicals. While, we have incorporated the calculations of the γ_{N2O5} into the model as explained in Chapter 3.

6.2 Methods

6.2.1 Model updates

The model was further updated to include the reactions responsible for PNO_3^- formation. The pseudo first-order heterogeneous rate constant of N_2O_5 reactions with aerosol to form $ClNO_2$ and PNO_3^- are calculated by using equations Eq 6.1 and Eq 6.2:

$$\frac{dClNO_2}{dt} = \frac{\emptyset \gamma_{N_2O_5} \omega S_A}{4} \qquad Eq6.1$$

$$\frac{dPNO_3^-}{dt} = \frac{(1-\emptyset)\gamma_{N_2O_5} \omega S_A}{4} \qquad Eq6.2$$

Where, $\emptyset$ represents the production yield of $ClNO_2/PNO_3^-$, (γ) is the uptake coefficient of N_2O_5, which is the probability of collision of N_2O_5 with an aerosol particle that results in its uptake at the surface of the particle (Gržinić et al., 2016); S_A is the aerosol surface area density (cm^2cm^{-3} of air) upon which the reaction is taking place, and ω is the mean speed of the molecule N_2O_5 (ms^{-1}), which is determined as a function of temperature, which was calculated in the model by using Eq3:

$$\omega N_2O_5 = \sqrt{\frac{8RT}{\pi (M_{w_{N_2O_5}})}} \qquad Eq3.7$$

In the model, the pseudo first order loss rate coefficient of nitrate aerosol is determined as the inverse of its lifetime of 4 days (Xu and Penner, 2012). Atmospheric removal of aerosol, and hence their lifetime varies according to their size. Small particles; nucleation mode (0.01 μm < diameter < 0.1 μm) have short lifetimes (hours) due to their rapid atmospheric removal by coagulation and condensation onto the surfaces of other particles (Harrison and Yin, 2004; Vu et al., 2015). Particles in the accumulation mode (0.1 μm < diameter < 2 μm) have longer lifetimes (several days to weeks), and larger particles in the coarse mode (1 μm < diameter < 10 μm) have a short lifetimes again (hours to days) especially for particles > 10 μm as they can be efficiently removed by dry and wet deposition. Nitrate can be found in both fine (as ammonium nitrate) and coarse particles (Seinfeld and Pandis, 1998). In this study, we have assumed nitrate is found predominantly in coarse mode particles, and hence considered N_2O_5 reaction with them, with a lifetime of 4 days.

The aerosol lifetime in the boundary layer is controlled by wet and dry deposition of aerosol particles and of gases that are in equilibrium with the aerosol particles (Pusede et al., 2016).

The physical parameters (temperature, pressure, location and date), and chemical conditions that were used to initialise the model for the model validation (Chapter 3) were also used for this study. Any update to the model for this study is otherwise mentioned throughout the chapter.

Two model experiments have been conducted, based on different products of the heterogeneous reaction of N_2O_5 with aerosol: 1) to produce nitrate aerosol only (R6.4); 2) to produce nitrate aerosol and $ClNO_2$ (R6.5), which are included in the model for the final part of the study (explained in section 3.4) to evaluate the impact of $ClNO_2$ on the concentration of nitrate aerosol.

Initial conditions and the concentrations of the inorganic and organic compounds used within the model are summarised in Table 6.1.

The model was initialised for rural (Harwell) and urban polluted (London Kensington) locations, and the results compared with measurement data to evaluate the model performance and accuracy.

The measured mean concentrations of NO, NO_2, O_3, nitrate and chloride particulates for Harwell and London in August 2014 (Table 6.1) were used to initiate the model, with data taken from the Defra website (https://uk-air.defra.gov.uk/data/data_selector). The Harwell monitoring station is based on the Harwell Science Centre located in South East of England (latitude: 51.57, longitude: -1.32) and was selected as it represents a rural background environment could be used to validate the model. In addition to the species mentioned earlier, ten VOCs have been added to the model where their initial values are the mean mixing ratios that were measured in Essex as part of the Tropospheric Organic CHemistry experiment (TORCH) in 2003 (Lee et al., 2006). TORCH data was used because there were no measurements of VOCs available at the Harwell site.

The 10 VOCs (listed in Table 6.1), which are selected based on their reactivity toward chlorine atoms, as explained in Chapter 2, were multiplied by a factor to obtain a similar OH-VOC reactivity (3.396 s^{-1}) that was observed in Essex during the TORCH campaign (Lee et al., 2006).

The model was run for 8 days to allow the chemical species in the model, including those with a short and intermediate lifetime, to reach a steady state level and not be overly affected by the initial conditions of the experiment, and the 8th day of the model is used for the analysis.

Table 6. 1 Initial conditions used in the model for the Harwell case. VOC mixing ratio were taken from TORCH measurements in Essex 2012 but multiplied by 1.8 to obtain total OH reactivity (3.19 s^{-1}) close to the measurement. The differences in data used for the model validation (Table 3.6) and for this study are bolded.

Chemical parameters	Chemical formula	Model input	Physical parameters	Model input
Nitric oxide	NO	**0.65 ppb**	Latitude	**51° 57′ N**
Nitrogen dioxide	NO_2	**1.83 ppb**	Longitude	**-1 °32 W**
Ozone	O_3	**28 ppb**	Day	1
Methane	CH_4	1800 ppb	Month	8
Formaldehyde	HCHO	2898 ppt	Year	2014
Acetaldehyde	CH_3CHO	2750 ppt	Start time	12.0 Midnight (UTC)
Toluene	C_7H_8	506 ppt	Temperature	287.5 K
Mxylene	C_8H_{10}	243 ppt	Pressure	1013.25 hPa
Isoprene	C_5H_8	241 ppt	Ideal gas constant	$8.314 \text{ J K}^{-1} \text{ mol}^{-1}$
Ethene	C_2H_4	844 ppt	Water vapour (H_2O)	2%
Propene	C_3H_6	266 ppt	Nitrogen (N_2)	78.09%
Methanol	CH_3OH	6813 ppt	Oxygen (O_2)	20.79%
Ethanol	C_2H_5OH	2185 ppt		
Acetylene	C_2H_2	711 ppt		
Chloride aerosol	Cl	**1.34 µg m^{-3}**		
Nitrate aerosol	PNO_3	**1.67 µg m^{-3}**		

6.3 Results

6.3.1 Model configuration and validation of the modelled nitrate concentration with measured data

The modelled nitrate was validated with measured nitrate aerosol data from the Harwell monitoring station during August 2014 (the same date as used for model validation in Chapter 3).

The hourly measured data shows that the nitrate concentration is highly variable with both the time of the day and from day to day (Figure 6.3). This variation is related to

meteorology, temperature, relative humidity (Wang et al., 2006), wind speed (Xue et al., 2014), precursor gas levels (mainly NH_3 and NO_2, and nitric acid (Orel and Seinfeld, 1977, Wang et al., 2016), aerosol water content (Pathak et al., 2009), and pH of the droplets (nitrate concentration decreases with decreasing pH) (Orel and Seinfeld, 1977). Sulphate concentrations affect aerosol acidity, an increase in sulphate will decrease the acidity of the aerosol, especially in regions with limited concentrations of NH_3, because the latter can neutralise sulphate, thus the pH of the aerosol will increase (Ding et al., 2018). However, a high level of NH_3 at night may reduce the aerosol acidity and limit the N_2O_5 hydrolysis reactions as shown by (Wen et al., 2018). It has been suggested that a low aerosol pH may indicate that the N_2O_5 reaction with aerosol is a primary source of nitrate (Pathak et al., 2009, Battaglia Jr et al., 2017). Battaglia Jr et al. (2017) highlighted the differences in aerosol acidity between urban and rural areas in the USA and found that higher temperatures accompanied with lower relative humidity in urban areas triggered by Urban Heat Island factors especially in summer caused the aerosol to be more acidic compared to rural areas. However, aerosol pH varies according to location and aerosol composition (Craig et al., 2018). The aerosol water content is a limiting factor of its pH, as pH represents the concentration of H^+ in an aqueous solution (Guo et al., 2015). The presence of ammonia in the aerosol for example results in neutralization of the particle's acidity, forming dry ammonium sulphate salt (Jacob, 2000), which inhibits the N_2O_5 dissociation and nitrate production. Therefore, the rate of nitrate or $ClNO_2$ formation increases with increase aerosol acidity (Jacob, 2000).
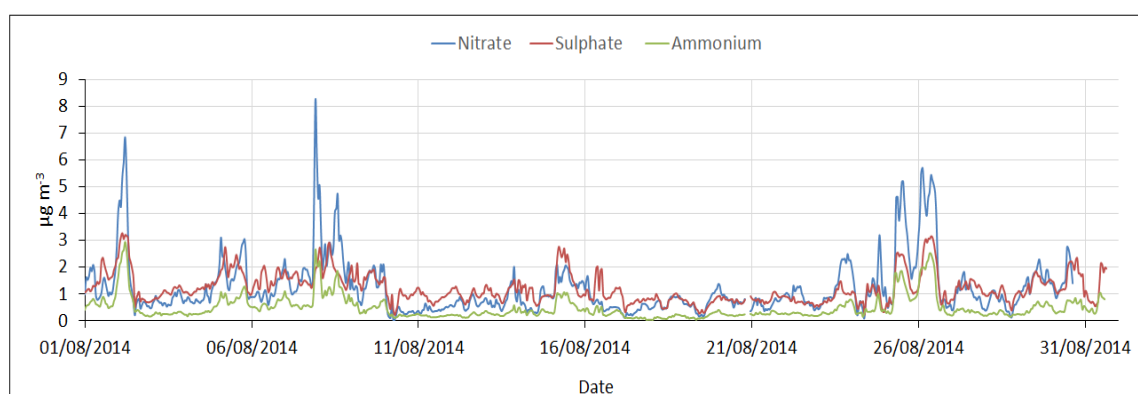
Figure 6. 3 Time series of the observed concentrations of nitrate, ammonium, and sulphate in Harwell, August 2014 (Defra, 2018)

The only nitrate formation pathway used in the model is the heterogeneous reaction of N_2O_5 on the aerosol surface. The homogenous reactions of HNO_3 with NH_3 have not been considered as this study is focused on the effect of N_2O_5 heterogeneous reaction on nitrate. Thus, the model represents a lower limit to PNO_3^- formation rate.

N_2O_5 can mainly accumulate during the nighttime as during the day the concentration is limited due to rapid photolysis of NO_3, the NO_3 reaction with NO, and N_2O_5 thermal decomposition. However, under certain conditions as mentioned in the introduction (cloudy, high levels of precursor gases) several pptv of N_2O_5 have been observed during the daytime, such as in the New England region in summer 2004 (Brown et al., 2005). It is acknowledged that in the atmosphere other chemistry contributes to nitrate formation, mainly the reaction of HNO_3 with NH_3 predominant in the daytime depending on the concentration of NH_3 (Richards, 1983)

The measured mean nitrate concentration in Harwell was 1.22 μgm^{-3} over August, and maximum and minimum concentrations of ~8 and 0.02 μgm^{-3} respectively were recorded on the 8th of August, 2014. The predicted mean nitrate concentration (1.07 μgm^{-3}) was close to the measured mean over 24 hours of the model 8th day (Figure 6.4).
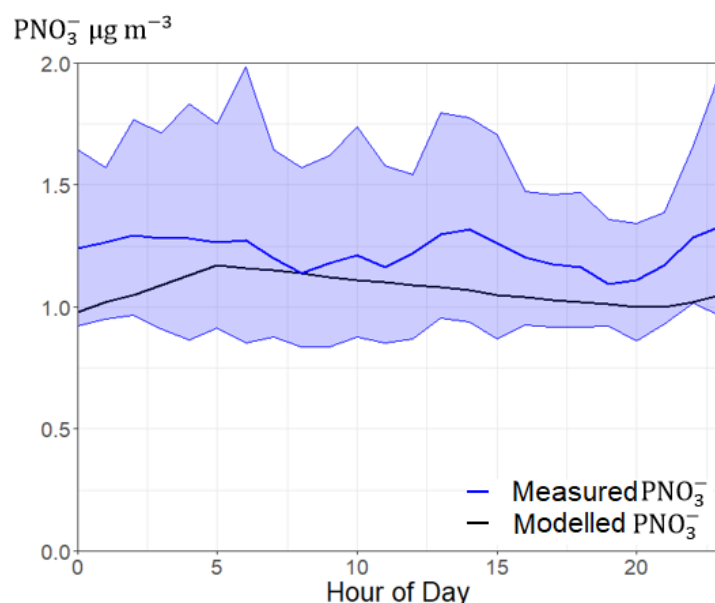
Figure 6. 4 Measured (averaged over August) and modelled nitrate for Harwell. The modelled nitrate is represented by the black line and the measured nitrate by the blue line, with the shaded areas representing 95% confidence intervals in the mean.

Although the model was able to predict nitrate (Figure 6.4) and NO, NO_2 close to measured concentrations (Figure 6.5a and 6.5b), the model predicted high O_3 mixing ratios (maximum of ~ 83 ppb) (Figure 6.5c), whereas no more than 45 ppb of O_3 was measured over August, as shown in Figure (6.6). Figure 6.7 presents the diurnal profiles of NO, NO_2, and O_3 mixing ratio that was measured in Harwell in August 2014.
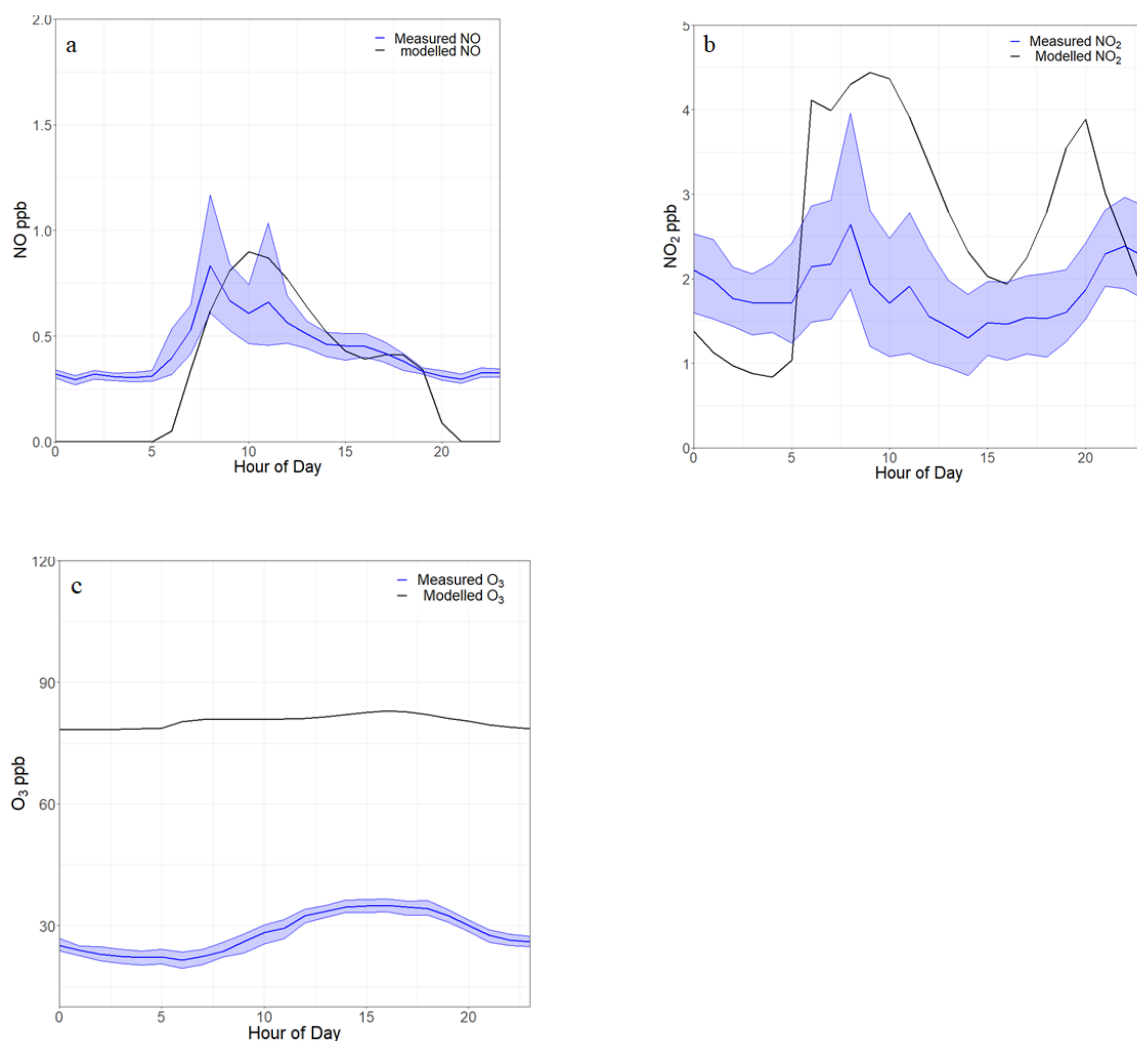
Figure 6. 5 Comparison between modelled and mean measured diurnal profiles (August 2014) of a) NO, b) NO_2, and c) O_3 for Harwell
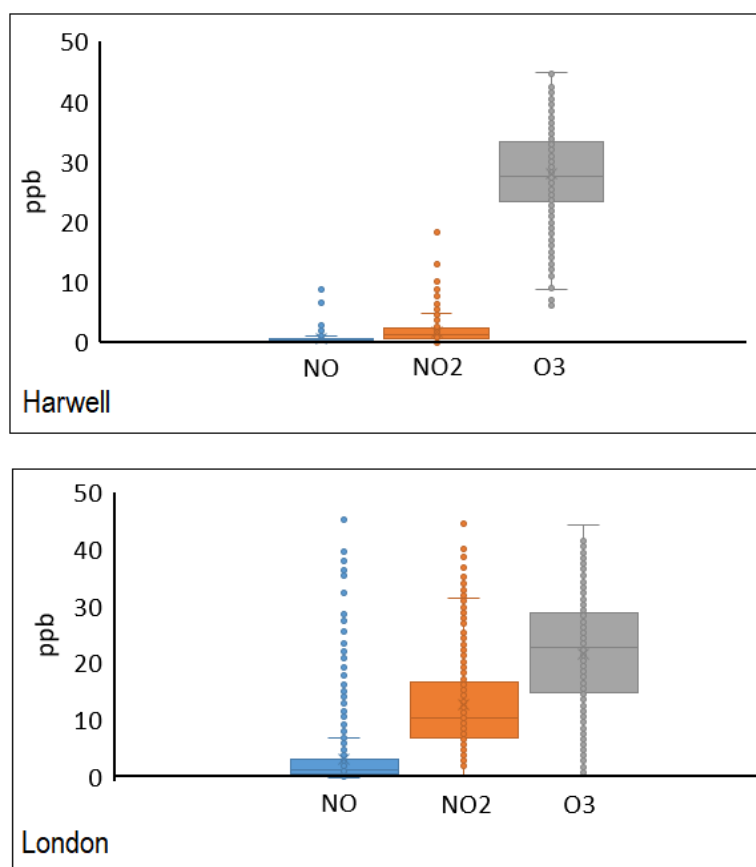
Figure 6. 6 Box plot showing mean, minimum, and maximum mixing ratios of NO, NO$_2$, and O$_3$ measured for Harwell and North Kensington, London across August 2014 (Defra, 2018). NO (blue box), NO$_2$ (orange box), and O$_3$ (grey box).
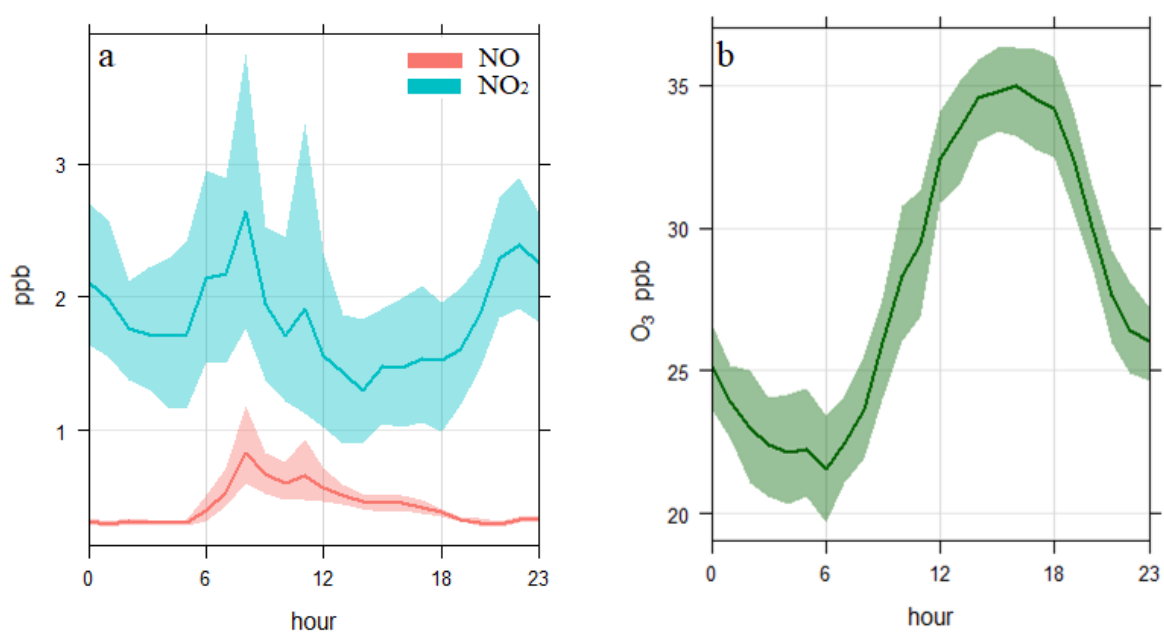
Figure 6. 7 Mean diurnal profiles for a) NO and NO$_2$, and b) O$_3$ that measured in Harwell over August 2014

In addition to the concentrations of O_3 precursors, many other factors influence O_3 which has a lifetime of several days to weeks in the troposphere (Young et al., 2013, Ni et al., 2018). Those factors are emissions, meteorological factors (wind speed and direction, temperature, radiation), the height of the boundary layer, topography, regional O_3 background, deposition, and atmospheric chemical processes (Tong et al., 2011).

In order to obtain a realistic O_3 level (close to the measurements), O_3 dry deposition near the ground was added as a major sink of O_3 at ground level (Osthoff et al., 2018, Sillman et al., 1990). The rate (flux) of O_3 deposition is the product of the dry deposition velocity of a pollutant and its concentration above the surface, which is negligible for O_3 due to lack of O_3 direct emissions from the surface as given by the following equation:

$$F = -V_d[O_{3\,(z)} - O_{3(0)}] \qquad\qquad Eq6.3$$

Where F is vertical dry deposition flux (molec cm^{-2} s^{-1}), vd is the deposition velocity (cm/s), $O_{3\,(z)}$ and $O_{3\,(0)}$ are the concentrations of O_3 (molec cm^{-3}) at a reference level above the surface and at the surface respectively. The O_3 concentration on the surface is zero as there is no direct emissions of O_3 from the ground. A typical deposition velocity of O_3 over the continents is estimated to be 0.4 cm s^{-1} (Hauglustaine et al., 1998). The height of the boundary layer (BLH) affects vertical mixing and thus O_3 dispersion (Haman et al., 2014, Tong et al., 2011). Therefore, the flux (F) was divided by the estimated boundary layer height (BLH) of 1000 metres to obtain the average deposition rate (Lin et al., 2010). An approximate, fixed boundary layer height throughout the day and night was used in the model which represents a typical daytime BLH in urban areas.

The rate coefficient for dry deposition *(k O_{3dry})* was then calculated by dividing the flux (rate) by the concentration of O_3 (Eq 6.4), giving a deposition rate of 4x10^{-6} s^{-1}, which was included in the model.

$$k_{O_{3dry}} = \frac{Flux_{O3\,dry}}{[O_3]} \qquad\qquad Eq6.4$$

The inclusion of the O_3 deposition equation in the model resulted in a decrease in the mixing ratio of NO, NO_2, O_3, (Figure 6.8a and 6.8b) and nitrate concentrations (Figure 6.8c). The model predicts a mean nitrate concentration of 0.71 µg m^{-3}, which is lower (~ 40%) than the observed mean (1.22 µg m^{-3}), but close to the observed range (95% confidence intervals in the mean) (Figure 6.9). The underestimation of nitrate is further investigated in section 6.3.2.

155
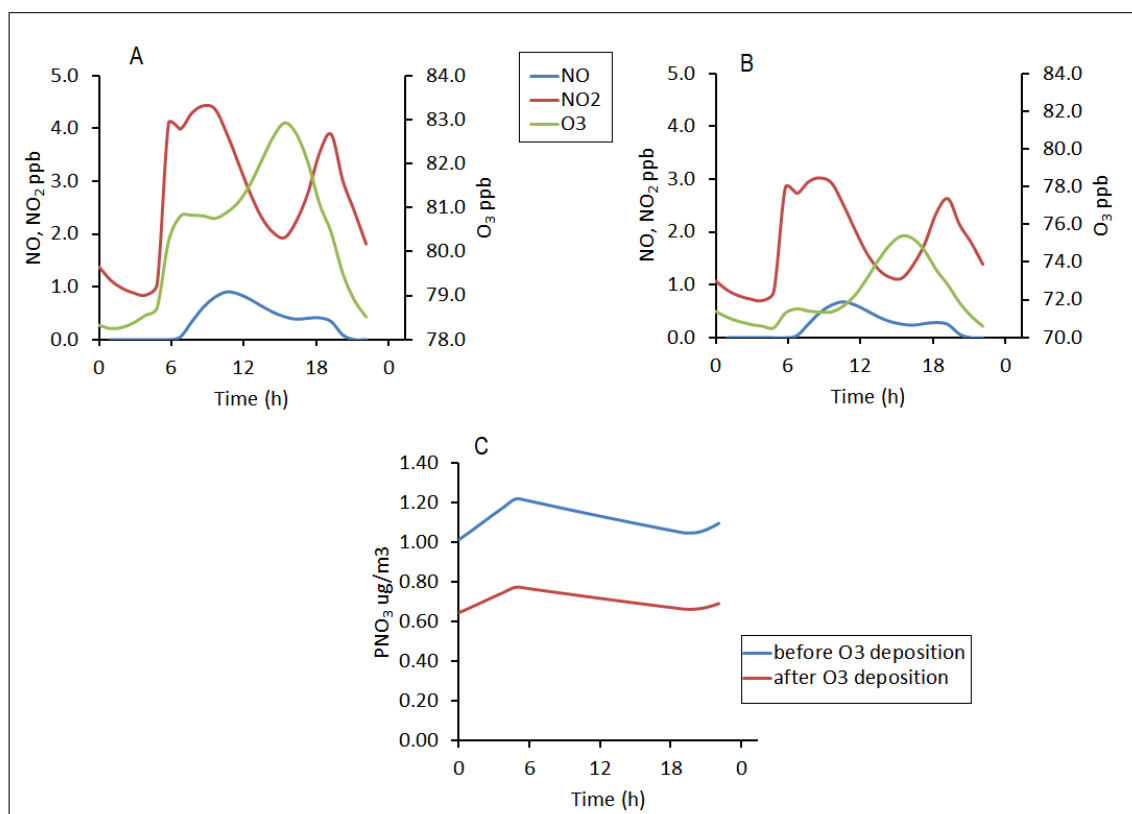
Figure 6. 8 Modelled NO, NO$_2$, and O$_3$ mixing ratios for A) before and B) after adding O$_3$ deposition reactions in the model; C) and PNO$^-_3$ concentrations for Harwell case
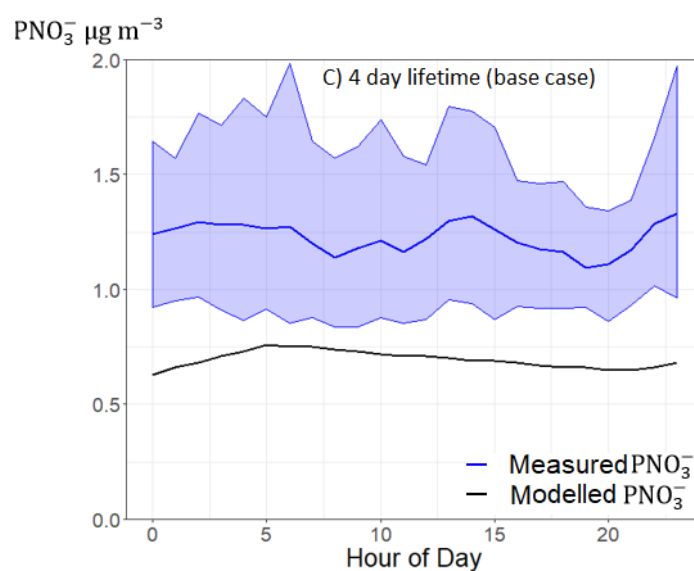
Figure 6. 9 Measured (averaged over August) and modelled nitrate for Harwell after O$_3$ deposition was added to the model (BLH is 1000 metres)

The simulated O_3 after including O_3 deposition in the model is reduced (maximum ~75 ppb), but still high relative to the measured O_3, and this may be related to how the MCM treats O_3 formation and loss according to different reactive mix of VOCs. The formation of O_3 starts from the reaction of OH reaction with hydrocarbons to form organic peroxy radicals.

To investigate the predicted O_3 mixing ratios as a function of the initial mixing ratio of NO_x, 11 model runs were conducted with varying mixing ratios of NO_x, whereas the initial O_3 mixing ratio was kept constant and all other parameters unchanged. The base case was the model that predicted maximum O_3 ~ 83 ppb, in which NO_x was ~ 2 ppb. The initial mixing ratios of NO_x used in the 11 model runs were: 1, 5, 10, 15, 20, 30, 40, 50, 60, 80, and 100 ppb, and the initial NO and NO_2 concentrations were assumed to be 40% and 60% of NO_x respectively.

 The model predicts high O_3 levels in low NO_x conditions, however, O_3 remain nearly constant for those runs with NO_x between 20 and 100 ppb.

Figure 6.10A and 6.10B show that the maximum O_3 (~75ppb) occurred in models with low NO_x mixing ratios (1, 2, and 5ppb) as low NO_x concentrations lead to high photochemical O_3 production (Sillman et al., 1990). O_3 decreased by 9 ppb when NO_x increased from 5ppb to 10 ppb, and decreased by 28 ppb when NO_x increased from 5 ppb to 15 ppb. There was a slight decrease in O_3 concentrations when NO_x was increased from 15 to 80 ppb.

This result indicates that O_3 is not sensitive to NO_x increases under low NO_x conditions (1-5 ppb), as O_3 remains nearly constant (~75 ppb), because NO_x is less available for O_3 titration. While, in high NO_x conditions (30 − 80 ppb), O_3 decreases slightly with increasing NO_x. However, O_3 becomes highly sensitive to NO_x when the latter ranged between 5-15 ppb. This implies the importance of NO_x titration in those areas when NO_x are in that range (5 − 15 ppb).

The maximum concentrations of OH and HO_2 were 1.94×10^7 and 2.28×10^8 molec cm^{-3} respectively when O_3 was high (~75 ppb), they, however, decreased sharply to 3.35×10^6 and 5×10^6 molec cm^{-3} respectively when NO_x was changed from 10 to 15 ppb and above; OH and HO_2 reached their minimum concentrations of 2.36×10^5 and 8.83×10^4 molec cm^{-3} respectively when NO_x was 100 ppb (Figure 6.8). This shows that OH and HO_2 did not increase with increasing NO_x mixing ratios, consequently, less OH is available to oxidise

VOCs, thus, less NO is converted to NO_2 and thus, less O_3 will be formed (Figure 1.2 in Chapter 1).
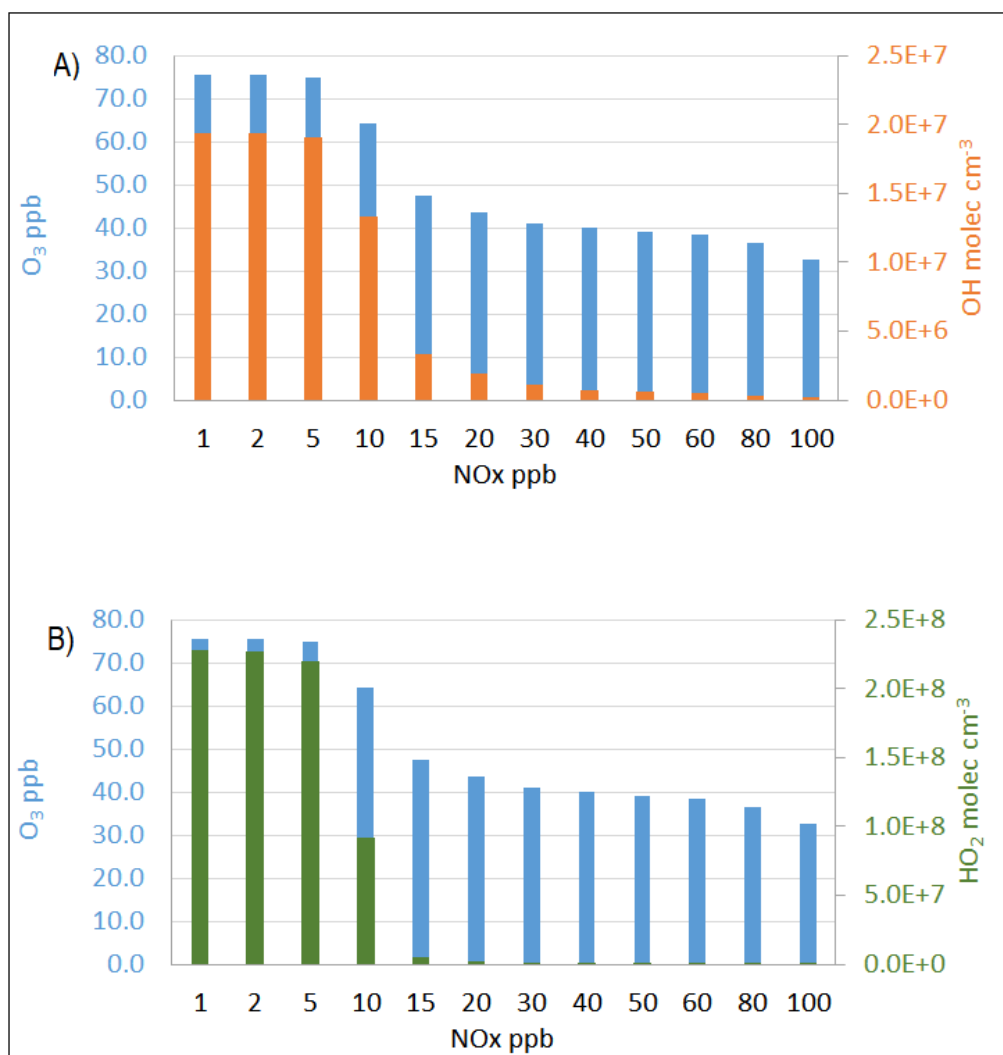
Figure 6. 10 Relationship of O_3 with **(A)** OH and **(B)** HO_2 as a function of varying concentrations of NO_x. O_3 (blue) on left axis, OH (orange), and HO_2 (green) on right.

6.3.2 Factors affecting particulate nitrate formation

The under predicted nitrate from the model is attributed to several factors, which are mentioned below:

6.3.2.1 Boundary layer high (BLH)

The boundary layer is the lowest part of the atmosphere, which is directly affected by the ground surface. Convective turbulence due to heating the earth's surface by the Sun enhances the vertical mixing and thus deepening of the BLH, resulting in diluting pollutants with clean air reducing pollutant concentrations. However, in stable conditions, when the air near the ground is cooler than the overlying air, a temperature inversion can occur that inhibits vertical mixing, thus the concentrations of pollutants increase and build up near the surface (Lutgens et al., 2010).

In China, in some locations higher concentrations of nitrate were observed at night than in the daytime, owed to lower temperature at night that inhibited decomposition of N_2O_5, or NH_4NO_3, and higher BLH during the daytime that encouraged dilution. Conversely, in other locations higher nitrate concentrations were observed during daytime than during the night, attributed to higher boundary layer heights that enhance regional transport of emissions to the area (Wen et al., 2018).

In this study, a BLH of 1000 metres was used for determining the rate constant of O_3 dry deposition. The effect of the BLH on nitrate concentrations was tested by changing the BLH to 500 metre in the O_3 deposition calculation. It was found that the mean nitrate concentrations (1.23 µg m^{-3}) increased by more than 70% (Figure 6.11), which is supporting the concept of increasing concentrations of pollutants associated with lower boundary layer height.
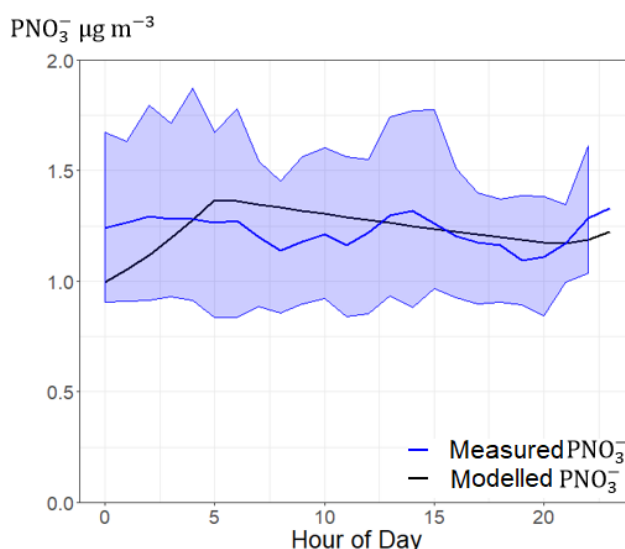
Figure 6. 11 Measured (averaged over August) and modelled nitrate for Harwell after O_3 deposition was added to the model and the BLH was reduced from 1000 to 500 m.

6.3.2.2 Atmospheric lifetime of nitrate

Direct nitrate deposition on the ground is thought to be the main removal pathway of nitrate from the atmosphere. However, generally the atmospheric lifetime of aerosols by dry deposition may be several days if not removed by precipitation or fog (Seinfeld and Pandis, 1998).

In addition, gas-phase HNO_3 which is the main precursor of nitrate formation, is rapidly removed from the atmosphere via dry deposition (Richards, 1983), with a typical dry deposition velocity estimated to be 4 cm s^{-1} (Hauglustaine et al., 1994). Production of nitrate from HNO_3 is not included in the model as the N_2O_5 heterogeneous reaction is the focus of this study.

The atmospheric lifetime of nitrate was assumed to be 4 days in the model as derived by Xu and Penner (2012). To diagnose the effect of changing nitrate lifetime on the concentration of nitrate, simulations was performed for four different lifetimes (2-5 days), and the rate coefficient of nitrate removal was changed accordingly for the additional scenarios. (Table 6.2).

Figure 6.12 shows the model better predicts of nitrate concentrations when the lifetime was 5 days, as this allows nitrate to build up when compared to case A (2 day lifetime) and the other cases.

Table 6. 2 The atmospheric lifetime of nitrate and calculated rate coefficient of nitrate dry deposition

Case	Lifetime (days)	k (s^{-1})
A	2	5.78×10^{-6}
B	3	3.85×10^{-6}
C (base case)	4	2.95×10^{-6}
D	5	2.3×10^{-6}
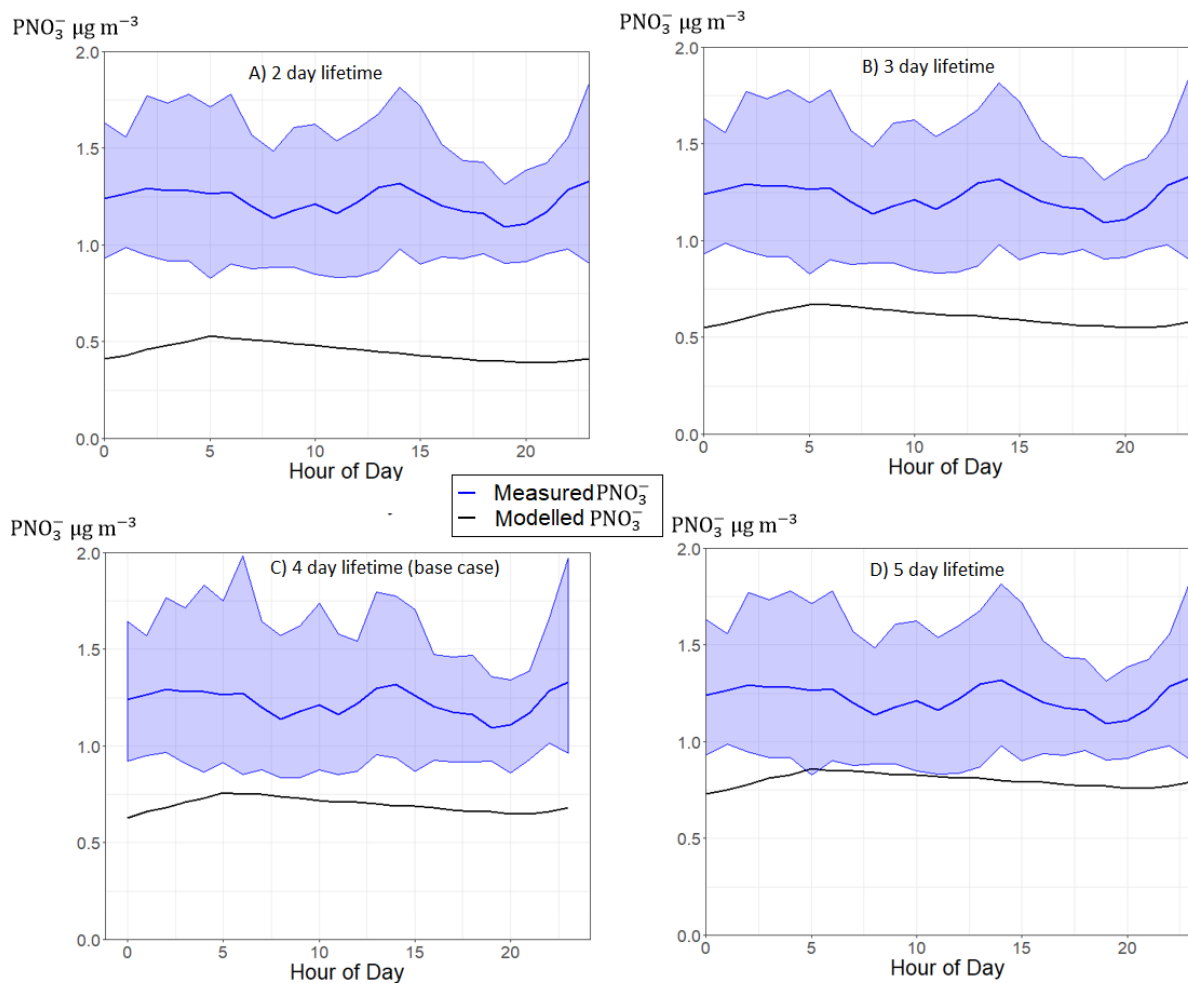
Figure 6. 12 Measured nitrate over the August with modelled nitrate with lifetime of **A)** 2day, B) 3day, **C)** 4 day, and **D)** 5 day.

6.3.3 Model evaluation for an urban area

Nitrate aerosol formation in urban areas is the focus of this study; therefore, the condition of the model has been adjusted from rural (Harwell) to urban background conditions (North Kensington, London).

The new initial conditions of the model are summarised in Table 6.3. The mean temperature was kept the same (15ºC) as for the rural case. The model was initiated with mean mixing ratios of NO, NO_2, O_3, and 10 VOCs as measured at North Kensington during the ClearfLo campaign in 2012 (Whalley et al., 2016). The mean, minimum, and maximum total OH reactivity for the ClearfLo campaign was ~18, ~15, and ~27 s^{-1} respectively (Whalley et al., 2016).

The total OH reactivity for inorganic species (NO, NO_2, and O_3), and for CH_4 and the ten VOCs are calculated to be 3.67 s^{-1} and 3.52 s^{-1} respectively for the North Kensington condition using equation 6.5 and 6.6:

$$k'_{(OH+inorganic)} = \Sigma k_{(OH+NO)}.[NO] + k_{(OH+NO2)}.[NO_2] + k_{(OH+O3)}.[O_3] + [CH_4] \qquad Eq6.5$$

$$k'_{(OH+VOC)} = \Sigma k_{(OH+voc1)}.[voc_1] + k_{(OH+voc2)}.[voc_2] \ldots\ldots\ldots.. k_{(OH+voc10)}.[voc_{10}] \qquad Eq6.6$$

$k'_{(OH+X)}$ is the rate coefficient taken from the MCM and the mean mixing ratios of NO, NO_2, O_3, CH_4, and VOCs measured for North Kensington during the campaign are used.

The mean total OH reactivity that was measured for North Kensington was 18 s^{-1}. Therefore, the initial mixing ratios of the 10 VOCs were multiplied by a factor of 4 to obtain the same measured reactivity. The reason for using a similar reactivity to that measured is to obtain the same radical chemistry, and thus ozone formation, from the reactions of OH with VOCs.

Table 6. 3 Initial conditions of the model adjusted for North Kensington. NO, NO_2 and O_3, VOC mixing ratio taken from ClearfLo measurements in North Kensington 2012 (Whalley et al., 2016). Nitrate and particulates chloride are the mean concentration over August 2014 measured in N Kensington derived from

https://uk-air.defra.gov.uk/data/data_selector?=l&1=&s=&o=#mid

Chemical parameters	Chemical formula	Model input
Nitric oxide	NO	5.95 ppb
Nitrogen dioxide	NO_2	10.93 ppb
Ozone	O_3	20.45 ppb
Methane	CH_4	1800 ppb
Formaldehyde	HCHO	2898 ppt
Acetaldehyde	CH_3CHO	2750 ppt
Toluene	C_7H_8	506 ppt
Mxylene	C_8H_{10}	243 ppt
Isoprene	C_5H_8	241 ppt
Ethene	C_2H_4	844 ppt
Propene	C_3H_6	266 ppt
Methanol	CH_3OH	6813 ppt
Ethanol	C_2H_5OH	2185 ppt
Acetylene	C_2H_2	711ppt
Chloride aerosol	Cl	0.71 $\mu g\ m^{-3}$
Nitrate aerosol	NO_3^-	0.93 $\mu g\ m^{-3}$
Total OH-VOC reactivity	R	18 s^{-1}

The predicted nitrate concentration was compared to the mean nitrate level recorded during August 2014 in North Kensington. As shown in Figure 6.13 the modelled nitrate concentrations agree well with the measured data.
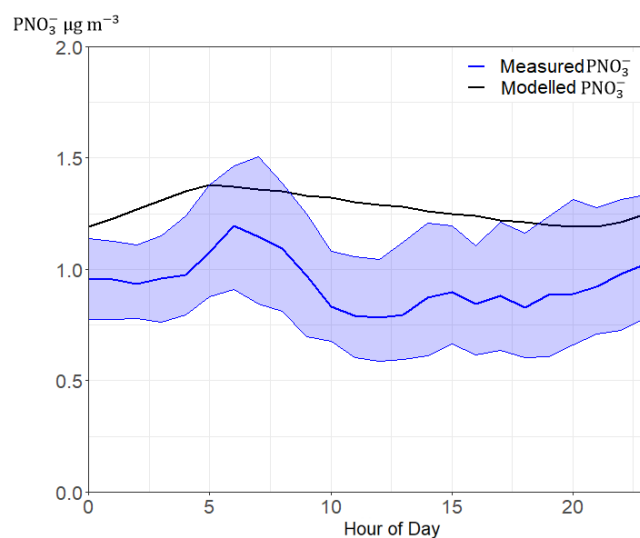
Figure 6. 13 Measured (averaged over August) and modelled particulate nitrate for London North Kensington

The model captured the typical temporal variation of NO, NO_2, and O_3 as expected in an urban areas. NO_2 peaked at 08:30 - 09:00 am in the morning and at 07:20 pm in the evening, while O_3 peaked at 3:00pm (Figure 6.15).
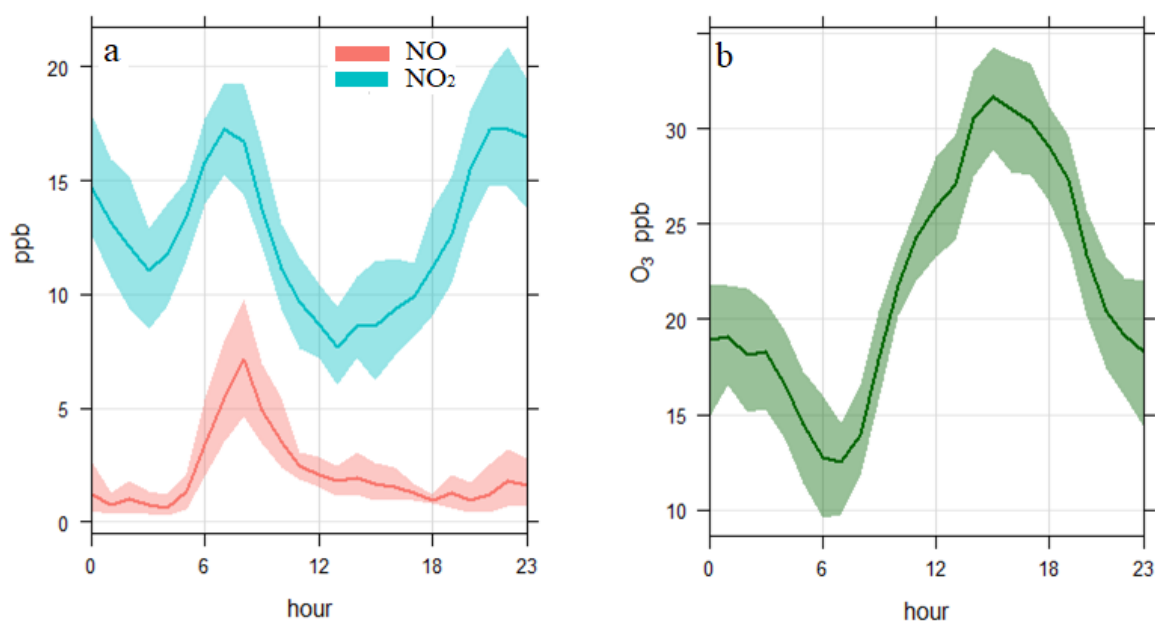
Figure 6. 14 Mean diurnal profiles for a) NO and NO_2, and b) O_3 that measured in London Kensington over August 2014

As shown in Figure 6.15, the model however extremely over predicted O_3, and under predicted NO and NO_2 mixing ratios relative to the measurements, which could be attributed to the increase in the VOC reactivity in the model. Changing reactivity means increasing the initial mixing ratio of the 10 VOCs, changing the NO_x emissions rate and the O_3 background sources to keep the key reactive chemical species such as OH, NO, NO_2, O_3, and intermediate species at steady state levels (Figure 6.16).

A sensitivity test was performed to investigate the production of O_3 and NO_2 in which the OH reactivity was decreased to 6 s^{-1}. The result demonstrated that decreasing OH reactivity caused a significant decrease of O_3 with maximum ~ 45 ppb (Figure 6.17). This result highlights the importance of controlling VOCs to reduce O_3 concentrations in the atmosphere.
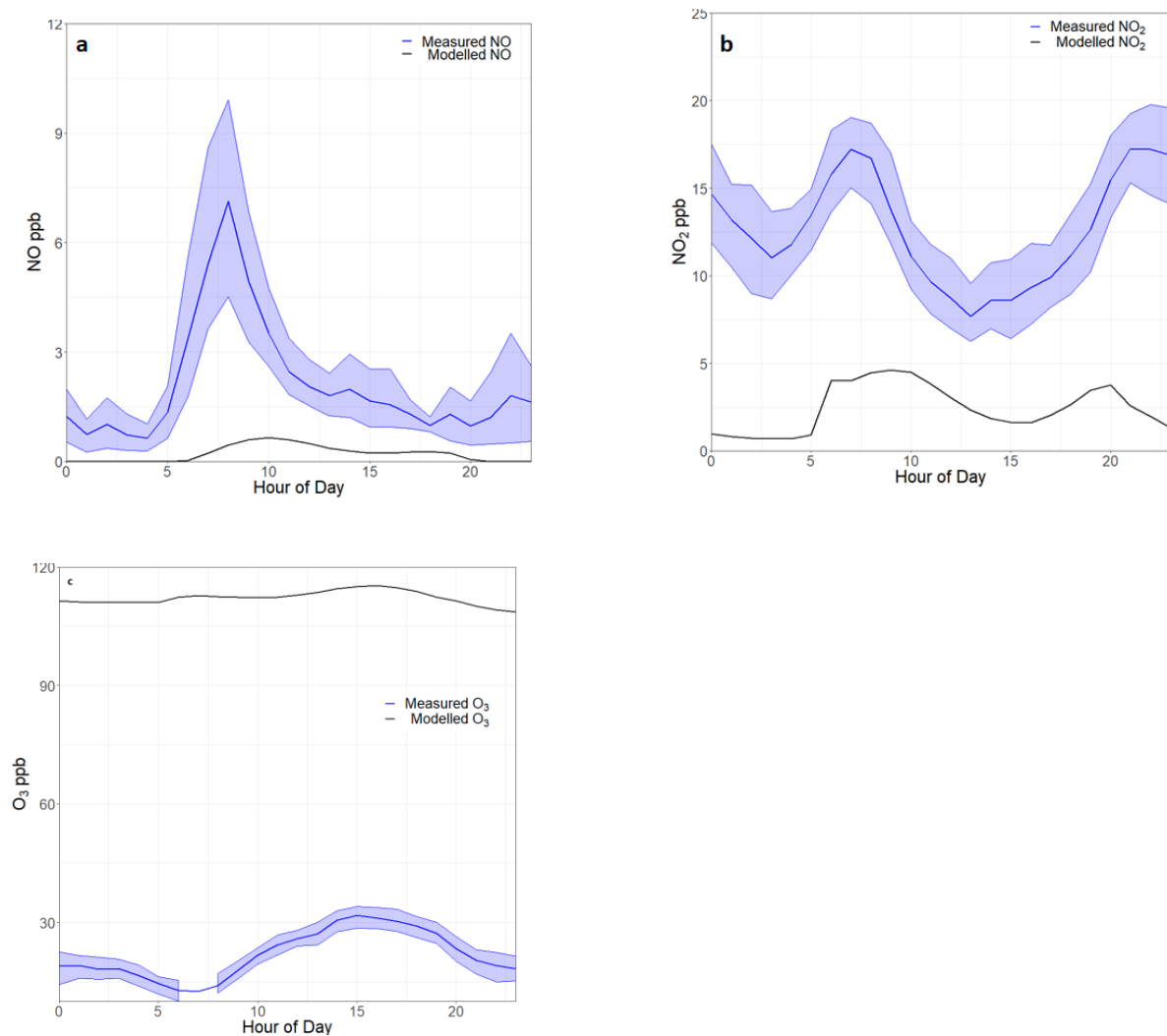
Figure 6. 15 Comparison between modelled and mean measured diurnal profiles (August 2014) of a) NO, b) NO_2, and c) O_3 for London North Kensington
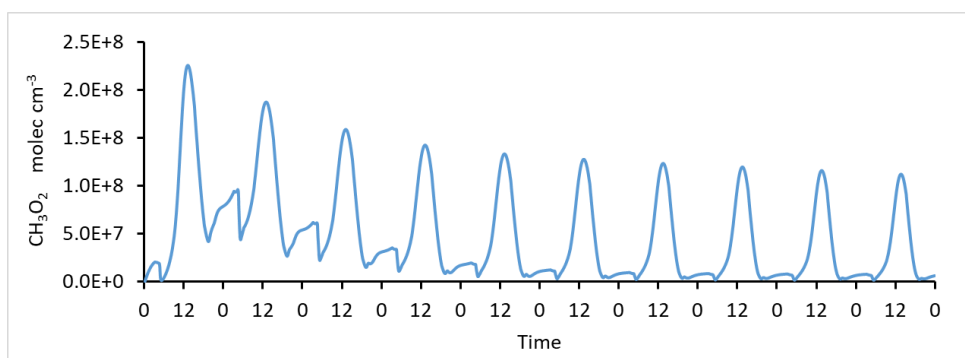
Figure 6. 16 Demonstrates a modelled intermediate species (CH_3O_2) at steady state level
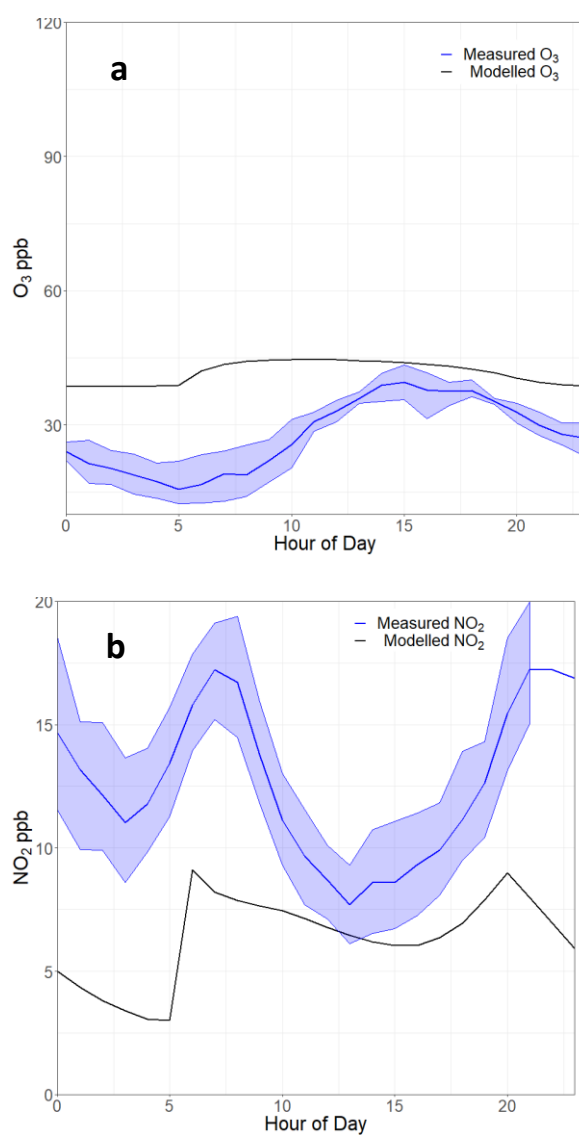
Figure 6. 17 Comparison between modelled a) O_3 and b) NO_2 mixing ratios and measured data for London after total OH+VOC reactivity decreased from ~18 s^{-1} to ~6 s^{-1}.

6.3.4 Comparison between Nitrate formation in rural and urban atmosphere

The results obtained from modelling nitrate levels in London and at Harwell were compared to demonstrate the differences in the abundance of nitrate and other pollutants between rural and urban areas. The model results reveal a higher mixing ratio of PNO_3^-, NO_2, O_3, and N_2O_5 for London than for Harwell as expected, however nearly similar NO levels were predicted for both locations, as shown in Figures 6.18 and 6.19.

NO_3 photolysis occurs at sunrise, thus the levels of NO_3 and N_2O_5 will fall during the day (in cloudless conditions). PNO_3 peaked at 5am, however, its concentration decreased at a slower rate than N_2O_5, which had a sharp decrease. This was due to the long lifetime of nitrate (4 days) compared to N_2O_5 which has ~ 40 second lifetime at 290 K due to thermal decomposition (Brown and Stutz, 2012).

The higher concentration of PNO_3 in the London case in relation to Harwell is mainly due to the differences in the initial mixing ratios of the precursor gases (NO_2, O_3, and N_2O_5) between the two locations, which are much higher in London than in Harwell, as summarised in Tables 6.1 and 6.2. Wen et al. (2018) showed that nitrate formation is highly sensitive to NO_2 and O_3 abundance, particularly at night. As the main source of NO and NO_2, thus N_2O_5 in an urban area like London is emissions from vehicles, it is important to know how NO_x emissions from traffic can influence nitrate in London.
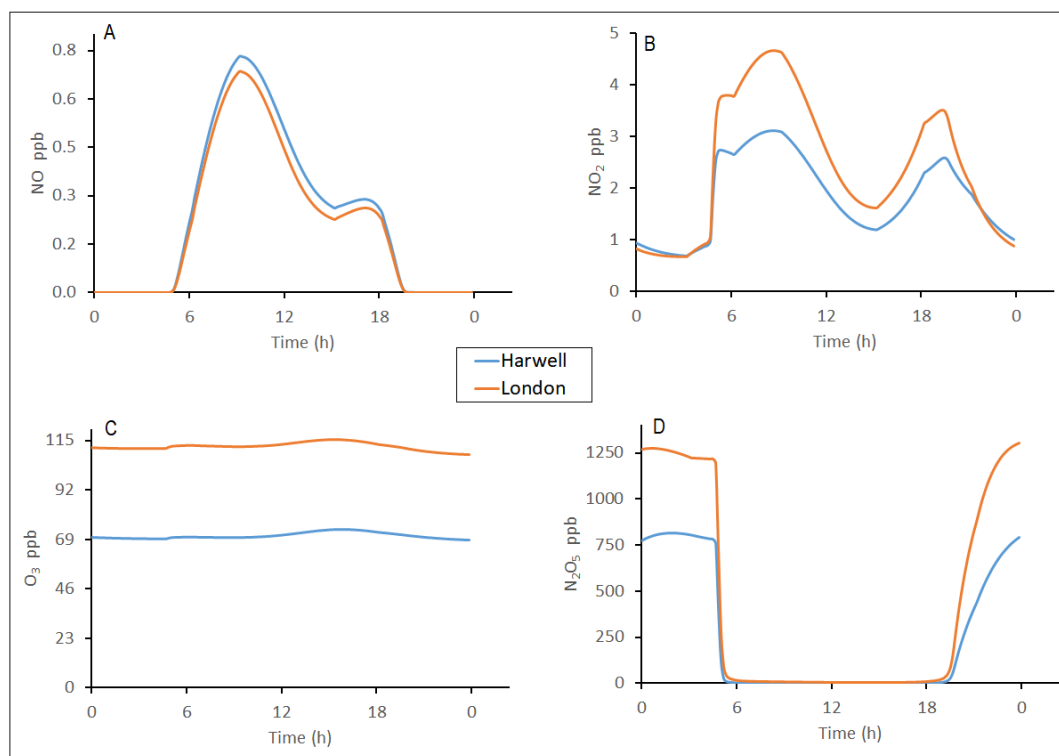
Figure 6. 18 Modelled **A)** NO, **B)** NO$_2$, **C)** O$_3$, and D) N$_2$O$_5$ for Harwell and London
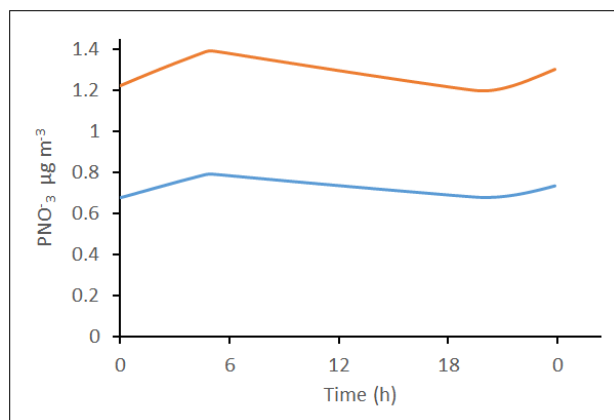
Figure 6. 19 Modelled particulate nitrate (PNO$^-_3$) for London and Harwell

6.4 Impacts of diurnal variations in emission distributions on particulate nitrate

It is being well documented that an increase in particulates nitrate and hazy days in urban areas is mainly due to traffic emissions (Ge et al., 2017, Pan et al., 2016, Sen-chao et al., 2009, Shon et al., 2013, Tan et al., 2009). As is the case with meteorological factors, NO_x emissions from human activities, e.g. traffic, vary from day to night, affecting the temporal variation of atmospheric aerosol (Galindo and Yubero, 2017). For example, Galindo and Yubero (2017) found a substantial decrease in PM_{10} concentrations at night, particularly in winter, due to lower traffic volume at night compared to daytime in an urban centre in southern Spain. Moreover, Pusede et al., (2016) observed a substantial decrease in winter nitrate aerosol from 2000 to 2013 because of the decline in surface NO_x emissions. In Beijing, China, heavy pollution days; where PM concentrations are above 100 µg m^{-3} were frequently found to be accompanied by high levels of NO_2 (and to lesser extent O_3) in ambient air, which are the main N_2O_5 precursor gases that enhance nitrate aerosol formation (Su et al., 2017; Wen et al., 2018). Therefore, it is important to examine the effect of NO_x emissions on nitrate formation.

In chapter 5, the effect of diurnal emission distributions on NO_2 and other pollutants were investigated by simulating six emission scenarios. It was found that the emission distribution in scenario D (emission peaks three times during the day) and scenario E (high emission at night, but low during the day) increased NO_2 levels, and as scenario D could represent a more polluted condition with three peaks of emissions, and E scenario represents a measure to reduce emissions in daytime. Therefore, these two scenarios (Figure 6.20) were selected to understand the relation between traffic emissions and nitrate in an urban area (London).

Scenario A (baseline) was included in the model for predicting nitrate and other species in Harwell and London as it represented a typical weekday emission pattern in urban/urban background areas in the UK. In scenario D it was assumed that emissions will peak three times during the day), and in scenario E emissions were assumed to be low during the day (3 am – 9pm), but high at night (from 9 pm – 3am). As mentioned in Chapter 5, the diurnal emissions were varied, however the total NO_x emission was maintained across all three scenarios.
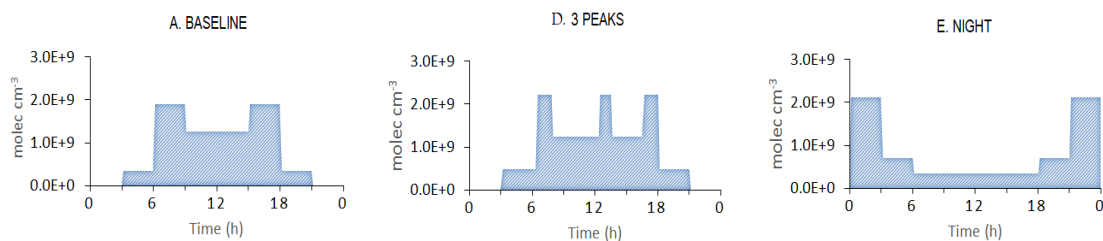
Figure 6. 20 Three emissions scenarios used in the model to asses PNO_3^- variation.
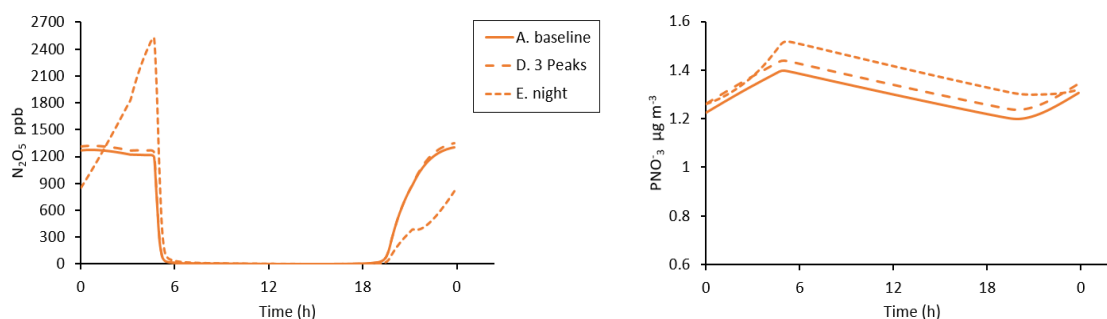
Figure 6. 21 Impact of variations in emission distributions on N_2O_5 (left) and particulate nitrate (right)

The variations in emission distribution have changed the N_2O_5 mixing ratio, which is a key source for nitrate formation in the model. The influence of the two scenarios (D and E) on the maximum predicted nitrate and N_2O_5 was assessed related to the base scenario (A). The maximum mixing ratio of N_2O_5 occurred at 4:40 am, while maximum nitrate concentration occurred at 5 am.

In the three peaks scenario, i.e., scenario D, N_2O_5 and nitrate were slightly higher than in the base case by 4% and 3%, respectively. However, N_2O_5 was significantly increased in the night scenario (E) related to the base scenario (A) by 112%, and nitrate was increased by 8% only (Figure 6.21).

During the night (from 7:30 pm to midnight) lower NO_2 (57%) occurred in scenario E relative to scenario A, as there were no emissions during the day in scenario E, resulting in a lower NO_2 mixing ratio (~ 60%) than in scenario A. As emissions increase from 9 pm to

3am, the NO_2 mixing ratio builds up to be double (8 ppb) of that in scenario A at ~5:30 am, as shown in Figure 6.22.
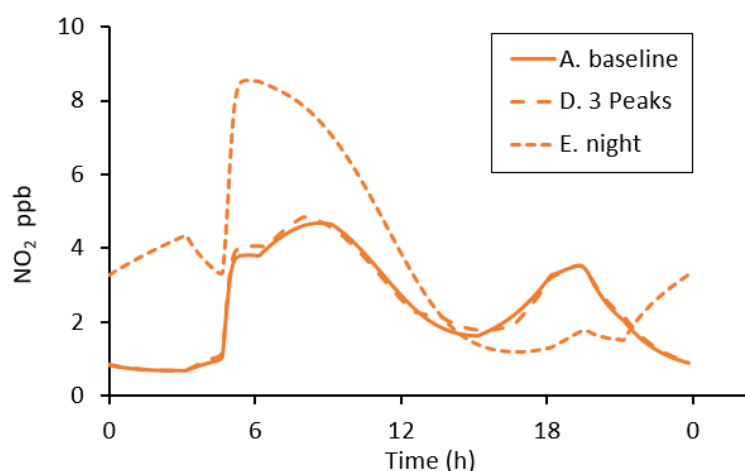
Figure 6. 22 Predicted NO_2 mixing ratios across the three different emission scenarios

In areas where heavy duty vehicle movements are restricted to nighttime, or where policy makers are considering inclusion of such measures to reduce air pollution, it is important to consider the consequences of such actions as it can increase pollutants such as NO_2 and nitrate in the mornings.

6.5 Influence of the formation of $ClNO_2$ on particulate nitrate

Modelling studies using the Community Multiscale Air Quality (CMAQ) and the Weather Research and Forecasting coupled with Chemistry (WRF-Chem) models, performed by (Sarwar et al. (2012) and Li et al. (2016), respectively, emphasise the effect of $ClNO_2$ formation from N_2O_5 hydrolysis chemistry on reducing particulate nitrate in the atmosphere. In this study, the MCM is used to assess the impact of this $ClNO_2$ formation on aerosol nitrate.

Recalling that the reaction of N_2O_5 with aerosols containing water produces either two PNO_3^- molecules or PNO_3^- and $ClNO_2$ if the aerosol contains chloride, the model simulations for nitrate were compared for with and without $ClNO_2$ chemistry. The model predicted peak $ClNO_2$ of ~75ppt (Figure 6.23B).

171

Inclusion of $ClNO_2$ chemistry in the model has considerable effects on nitrate concentrations (Figure 6.23A and 6.24). Relative to the model without $ClNO_2$ formation, nitrate concentrations decreased by ~0.6 µg m^{-3} (~50%) on average over 24 hours when $ClNO_2$ formation was included in the model. Sarwar et al. (2014) observed decreases in monthly mean total nitrate (HNO_3 and PNO_3^-) in winter by 25% over the whole Northern Hemisphere by including $ClNO_2$ chemistry in their CMAQ model, however, they also observed an increase in total nitrate in some remote areas.

It should be noted that there are uncertainties in the results obtained in this study. For example, the loss rate coefficient of particulate nitrate loss was based on a constant lifetime (4 days), whereas, in reality the lifetime of aerosol is highly variable (as shown in Figure 6.12) according to meteorological factors, the abundance of precursor gases (Battaglia Jr et al., 2017, Xue et al., 2014), and the pre-existing aerosol abundance. Moreover, the N_2O_5 parameterization in this study lack some uncertainty, such as organic constitute of the particle that can decrease the N_2O_5 uptake (Bertram and Thornton, 2009). In this study, the bulk composition of the particle is assumed to be either sodium chloride, or water, and the particles are assumed to be homogeneous in chemical composition and internally mixed.
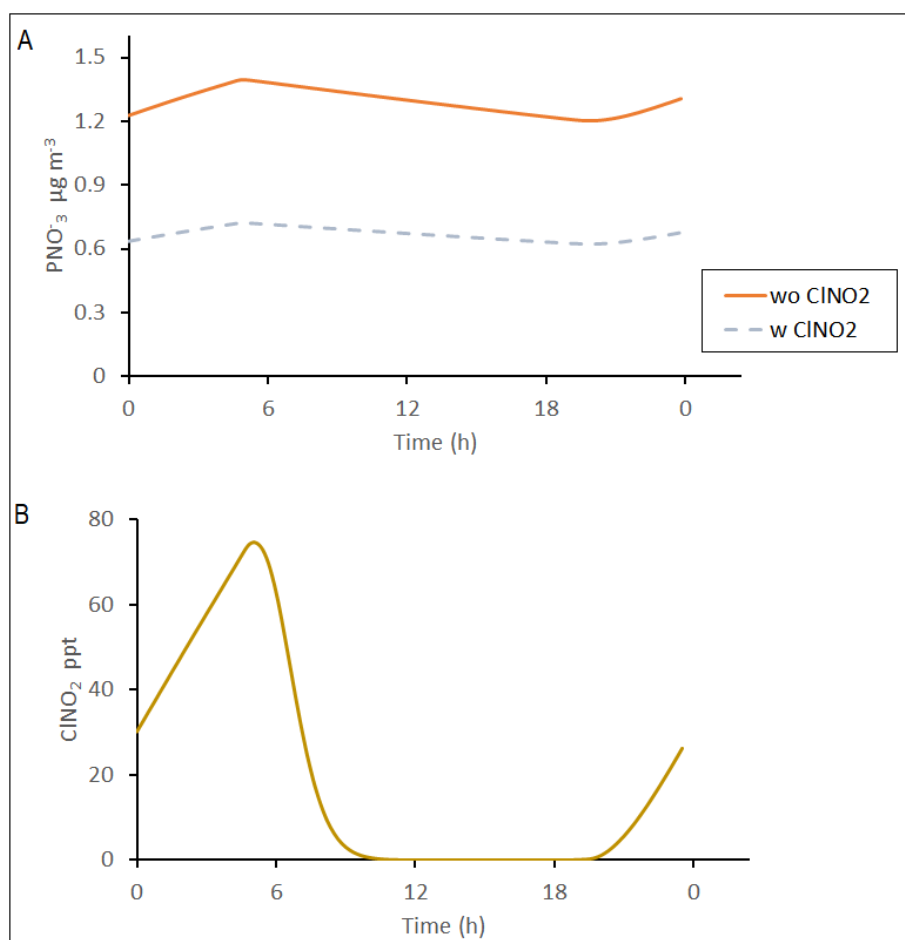
Figure 6. 23 A) Predicted particulate nitrate concentrations for the models where ClNO$_2$ formation included (blue dashed line) /excluded (orange solid line); **B)** ClNO$_2$ mixing ratio from N$_2$O$_5$ hydrolysis as predicted by the model.
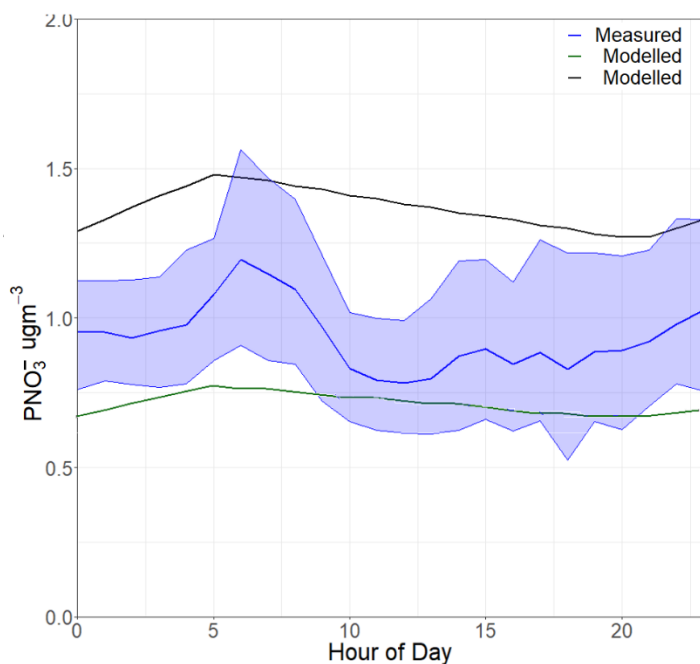
Figure 6. 24 Comparison between modelled nitrate aerosol, when ClNO$_2$ chemistry excluded (black line), and included (green line) in the model, with average diurnal nitrate aerosol measured in London North Kensington

6.6 Summary and Conclusion

The extended MCM mechanism has been evaluated for nitrate formation by comparison with measured concentrations for a rural area (Harwell) and an urban area (North Kensington, London). Overall, the model slightly under predicted nitrate for Harwell, but the model better predicted the simulated nitrate levels for the urban area than for the rural area. The results of sensitivity tests to assess the response of the particulate nitrate concentration to its atmospheric lifetime showed better model performance in predicting particulate nitrate with a longer lifetime (5 days), than when compared to a shorter (2 days) lifetime.

The model however substantially under predicted NO$_2$, and over predicted O$_3$ for Harwell compared with London. This could be related to the way O$_3$ is treated in the model, which appeared from the sensitivity test performed to be due to the model initial condition in terms of NO$_x$ - VOC reactivity. The model performed better (the maximum O$_3$ formed was 45 ppb) when the OH reactivity was reduced from 18 to ~6 s^{-1}. Therefore, the prediction of

174

NO_2 and O_3 is dependent on the initial conditions including NO, NO_2, and VOC mixing ratios.

The performance of the model for O_3 for rural areas was, however, improved when dry deposition of O_3 was added into the model, decreasing O_3 by 8 ppb. Further tests were performed for O_3 by changing the initial NO_x mixing ratio. The result shows very high-simulated O_3 mixing ratio (83 ppb) at low NO_x initial mixing ratio (1-5 ppb) and ~30 ppb at a high initial mixing ratio (100 ppb). The OH and HO_2 concentrations were very low when NO_x was 15 - 100 ppb.

The sensitivity analysis showed that when the initial mixing ratio of NO_x in the model was 15 ppb or above, very little HO_2 was produced, because of the high removal of HO_2 by NO.

The box model has limitations and may not represent the real atmosphere as we are effectively assuming that this box represents the entire London / Harwell Boundary Layer. For prediction of the short lived and intermediate chemical species (such as NO and NO_2) using the zero dimensional box model was satisfactory and agreed with measurements for the Harwell case (Figure 6.5), however it depends on the OH-VOC reactivity as the agreement between modelled and measured NO and NO_2 became less satisfactory for London North Kensington when reactivity increased to 18 s^{-1} (Figure 6.15), and it improved when the reactivity decreased to 6 s^{-1} (Figure 6.17).

For a long lived species like O_3 the agreement between measurement and the model was not satisfactory for both Harwell and London North Kensington cases (Figures 6.4 and 6.13), but the agreement improved for the latter case when the OH reactivity was decreased from 18 to 6 s^{-1} (Figure 6.15). The concentrations of the long-lived species in the atmosphere are influenced by the background conditions, boundary layer, and the meteorological factors. The horizontal and vertical transport, which affect chemical species abundance, are not presented in a box model (Wolfe et al., 2016). Additionally, the calculation of the concentrations of a chemical species is based on the initial conditions in the model at a specific grid point (Saunders, 2017). When the OH reactivity was decreased from 18 s^{-1} to ~6 s^{-1}, predicted NO_2 and O_3 levels were close to monitored values (Figure 6.17), meaning that increasing the concentrations of VOCs in the model to increase the reactivity may have resulted in an imbalanced effect on the RO_2 production, which resulted in high O_3 levels.

Comparison between the two sites showed that higher NO_2, O_3, N_2O_5, and nitrate was formed in London than at Harwell due to higher initial NO_x mixing ratios and NO_x emissions input in the London case. Therefore, the effect of varying emission distributions was also examined on nitrate formation in which two simulations were conducted for different emission scenarios. The results showed a maximum increase of 112% and 8% in N_2O_5 and nitrate respectively in scenario E (night emissions) compared with the base case (scenario A) that have two emission peaks during the day. Therefore, controlling temporal NO_x emissions in urban areas is important to reduce particulate nitrate contributions to urban air pollution.

Finally, including $ClNO_2$ formation in the model reduced nitrate by $\sim$ 50% compared to the model without $ClNO_2$ chemistry. This suggests that $ClNO_2$ and nitrate are negatively correlated; less nitrate aerosol can be expected in areas with high $ClNO_2$ concentrations. However, this depends on the location, season, and the condition, i.e. urban, polluted or remote, clean areas (Sarwar et al., 2014).

Another removal pathway of nitrate is photolysis. Recent modelling studies have confirmed fast particulate nitrate photolysis, which is considered an important source for NO_x and nitrous acid (HONO) in marine environments (Romer et al., 2018, Ye et al., 2017). In laboratory studies, the mean nitrate photolysis rate was determined to be as high as $\sim 1.8 \times 10^{-4}$ s^{-1} in suburban and remote environment (Ye et al., 2017). Photolysis could therefore present another sink of nitrate aerosol alongside deposition, which can affect aerosol budget in the atmosphere. Therefore, to more accurately simulate PNO_3^- formation, it is useful to include the nitrate photolysis frequency in the model.

Chapter 7 Conclusion and Future Work

7.1 Conclusion

This study sets out to use a zero-dimensional box model based on the near explicit Master Chemical Mechanism to model air pollution associated primarily with NO_x emitted from vehicles in an urban environment.

The focus of this study was on a $ClNO_2$, NO_2, and nitrate aerosol particulates with aims to assess the effect of temperature on $ClNO_2$ formation and its impact on air quality; to investigate the impact of the temporal emission distribution from vehicles on the formation of NO_2 and other chemical species; and finally to explore nitrate aerosol formation from heterogeneous N_2O_5 reaction with aerosol.

An MCM-based 0-D box model was developed primarily for $ClNO_2$ formation and its consequent effects on the concentrations of O_3 and other chemical species. This established model was also used, but with changing NO_x emissions scenario to investigate the impact of temporal changing emissions on different species. The same model was further updated to include nitrate aerosol formation and loss, O_3 deposition as another O_3 loss source.

7.1.1 Mechanism and model development

The MCM was modified to include the potential sources of chlorine atoms. These sources are $ClNO_2$, $ClONO_2$, $HOCl$ and Cl_2 photolysis, with thermal decomposition of $ClONO_2$, and the reaction of HCl with OH. The photolysis rates of these compounds are calculated more accurately than other studies performed before, as the scaling factors used for the calculation of the photolysis rate coefficient are not constant, but vary with the SZA, which provided more accurate photolysis diurnal profile. The mechanism was further extended to include 15 inorganic and 43 organic reactions with chlorine (Table 7.1).

The model development also included comprehensive parameters and reactions required for calculation of the chemistry of $ClNO_2$ formation (from the N_2O_5 reaction with aerosol), and yield. N_2O_5 uptake coefficient was calculated in the model based on the

parameterization from Bertram and Thornton (2009). Most previous studies used a constant value for the N_2O_5 uptake and yield of $ClNO_2$. Moreover, aerosol water content based on Petters and Kreidenweis (2007) was calculated within the model, driven by ambient temperature and relative humidity.

Table 7. 1 Demonstrates all chemical reactions included in the model

NO	group	Reactions
1		$ClNO_2 + hv \rightarrow Cl + NO_2$
2		$HOCl + hv \rightarrow Cl + OH$
3	Cl sources	$Cl_2 + hv \rightarrow 2Cl$
4		$ClONO_2 + hv \rightarrow Cl + NO_3$
5		$ClONO_2 + hv \rightarrow ClO + NO_2$
Sum = 5		
1		$Cl + O_3 \rightarrow ClO + O_2$
2		$Cl + HO_2 \rightarrow HCl + O_2$
3		$Cl + HO_2 \rightarrow ClO + OH$
4		$Cl + H_2O_2 \rightarrow HCl + HO_2$
5		$Cl + NO_3 \rightarrow NO_2 + ClO$
6		$Cl + ClONO_2 \rightarrow Cl_2 + NO_3$
7		$OH + HOCl \rightarrow ClO + H_2O$
8	Inorganic	$OH + Cl_2 \rightarrow HOCl + Cl$
9	reactions	$OH + HCl \rightarrow Cl + H_2O$
10		$ClO + NO \rightarrow Cl + NO_2$
11		$ClO + HO_2 \rightarrow HOCl + O_2$
12		$ClO + OH \rightarrow Cl + HO_2$
13		$ClO + OH \rightarrow HCl + O_2$
14		$ClO + NO_2 + M \rightarrow ClONO_2 + M$
15		$ClONO_2 + M \rightleftarrows ClO + NO_2 + M$
Sum	15	
No	**group**	**Reactions**

1		$Cl + CH_3OH \rightarrow HO_2 + HCHO + HCl$
2		$Cl + C_2H_5OH \rightarrow CH_3CHO + HO_2 + HCl$
3		$Cl + C_2H_5OH \rightarrow HOCH_2CH_2O_2 + HCl$
4		$Cl + HCHO \rightarrow HO_2 + CO + HCl$
5		$Cl + CH_3CHO \rightarrow CH_3CO_3 + HCl$
6		$Cl + CH_3CHO \rightarrow HCOCH_2O_2 + HCl$
7		$Cl + C_5H_8 \rightarrow ISOClO_2$
8		$ISOClO_2 + NO \rightarrow ISOPAO + NO_2$
9		$Cl + C_7H_8 \rightarrow C_6H_5CH_2O_2 + HCl$
10		$Cl + C_8H_{10} \rightarrow C_8H_{10}O_2 + HCl$
11		$Cl + C_2H_4 \rightarrow CH_2ClCH_2O_2$
12		$Cl + C_3H_6 \rightarrow CH_2C_2H_3O_2 + HCl$
13		$CH_2C_2H_3O_2 + NO \rightarrow ACR + HCl$
14		$Cl + C_3H_6 \rightarrow CH_2ClCHOOCH_3$
15		$CH_2ClCHOOCH_3 + NO \rightarrow H_2ClCOCH_3$
16		$Cl + C_3H_6 \rightarrow CH_3CHClCH_2OO$
17		$CH_3CHClCH_2OO + NO \rightarrow CHOCHClCH_3$
18		$CHOCHClCH_3 + OH \rightarrow C_2H_5OClCO_3$
19		$C_2H_5OClCO_3 + HO_2 \rightarrow CH_3CHClO_2$
20		$C_2H_5OClCO_3 + HO_2 \rightarrow CH_3CHClCO_3H$
21		$CH_3CHClCO_3H + OH \rightarrow C_2H_5ClCO_3$
22	Organic reactions	$CH_3CHClCO_3H \rightarrow CH_3CHClO_2 + OH$
23		$C_2H_5ClCO_3 + HO_2 \rightarrow CH_3CHClCOOH + O_3$
24		$CH_3CHClCOOH + OH \rightarrow CH_3CHClO_2$
25		$C_2H_5OClCO_3 + NO \rightarrow CH_3CHClO_2 + NO_2$
26		$C_2H_5OClCO_3 + NO_2 \rightarrow 2\ ClPPN$
27		$2\ ClPPN + OH \rightarrow ClETAl + CO + NO_2$
28		$2\ ClPPN \rightarrow C_2H_5ClO_3 + NO_2$
29		$C_2H_5ClO_3 + NO_2 \rightarrow CH_3CHClO_2$
30		$C_2H_5ClO_3 \rightarrow CH_3CHClO_2$
31		$C_2H_5ClO_3 \rightarrow CH_3CHClCOOH$
32		$CHOCHClCH_3 + hv \rightarrow CH_3CHClO_2 + HO_2 + CO$
33		$Cl + C_2H_2 + M \rightarrow ClCHO + CO + HO_2 + M$
34		$Cl + CH_3OOH \rightarrow CH_3O_2 + HCl$
35		$Cl + CH_3OOH \rightarrow HCHO + OH + HCl$
36		$Cl + HCOOH \rightarrow HO_2 + HCl$
37		$Cl + CH_3CO_2H \rightarrow CH_3O_2 + HCl$
38		$Cl + PROPACID \rightarrow C_2H_5O_2 + HCl$
39		$Cl + CH_3NO_3 \rightarrow HCHO + NO_2 + HCl$
40		
41		$Cl + C_2H_5NO_3 \rightarrow CH_3CHO + NO_2 + HCl$

179

Sum	43	
Total	63	All reactions included in the model

7.1.2 Model evaluation

The model was evaluated by comparing the modelled $ClNO_2$, NO, NO_2, and O_3 concentrations with mean measured data in an urban area during August 2014. The model reproduced the diurnal profile of NO_2, O_3, and $ClNO_2$ well and the frequency distribution test revealed that the modelled and measured $ClNO_2$ have the same distribution. Discrepancies in the $ClNO_2$ trends are however observed between the model and measurements, which are suggested to be related to meteorological factors, as $ClNO_2$ formation is temperature and RH dependent and the concentrations of $ClNO_2$ precursor gases (NO_2, O_3, NO_3, and N_2O_5) can be highly affected by ventilation/transport of the air, which a simple model like a 0-D box model is not able to take into account these factors.

Contributions and Implications:

The developed model is more comprehensive than models developed in previous studies in treating N_2O_5 heterogeneous loss and photolysis of chlorine sources, as the model well reproduced $ClNO_2$ measured in an urban area (section 7.1.2). The agreement between modelled and measured $ClNO_2$ (and NO_2, O_3) demonstrates the ability of the model in predicting atmospheric chemical species in the atmosphere. Therefore, this model can be used with confidence to investigate N_2O_5 heterogeneous and $ClNO_2$ chemistry for future field studies, and can be used to predict the abundance of other chemical species in those areas that measurement is difficult or to assess the impact of climate change on tropospheric chemistry.

7.1.3 Effects of projected future temperature increase on $ClNO_2$ formation and chemistry

The UKCP09 projected a future mean summer temperature increase of 2.9 ^oC by 2050 relative to a baseline period (1961-1990) with the central year 1975, under high CO_2 emissions scenario for the West Midlands, UK. In Chapter 4, the impact of this temperature increase on the formation and potential effects of $ClNO_2$ chemistry was

explored. Relative to baseline conditions (mean temperature 15 ^{o}C), an increase in temperature by 2.9 ^{o}C, resulted in a decrease of $ClNO_2$ concentration by 10%. Accordingly, the enhancement in the concentrations of the radicals (OH, HO_2, and RO_2) by $ClNO_2$ chemistry was less than that at lower temperatures with differences of approximately 15%, 34%, and 33% respectively (Table 4.1), but the temperature effect on O_3 enhancements by $ClNO_2$ was small (0.3%). To further our understanding of the temperature-$ClNO_2$ relationship as a function of NO_x, a sensitivity test was conducted. The results showed maximum $ClNO_2$ concentrations at temperatures ranging from 279K (6 ^{o}C) to 287K (14 ^{o}C), and when NO_x is between 25 and 35 ppb, representing a polluted area with low -moderate temperature. Meaning that, in this location (urban area in the UK), air quality will be worse due to $ClNO_2$ contribution to air pollution if NO_x mixing ratios are 35-35 ppb and the ambient temperatures are 6 – 14 ^{o}C.

Contributions: This study provides a framework for more future research on assessing the effect of changing temperature due to climate change on air quality, interrelated with traffic emissions (i.e. based on emission rates), and also to predict the effect of urban heat island on pollutant concentrations.

Implications and future work

In terms of modelling, ongoing development of the MCM is necessary for chlorine chemistry. Despite the existence of a number of suggested chlorine mechanisms developed by many researchers, to date this mechanism (except for alkanes) including the photolysis of the chlorine sources have not been integrated into the MCM. Based on this study and previous studies, a detailed chlorine mechanism should be added into the MCM framework by the development team. This will reduce uncertainties concerning chlorine loss or recycling into the atmosphere, and on the effect of chlorine on photochemical chemistry.

In terms of the results, This model can be used for any environment/locations, thus it is recommended to use the model to investigate $ClNO_2$ abundance and its impacts around the world, in particular in those places, which are hot (summer mean temperature > 40 ^{o}C), close to chloride sources, and have moderate to high NO_x emissions, especially in areas that no measurements have conducted before, such as in oil producing countries in the Middle East which have all sources (chlorine, NO_x, VOCs) from oil industries contributing

to $ClNO_2$ formation. The concentrations of $ClNO_2$ can be then compared with results obtained for cold environments with nearly same background (oil producing countries and close to the sea) such as in Russia. The results alongside previous and current literature will provide a comprehensive profile on $ClNO_2$ chemistry and its impacts around the world with different climate.

Decreases in NO_x emissions, especially in cold environments, would decrease $ClNO_2$ formation (as found from the sensitivity tests of $ClNO_2$-NO_x and temperature), and thus its impact on O_3 enhancements. i.e. less extra O_3 from $ClNO_2$ chemistry will be formed in the atmosphere. This implies that $ClNO_2$ effects on O_3 are significant in cold environments, so reducing emissions at temperature ranging 6-14 ^{o}C could be necessary to avoid poor air quality.

Finally, this model can be used by air quality policy makers to forecast the levels of pollutants for a projected temperature change (increase or decrease), particularly to predict traffic related pollutants increase during summer heat waves or cold temperature.

7.1.4 Impact of changing emission distributions from vehicles with time on NO_2 mixing ratios

Exposure to traffic related emissions has been found to have an adverse impact on human health. In Chapter 5, the model was updated to include six contrasting NO_x emissions distributions scenarios, reflecting the temporal differences in traffic, whilst at the same time maintaining a constant total NO_x emission over a twenty-four hour period. The results were compared with the baseline scenario (two emission peaks during the day). Other scenarios were: when the duration of the emission peaks from the baseline are reduced from two hours to thirty minutes, if there is one emissions peak during the day; if there are three emissions peaks; if emissions are low during the day, but high at night; and finally, if there is a constant emission source over 24 hours.

The effects of these scenarios on the concentrations of OH, HO_2, NO, NO_2, NO_3, N_2O_5, O_3, and $ClNO_2$ were investigated. Based on the model simulations, related to the baseline case, the largest differences in the concentrations of NO_2, NO_3, N_2O_5, and $ClNO_2$ were found for the scenarios where emissions were high at night, and when they were constant.

The results show maximum NO_2 concentrations in the morning, around 6 to 10 am, when the number of people walking near the road, and/or cycling on the road are usually high. This finding was related to the number of deaths due to exposure to NO_2 in the UK, and compared to the number of deaths in other scenarios. From a simple calculation, we found that the number of deaths would decrease by 1.2% if the duration of peak emissions were reduced from two hours to thirty minutes. However, for morning (6-10am), the number of deaths decreases by 2.5%, equivalent to ~19 people/year. Alternatively, for the night scenario in which emissions are high at night and low during the day, the number of deaths increases by 14% (over 24hours) and 18.6% (in the morning) related to the base case, equivalent to ~92 and 142 deaths per year respectively.

The two emissions scenarios (when emissions are high at night or constant), which have the largest effects on NO_2 level were implemented into a case study (Delhi, India), where there is high emission at night. For this six more model runs were performed, and in each run the total NO_x emission was changed (decreased or increased from the base case). The results show a decrease in NO_2 concentrations by 88% if total NO_x emissions decreased to half of the baseline, alternatively, the concentration of NO_2 approximately increases linearly with increasing NO_x emission.

The findings from this study contribute to the current literature. Temporal NO_x emission distributions can shape pollutant concentrations in the troposphere, as daytime chemistry is different from nighttime chemistry.

Implications and future work:

This model in combination with models that are developed specifically to simulate boundary layer conditions and meteorological factors such as the Weather Research and Forecasting (WRF) model can enable more accurate prediction of O_3 concentrations in the air.

The results from this study can support future work to find a relationship between high NO_x emissions at night at a particular place, which have a high volume of traffic (for example due to an event) on the next day people admissions to hospital or with increase in the number of ambulance call (due to respiratory or cardiovascular disease).

7.1.5 Prediction of nitrate aerosol formation from the heterogeneous reactions

In Chapter 5, the model was updated further to include the formation and loss of nitrate aerosol, and O_3 deposition as a function of boundary layer height. The updated model was used to assess the concentration of nitrate aerosol produced from the heterogeneous N_2O_5 reaction with aerosol particulates.

The model was evaluated by comparing the modelled nitrate, NO, NO_2, and O_3 concentrations with mean measurement data for rural and urban conditions in the UK. Generally, the agreement between the modelled and the measured nitrate aerosol was reasonable (the diurnal nitrate profile was close to the 95% confidence interval in the mean). The model under predicted mean nitrate concentrations by ~40%, but the modelled values represent a lower limit as only the N_2O_5 heterogeneous source was included in the model. The simulated nitrate for an urban area was better predicted than for a rural area. The discrepancies were related to the uncertainties about the lifetime of aerosol nitrate as found from a sensitivity test. The agreement between the model and the measurements was considerably better when the lifetime of nitrate aerosol was increased from 4 to 5 days.

The model, however, substantially over-predicted O_3 for the urban area compared with the rural area. This was attributed to the way O_3 was treated in the model, as the concentrations of NO_2 and O_3 are sensitive to the OH reactivity with VOCs in the model. Decreasing OH reactivity resulted in better prediction of NO_2, and O_3 by the model. The over-predicted O_3 was also attributed to the initial concentration of NO_x in the model. Results from a sensitivity test conducted for $O_3 - NO_x$ relationship (in terms of mixing ratio), showed that the model predicted very high O_3 concentrations at low NO_x conditions (1-5 ppb).

The effect of temporal emission distributions on nitrate aerosol formation was also examined. When compared to the baseline case (two peaks in NO_x emissions during the day), a 8% increase in nitrate aerosol concentrations was predicted when NO_x emissions are low during the day, but high at night. This result shows a strong link between NO_x emissions and nitrate, therefore controlling temporal NO_x emissions is important to reduce nitrate aerosol.

Including ClNO$_2$ chemistry in the model lead to a ~50% (~0.6 μg m^{-3}) decrease in nitrate aerosol concentrations, which suggest the anti-correlated relationships between ClNO$_2$ and nitrate, which was in agreement with other previous studies such as (Sarwar et al., 2014) that observed 25% reduction in average total nitrate (HNO$_3$ gas + nitrate) over the entire Northern Hemisphere. However, they proposed that the ClNO$_2$ impacts on the levels of total nitrate in the atmosphere depend on local environmental conditions (atmospheric chemical condition and meteorological effects). The reduction in nitrate aerosol by 50% due to ClNO$_2$ is expected as the modelled nitrate formation in this study was highly simplified in which N$_2$O$_5$ hydrolysis is the only source for nitrate formation, thus in the model with ClNO$_2$ formation, a fraction of N$_2$O$_5$ is consumed to form ClNO$_2$, hence nitrate aerosol reduced by half.

Despite that aerosol formation is a complex process, the developed box model in this study was able to reproduce aerosol nitrate close to the measurements. However, this was not the case for O$_3$.

Implications and future work:

This model can be improved, thus predicting aerosol nitrate concentrations more accurately (close to the measurements) by adding more reactions (listed below) including homogeneous and heterogeneous process and nitrate aerosol photolysis reaction:

$$NH_{3_{gas}} \; + \; HNO_{3_{gas}} \; \leftrightarrow \; NH_4^+ \; + \; NO_3^- \qquad\qquad R7.1$$

$$NH_{3_{gas}} \; + \; HNO_{3_{gas}} \; \leftrightarrow \; H_4NO_{3_{solid}} \qquad\qquad R7.2$$

$$HNO_{3_{gas}} \; + \; aerosol \; \rightarrow \; NO_3^- \qquad\qquad R7.3$$

$$NO_{3_{aerosol}} \; + \; hv \; \rightarrow \; HONO + \; NO_2 \qquad\qquad R7.4$$
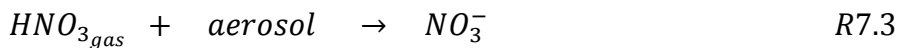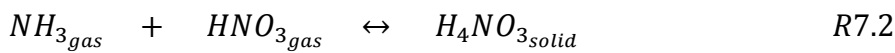
7.1.6 Future direction

The main points (In terms of modelling) were suggested for future works is reiterated below:

Ongoing development of the MCM: A detailed chlorine mechanism should be added into the MCM framework. This will reduce uncertainties concerning chlorine loss / recycling into the atmosphere, and on the effect of chlorine on photochemical chemistry.

Coupling with other models that can simulate meteorological factors, emissions, and transport**,** could improve the model performance and produce more accurate concentrations of the atmospheric chemical species.

A 0-D box model can be improved to predict aerosol nitrate concentrations more accurately **by adding more reactions** (listed in section 7.1.5) including homogeneous and heterogeneous process and nitrate aerosol photolysis reaction.

References

AGUADO, E. & BURT, J. E. 2010. *Understanding weather and climate*.

ARYA, S. P. 1999. *Air pollution meteorology and dispersion*, Oxford University Press New York.

ATKINSON, R. & ASCHMANN, S. M. 1985. Kinetics of the gas phase reaction of Cl atoms with a series of organics at 296±2 K and atmospheric pressure. *International journal of chemical kinetics,* 17**,** 33-41.

ATKINSON, R., BAULCH, D., COX, R., CROWLEY, J., HAMPSON JR, R., KERR, J., ROSSI, M. & TROE, J. 2001. Summary of evaluated kinetic and photochemical data for atmospheric chemistry. *IUPAC Subcommittee on gas kinetic data evaluation for atmospheric chemistry***,** 1-56.

ATKINSON, R., BAULCH, D., COX, R., CROWLEY, J., HAMPSON, R., HYNES, R., JENKIN, M., ROSSI, M. & TROE, J. 2006a. Evaluated kinetic and photochemical data for atmospheric chemistry: Volume III? reactions of inorganic halogens. *Atmospheric Chemistry and Physics Discussions,* 6**,** 2281-2702.

ATKINSON, R., BAULCH, D., COX, R., CROWLEY, J., HAMPSON, R., HYNES, R., JENKIN, M., ROSSI, M., TROE, J. & SUBCOMMITTEE, I. 2006b. Evaluated kinetic and photochemical data for atmospheric chemistry: Volume II–gas phase reactions of organic species. *Atmospheric chemistry and physics,* 6**,** 3625-4055.

ATKINSON, R., WINER, A. M. & PITTS JR, J. N. 1986. Estimation of night-time N2O5 concentrations from ambient NO2 and NO3 radical concentrations and the role of N2O5 in night-time chemistry. *Atmospheric Environment (1967),* 20**,** 331-339.

AUMONT, B., MADRONICH, S., BEY, I. & TYNDALL, G. S. 2000. Contribution of secondary VOC to the composition of aqueous atmospheric particles: A modeling approach. *Journal of Atmospheric Chemistry,* 35**,** 59-75.

AUMONT, B., SZOPA, S. & MADRONICH, S. 2005. Modelling the evolution of organic carbon during its gas-phase tropospheric oxidation: development of an explicit model based on a self generating approach. *Atmospheric Chemistry and Physics,* 5**,** 2497-2517.

BADIA, A., REEVES, C. E., BAKER, A. R., SAIZ-LOPEZ, A., VOLKAMER, R., APEL, E. C., HORNBROOK, R. S., CARPENTER, L. J., ANDREWS, S. J. & VON GLASOW, R. 2017. Importance of reactive halogens in the tropical marine atmosphere: A regional modelling study using WRF-Chem. *Atmos. Chem. Phys. Discuss.,* https://doi. *org/10.5194/acp-2017-903, in review*.

BAKER, A. K., SAUVAGE, C., THORENZ, U. R., VAN VELTHOVEN, P., ORAM, D. E., ZAHN, A., BRENNINKMEIJER, C. A. & WILLIAMS, J. 2016. Evidence for strong, widespread chlorine radical chemistry associated with pollution outflow from continental Asia. *Scientific reports,* 6**,** 36821.

BANNAN, T. J., BOOTH, A. M., BACAK, A., MULLER, J. B., LEATHER, K. E., LE BRETON, M., JONES, B., YOUNG, D., COE, H. & ALLAN, J. 2015. The first UK measurements of nitryl chloride using a chemical ionization mass spectrometer in central London in the summer of 2012, and an investigation of the role of Cl atom oxidation. *Journal of Geophysical Research: Atmospheres,* 120**,** 5638-5657.

BARRY, R. G. & CHORLEY, R. J. 2010. *Atmosphere, weather and climate*, Routledge.

BATTAGLIA JR, M. A., DOUGLAS, S. & HENNIGAN, C. J. 2017. Effect of the urban heat island on aerosol pH. *Environmental science & technology,* 51**,** 13095-13103.

BAUER, S., KOCH, D., UNGER, N., METZGER, S., SHINDELL, D. & STREETS, D. 2007. Nitrate aerosols today and in 2030: a global simulation including aerosols and tropospheric ozone. *Atmospheric Chemistry and Physics,* 7**,** 5043-5059.

BEHNKE, W., GEORGE, C., SCHEER, V. & ZETZSCH, C. 1997. Production and decay of ClNO2 from the reaction of gaseous N2O5 with NaCl solution: Bulk and aerosol experiments. *Journal of Geophysical Research: Atmospheres,* 102**,** 3795-3804.

BERTRAM, T. & THORNTON, J. 2009. Toward a general parameterization of N 2 O 5 reactivity on aqueous particles: the competing effects of particle liquid water, nitrate and chloride. *Atmospheric Chemistry and Physics,* 9**,** 8351-8363.

BERTRAM, T. H., THORNTON, J. A., RIEDEL, T. P., MIDDLEBROOK, A. M., BAHREINI, R., BATES, T. S., QUINN, P. K. & COFFMAN, D. J. 2009. Direct observations of N2O5 reactivity on ambient aerosol particles. *Geophysical Research Letters,* 36.

BLOSS, C., WAGNER, V., BONZANINI, A., JENKIN, M., WIRTZ, K., MARTIN-REVIEJO, M. & PILLING, M. 2005a. Evaluation of detailed aromatic mechanisms (MCMv3 and MCMv3. 1) against environmental chamber data. *Atmospheric Chemistry and Physics,* 5**,** 623-639.

BLOSS, C., WAGNER, V., JENKIN, M., VOLKAMER, R., BLOSS, W., LEE, J., HEARD, D., WIRTZ, K., MARTIN-REVIEJO, M. & REA, G. 2005b. Development of a detailed chemical mechanism (MCMv3. 1) for the atmospheric oxidation of aromatic hydrocarbons. *Atmospheric Chemistry and Physics,* 5**,** 641-664.

BLOSS, W. 2009. Atmospheric chemical processes of importance in cities. *Issues in Environmental Science and Technology,* 28**,** 42.

BLOSS, W. J., EVANS, M. J., LEE, J. D., SOMMARIVA, R., HEARD, D. E. & PILLING, M. J. 2005c. The oxidative capacity of the troposphere: Coupling of field measurements of OH and a global chemistry transport model. *Faraday discussions,* 130**,** 425-436.

BRASSEUR, G., ORLANDO, J. J. & TYNDALL, G. S. 1999. *Atmospheric chemistry and global change*, Oxford University Press.

BRIGHT, V. B., BLOSS, W. J. & CAI, X. 2011. Street canyon atmospheric composition: Coupling dynamics and chemistry. *Air Pollution Modeling and its Application XXI.* Springer.

BROWN, S., RYERSON, T., WOLLNY, A., BROCK, C., PELTIER, R., SULLIVAN, A., WEBER, R., DUBE, W., TRAINER, M. & MEAGHER, J. F. 2006. Variability in nocturnal nitrogen oxide processing and its role in regional air quality. *Science,* 311**,** 67-70.

BROWN, S. S., DUBÉ, W. P., FUCHS, H., RYERSON, T. B., WOLLNY, A. G., BROCK, C. A., BAHREINI, R., MIDDLEBROOK, A. M., NEUMAN, J. A. & ATLAS, E. 2009. Reactive uptake coefficients for N2O5 determined from aircraft measurements during the Second Texas Air Quality Study: Comparison to current model parameterizations. *Journal of Geophysical Research: Atmospheres,* 114.

BROWN, S. S., OSTHOFF, H. D., STARK, H., DUBÉ, W. P., RYERSON, T. B., WARNEKE, C., DE GOUW, J. A., WOLLNY, A. G., PARRISH, D. D. & FEHSENFELD, F. C. 2005. Aircraft observations of daytime NO3 and N2O5 and their implications for tropospheric chemistry. *Journal of Photochemistry and Photobiology A: Chemistry,* 176**,** 270-278.

BROWN, S. S. & STUTZ, J. 2012. Nighttime radical observations and chemistry. *Chemical Society Reviews,* 41**,** 6405-6447.

CARDELINO, C. 1998. Daily variability of motor vehicle emissions derived from traffic counter data. *Journal of the Air & Waste Management Association,* 48**,** 637-645.

CARSLAW, D. C. 2005. Evidence of an increasing NO2/NOx emissions ratio from road traffic emissions. *Atmospheric Environment,* 39**,** 4793-4802.

CARSLAW, D. C., BEEVERS, S. D., TATE, J. E., WESTMORELAND, E. J. & WILLIAMS, M. L. 2011. Recent evidence concerning higher NOx emissions from passenger cars and light duty vehicles. *Atmospheric Environment,* 45**,** 7053-7063.

CARSLAW, D. C., MURRELLS, T. P., ANDERSSON, J. & KEENAN, M. 2016. Have vehicle emissions of primary NO 2 peaked? *Faraday discussions,* 189**,** 439-454.

CARTER, W. P. 2000. Documentation of the SAPRC-99 chemical mechanism for VOC reactivity assessment. *Contract,* 92**,** 95-308.

CARTER, W. P. 2010. Development of the SAPRC-07 chemical mechanism. *Atmospheric Environment,* 44**,** 5324-5335.

CHANG, W. L., BHAVE, P. V., BROWN, S. S., RIEMER, N., STUTZ, J. & DABDUB, D. 2011. Heterogeneous atmospheric chemistry, ambient measurements, and model calculations of N2O5: A review. *Aerosol Science and Technology,* 45**,** 665-695.

CHARLTON, S. G. & BAAS, P. H. 2002. Road User Interactions: Patterns of Road Use and Perception of Driving Risk.

COLLETT, R. S. & ODUYEMI, K. 1997. Air quality modelling: a technical review of mathematical approaches. *Meteorological Applications,* 4**,** 235-246.

COLVILE, R., HUTCHINSON, E., MINDELL, J. & WARREN, R. 2001. The transport sector as a source of air pollution. *Atmospheric environment,* 35**,** 1537-1565.

CRAIG, R. L., PETERSON, P. K., NANDY, L., LEI, Z., HOSSAIN, M. A., CAMARENA, S., DODSON, R. A., COOK, R. D., DUTCHER, C. S. & AULT, A. P. 2018. Direct Determination of Aerosol pH: Size-Resolved Measurements of Submicrometer and Supermicrometer Aqueous Particles. *Analytical chemistry,* 90**,** 11232-11239.

CURTIS, A. & SWEETENHAM, W. 1987. *FACSIMILE/CHECKMAT user's manual*, UKAEA Atomic Energy Research Establishment Computer Science and Systems Division.

DALY, A. & ZANNETTI, P. 2007. Air pollution modeling–An overview. *Ambient air pollution***,** 15-28.

DEMORE, W. B., SANDER, S. P., GOLDEN, D., HAMPSON, R. F., KURYLO, M. J., HOWARD, C. J., RAVISHANKARA, A., KOLB, C. & MOLINA, M. 1997. Chemical Kinetics and Photochemical Data for Use in Stratospheric Modeling. Evaluation No. 12.

DENG, J., WANG, T., LIU, L. & JIANG, F. 2010. Modeling heterogeneous chemical processes on aerosol surface. *Particuology,* 8**,** 308-318.

DERWENT, D., FRASER, A., ABBOTT, J., JENKIN, M., WILLIS, P. & MURRELLS, T. 2010. Evaluating the performance of air quality models. *Report prepared for the UK Department for Environment, Food and Rural Affairs*.

ELLIOT, P. & CUZICK, J. 1992. *Geographical and environmental epidemiology: methods for Small area studies*, World Health Organization [Geneva].

ELSTON, J. C. 1979. Offsetting Stationary Source Emissions with Transportation Control Measures. *Journal of the Air Pollution Control Association,* 29**,** 1066-1069.

ESCORCIA, E. N. 2010. *Laboratory Aerosol Kinetics Studies of the Hydrolysis Reaction of N2O5 Using a Flow Tube Coupled to a New Chemical Ionization Mass Spectrometer.*

EZELL, M. J., WANG, W., EZELL, A. A., SOSKIN, G. & FINLAYSON-PITTS, B. J. 2002. Kinetics of reactions of chlorine atoms with a series of alkenes at 1 atm and 298 K: structure and reactivity. *Physical Chemistry Chemical Physics,* 4**,** 5813-5820.

FAN, J. & ZHANG, R. 2004. Atmospheric oxidation mechanism of isoprene. *Environmental Chemistry,* 1**,** 140-149.

FAXON, C. B., BEAN, J. K. & RUIZ, L. H. 2015. Inland concentrations of Cl2 and ClNO2 in Southeast Texas suggest chlorine chemistry significantly contributes to atmospheric reactivity. *Atmosphere,* 6**,** 1487-1506.

FINLAYSON-PITTS, B. 2003. The tropospheric chemistry of sea salt: A molecular-level view of the chemistry of NaCl and NaBr. *Chemical reviews,* 103**,** 4801-4822.

FINLAYSON-PITTS, B., EZELL, M. & PITTS JR, J. 1989. Formation of chemically active chlorine compounds by reactions of atmospheric NaCl particles with gaseous N2O5 and ClONO2. *Nature,* 337**,** 241.

FINLAYSON-PITTS, B. J. & PITTS JR, J. N. 1999. *Chemistry of the upper and lower atmosphere: theory, experiments, and applications*, Elsevier.

FOWLER, D., AMANN, M., ANDERSON, F., ASHMORE, M., COX, P., DEPLEDGE, M., DERWENT, D., GRENNFELT, P., HEWITT, N. & HOV, O. 2008. Ground-level ozone in the 21st century: future trends, impacts and policy implications. *Royal Society Science Policy Report,* 15.

FUENTES, J. D., LERDAU, M., ATKINSON, R., BALDOCCHI, D., BOTTENHEIM, J., CICCIOLI, P., LAMB, B., GERON, C., GU, L. & GUENTHER, A. 2000. Biogenic hydrocarbons in the atmospheric boundary layer: a review. *Bulletin of the American Meteorological Society,* 81**,** 1537-1576.

FUJITA, K. 2013. *Cities and crisis: new critical urban theory*, Sage.

GALINDO, N. & YUBERO, E. 2017. Day-night variability of water-soluble ions in PM 10 samples collected at a traffic site in southeastern Spain. *Environmental Science and Pollution Research,* 24**,** 805-812.

GAO, H. O. 2007. Day of week effects on diurnal ozone/NOx cycles and transportation emissions in Southern California. *Transportation Research Part D: Transport and Environment,* 12**,** 292-305.

GE, X., HE, Y., SUN, Y., XU, J., WANG, J., SHEN, Y. & CHEN, M. 2017. Characteristics and formation mechanisms of fine particulate nitrate in typical urban areas in China. *Atmosphere,* 8**,** 62.

GEORGE, C., PONCHE, J., MIRABEL, P., BEHNKE, W., SCHEER, V. & ZETZSCH, C. 1994. Study of the uptake of N2O5 by water and NaCl solutions. *The Journal of Physical Chemistry,* 98**,** 8780-8784.

GERY, M., WHITTEN, G. & KILLUS, J. 1988. *Development and Testing of the CBM-IV for Urban and Regional Modeling: Project Summary*, US Environmental Protection Agency, Atmospheric Sciences Research Laboratory.

GERY, M. W., WHITTEN, G. Z., KILLUS, J. P. & DODGE, M. C. 1989. A photochemical kinetics mechanism for urban and regional scale computer modeling. *Journal of Geophysical Research: Atmospheres,* 94**,** 12925-12956.

GEYER, A. 2000. The role of the nitrate radical in the boundary layer. *Atmospheric Chemistry of HOx and ROx Radicals" ISBN***,** 3-89825.

GRANGE, S. K., LEWIS, A. C., MOLLER, S. J. & CARSLAW, D. C. 2017. Lower vehicular primary emissions of NO 2 in Europe than assumed in policy projections. *Nature Geoscience,* 10**,** 914.

GRENFELL, J., SAVAGE, N., HARRISON, R., PENKETT, S., FORBERICH, O., COMES, F., CLEMITSHAW, K., BURGESS, R., CARDENAS, L. & DAVISON, B. 1999. Tropospheric box-modelling and analytical studies of the hydroxyl (OH) radical and related species: Comparison with observations. *Journal of atmospheric chemistry,* 33**,** 183-214.

GRICE, S., STEDMAN, J., KENT, A., HOBSON, M., NORRIS, J., ABBOTT, J. & COOKE, S. 2009. Recent trends and projections of primary NO2 emissions in Europe. *Atmospheric Environment,* 43**,** 2154-2167.

GROSJEAN, D. 1997. Atmospheric chemistry of alcohols. *Journal of the Brazilian Chemical Society,* 8**,** 433-442.

GULIA, S., NAGENDRA, S. S., BARNES, J. & KHARE, M. 2018. Urban local air quality management framework for non-attainment areas in Indian cities. *Science of the Total Environment,* 619**,** 1308-1318.

GUO, H., XU, L., BOUGIATIOTI, A., CERULLY, K. M., CAPPS, S. L., HITE JR, J., CARLTON, A., LEE, S.-H., BERGIN, M. & NG, N. 2015. Fine-particle water and pH in the southeastern United States. *Atmospheric Chemistry & Physics,* 15.

GUTTIKUNDA, S. K. & GOEL, R. 2013. Health impacts of particulate pollution in a megacity— Delhi, India. *Environmental Development,* 6**,** 8-20.

HABY, J. 2011. The Planetary Boundary Layer. *Weather Education Website,* [http://www.](http://www). theweatherprediction. com/basic/pbl*.*

HAMAN, C., COUZO, E., FLYNN, J., VIZUETE, W., HEFFRON, B. & LEFER, B. 2014. Relationship between boundary layer heights and growth rates with ground- level ozone in Houston, Texas. *Journal of Geophysical Research: Atmospheres,* 119**,** 6230-6245.

HARRISON, R. & YIN, J. 2004. Characterisation of particulate matter in the United Kingdom. *Report produced for Defra, the National Assembly for Wales, the Department of the Environment in Northern Ireland and the Scottish Executive, The University of Birmingham.*

HARRISON, R. M. & YIN, J. 2008. Sources and processes affecting carbonaceous aerosol in central England. *Atmospheric Environment,* 42**,** 1413-1423.

HAUGLUSTAINE, D., BRASSEUR, G., WALTERS, S., RASCH, P., MÜLLER, J. F., EMMONS, L. & CARROLL, M. 1998. MOZART, a global chemical transport model for ozone and related chemical tracers: 2. Model results and evaluation. *Journal of Geophysical Research: Atmospheres,* 103**,** 28291-28335.

HAUGLUSTAINE, D., GRANIER, C., BRASSEUR, G. & MEGIE, G. 1994. The importance of atmospheric chemistry in the calculation of radiative forcing on the climate system. *Journal of Geophysical Research: Atmospheres,* 99**,** 1173-1186.

HEWITT, C. N. & JACKSON, A. V. 2009. *Atmospheric science for environmental scientists*, John Wiley & Sons.

HITCHCOCK, G., CONLAN, B., KAY, D., BRANNIGAN, C. & NEWMAN, D. 2014. Air quality and road transport. *London: Impacts and solutions. RAC Foundation*.

HOLGATE, S. T. 2017. 'Every breath we take: the lifelong impact of air pollution'–a call for action. *Clinical Medicine,* 17**,** 8-12.

HOLLOWAY, A. M. & WAYNE, R. P. 2010. *Atmospheric chemistry*, Royal Society of Chemistry.

HOOD, C., MACKENZIE, I., STOCKER, J., JOHNSON, K., CARRUTHERS, D., VIENO, M. & DOHERTY, R. Air quality simulations for London using a coupled regional-to-local modelling system.

HOYLE, C., BOY, M., DONAHUE, N., FRY, J., GLASIUS, M., GUENTHER, A., HALLAR, A., HUFF HARTZ, K., PETTERS, M. & PETÄJÄ, T. 2011. A review of the anthropogenic influence on biogenic secondary organic aerosol. *Atmospheric Chemistry and Physics,* 11**,** 321-343.

HYNES, R., ANGOVE, D., SAUNDERS, S., HAVERD, V. & AZZI, M. 2005. Evaluation of two MCM v3. 1 alkene mechanisms using indoor environmental chamber data. *Atmospheric Environment,* 39**,** 7251-7262.

JACOB, D. J. 2000. Heterogeneous chemistry and tropospheric ozone. *Atmospheric Environment,* 34**,** 2131-2159.

JACOBSON, M. Z. 2012. *Air pollution and global warming: History, science, and solutions*, Cambridge University Press.

JENKIN, M., WATSON, L., UTEMBE, S. & SHALLCROSS, D. 2008. A Common Representative Intermediates (CRI) mechanism for VOC degradation. Part 1: Gas phase mechanism development. *Atmospheric Environment,* 42**,** 7185-7195.

JENKIN, M., WYCHE, K., EVANS, C., CARR, T., MONKS, P., ALFARRA, M., BARLEY, M., MCFIGGANS, G., YOUNG, J. & RICKARD, A. 2012. Development and chamber evaluation of the MCM v3. 2 degradation scheme for β-caryophyllene. *Atmospheric Chemistry and Physics,* 12**,** 5275-5308.

JENKIN, M., YOUNG, J. & RICKARD, A. 2015a. The MCM v3. 3.1 degradation scheme for isoprene. *Atmospheric Chemistry and Physics,* 15**,** 11433.

JENKIN, M., YOUNG, J. & RICKARD, A. 2015b. The MCM v3. 3.1 degradation scheme for isoprene. *Atmospheric Chemistry & Physics,* 15.

JENKIN, M. E., SAUNDERS, S. M. & PILLING, M. J. 1997. The tropospheric degradation of volatile organic compounds: a protocol for mechanism development. *Atmospheric Environment,* 31**,** 81-104.

JENKINS, G. J. 2009. *UK climate projections: briefing report*, Met Office Hadley Centre.

JIMENEZ, J. L., CANAGARATNA, M., DONAHUE, N., PREVOT, A., ZHANG, Q., KROLL, J. H., DECARLO, P. F., ALLAN, J. D., COE, H. & NG, N. 2009. Evolution of organic aerosols in the atmosphere. *Science,* 326**,** 1525-1529.

JIN, L., TONSE, S., COHAN, D. S., MAO, X., HARLEY, R. A. & BROWN, N. J. 2008. Sensitivity analysis of ozone formation and transport for a central California air pollution episode. *Environmental science & technology,* 42**,** 3683-3689.

KASSOMENOS, P., KARAKITSIOS, S. & PAPALOUKAS, C. 2006. Estimation of daily traffic emissions in a South-European urban agglomeration during a workday. Evaluation of several "what if" scenarios. *Science of the Total Environment,* 370**,** 480-490.

KEIL, A. D. & SHEPSON, P. B. 2006. Chlorine and bromine atom ratios in the springtime Arctic troposphere as determined from measurements of halogenated volatile organic compounds. *Journal of Geophysical Research: Atmospheres,* 111.

KERCHER, J., RIEDEL, T. & THORNTON, J. 2009. Chlorine activation by N 2 O 5: simultaneous, in situ detection of ClNO 2 and N 2 O 5 by chemical ionization mass spectrometry. *Atmospheric Measurement Techniques,* 2**,** 193-204.

KHANIABADI, Y. O., GOUDARZI, G., DARYANOOSH, S. M., BORGINI, A., TITTARELLI, A. & DE MARCO, A. 2017. Exposure to PM 10, NO 2, and O 3 and impacts on human health. *Environmental science and pollution research,* 24**,** 2781-2789.

KIM, M. J., FARMER, D. K. & BERTRAM, T. H. 2014. A controlling role for the air− sea interface in the chemical processing of reactive nitrogen in the coastal marine boundary layer. *Proceedings of the National Academy of Sciences,* 111**,** 3943-3948.

KNIBBS, L. D., COLE-HUNTER, T. & MORAWSKA, L. 2011. A review of commuter exposure to ultrafine particles and its health effects. *Atmospheric Environment,* 45**,** 2611-2622.

KROLL, J. H., NG, N. L., MURPHY, S. M., FLAGAN, R. C. & SEINFELD, J. H. 2006. Secondary organic aerosol formation from isoprene photooxidation. *Environmental science & technology,* 40**,** 1869-1877.

KROLL, J. H. & SEINFELD, J. H. 2008. Chemistry of secondary organic aerosol: Formation and evolution of low-volatility organics in the atmosphere. *Atmospheric Environment,* 42**,** 3593-3624.

KUMAR, P., KHARE, M., HARRISON, R. M., BLOSS, W. J., LEWIS, A., COE, H. & MORAWSKA, L. 2015. New directions: air pollution challenges for developing megacities like Delhi. *Atmospheric Environment,* 122**,** 657-661.

KUMAR, R., ELIZABETH, A. & GAWANE, A. 2006. Air quality profile of inorganic ionic composition of fine aerosols at two sites in Mumbai City. *Aerosol science and technology,* 40**,** 477-489.

KWOK, E. S. & ATKINSON, R. 1995. Estimation of hydroxyl radical reaction rate constants for gas-phase organic compounds using a structure-reactivity relationship: an update. *Atmospheric Environment,* 29**,** 1685-1696.

LEE, J. D., LEWIS, A. C., MONKS, P. S., JACOB, M., HAMILTON, J. F., HOPKINS, J. R., WATSON, N. M., SAXTON, J. E., ENNIS, C. & CARPENTER, L. J. 2006. Ozone photochemistry and elevated isoprene during the UK heatwave of August 2003. *Atmospheric Environment,* 40**,** 7598-7613.

LELIEVELD, J., DENTENER, F., PETERS, W. & KROL, M. 2004. Hydroxyl radicals maintain the self-cleansing capacity of the troposphere. *Atmospheric Chemistry and Physics Discussions,* 4**,** 3699-3720.

LI, Q., ZHANG, L., THAM, Y. J., AHMADOV, R., XUE, L., ZHANG, Q. & ZHENG, J. 2016. Impacts of heterogeneous uptake of dinitrogen pentoxide and chlorine activation on ozone and reactive nitrogen partitioning: improvement and application of the WRF-Chem model in southern China. *Atmospheric Chemistry and Physics,* 16**,** 14875.

LIN, Y. C., CHENG, M. T., LIN, W. H., LAN, Y.-Y. & TSUANG, B.-J. 2010. Causes of the elevated nitrate aerosol levels during episodic days in Taichung urban area, Taiwan. *Atmospheric Environment,* 44**,** 1632-1640.

LINGARD, J. J., AGUS, E. L., YOUNG, D. T., ANDREWS, G. E. & TOMLIN, A. S. 2006. Observations of urban airborne particle number concentrations during rush-hour conditions: analysis of the number based size distributions and modal parameters. *Journal of Environmental Monitoring,* 8**,** 1203-1218.

LIU, X., QU, H., HUEY, L. G., WANG, Y., SJOSTEDT, S., ZENG, L., LU, K., WU, Y., HU, M. & SHAO, M. 2017. High levels of daytime molecular chlorine and nitryl chloride at a rural site on the North China Plain. *Environmental science & technology,* 51**,** 9588-9595.

LIU, Y., FAN, Q., CHEN, X., ZHAO, J., LING, Z., HONG, Y., LI, W., CHEN, X., WANG, M. & WEI, X. 2018. Modeling the impact of chlorine emissions from coal combustion and prescribed waste incineration on tropospheric ozone formation in China. *Atmospheric Chemistry and Physics,* 18**,** 2709-2724.

LUTGENS, F. K., TARBUCK, E. J. & TUSA, D. 2010. *The atmosphere*, Prentice Hall Upper Saddle River, NJ.

MADRONICH, S. & CALVERT, J. G. 1990. Permutation reactions of organic peroxy radicals in the troposphere. *Journal of Geophysical Research: Atmospheres,* 95**,** 5697-5715.

MADRONICH, S. & FLOCKE, S. 1999. The role of solar radiation in atmospheric chemistry. *Environmental photochemistry.* Springer.

MALLEY, C., VON SCHNEIDEMESSER, E., MOLLER, S. J., HICKS, W. K., BRABAN, C. & HEAL, M. 2018. Analysis of the distributions of hourly NO2 concentrations contributing to annual average NO2 concentrations across the European monitoring network between 2000 and 2014. *Atmospheric Chemistry and Physics***,** 3563-3587.

MANDERS, A., SCHAAP, M., QUEROL, X., ALBERT, M., VERCAUTEREN, J., KUHLBUSCH, T. & HOOGERBRUGGE, R. 2010. Sea salt concentrations across the European continent. *Atmospheric Environment,* 44**,** 2434-2442.

MCLAREN, R., WOJTAL, P., MAJONIS, D., MCCOURT, J., HALLA, J. & BROOK, J. 2010. NO 3 radical measurements in a polluted marine environment: links to ozone formation. *Atmospheric Chemistry and Physics,* 10**,** 4187-4206.

MILLS, I., ATKINSON, R., ANDERSON, H., MAYNARD, R. & STRACHAN, D. 2016. Distinguishing the associations between daily mortality and hospital admissions and nitrogen dioxide from those of particulate matter: a systematic review and meta-analysis. *BMJ open,* 6**,** e010751.

MOHAMED, M. F., KANG, D. & ANEJA, V. P. 2002. Volatile organic compounds in some urban locations in United States. *Chemosphere,* 47**,** 863-882.

MONKS, P. S. 2005. Gas-phase radical chemistry in the troposphere. *Chemical Society Reviews,* 34**,** 376-395.

MONKS, P. S., ARCHIBALD, A., COLETTE, A., COOPER, O., COYLE, M., DERWENT, R., FOWLER, D., GRANIER, C., LAW, K. S. & MILLS, G. 2015. Tropospheric ozone and its precursors from the urban to the global scale from air quality to short-lived climate forcer. *Atmospheric Chemistry and Physics,* 15**,** 8889-8973.

MORGAN, W., OUYANG, B., ALLAN, J., ARUFFO, E., DI CARLO, P., KENNEDY, O., LOWE, D., FLYNN, M., ROSENBERG, P. & WILLIAMS, P. 2015. Influence of aerosol chemical composition on N 2 O 5 uptake: airborne regional measurements in northwestern Europe. *Atmospheric Chemistry and Physics,* 15**,** 973-990.

MURPHY, J. M., SEXTON, D., JENKINS, G., BOOTH, B., BROWN, C., CLARK, R., COLLINS, M., HARRIS, G., KENDON, E. & BETTS, R. 2009. UK climate projections science report: climate change projections.

NHUNG, N. T. T., SCHINDLER, C., DIEN, T. M., PROBST-HENSCH, N., PEREZ, L. & KÜNZLI, N. 2018. Acute effects of ambient air pollution on lower respiratory infections in hanoi children: an eight-year time series study. *Environment international,* 110**,** 139-148.

NI, R., LIN, J., YAN, Y. & LIN, W. 2018. Foreign and domestic contributions to springtime ozone over China. *Atmospheric Chemistry & Physics,* 18.

OHTA, T., BANDOW, H. & AKIMOTO, H. 1982. Gas- phase chlorine- initiated photooxidation of methanol and isopropanol. *International Journal of Chemical Kinetics,* 14**,** 173-182.

OIKONOMAKIS, E., AKSOYOGLU, S., CIARELLI, G., BALTENSPERGER, U., PRÉVÔT, H. & STEPHAN, A. 2018. Low modeled ozone production suggests underestimation of precursor emissions (especially NO x) in Europe. *Atmospheric Chemistry & Physics,* 18.

OREL, A. E. & SEINFELD, J. H. 1977. Nitrate formation in atmospheric aerosols. *Environmental Science & Technology,* 11**,** 1000-1007.

OSTHOFF, H. D., ODAME-ANKRAH, C. A., TAHA, Y. M., TOKAREK, T. W., SCHILLER, C. L., HAGA, D., JONES, K. & VINGARZAN, R. 2018. Low levels of nitryl chloride at ground level: nocturnal nitrogen oxides in the Lower Fraser Valley of British Columbia. *Atmospheric Chemistry and Physics,* 18**,** 6293-6315.

OSTHOFF, H. D., ROBERTS, J. M., RAVISHANKARA, A., WILLIAMS, E. J., LERNER, B. M., SOMMARIVA, R., BATES, T. S., COFFMAN, D., QUINN, P. K. & DIBB, J. E. 2008.

High levels of nitryl chloride in the polluted subtropical marine boundary layer. *Nature Geoscience,* 1**,** 324.

PACIFICO, F., HARRISON, S., JONES, C. & SITCH, S. 2009. Isoprene emissions and climate. *Atmospheric Environment,* 43**,** 6121-6135.

PAN, Y., WANG, Y., ZHANG, J., LIU, Z., WANG, L., TIAN, S., TANG, G., GAO, W., JI, D. & SONG, T. 2016. Redefining the importance of nitrate during haze pollution to help optimize an emission control strategy. *Atmospheric Environment,* 141**,** 197-202.

PATHAK, R. K., WU, W. S. & WANG, T. 2009. Summertime PM 2.5 ionic species in four major cities of China: nitrate formation in an ammonia-deficient atmosphere. *Atmospheric Chemistry and Physics,* 9**,** 1711-1722.

PEÑUELAS, J. & STAUDT, M. 2010. BVOCs and global change. *Trends in plant science,* 15**,** 133-144.

PETETIN, H., SCIARE, J., BRESSI, M., GROS, V., ROSSO, A., SANCHEZ, O., SARDA-ESTÈVE, R., PETIT, J.-E. & BEEKMANN, M. 2016. Assessing the ammonium nitrate formation regime in the Paris megacity and its representation in the CHIMERE model. *Atmospheric Chemistry and Physics,* 16**,** 10419-10440.

PETTERS, M. & KREIDENWEIS, S. 2007. A single parameter representation of hygroscopic growth and cloud condensation nucleus activity. *Atmospheric Chemistry and Physics,* 7**,** 1961-1971.

PINHO, P., PIO, C., CARTER, W. & JENKIN, M. 2006. Evaluation of alkene degradation in the detailed tropospheric chemistry mechanism, MCM v3, using environmental chamber data. *Journal of Atmospheric Chemistry,* 55**,** 55-79.

POLONIECKI, J. D., ATKINSON, R. W., DE LEON, A. P. & ANDERSON, H. R. 1997. Daily time series for cardiovascular hospital admissions and previous day's air pollution in London, UK. *Occupational and environmental medicine,* 54**,** 535-540.

POPE III, C. A., EZZATI, M. & DOCKERY, D. W. 2009. Fine-particulate air pollution and life expectancy in the United States. *New England Journal of Medicine,* 360**,** 376-386.

PUSEDE, S., DUFFEY, K., SHUSTERMAN, A., SALEH, A., LAUGHNER, J., WOOLDRIDGE, P., ZHANG, Q., PARWORTH, C., KIM, H. & CAPPS, S. 2016. On the effectiveness of nitrogen oxide reductions as a control over ammonium nitrate aerosol. *Atmospheric Chemistry and Physics,* 16**,** 2575-2596.

PUTAUD, J.-P., VAN DINGENEN, R., ALASTUEY, A., BAUER, H., BIRMILI, W., CYRYS, J., FLENTJE, H., FUZZI, S., GEHRIG, R. & HANSSON, H.-C. 2010. A European aerosol phenomenology–3: Physical and chemical characteristics of particulate matter from 60 rural, urban, and kerbside sites across Europe. *Atmospheric Environment,* 44**,** 1308-1320.

RAGETTLI, M. S., CORRADI, E., BRAUN-FAHRLÄNDER, C., SCHINDLER, C., DE NAZELLE, A., JERRETT, M., DUCRET-STICH, R. E., KÜNZLI, N. & PHULERIA, H.

C. 2013. Commuter exposure to ultrafine particles in different urban locations, transportation modes and routes. *Atmospheric environment, 77*, 376-384.

RAVISHANKARA, A. 1997. Heterogeneous and multiphase chemistry in the troposphere. *Science, 276*, 1058-1065.

RICHARDS, L. W. 1983. Comments on the oxidation of NO2 to nitrate—day and night. *Atmospheric Environment (1967), 17*, 397-402.

RIEDEL, K. & LASSEY, K. 2008. Detergent of the atmosphere. *Water Atmos, 16*.

RIEDEL, T., WOLFE, G., DANAS, K., GILMAN, J., KUSTER, W., BON, D., VLASENKO, A., LI, S.-M., WILLIAMS, E. & LERNER, B. 2014. An MCM modeling study of nitryl chloride (ClNO 2) impacts on oxidation, ozone production and nitrogen oxide partitioning in polluted continental outflow. *Atmospheric Chemistry and Physics, 14*, 3789-3800.

ROBERTS, J. M., OSTHOFF, H. D., BROWN, S. S., RAVISHANKARA, A., COFFMAN, D., QUINN, P. & BATES, T. 2009. Laboratory studies of products of N2O5 uptake on Cl− containing substrates. *Geophysical Research Letters, 36*.

ROMER, P. S., WOOLDRIDGE, P. J., CROUNSE, J. D., KIM, M. J., WENNBERG, P. O., DIBB, J. E., SCHEUER, E., BLAKE, D. R., MEINARDI, S. & BROSIUS, A. L. 2018. Constraints on aerosol nitrate photolysis as a potential source of HONO and NO x. *Environmental science & technology, 52*, 13738-13746.

RYAN, P. H., REPONEN, T., SIMMONS, M., YERMAKOV, M., SHARKEY, K., GARLAND-PORTER, D., EGHBALNIA, C. & GRINSHPUN, S. A. 2013. The impact of an anti-idling campaign on outdoor air quality at four urban schools. *Environmental Science: Processes & Impacts, 15*, 2030-2037.

SAIZ-LOPEZ, A. & VON GLASOW, R. 2012. Reactive halogen chemistry in the troposphere. *Chemical Society Reviews, 41*, 6448-6472.

SALMOND, J. A. & MCKENDRY, I. 2009. Influences of Meteorology on Air Pollution Concentrations and Processes in Urban Areas. *Air Quality in Urban Environments, 28*, 23.

SANDER, S. 2011. Chemical kinetics and photochemical data for use in atmospheric studies, evaluation no. 17 of the NASA panel for data evaluation, JPL Publ., 10-6, Jet Propul. *Lab., Pasadena*.

SANDER, S. P., FRIEDL, R., BARKER, J., GOLDEN, D., KURYLO, M., WINE, P., ABBATT, J., BURKHOLDER, J., KOLB, C. & MOORTGAT, G. 2009. Chemical kinetics and photochemical data for use in Atmospheric Studies Evaluation Number 16: supplement to Evaluation 15: update of key reactions. Pasadena, CA: Jet Propulsion Laboratory, National Aeronautics and Space Administration, 2009.

SARWAR, G., SIMON, H., BHAVE, P. & YARWOOD, G. 2012. Examining the impact of heterogeneous nitryl chloride production on air quality across the United States. *Atmospheric Chemistry and Physics, 12*, 6455-6473.

SARWAR, G., SIMON, H., XING, J. & MATHUR, R. 2014. Importance of tropospheric ClNO2 chemistry across the Northern Hemisphere. *Geophysical Research Letters,* 41**,** 4050-4058.

SAUNDERS, E. 2017. *Modeling Regional & Global Atmospheric Chemistry Mechanisms: Observing Adverse Respiratory Health Effects due to Tropospheric Ozone Air Pollution from Modeling Output.* Howard University.

SAUNDERS, S. M., JENKIN, M. E., DERWENT, R. & PILLING, M. 2003. Protocol for the development of the Master Chemical Mechanism, MCM v3 (Part A): tropospheric degradation of non-aromatic volatile organic compounds. *Atmospheric Chemistry and Physics,* 3**,** 161-180.

SEINFELD, J. H. 1989. Urban air pollution: state of the science. *Science,* 243**,** 745-752.

SEINFELD, J. H. & PANDIS, S. N. 1997. *Atmospheric chemistry and physics: from air pollution to climate change*, John Wiley & Sons.

SEINFELD, J. H. & PANDIS, S. N. 1998. *Atmospheric chemistry and physics: from air pollution to climate change*, John Wiley & Sons.

SEINFELD, J. H. & PANDIS, S. N. 2012. *Atmospheric chemistry and physics: from air pollution to climate change*, John Wiley & Sons.

SEINFELD, J. H. & PANDIS, S. N. 2016. *Atmospheric chemistry and physics: from air pollution to climate change*, John Wiley & Sons.

SEN-CHAO, L., SHI-CHUN, Z., JUN-JI, C., SHUN-CHENG, L. & KIN-FAI, H. 2009. Characterizing ionic species in PM2. 5 and PM10 in four Pearl River Delta cities, South China. *Journal of Environmental Sciences,* 19**,** 939-947.

SHI, J. & BERNHARD, M. J. 1997. Kinetic studies of Cl- atom reactions with selected aromatic compounds using the photochemical reactor- FTIR spectroscopy technique. *International journal of chemical kinetics,* 29**,** 349-358.

SHON, Z.-H., GHOSH, S., KIM, K.-H., SONG, S.-K., JUNG, K. & KIM, N.-J. 2013. Analysis of water-soluble ions and their precursor gases over diurnal cycle. *Atmospheric research,* 132**,** 309-321.

SILLMAN, S. 1999. The relation between ozone, NOx and hydrocarbons in urban and polluted rural environments. *Atmospheric Environment,* 33**,** 1821-1845.

SILLMAN, S. 2003. Overview: Tropospheric ozone, smog and ozone-NOx-VOC sensitivity. *Treatise on Geochemistry*.

SILLMAN, S., LOGAN, J. A. & WOFSY, S. C. 1990. The sensitivity of ozone to nitrogen oxides and hydrocarbons in regional ozone episodes. *Journal of Geophysical Research: Atmospheres,* 95**,** 1837-1851.

SIMON, H., BECK, L., BHAVE, P. V., DIVITA, F., HSU, Y., LUECKEN, D., MOBLEY, J. D., POULIOT, G. A., REFF, A. & SARWAR, G. 2010. The development and uses of EPA's SPECIATE database. *Atmospheric Pollution Research,* 1**,** 196-206.

SIMON, H., KIMURA, Y., MCGAUGHEY, G., ALLEN, D., BROWN, S., OSTHOFF, H., ROBERTS, J., BYUN, D. & LEE, D. 2009. Modeling the impact of ClNO2 on ozone formation in the Houston area. *Journal of Geophysical Research: Atmospheres,* 114.

SINGH, A. & AGRAWAL, M. 2007. Acid rain and its ecological consequences. *Journal of Environmental Biology,* 29**,** 15.

SOLOMON, S., QIN, D., MANNING, M., AVERYT, K. & MARQUIS, M. 2007. *Climate change 2007-the physical science basis: Working group I contribution to the fourth assessment report of the IPCC*, Cambridge university press.

SOMMARIVA, R., HOLLIS, L. D., SHERWEN, T., BAKER, A. R., BALL, S. M., BANDY, B. J., BELL, T. G., CHOWDHURY, M. N., CORDELL, R. L. & EVANS, M. J. 2018. Seasonal and geographical variability of nitryl chloride and its precursors in Northern Europe. *Atmospheric Science Letters,* 19**,** e844.

SPITTLER, M., BARNES, I., BEJAN, I., BROCKMANN, K., BENTER, T. & WIRTZ, K. 2006. Reactions of NO3 radicals with limonene and α-pinene: Product and SOA formation. *Atmospheric Environment,* 40**,** 116-127.

STOCKWELL, W. R., LAWSON, C. V., SAUNDERS, E. & GOLIFF, W. S. 2011. A review of tropospheric atmospheric chemistry and gas-phase chemical mechanisms for air quality modeling. *Atmosphere,* 3**,** 1-32.

STUTZ, J., ALICKE, B., ACKERMANN, R., GEYER, A., WHITE, A. & WILLIAMS, E. 2004. Vertical profiles of NO3, N2O5, O3, and NOx in the nocturnal boundary layer: 1. Observations during the Texas Air Quality Study 2000. *Journal of Geophysical Research: Atmospheres,* 109.

SU, X., TIE, X., LI, G., CAO, J., HUANG, R., FENG, T., LONG, X. & XU, R. 2017. Effect of hydrolysis of N 2 O 5 on nitrate and ammonium formation in Beijing China: WRF-Chem model simulation. *Science of the Total Environment,* 579**,** 221-229.

SUH, I. & ZHANG, R. 2000. Kinetic studies of isoprene reactions initiated by chlorine atom. *The Journal of Physical Chemistry A,* 104**,** 6590-6596.

SUNYER, J., SPIX, C., QUENEL, P., PONCE-DE-LEON, A., PÖNKA, A., BARUMANDZADEH, T., TOULOUMI, G., BACHAROVA, L., WOJTYNIAK, B. & VONK, J. 1997. Urban air pollution and emergency admissions for asthma in four European cities: the APHEA Project. *Thorax,* 52**,** 760-765.

SYAFEI, A. D. & ZHANG, J. 2015. Temporal and spatial analysis of peak-concentration times for NO and NO2 in morning and evening events: a case study of Surabaya city. *Procedia Environmental Sciences,* 28**,** 509-518.

TAN, J., DUAN, J., HE, K., MA, Y., DUAN, F., CHEN, Y. & FU, J. 2009. Chemical characteristics of PM2. 5 during a typical haze episode in Guangzhou. *Journal of Environmental Sciences,* 21**,** 774-781.

TANAKA, P. L., ALLEN, D. T., MCDONALD- BULLER, E. C., CHANG, S., KIMURA, Y., MULLINS, C. B., YARWOOD, G. & NEECE, J. D. 2003. Development of a chlorine mechanism for use in the carbon bond IV chemistry model. *Journal of Geophysical Research: Atmospheres,* 108.

THORNTON, J. A. & ABBATT, J. P. 2005. N2O5 reaction on submicron sea salt aerosol: Kinetics, products, and the effect of surface active organics. *The Journal of Physical Chemistry A,* 109**,** 10004-10012.

TONG, N. Y., LEUNG, D. Y. & LIU, C.-H. 2011. A review on ozone evolution and its relationship with boundary layer characteristics in urban environments. *Water, Air, & Soil Pollution,* 214**,** 13-36.

TURNBULL, A. B. & HARRISON, R. M. 2000. Major component contributions to PM10 composition in the UK atmosphere. *Atmospheric Environment,* 34**,** 3129-3137.

VARDOULAKIS, S., FISHER, B. E., PERICLEOUS, K. & GONZALEZ-FLESCA, N. 2003. Modelling air quality in street canyons: a review. *Atmospheric environment,* 37**,** 155-182.

VU, T. V., DELGADO-SABORIT, J. M. & HARRISON, R. M. 2015. Particle number size distributions from seven major sources and implications for source apportionment studies. *Atmospheric Environment,* 122**,** 114-132.

VUTUKURU, S., GRIFFIN, R. J. & DABDUB, D. 2006. Simulation and analysis of secondary organic aerosol dynamics in the South Coast Air Basin of California. *Journal of Geophysical Research: Atmospheres,* 111.

WAGNER, N., RIEDEL, T., YOUNG, C., BAHREINI, R., BROCK, C., DUBÉ, W., KIM, S., MIDDLEBROOK, A., ÖZTÜRK, F. & ROBERTS, J. 2013. N2O5 uptake coefficients and nocturnal NO2 removal rates determined from ambient wintertime measurements. *Journal of Geophysical Research: Atmospheres,* 118**,** 9331-9350.

WAHNER, A., MENTEL, T. F. & SOHN, M. 1998. Gas- phase reaction of N2O5 with water vapor: Importance of heterogeneous hydrolysis of N2O5 and surface desorption of HNO3 in a large Teflon chamber. *Geophysical Research Letters,* 25**,** 2169-2172.

WALLINGTON, T., ANDINO, J., LORKOVIC, I., KAISER, E. & MARSTON, G. 1990. Pressure dependence of the reaction of chlorine atoms with ethene and acetylene in air at 295 K. *Journal of Physical Chemistry,* 94**,** 3644-3648.

WANG, H., LU, K., GUO, S., WU, Z., SHANG, D., TAN, Z., WANG, Y., BRETON, M. L., LOU, S. & TANG, M. 2018. Efficient N 2 O 5 uptake and NO 3 oxidation in the outflow of urban Beijing. *Atmospheric Chemistry and Physics,* 18**,** 9705-9721.

WANG, T., THAM, Y. J., XUE, L., LI, Q., ZHA, Q., WANG, Z., POON, S. C., DUBÉ, W. P., BLAKE, D. R. & LOUIE, P. K. 2016. Observations of nitryl chloride and modeling its source and effect on ozone in the planetary boundary layer of southern China. *Journal of Geophysical Research: Atmospheres,* 121**,** 2476-2489.

WANG, W. & FINLAYSON- PITTS, B. J. 2001. Unique markers of chlorine atom chemistry in coastal urban areas: The reaction with 1, 3- butadiene in air at room temperature. *Journal of Geophysical Research: Atmospheres,* 106**,** 4939-4958.

WANG, X. & MAUZERALL, D. L. 2004. Characterizing distributions of surface ozone and its impact on grain production in China, Japan and South Korea: 1990 and 2020. *Atmospheric Environment,* 38**,** 4383-4402.

WANG, X., WANG, H., XUE, L., WANG, T., WANG, L., GU, R., WANG, W., THAM, Y. J., WANG, Z. & YANG, L. 2017. Observations of N2O5 and ClNO2 at a polluted urban surface site in North China: High N2O5 uptake coefficients and low ClNO2 product yields. *Atmospheric environment,* 156**,** 125-134.

WATSON, L., SHALLCROSS, D., UTEMBE, S. & JENKIN, M. 2008. A Common Representative Intermediates (CRI) mechanism for VOC degradation. Part 2: Gas phase mechanism reduction. *Atmospheric Environment,* 42**,** 7196-7204.

WAYNE, R. P., BARNES, I., BIGGS, P., BURROWS, J., CANOSA-MAS, C., HJORTH, J., LE BRAS, G., MOORTGAT, G., PERNER, D. & POULET, G. 1991. The nitrate radical: Physics, chemistry, and the atmosphere. *Atmospheric Environment. Part A. General Topics,* 25**,** 1-203.

WEN, L., XUE, L., WANG, X., XU, C., CHEN, T., YANG, L., WANG, T., ZHANG, Q. & WANG, W. 2018. Summertime fine particulate nitrate pollution in the North China Plain: increasing trends, formation mechanisms and implications for control policy. *Atmospheric Chemistry and Physics,* 18**,** 11261-11275.

WHALLEY, L., STONE, D., BANDY, B., DUNMORE, R., HAMILTON, J. F., HOPKINS, J., LEE, J. D., LEWIS, A. C. & HEARD, D. E. 2016. Atmospheric OH reactivity in central London: observations, model predictions and estimates of in situ ozone production. *Atmospheric Chemistry and Physics,* 16**,** 2109-2122.

WINER, A. M., AREY, J., ATKINSON, R., ASCHMANN, S. M., LONG, W. D., MORRISON, C. L. & OLSZYK, D. M. 1992. Emission rates of organics from vegetation in California's Central Valley. *Atmospheric Environment. Part A. General Topics,* 26**,** 2647-2659.

WISE, M. E., MARTIN, S. T., RUSSELL, L. M. & BUSECK, P. R. 2008. Water uptake by NaCl particles prior to deliquescence and the phase rule. *Aerosol Science and Technology,* 42**,** 281-294.

WOFSY, S. C. & MCELROY, M. B. 1974. HO x, NO x, and ClO x: Their role in atmospheric photochemistry. *Canadian Journal of Chemistry,* 52**,** 1582-1591.

WOLFE, G. M., MARVIN, M. R., ROBERTS, S. J., TRAVIS, K. R. & LIAO, J. 2016. The Framework for 0-D Atmospheric Modeling (F0AM) v3. 1. *Geoscientific Model Development,* 9**,** 3309-3319.

WOOD, E., BERTRAM, T., WOOLDRIDGE, P. & COHEN, R. 2005. Measurements of N 2 O 5, NO 2, and O 3 east of the San Francisco Bay. *Atmospheric Chemistry and Physics,* 5**,** 483-491.

XIE, R., JACKSON, K. A., SEIP, H. M., MCLEOD, C. W., WIBETOE, G., SCHOFIELD, M. J., ANDERSON, D. & HANSSEN, J. E. 2009. Characteristics of water-soluble inorganic chemical components in size-resolved airborne particulate matters-Sheffield, UK. *Journal of Environmental Monitoring,* 11**,** 336-343.

XU, L. & PENNER, J. 2012. Global simulations of nitrate and ammonium aerosols and their radiative effects. *Atmospheric Chemistry and Physics,* 12**,** 9479-9504.

XUE, J., YUAN, Z., LAU, A. K. & YU, J. Z. 2014. Insights into factors affecting nitrate in PM2. 5 in a polluted high NOx environment through hourly observations and size distribution measurements. *Journal of Geophysical Research: Atmospheres,* 119**,** 4888-4902.

XUE, L., SAUNDERS, S., WANG, T., GAO, R., WANG, X., ZHANG, Q. & WANG, W. 2015. Development of a chlorine chemistry module for the Master Chemical Mechanism. *Geoscientific model development,* 8**,** 3151-3162.

YE, C., ZHANG, N., GAO, H. & ZHOU, X. 2017. Photolysis of Particulate Nitrate as a Source of HONO and NO x. *Environmental Science & Technology,* 51**,** 6849-6856.

YOUNG, C., WASHENFELDER, R., EDWARDS, P., PARRISH, D., GILMAN, J., KUSTER, W., MIELKE, L., OSTHOFF, H., TSAI, C. & PIKELNAYA, O. 2014. Chlorine as a primary radical: evaluation of methods to understand its role in initiation of oxidative cycles. *Atmospheric Chemistry and Physics,* 14**,** 3427-3440.

YOUNG, P., ARCHIBALD, A., BOWMAN, K., LAMARQUE, J.-F., NAIK, V., STEVENSON, D., TILMES, S., VOULGARAKIS, A., WILD, O. & BERGMANN, D. 2013. Pre-industrial to end 21st century projections of tropospheric ozone from the Atmospheric Chemistry and Climate Model Intercomparison Project (ACCMIP). *Atmospheric Chemistry and Physics,* 13**,** 2063-2090.

YUN, H., WANG, T., WANG, W., THAM, Y. J., LI, Q., WANG, Z. & POON, S. C. 2018. Nighttime NO x loss and ClNO 2 formation in the residual layer of a polluted region: Insights from field measurements and an iterative box model. *Science of The Total Environment,* 622**,** 727-734.

ZHANG, L., LI, Q., WANG, T., AHMADOV, R., ZHANG, Q., LI, M. & LV, M. 2017. Combined impacts of nitrous acid and nitryl chloride on lower-tropospheric ozone: new module development in WRF-Chem and application to China. *Atmospheric Chemistry & Physics,* 17.

ZHENG, B., ZHANG, Q., ZHANG, Y., HE, K., WANG, K., ZHENG, G., DUAN, F., MA, Y. & KIMOTO, T. 2015. Heterogeneous chemistry: a mechanism missing in current models to

explain secondary inorganic aerosol formation during the January 2013 haze episode in North China. *Atmospheric Chemistry and Physics (Online),* 15.

ZMIROU, D., BARUMANDZADEH, T., BALDUCCI, F., RITTER, P., LAHAM, G. & GHILARDI, J. 1996. Short term effects of air pollution on mortality in the city of Lyon, France, 1985-90. *Journal of Epidemiology & Community Health,* 50**,** S30-S35.

 DFT (2009). Transport Statistics Bulletin. Road Statistics 2008: Traffic, Speeds and Congestion. ? [Accessed 09 June 2019] from < http://www.ukroads.org/ukroadsignals/articlespapers/roadstats08tsc.pdf**>**

Hitchcock, G. And Carslaw, D., (2016) Road transport and air pollution - where are we now? [Accessed 8 February 2018] from <https://www.racfoundation.org/wp-content/uploads/2017/11/Ricardo_EAE_air_quality_report_Hitchcock_Carslaw_December _2016.pdf >

The City of London Traffic Composition Surveys (2018). Traffic in the City 2018. Available online < http://democracy.cityoflondon.gov.uk/documents/s91800/Appendix+1+-+Traffic+in+the+City+2018.pdf > [Accessed 26th Oct 2018]

Defra (2004), 'Nitrogen Dioxide in the United Kingdom'. available online from< https://uk-air.defra.gov.uk/assets/documents/reports/aqeg/nd-summary.pdf > revised [16th July 2018]

Defra (2015) Valuing impacts on air quality: Updates in valuing changes in emissions of Oxides of Nitrogen (NOX) and concentrations of Nitrogen Dioxide (NO2). Online from < file:///C:/Users/txr326/AppData/Local/Microsoft/Windows/INetCache/IE/2J8M1IYS/air-quality-econanalysis-nitrogen-interim-guidance.pdf > [Accsessed 7June2018]

Defra (2016b). Local Air Quality Management: Policy guidance (PG16) [Accessed 9 February 2018] online from< https://consult.defra.gov.uk/communications/laqm_changes/supporting_documents/LAQM %20Policy%20Guidance%202016.pdf >

Defra (2018) Defra National Statistics Release: Air quality statistics in the UK 1987 to 2017 [Accessed 7June2018] online from <https://assets.publishing.service.gov.uk/government/uploads/system/uploads/attachment_dat a/file/796887/Air_Quality_Statistics_in_the_UK_1987_to_2018.pdf>